

DISSERTATION

INVESTIGATIONS OF THE IDENTITY OF THE TRUE CATALYST IN THREE
SYSTEMS, INCLUDING THE DEVELOPMENT OF CATALYST POISONING
METHODOLOGY

Submitted by

Ercan Bayram

Department of Chemistry

In partial fulfillment of the requirements

For the Degree of Doctor of Philosophy

Colorado State University

Fort Collins, Colorado

Summer 2012

Doctoral Committee:

Advisor: Richard G. Finke

Eugene Y.-X. Chen

Amy L. Prieto

Elliot R. Bernstein

David S. Dandy

ABSTRACT

INVESTIGATIONS OF THE IDENTITY OF THE TRUE CATALYST IN THREE SYSTEMS, INCLUDING THE DEVELOPMENT OF CATALYST POISONING METHODOLOGY

Following brief reviews of the pertinent “who is the catalyst?” and “M₄ (M= transition-metal) cluster catalysis” literature, the research presented herein is focused on the investigations of the true catalyst for three different catalytic systems. The studies include: (i) the investigation of the true catalyst for neat benzene hydrogenation beginning with commercially available [Ir(cod)Cl]₂ (cod= 1,5-cyclooctadiene) at 22 °C and 40 psig initial H₂ pressure; (ii) the investigation of the true catalyst for benzene hydrogenation beginning with commercially available [RhCp*Cl]₂ (Cp*= pentamethylcyclopentadienyl) at 100 °C and 50 atm (740 psig) initial H₂ pressure; and (iii) the investigation of the true catalyst for cyclohexene hydrogenation beginning with the well-characterized, site isolated [Ir(C₂H₄)₂]/zeolite-Y complex at 22 °C and 40 psig initial H₂ pressure, studies done collaboratively with Professor Bruce C. Gates and his group at the University of California-Davis.

All three investigations aimed at identifying the true catalyst were studied via an arsenal of complimentary techniques including kinetics, *in operando* and post-catalysis X-ray absorption fine structure (XAFS) spectroscopy, kinetic quantitative poisoning experiments, transmission electron microscopy (TEM), X-ray photoelectron spectroscopy (XPS), and high-angle annular dark-field scanning electron microscopy (HAADF-STEM). The data obtained for each system

presented herein provide compelling evidence that the proposed species in each chapter are the true catalyst of the given system, specifically (and respectively) for (i), (ii), and (iii) above Ir(O)_n nanoparticles and aggregates, Rh₄ sub-nanometer clusters, and atomically dispersed, mononuclear Ir₁/zeolite Y catalysts. The results emphasize the need to use complimentary, multiple methods in order to correctly identify the true catalyst in such catalytic systems.

The final study elucidates kinetic quantitative catalyst poisoning via two model catalysts: Rh(O)_n nanoparticles and Rh₄ clusters, providing detailed analyses of linear as well as non-linear kinetic quantitative poisoning plots. The resulting quantitative kinetic catalyst poisoning studies of Rh(O)_n nanoparticles and Rh₄ clusters led to estimates of the equivalents of poison bound, quantitative catalyst poisoning association constants, and the numbers of active sites for each catalyst.

ACKNOWLEDGMENTS

Although only my name appears on the cover of this dissertation, a great many people have contributed to its production. First and foremost, I would like to express my sincere gratitude to Prof. Richard G. Finke for his encouragement, never-ending support, valuable criticism, advice, and supervision throughout this study. And, my beautiful wife, Hanife, is most gratefully acknowledged for her endless support and encouragement. This thesis would have been only a dream without these two people.

I would like to extend my gratitude to the Finke Group members that have been at Colorado State University over the course of the past six years for their valuable criticism and feedback that made the studies within this thesis possible.

My sincere appreciation is also extended to Prof. Saim Özkar, Prof. Bruce C. Gates and coworkers, Dr. John C. Linehan, and Dr. John L. Fulton for their valuable contribution to the science presented in this thesis.

TABLE OF CONTENTS

CHAPTER I	INTRODUCTION.....	1
CHAPTER II	A BRIEF REVIEW OF THE PROBLEM OF IDENTIFICATION OF THE TRUE CATALYST: WHAT IS THE BEST AND MOST EFFICIENT APPROACH?.....	4
	References.....	18
CHAPTER III	A CONCISE REVIEW OF SUB-NANOMETER M ₄ (M= TRANSITION-METAL) CLUSTERS IN CATALYSIS.....	22
	Carbonyl/Hydride Tetrametallic Cluster Precatalysts/Catalysts	22
	Other, Non-Carbonyl Tetrametallic Cluster Catalysts.....	32
	References.....	40
CHAPTER IV	IN-SITU FORMED “WEAKLY LIGATED/LABILE LIGAND IRIIDIUM(0) NANOPARTICLES AND AGGREGATES AS CATALYSTS FOR THE COMPLETE HYDROGENATION OF NEAT BENZENE AT ROOM TEMPERATURE AND MILD PRESSURES.....	43
	Overview.....	44
	Introduction.....	45
	Experimental.....	47
	Results and Discussion.....	55
	Conclusions.....	69
	Acknowledgments.....	71
	References.....	72
APPENDIX A	SUPPORTING INFORMATION FOR: IN-SITU FORMED “WEAKLY LIGATED/LABILE LIGAND IRIIDIUM(0) NANOPARTICLES AND AGGREGATES AS CATALYSTS FOR THE COMPLETE HYDROGENATION OF NEAT BENZENE AT ROOM TEMPERATURE AND MILD PRESSURES	77

CHAPTER V	<p>IS IT HOMOGENEOUS OR HETEROGENEOUS CATALYSIS DERIVED FROM [RhCp*Cl₂]₂? <i>IN OPERANDO</i> XAFS, KINETIC, AND CRUCIAL KINETIC POISONING EVIDENCE FOR SUBNANOMETER Rh₄ CLUSTER-BASED BENZENE HYDROGENATION CATALYSIS.....</p>	<p>83 84 85 92 116 117 127 128</p>
APPENDIX B	<p>SUPPORTING INFORMATION FOR: IS IT HOMOGENEOUS OR HETEROGENEOUS CATALYSIS DERIVED FROM [RhCp*Cl₂]₂? <i>IN OPERANDO</i> XAFS, KINETIC, AND CRUCIAL KINETIC POISONING EVIDENCE FOR SUBNANOMETER Rh₄ CLUSTER-BASED BENZENE HYDROGENATION CATALYSIS.....</p>	<p>134</p>
CHAPTER VI	<p>A MONONUCLEAR ZEOLITE-SUPPORTED IRIDIUM CATALYST: KINETIC, SPECTROSCOPIC, ELECTRON MICROSCOPIC, SIZE SELECTIVE POISONING EVIDENCE FOR AN ATOMICALLY DISPERSED TRUE CATALYST AT 22 °C.....</p>	<p>153 155 156 160 169 180 182 183</p>
APPENDIX C	<p>SUPPORTING INFORMATION FOR: A MONONUCLEAR ZEOLITE-SUPPORTED IRIDIUM CATALYST: KINETIC, SPECTROSCOPIC, ELECTRON MICROSCOPIC, SIZE SELECTIVE POISONING EVIDENCE FOR AN ATOMICALLY DISPERSED TRUE CATALYST AT 22 °C.....</p>	<p>189</p>

CHAPTER VII	<p>QUANTITATIVE 1,10-PHENANTHROLINE CATALYST POISONING KINETIC STUDIES OF Rh(0) NANOPARTICLE AND Rh₄ CLUSTER BENZENE HYDROGENATION CATALYSTS: ESTIMATES OF THE POISON $K_{\text{association}}$ BINDING CONSTANTS, OF THE EQUIVALENTS OF POISON BOUND AND OF THE NUMBER OF CATALYTICALLY ACTIVE SITES FOR EACH CATALYST.....</p>	204
	Overview.....	205
	Introduction.....	206
	Experimental.....	212
	Results and Discussion.....	214
	Conclusions.....	223
	Acknowledgments.....	225
	References.....	226
APPENDIX D	<p>SUPPORTING INFORMATION FOR: QUANTITATIVE 1,10-PHENANTHROLINE CATALYST POISONING KINETIC STUDIES OF Rh(0) NANOPARTICLE AND Rh₄ CLUSTER BENZENE HYDROGENATION CATALYSTS: ESTIMATES OF THE POISON $K_{\text{association}}$ BINDING CONSTANTS, OF THE EQUIVALENTS OF POISON BOUND AND OF THE NUMBER OF CATALYTICALLY ACTIVE SITES FOR EACH CATALYST.....</p>	232
CHAPTER VIII	<p>SUMMARY.....</p>	247
	References.....	250
APPENDIX E	<p>GENERAL STATEMENT ON “JOURNALS-FORMAT THESES”.....</p>	251

CHAPTER I

INTRODUCTION

The broad theme of this dissertation is the investigation of the true catalyst—that is, the actual catalytically active form or forms—for three different catalytic systems. This dissertation is written in the “journals-format” style (see Appendix A for a more detailed discussion of this type of dissertation). It is based on four separate publications/chapters written in the format set by the American Chemical Society, plus brief reviews of the pertinent literature. Consistency of this dissertation as a single document is achieved by (i) this introduction, (ii) brief reviews of the pertinent literature, (iii) the use of bridging paragraphs at the beginning of each chapter, and (iv) a final summary chapter. Detailed accounts of individual contributions of the authors of each paper/chapter to both the experimental and written aspects of this dissertation, are given at the beginning of each chapter. A concise overview of each chapter’s contents is presented below.

Chapter II is a brief literature review of the “who is the catalyst?” phenomena emphasizing the importance of the identification of the true catalyst which, often times, is challenging and requires multiple, complimentary methods since no single experiment can convincingly identify the true catalyst of any catalytic system.

Chapter III is a brief literature review of “ M_4 (M= transition metal) cluster catalysis”; an interesting, increasingly important and evolving area in chemical catalysis since M_4 sub-

nanometer clusters are poised between single-metal homogeneous and multiple-metal heterogeneous catalysts, offering their own, sometimes distinctive, catalytic properties.

Chapter IV is an investigation of the true catalyst in neat benzene hydrogenation beginning with commercially available $[\text{Ir}(\text{cod})\text{Cl}]_2$ (cod= 1,5-cyclooctadiene) at 22 °C and 40 psig initial H_2 pressure. The results allow identification of “weakly ligated/labile ligand” $\text{Ir}(\text{O})_n$ nanoparticles and their aggregates as the true catalyst via kinetics, transmission electron microscopy (TEM), control experiments employing similar iridium precatalysts (i.e., $[\text{Ir}(\text{cod})(\text{CH}_3\text{CN})_2][\text{X}]_2$ where X: PF_6 and BF_4 and Ir-black), plus CS_2 kinetic quantitative catalyst poisoning experiments.

Chapter V is an investigation of true catalyst for benzene hydrogenation beginning with commercially available $[\text{RhCp}^*\text{Cl}_2]_2$ (Cp^* = pentamethylcyclopentadienyl) at 100 °C and 50 atm initial H_2 pressure. In this case identification of ligated, on average $\text{Rh}_4\text{Cp}^*_{2.4}\text{Cl}_4\text{H}_c$ clusters as the true catalyst is detailed via a combination of *in operando* extended X-ray absorption fine structure (EXAFS) spectroscopy, kinetics and, crucial quantitative 1,10-phenanthroline catalyst-poisoning experiments.

Chapter VI provides kinetic, post-catalysis EXAFS spectroscopy, post-catalysis high-angle annular dark-field scanning transmission electron microscopy (HAADF-STEM), and again crucial quantitative and size-selective catalyst poisoning evidence for atomically dispersed mononuclear iridium species supported on zeolite Y as the true catalyst in cyclohexene hydrogenation beginning with well-defined $[\text{Ir}(\text{C}_2\text{H}_4)_2]/\text{zeolite Y}$ complex at 22 °C under 40 psig initial H_2 pressure.

Chapter VII is a more detailed analysis of the quantitative 1,10-phenanthroline catalyst poisoning results of Chapter V en route to estimating the equivalents of poison bound, the quantitative catalyst poisoning association constants, and the numbers of active sites for both

Rh(0)_n nanoparticles and Rh₄ cluster-based catalysts. In terms of new methodology that promises to have a broader impact on the “who is the catalyst?” problem, the catalyst poisoning phenomenon developed in this thesis and examined in greater depth in Chapter VII is that new methodology.

Chapter VIII presents a concise summary of the material presented in this dissertation.

CHAPTER II

A BRIEF REVIEW OF THE PROBLEM OF IDENTIFICATION OF THE TRUE CATALYST: WHAT IS THE BEST AND MOST EFFICIENT APPROACH?

Identification of the true catalytically active species for any and all catalytic reactions is a forefront, challenging and often perplexing topic in catalysis science.^{1,2,3,4,5,6,7,8,9} Key catalytic properties such as activity, selectivity, stability, and lifetime depend on the identity of the true catalyst; these key properties are inherently different for discrete metal complex homogeneous vs multiple metal heterogeneous catalysts [1].^{10,11,12} Hence, rational design of a new catalyst, or improvements of existing catalysts, first require the identification of the true catalyst of the system.

The literature in this area dates back to the 1980s and includes contributions from Maitlis and coworkers,¹³ Whitesides and coworkers,^{14,15} Crabtree and coworkers,^{16,17} Collman and coworkers,¹⁸ and Lewis and coworkers.^{19,20} These prior literature methods focused on tests such as filtration or poisoning to attempt to identify the true catalyst for a given system. Each method has its own limitations as detailed elsewhere.¹ More recently, an arsenal of experiments have been used to investigate the true catalyst, including transmission electron microscopy (TEM) as

[1] The modern definitions of homogeneous vs heterogeneous catalysts by Schwartz¹⁰ are used within this thesis rather than the classical definitions of the solubility of the catalyst (“homogeneous”) vs insolubility (“heterogeneous”) in the reaction solution. That is, homogeneous catalysts have single active sites whereas heterogeneous catalysts have multiple active sites.

well as X-ray absorption fine structure (XAFS) spectroscopy.²¹ The details of these methods, their limitations, and their advantages/disadvantages are briefly tabulated in Table 2.1.

Table 2.1. Critical analyses of the common literature methods to attempt to identify the true catalyst.

<i>Method</i>	<i>Description/Details</i>	<i>Disadvantages/Pitfalls</i>
<i>Reaction Kinetics</i>	<ul style="list-style-type: none"> • Catalysis is a “wholly kinetic phenomenon”²² and hence, reaction kinetics is crucial for identifying the true catalyst. • Reaction kinetics with induction periods (e.g., sigmoidal curves) that fit, for example, the $A \rightarrow B$, $A+B \rightarrow 2B$ 2-step mechanism²³ rule out the starting material, A, as the true catalyst. • Control kinetic experiments with the authentic form of the proposed true catalyst are also essential. 	<ul style="list-style-type: none"> • Reproducible kinetics previously was interpreted as evidence for homogeneous catalysis;²⁴ however, reproducible heterogeneous transition metal nanoparticle catalysis is now known.¹¹ • The absence of an induction period is not necessarily an indication of starting material being the true catalyst. An alternative hypothesis is that the true catalyst is formed immediately and obscuring the induction period.
<i>TEM</i>	<ul style="list-style-type: none"> • TEM is a commonly employed characterization technique for transition metal nanoparticles; controls examining the TEM of precursors, and the stability 	<ul style="list-style-type: none"> • TEM evidence for the presence of nanoparticles at the end of the reaction is not, by itself, evidence that those nanoparticles are the true catalyst. TEM

	<p>of the sample under the TEM beam, are essential, however.</p>	<p>is <i>only one</i> characterization technique.</p> <ul style="list-style-type: none"> • One needs to be aware of the instrumental limitations of TEM (such as beam damage²⁵); hence, all other complimentary physical characterization techniques should be employed to further support or refute the TEM results (such as XAFS, SEM, AFM, or XPS). • The reductive nature of the TEM beam can cause formation of nanoparticles from organometallic complexes.²⁶
<p><i>Qualitative Poisoning</i></p>	<ul style="list-style-type: none"> • Hg(0) amalgamation of metal surfaces has been known in the literature for almost a century²⁷ and has been widely used since then. • Poisoning of the catalyst via excess Hg(0) (≥ 300 equiv per metal) addition suggests an operating heterogeneous catalyst, while negative poisoning 	<ul style="list-style-type: none"> • Hg(0) poisoning by itself is not definitive and is not universally applicable. Poisoning experiments with other possible poison candidates—specifically quantitative poisoning experiments—should be employed whenever applicable to compliment Hg(0) poisoning studies.

	evidence is consistent with, but not proof of, a homogeneous catalyst.	<ul style="list-style-type: none"> • Adding excess Hg(0) (≥ 300 equiv per metal) when the catalyst evolution is complete, and good stirring, are keys to perform Hg(0) poisoning experiments correctly. In addition, the catalytic activity should be checked without decanting the added Hg(0). • Control experiments, poisoning authentic catalyst and precatalyst, are also needed.
<i>Quantitative Poisoning</i>	<ul style="list-style-type: none"> • Quantitative poisoning experiments are another set of kinetic-based experiments to test the nature and identity of the catalyst. • Ligands that poison the catalytically active sites of the metal in preference to the substrate are utilized for this purpose, such as (but not limited to), sulfur-, phosphorus-, and nitrogen-based ligands.²⁸ • The complete poisoning of the catalyst system upon 	<ul style="list-style-type: none"> • The dissociation energy of the poison from the catalyst should be considered in order not to misinterpret the result. For instance, at higher temperatures (usually above 50 °C), ligands such as CS₂ dissociate and can yield erroneous results.¹¹ • If a catalyst system has more than one possible forms of kinetically competent catalysts, the

	<p>the addition of $\ll 1.0$ equiv of poison ligand per total metal present strongly suggests the presence of a heterogeneous nanoparticle catalyst since only a fraction of a nanoparticles' surface area is available for catalysis.</p> <ul style="list-style-type: none"> • Complete poisoning of a homogeneous catalyst system is believed to often require >1.0 equiv of poison ligand per total metal present. 	<p>relative association constants of the poison to both forms is needed to interpret the results.²⁹</p> <ul style="list-style-type: none"> • The limitations of the used poison should be considered, such as difficult synthesis of dibenzo[<i>a,e</i>]cyclooctatetraene (dct).¹¹ • Control experiments with authentic catalyst and precatalyst are also needed.
<p><i>Reactivity Pattern</i></p>	<ul style="list-style-type: none"> • The fully formed catalyst should yield comparable—not slower—activity upon the addition of fresh substrate. • Using a reaction that can be catalyzed only by heterogeneous or homogeneous catalyst. • Historically, monocyclic arene—that is, benzene³⁰—hydrogenation was interpreted as an indication of a heterogeneous catalyst (i.e., due to the high 	<ul style="list-style-type: none"> • It is occasionally possible to find a reaction that can be catalyzed only by heterogeneous or homogeneous catalysts. • Not all heterogeneous catalysts are necessarily active for arene hydrogenation. • A few homogeneous arene hydrogenation catalysts are known.¹¹ • Smaller heterogeneous transition metal

	<p>resonance stabilization of benzene and, therefore, the relative difficulty of its reduction).¹</p> <ul style="list-style-type: none"> • Hydrogenation of polymer-bound substrates can be an indication of a homogeneous catalyst due lack of mobility of a heterogeneous catalysts in a polymer-matrix (at least in favorable cases where heterogeneous catalysts are >8 nm).³¹ 	<p>nanoparticles (i.e., <8 nm) can hydrogenate polymer-matrix bound substrates.³²</p>
<p><i>XAFS Spectroscopy</i>³³</p>	<ul style="list-style-type: none"> • A powerful characterization method—especially, when used <i>in operando</i> [2],³⁴—to obtain local, average structural information around the scattering metal atom. • Yields qualitative (to semi-quantitative³⁵) information about the metal oxidation state, the ligand environment and the covalency of the metal atom. 	<ul style="list-style-type: none"> • Beam damage due high energy X-rays can occur. Hence, control experiments may be required. • Rigorous structural information is available only if a good fit is observed between a known model structure (e.g., a single crystal XRD structure) and the experimental data. • Even a good fit might not be enough as noted elsewhere³⁶ by Gates and coworkers: “...(the

[2] *In operando* studies define any spectroscopic technique in which the catalyst is not only present in the reaction solvent at the operating temperature and pressure (i.e., in-situ), but also under the working conditions of the catalyst system.³⁴

	<ul style="list-style-type: none"> • Yields quantitative information about neighbor atom distances (up to 4-5 Å with ± 0.2 Å precision) and coordination numbers. 	<p>fitting procedure can) lead to more than one statistically valid and physically reasonable structural model.”³⁶</p> <ul style="list-style-type: none"> • Hence, the reliable use of XAFS spectroscopy requires at least one complimentary physical method³⁷ [3] and ideally several physical methods. • Requires the use of continuum (3-30 keV) synchrotron sources (10^{10} flux compared to 10^3 flux for an X-ray tube). • Requires the knowledge and experience with sophisticated software programs (e.g., Athena, IFEFFIT,³⁸ etc.) to fit the experimental data to known models.
--	---	--

[3] A nice example from the literature is the use of in situ XAFS, combined with in situ ^{11}B -NMR, to follow the evolution of $[\text{Rh}(\text{cod})\text{Cl}]_2$ (precatalyst) and to follow the progress of dehydrocoupling of dimethylaminoborane to give cyclic $((\text{CH}_3)_2\text{N}-\text{BH}_2)_2$ product. The results reveal that ca. 45% of the dehydrocoupling reaction is completed (via ^{11}B -NMR) upon the formation of soluble, on average Rh_{4-6} clusters (via XAFS).³⁷

<p><i>Filtration</i></p>	<ul style="list-style-type: none"> • The filtration test is basically the comparison of the catalyst activity of the filtrate vs the filtered solution. • The addition of fresh solvent, and repeating the catalytic reaction with both the filtrate and the filtered solution separately, can reveal where the true catalyst resides. 	<ul style="list-style-type: none"> • Filter papers, or filter aids, are not necessarily effective in filtering out the true catalyst. This can yield erroneous results, such as observing the catalytic activity in both phases. • The possible inability of the filter paper (i.e., with its large, micron-sized pores) in filtering out nanometer-sized metal particles is another possible pitfall. • The filtration procedure might decompose or otherwise change the true catalyst structure. • Control experiments with authentic catalyst and precatalyst are essential. • Cases where, both phases are active, or more than one active form of the catalyst exists, can be complicated to interpret correctly.
--------------------------	--	---

A common pitfall for many of the studies attempting to identifying the true catalyst in the literature is the use of only one (or two similar, rather than two complimentary) method(s) to identify the true catalyst. For example, the recovery of >98-99% of the starting material at the end of the reaction, and demonstrating the same or closely similar FT-IR spectrum for both the starting metal complex and the recovered material, is—commonly but erroneously— believed to be a strong indication that the starting material is the true catalyst.³⁹ Similarly, in the literature an ex-situ TEM image obtained at the end of the catalytic reaction showing the presence of nanoparticles is commonly believed to be enough evidence for nanoparticle catalysis!

However, and as emphasized elsewhere^{1,11,40,41} *no single experiment can convincingly determine the true nature of the catalyst*; rather, it is necessary to perform a series of experiments to arrive at a compelling conclusion (“the Finke strategy”³). In this context, a more general approach for distinguishing homogeneous vs heterogeneous catalysts was developed in 1994 by Finke and coworkers,⁴⁰ the so-called 4-prong method—that resulted in the discovery of polyoxoanion-stabilized Ir(0)_n nanoparticles.^{40,42} More recently, this approach has been updated to a “5-prong method” that emphasizes the importance of *in operando* spectroscopy,² Figure 2.1. Indeed, the 5-prong approach is in some sense the combination of all the methodologies outlined in Table 2.1. Briefly, this approach emphasizes the following:

- 1) *In operando* spectroscopy, for example *in operando* XAFS, to provide structural details by providing “motion pictures”³⁴ under working conditions (for details of *in operando* instrumentation and the list of *in operando* physical characterization tools for catalysis, see Table 1 elsewhere³⁴).
- 2) Catalyst isolation and characterization investigation to identify where, and in what form, the metal mass resides before and after the catalytic reaction. The results of this set of

experiments are solely “road-signs” possibly pointing toward the true catalyst, not necessarily the identity of the true catalyst, even if a large percentage (e.g., 98-99%) of the starting material is recovered at the end of the reaction, for instance. The use of physical characterization methods such as (but not limited to) XAFS, XRD, XPS, TEM, SEM, or AFM is the essence of this step. Then, a crucial and very important control experiment is the use of the authentic form of the proposed catalyst under the otherwise identical conditions, to compare the observed catalytic activity, selectivity, lifetime, and other catalytic properties.

- 3) Because catalysis is a “wholly kinetic phenomenon”,²² kinetic studies are the next step. One needs to establish the stoichiometry according to step-2 above and then design conclusive kinetic experiments to rule out the alternative hypotheses for the other possible form(s) of the catalyst. One important “tell-tale” sign is the observation of an induction period when the starting material has not been pretreated. That induction period rules out the hypothesis that the starting material is the true catalyst; instead, it is a *precatalyst* en route to the true catalyst. A control experiment involving the addition of fresh substrate to the fully evolved catalyst should catalyze the given reaction at a competent rate *without* any induction period. Note also that, when the (pre)catalyst is pretreated, then the absence of an induction period might not necessarily indicate that the starting material is the catalyst. An alternative hypothesis in this case is that the true catalyst is formed effectively immediately, without an observable induction period.
- 4) Quantitative phenomenological tests, emphasizing the use of poisoning experiments whenever applicable, are the next key tool in the quest to identify the true catalyst. The most common poisoning test to distinguish heterogeneous vs. homogeneous catalysts is the use of

Hg(0).^{1,11} The complete poisoning of the catalyst system upon the addition of excess (≥ 300 metal equiv) Hg(0) implies the presence of heterogeneous catalysts. However, and as detailed in Table 2.1, Hg(0) is not definitive by itself and is not universally applicable. Hence, quantitative poisoning experiments should be preferred over Hg(0) poisoning experiment since quantitative poisoning experiments can provide kinetic-based, often compelling evidence for the nature and the identity of the true catalyst, as well as to calculate the “real”, per active site corrected turnover frequency (the moles of product/(moles of *active sites* \times time)).⁴³ As a guideline for interpreting the results, the required equivalents of poisoning ligand per metal is often >1 for discrete metal complex homogeneous catalysts, but $\ll 1$ for multiple metal heterogeneous catalysts (e.g., ca. 0.10 in some of the studies that follow for a Rh(0)_n nanoparticle catalyst).

- 5) The last prong emphasizes that one should gather any other mechanistic information by any new, updated, or improved methodology that appears in the literature. Ultimately, one should keep in mind that the correct hypothesis for the true catalyst should explain all the results and should have a predictive value for future investigations.

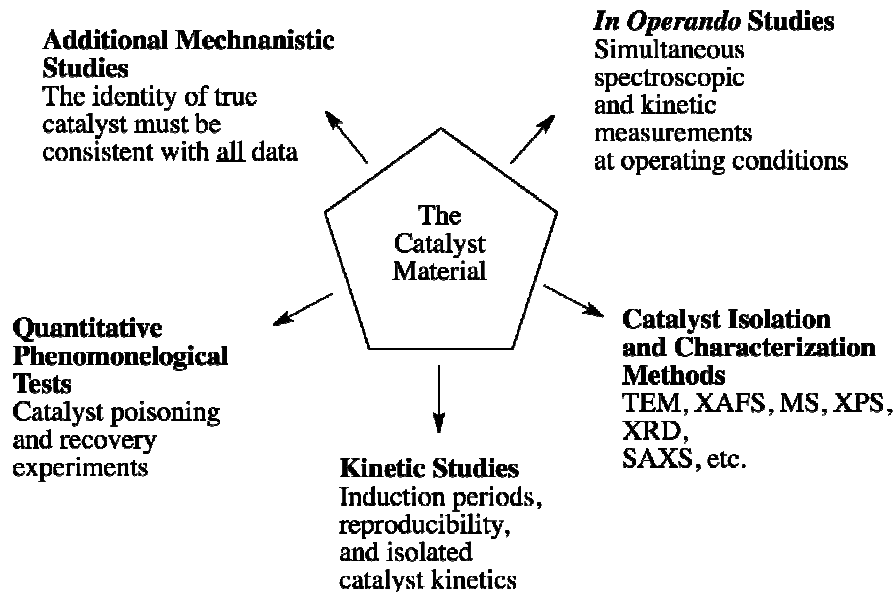


Figure 2.1. The updated “5-prong approach” for distinguishing homogeneous vs heterogeneous catalysts.² Reproduced with permission.

Even with the “5-prong approach”, the “identification of the true catalyst” problem is made even more intriguing, as well as compounded in complexity, by the recent findings that *sub-nanometer clusters*, such as M_4 species (M = metal), can be active catalysts.^{21,44,45,46,47,48} Sub-nanometer clusters lie between the discrete metal complex homogeneous catalysts and multiple metal, nanoparticle heterogeneous catalysts. Hence, and since they are important to the thesis work that follows, a concise summary of M_4 clusters follows in the next chapter.

Overall, then, and in conclusion:

- Identification of the true catalyst is important for any and all catalytic reactions—yet is often challenging in many if not most cases.
- No single experiment can convincingly determine the true identity of the catalyst; multiple, complimentary methods are a must.
- In this context, one should start the investigation to identify the true catalyst of a given system by: (i) performing *in operando*³⁴ studies to write the complete

stoichiometry for the catalyst evolution (to what form(s) the metal mass resides); (ii) performing kinetic experiments according to this proposed stoichiometry, since catalysis is a “wholly kinetic phenomenon”,²² and (iii) performing catalyst kinetic poisoning experiments. These three crucial investigations of the 5-prong method often are able to provide key evidence to answer the question “who is the true catalyst?” Indeed, the author of this thesis envisages that the 5-prong method, with emphasis on the above 3 steps, will become one indispensable part of “who is the true catalyst?” investigations. Time will tell.

REFERENCES

- ¹ Widegren, J.A.; Finke, R.G. *J. Mol. Catal. A: Chem.* **2003**, *191*, 187.
- ² Alley, W.M.; Kayiran, I.K.; Johnson, K.A.; Finke, R.G. *J. Mol. Catal. A: Chem.* **2010**, *315*, 1.
- ³ Crabtree, R.H. *Chem. Rev.* doi: dx.doi.org/10.1021/cr2002905.
- ⁴ Astruc, D.; Lu, F.; Aranzaes, J.R. *Angew. Chem. Int. Ed.* **2005**, *44*, 7852.
- ⁵ Phan, N.T.S.; van der Sluys, M.; Jones, C.W. *Adv. Synth. Catal.* **2006**, *348*, 609.
- ⁶ de Vries, J.G. *Dalton Trans.* **2006**, 421.
- ⁷ Dyson, P.J. *Dalton Trans.* **2003**, 2964.
- ⁸ Astruc, D. *Inorg. Chem.* **2007**, *46*, 1884.
- ⁹ Corma, A.; Garcia, H. *Top. Catal.* **2008**, *48*, 8.
- ¹⁰ Schwartz, J. *Acc. Chem. Res.* **1985**, *18*, 302.
- ¹¹ Widegren, J.A.; Finke, R.G. *J. Mol. Catal. A: Chem.* **2003**, *198*, 317.
- ¹² Bell, A.T. *Science* **2003**, *299*, 1688.
- ¹³ Hamlin, J.E.; Hirai, K.; Millan, A.; Maitlis, P.M. *J. Mol. Catal.* **1980**, *7*, 543.
- ¹⁴ Staudt, E.M.; Brown, D.W.; Moore, S.S.; Izumi, A.N.; Sowinski, A.F.; Lavalleye, J.P.P.M.; Brainard, R.L.; Hackett, M.; Whitesides, G.M. *Organometallics* **1985**, *4*, 1819.

- ¹⁵ Foley, P.; DiCosimo, R.; Whitesides, G.M. *J. Am. Chem. Soc.* **1980**, *102*, 6713.
- ¹⁶ Anton, D.R.; Crabtree, R.H. *Organometallics* **1983**, *2*, 855.
- ¹⁷ Mellea, M.F.; Mihelcic, J.M.; Quirk, J.M.; Crabtree, R.H. *J. Am. Chem. Soc.* **1982**, *104*, 107.
- ¹⁸ Kosydar, K.M.; Bressan, M.; Lamanna, W.; Garret, T.; Collman, J.P. *J. Am. Chem. Soc.* **1984**, *106*, 2569.
- ¹⁹ Lewis, L.N. *J. Am. Chem. Soc.* **1990**, *112*, 5998.
- ²⁰ Lewis, L.N.; Lewis, N. *J. Am. Chem. Soc.* **1986**, *108*, 7228.
- ²¹ Fulton, J.L.; Linehan, J.C.; Autrey, T.; Balasubramanian, M.; Chen, Y.; Szymczak, N.K. *J. Am. Chem. Soc.* **2007**, *129*, 11936.
- ²² (a) Halpern, J. *Inorg. Chim. Acta* **1981**, *50*, 11. (b) Landis, C.R.; Halpern, J. *J. Am. Chem. Soc.* **1987**, *109*, 1746.
- ²³ Watzky, M.A.; Finke, R.G. *J. Am. Chem. Soc.* **1997**, *119*, 10382. (b) Watzky, M.A.; Finke, R.G. *Chem. Mater.* **1997**, *9*, 3083. (c) Aiken, J.D. III; Finke, R.G. *J. Am. Chem. Soc.* **1998**, *120*, 9545. (d) Widegren, J.A.; Aiken, J.D. III; Özkar, S.; Finke, R.G. *Chem. Mater.* **2001**, *13*, 312.
- ²⁴ Laine, R.M. *J. Mol. Catal.* **1982**, *14*, 137.
- ²⁵ Egerton, R.F.; Li, P.; Malac, M. *Micron* **2004**, *35*, 399.
- ²⁶ Hagen, C.M.; Widegren, J.A.; Maitlis, P.M.; Finke, R.G. *J. Am. Chem. Soc.* **2005**, *127*, 4423.
- ²⁷ Paal, C.; Hartmann, W. *Chem. Ber.* **1918**, *51*, 711.
- ²⁸ Maxted, E.B. *Adv. Catal.* **1951**, *3*, 129.

- ²⁹ Bayram, E.; Finke, R.G. *submitted to ACS-Catalysis*.
- ³⁰ Bayram, E.; Zahmakıran, M.; Özkar, S.; Finke, R.G. *Langmuir* **2010**, *26*, 12455.
- ³¹ Collman, J.P.; Kosydar, K.M.; Bressan, M.; Lamanna, W.; Garrett, T. *J. Am. Chem. Soc.* **1984**, *106*, 2569.
- ³² Johnson, K.A. *Polymer Preprints* **2000**, *41*, 1525.
- ³³ Koningsberger, D.C.; Prins, R. (Eds.) *X-Ray Absorption: Principles, Applications, Techniques of EXAFS, SEXAFS and XANES*. John Wiley&Sons:New York, 1988.
- ³⁴ Tinnemans, S.J.; Mesu, J.G.; Kervinen, K.; Visser, T.; Nijhuis, T.A.; Beale, A.M.; Keller, D.E.; van der Eerden, A.M.J.; Weckhuysen, B.M. *Cat. Today* **2006**, *113*, 3.
- ³⁵ Rehr, J.J.; Ankudinov, A.L. *Coord. Chem. Rev.* **2005**, *249*, 131.
- ³⁶ Kulkarni, A.; Lobo-Lapidus, R.J.; Gates, B.C.; *Chem. Commun.* **2010**, *46*, 5997.
- ³⁷ Chen, Y.; Fulton, J.L.; Linehan, J.C.; Autrey, T. *J. Am. Chem. Soc.* **2005**, *127*, 3254.
- ³⁸ Newville, M.; Ravel, B.; Haskel, D.; Rehr, J.J. Stern, E.A.; Yacoby, Y. *Physica B* **1995**, *208/209*, 154.
- ³⁹ (a) Ohgomori, Y.; Mori, S.; Yoshida, S.-I.; Watanabe, Y. *J. Mol. Cat.* **1987**, *40*, 223. (b) Galletti, A.M.R.; Braca, G.; Sbrana, G. *J. Organomet. Chem.* **1988**, *356*, 221.
- ⁴⁰ Lin, Y.; Finke, R.G. *Inorg. Chem.* **1994**, *33*, 4891.
- ⁴¹ Gómez, M.; Favier, I. In *Metal Nanoclusters in Catalysis and Materials Science: The Issue of Size Control* Ch. 31 pp. 427-436. Eds. Corain, B.; Schmid, G.; Toshima, N. Elsevier 2008.

- ⁴² (a) Lin, Y.; Finke, R.G. *J. Am. Chem. Soc.* **1994**, *116*, 8335. (b) Aiken III, J.D.; Lin, Y.; Finke, R.G. *J. Mol. Cat. A: Chem.* **1996**, *114*, 29. (c) Weiner, H.; Trovarelli, A.; Finke, R.G. *J. Mol. Cat.* **2003**, *191*, 253. (d) Hornstein, B.J.; Finke, R.G. *Chem. Mater.* **2003**, *15*, 899.
- ⁴³ Hornstein, B.J.; Aiken, J.D. III; Finke, R.G. *Inorg. Chem.* **2002**, *41*, 1625.
- ⁴⁴ Bayram, E.; Linehan, J.C.; Fulton, J.L.; Roberts, J.A.S.; Szymczak, N.; Smurthwaite, T.D.; Özkar, S.; Balasubramanian, M.; Finke, R.G. *J. Am. Chem. Soc.* **2011**, *133*, 18889.
- ⁴⁵ Alley, W.M.; Kayiran, I.K.; Wang, Q.; Frenkel, A.I.; Li, L.; Yang, J.C.; Menard, L.D.; Nuzzo, R.G.; Özkar, S.; Johnson, K.A.; Finke, R.G. *Inorg. Chem.* **2010**, *49*, 8131.
- ⁴⁶ Alley, W.M.; Kayiran, I.K.; Wang, Q.; Frenkel, A.I.; Li, L.; Yang, J.C.; Menard, L.D.; Nuzzo, R.G.; Özkar, S.; Yih, K.-H.; Johnson, K.A.; Finke, R.G. *Langmuir* **2011**, *27*, 6279.
- ⁴⁷ (a) Uzun, A.; Gates, B.C. *Angew. Chem. Int. Ed.* **2008**, *47*, 9245. (b) Uzun, A.; Gates, B.C. *J. Am. Chem. Soc.* **2009**, *131*, 15887.
- ⁴⁸ Bayram, E.; Lu, J.; Aydin, C.; Uzun, A.; Browning, N.G.; Gates, B.C.; Finke, R.G. *to be submitted*.

CHAPTER III

A CONCISE REVIEW OF SUB-NANOMETER M_4 (M= TRANSITION-METAL) CLUSTERS IN CATALYSIS

Molecular metal clusters^{1,2} containing four metal atoms (e.g., tetrahedral M_4 clusters) are an interesting, increasingly important, and evolving area for catalysis since they are poised between mononuclear metal complexes and larger, $M(0)_n$ metal nanoparticles. Hence, they offer intermediate, or their own, distinctive catalytic properties in-between single-metal homogeneous and polymetallic-nanoparticle heterogeneous catalysis.³

Carbonyl/Hydride Tetrametallic Cluster Precatalysts/Catalysts

Tetrametallic clusters of different metals (e.g., Rh, Ir, Os, etc.) have been successfully synthesized, characterized,⁴ and used as precatalysts or catalysts for a range of applications, specifically for: hydrodesulfurization,⁵ hydroformylation,⁶ hydrosilylation,⁷ carbonylation,⁸ Fischer-Tropsch synthesis,⁹ and simple olefin hydrogenation.¹⁰ Table 3.1 summarizes 13 selected studies from the literature where: (i) a M_4 cluster is the starting material (i.e., at least a precatalyst), and where (ii) the authors propose a M_4 species as the true catalyst for the system via kinetic and other studies.

Table 3.1. Literature table of tetrametallic, M_4 clusters that have been employed as a precatalyst or a catalyst for a variety of catalytic reactions.

<i>Entry</i>	<i>Authors</i>	<i>Starting Tetrahedral Metal Cluster (Catalyst System)</i>	<i>Details</i>	<i>Reference</i>
1	Heil, B.; Markó, L.	$Rh_4(CO)_{12}$ (hydroformylation of <i>n</i> -heptene at 75 °C)	Claimed catalytically active species: $Rh_4(CO)_{12}$. The reaction is first-order with respect to $Rh_4(CO)_{12}$.	<i>Chem. Ber.</i> 1968 , <i>101</i> , 2209.
2	Heil, B.; Markó, L.	$Rh_4(CO)_{12}$ (hydrogenation of aldehydes at 160 °C)	Claimed catalytically active species: $HRh(CO)_3$. The reaction is $1/6$ order with respect to $Rh_6(CO)_{16}$.	<i>Act. Chim. Acad. Sci. Hung.</i> 1968 , <i>55</i> , 107.
3	Csontos, G.; Heil, B.; Markó, L.; Chini, P.	$Rh_4(CO)_{12}$ (hydroformylation of propylene at 23 °C)	Claimed catalytically active species: $(HRh(CO)_x)$. The reaction is first-order with respect to $Rh_4(CO)_{12}$, and H_2 -pressure. It is also inverse-first-order with respect to	<i>Hung. J. Ind. Chem.</i>

			<p>CO-pressure.</p> <p>The studied reaction was stoichiometric, not catalytic.</p> <p>Although the authors found that the reaction is first-order with respect to $\text{Rh}_4(\text{CO})_{12}$, the authors claim that the mononuclear rhodium hydride compound, $\text{HRh}(\text{CO})_x$, is the catalytically active species. The authors proposed a mechanism in which $\text{Rh}_4(\text{CO})_{12}$ is fragmented into mononuclear rhodium-carbonyl species and assign this step as the rate-determining step.</p>	<p>1974, 1, 53.</p>
4	Csontos, G.; Heil, B.; Markó, L.	$\text{Rh}_4(\text{CO})_{12}$ (hydroformylation of cyclohexene at 75 °C)	<p>Claimed catalytically active species: $\text{HRh}(\text{CO})_3$.</p> <p>The reaction is $\frac{1}{4}$ order with respect to $\text{Rh}_4(\text{CO})_{12}$.</p> <p>IR-spectroscopic investigation supports the presence of $\text{HRh}(\text{CO})_3$. The authors proposed a mechanism for the formation of the catalytically active species and for the catalytic cycle. The authors also propose olefin addition to the claimed mononuclear rhodium species (i.e., to</p>	<p><i>Ann. N. Y.</i> <i>Acad. Sci.</i> 1974, 239, 47.</p>

			HRh(CO) ₃) as the rate-determining step.	
5	Frediani, P.; Matteoli, U.; Bianchi, M.; Piacenti, F.; Menchi, G.	H ₄ Ru ₄ (CO) ₁₂ (Hydrogenation of cyclohexanone at 100 °C)	Claimed catalytically active species: H ₄ Ru ₄ (CO) ₁₂ . The reaction is first-order with respect to H ₄ Ru ₄ (CO) ₁₂ which was recovered unchanged (by IR) at the end of the reaction. However, the authors did not propose any alternative hypotheses; an IR-undetectable ruthenium species might be responsible for the observed catalysis, for example.	<i>J. Organomet. Chem.</i> 1978 , 150, 273.
6	Bradley, J.S.	[H ₄ Ru ₄ (CO) ₁₂] ²⁻ and [H ₃ Ru ₄ (CO) ₁₂] ³⁻ (Hydrogenation of CO to methanol at 268 °C)	Claimed catalytically active species: Ru(CO) ₅ . The reaction is first-order with respect to Ru(acac) ₃ . The IR spectrum in the 2000 cm ⁻¹ region revealed absorptions due only to Ru(CO) ₅ . An increase in the CO-pressure suppressed the catalytic activity. The authors observed only one ruthenium species (i.e., Ru(CO) ₅ when starting with [H ₄ Ru ₄ (CO) ₁₂] ²⁻ , [H ₃ Ru ₄ (CO) ₁₂] ³⁻ , or Ru(acac) ₃) via IR, and each exhibited similar activities.	<i>J. Am. Chem. Soc.</i> 1979 , 101, 7419.

			<p>The authors employed Ru(acac)₃ for their kinetic studies since it was more convenient. Although Ru(acac)₃ yields the same ruthenium species by IR, the detection limit of IR is probably limited to ca. ±10% and could miss minor species.</p>	
7	Doi, Y.; Koshizuka, K.; Keii, T.	<p>H₄Ru₄(CO)₁₂ (Hydrogenation of ethylene at 72 °C)</p>	<p>Claimed catalytically active species: H₄Ru₄(CO)₁₂. The reaction is first-order with respect to H₄Ru₄(CO)₁₂. Increasing CO-pressure decreased the rate of reaction; hence, the authors propose CO-dissociation and formation of the catalytically active species without either cluster fragmentation or higher cluster formation. H/D exchange, UV-vis measurements, and the kinetic order of each reactant yielded the same conclusion that H₄Ru₄(CO)₁₂ provides the catalytically active site. The kinetics were followed by syringing out aliquots of the gases above the reaction solution and analyzing them via GLC. Finally, a</p>	<p><i>Inorg. Chem.</i> 1982, <i>21</i>, 2732.</p>

			<p>mechanism was proposed which is consistent with all the observed data.</p> <p>This study appears to be an early, if not the first, complete kinetic study to provide not only kinetic data, but also a mechanism and a rate equation consistent with all the data.</p>	
8	Doi, Y.; Koshizuka, K.; Tamura, S.	$\text{H}_4\text{Ru}_4(\text{CO})_{12}$ (Hydrogenation of ethylene at 35 °C)	<p>Claimed catalytically active species: $\text{H}_4\text{Ru}_4(\text{CO})_{12}$.</p> <p>The reaction is first-order with respect to $\text{H}_4\text{Ru}_4(\text{CO})_{12}$.</p> <p>This study is the extension of the previous study of the same group (entry 7): The same ethylene hydrogenation catalytic reaction was examined, but was photoinduced rather than thermally induced at a lower temperature (72 °C vs 35 °C). A mechanism was proposed and a rate equation was derived consistent with the experimental results.</p>	<i>J. Mol. Cat.</i> 1983 , <i>19</i> , 213.
9	Sánchez-Delgado,	$[\text{H}_4\text{Os}_4(\text{CO})_{12}]$,	Claimed catalytically active species: fragmented, lower	<i>Inorg.</i>

	<p>R.A.; Andriollo, A.; Puga, J.; Martin, G.</p>	<p>$[\text{H}_2\text{Os}_4(\text{CO})_{12}(\text{I})]^-$, $[\text{H}_3\text{Os}_4(\text{CO})_{12}]^-$ (Hydrogenation of styrene at 140 °C)</p>	<p>nuclearity osmium species, such as $\text{Os}_{<4}$ species. Kinetics results yielded non-linear dependence on the total concentration of either $[\text{H}_2\text{Os}_4(\text{CO})_{12}(\text{I})]^-$ or $[\text{H}_3\text{Os}_4(\text{CO})_{12}]^-$ in independent investigations. After the catalytic run, the solution was filtered through celite which showed ~100% of the observed activity as seen in the first run beginning with the stated Os_4 clusters. When $\text{Hg}(0)$ was added to this solution, no poisoning was observed. However, $\text{Hg}(0)$ did not poison the filtrate, either. As a separate control experiment, metallic osmium was generated from $\text{OsCl}_2(\text{Me}_2\text{SO})_4$ which gave an activity less than 10% of the activity found for the osmium clusters' solution. However, the surface area of the $\text{Os}(0)_n$ nanoparticles was not established. Identical IR spectra before and after the reaction favors fragmentation of the starting Os_4 clusters with IR-undetectable, low</p>	<p><i>Chem.</i> 1987, 26, 1867.</p>
--	--	--	---	--

			concentrations of Os ₂ or Os ₁ species.	
10	Bhaduri, S.; Sharma, K.	H ₄ Ru ₄ (CO) ₈ (PBU ⁿ ₃) ₄ (Selective transfer hydrogenation of α,β-unsaturated aldehydes at 82 °C)	Claimed catalytically active species: H ₄ Ru ₄ (CO) ₈ (PBU ⁿ ₃) ₄ . The reaction is first-order with respect to H ₄ Ru ₄ (CO) ₈ (PBU ⁿ ₃) ₄ . Catalytic activity is inhibited by the addition of free phosphine or CO, indicating phosphine and CO dissociative equilibria. After the catalytic run, the starting Ru ₄ cluster, H ₄ Ru ₄ (CO) ₈ (PBU ⁿ ₃) ₄ , could be recovered “quantitatively” (although no quantitative value was reported) and reused; however, the activity in the 2 nd run was not reported.	<i>J. Chem. Soc. Chem. Commun.</i> 1988 , 173.
11	Rosas, N.; Màrquez, C.; Hernàndez, H.; Gómez, R.	Rh ₄ (CO) ₁₂ (Hydroformylation of cyclohexene at 125 °C)	Claimed catalytically active species: Rh ₄ (CO) ₁₂ . The reaction is first-order with respect to Rh ₄ (CO) ₁₂ . Color of the solution remained the same, pale-yellow during the reaction. Rh ₄ (CO) ₁₂ was recovered 92% spectrophotometrically and 88% gravimetrically. Also, identical IR spectra were obtained for the cluster before	<i>J. Mol. Cat.</i> 1988 , 48, 59.

			<p>and after the reaction. The authors proposed a catalytic cycle (including a cluster reorganization) consistent with all the data in which Rh₄ cluster is proposed as the catalyst.</p> <p>Although the evidence is solid, the alternative hypothesis of the formation of an IR-undetectable, low concentration of lower (or higher) nuclearity species was not, but should have been, considered, since only ~90% of the starting Rh₄(CO)₁₂ cluster was recovered.</p>	
12	Bhaduri, S.; Sharma, K.; Mukesh, D.	<p>[Ru₄H₄(CO)₈L₄] where L= PBuⁿ₃, P(OEt)₃, P(OMe)₃, PMe₃, PPh₃</p> <p>(Selective transfer hydrogenation of α,β-unsaturated aldehydes at 82.5 °C)</p>	<p>Claimed catalytically active species: [Ru₄H₄(CO)₈L₄] where L= PBuⁿ₃, P(OEt)₃, P(OMe)₃, PMe₃, or PPh₃.</p> <p>The reaction is first-order with respect to [Ru₄H₄(CO)₈L₄].</p> <p>At the end of catalytic reactions, the starting clusters were recovered “quantitatively” (no quantitative value was reported) by column chromatography. The authors provide evidence against a radical mechanism by showing</p>	<p><i>J. Chem. Soc. Dalton Trans.</i> 1992, 77.</p>

			that added 2,6-di- <i>tert</i> -butyl- <i>p</i> -cresol had no effect. This study is an extension of the previous study of the same group (entry 10).	
13	Adams, R.D.; Falloon, S.B.	Os ₄ (CO) ₁₁ (NCMe)(μ-H) ₄ (Cyclooligomerization of thietane)	<p>Claimed catalytically active species: Os₄(CO)₁₁(SCH₂CH₂CH₂)(μ-H)₄ and Os₄(CO)₁₁(1,5,9-trithiacyclododecane)(μ-H)₄.</p> <p>The reaction is first-order with respect to Os₄(CO)₁₁(NCMe)(μ-H)₄.</p> <p>The ¹H-NMR analysis of the residue yielded both claimed catalytically active species, Os₄(CO)₁₁(SCH₂CH₂CH₂)(μ-H)₄ and Os₄(CO)₁₁(1,5,9-trithiacyclododecane)(μ-H)₄.</p> <p>The authors claimed that the both species have almost identical activities, but failed to check this claim by examining the activities of Os₄(CO)₁₁(SCH₂CH₂CH₂)(μ-H)₄ and Os₄(CO)₁₁(1,5,9-trithiacyclododecane)(μ-H)₄ in separate experiments.</p>	<i>Organometallics</i> 1995 , <i>14</i> , 4594.

All the studies in Table 3.1 reported the reaction order with respect to the starting tetrametallic cluster. However, one common pitfall is the failure to disprove alternative hypotheses/alternative possible mechanisms (except, for example, entries 7, 9, and 12). Moreover, even when the reaction is first-order with respect to the starting M_4 cluster, it does not necessarily indicate that the starting material is the true catalyst. The alternative hypothesis is rate-determining cleavage to undetectable entities, such as—but not limited to—mononuclear species or nanoparticles upon the addition of substrate and solvent, and that one or more of those species are then the true catalyst. None of the studies in Table 3.1 reported the presence or absence of induction periods. Overall, and as stated in the previous chapter, *no single experiment can convincingly determine the true nature of the catalyst*; rather, it is necessary to perform a series of *complimentary* experiments to arrive at a compelling conclusion about the true catalyst.

All the studies employing stable metal-carbonyl/hydride M_4 clusters as the precatalyst or catalyst given in Table 3.1 were reported up to the late 1990s. However, more recently M_4 clusters with labile ligands (and often times, as $(M_4)^{n+}$, not $(M_4)^0$) have been suggested to be the true catalyst.^{11,12,13,14} Hence, a concise, critical analysis of those selected studies is provided next.

Other, Non-Carbonyl Tetrametallic Cluster Catalysts

Table 3.2 lists the recent studies where non-carbonyl M_4 clusters have been found to evolve during catalysis, followed by details and critical analysis of each system.

Table 3.2. List of recent studies where M_4 clusters have been found to evolve during catalysis.

<i>Entry</i>	<i>Authors</i>	<i>Catalyst System</i>	<i>Details</i>	<i>Reference</i>
1	Uzun, A.; Gates, B.C.	Solid-gas phase ethylene hydrogenation beginning with $[\text{Ir}(\text{C}_2\text{H}_4)_2]/\text{zeolite Y}$ at $80\text{ }^\circ\text{C}$. ¹¹	Formation of $\text{Ir}_4/\text{zeolite Y}$ as the proposed true ethylene hydrogenation catalyst via XAFS and IR spectroscopies. <i>Needed studies to verify or to refute the hypothesis for the true catalyst:</i> Kinetics starting with the $\text{Ir}_4/\text{zeolite Y}$, the full rate law of the reaction, and quantitative kinetic poisoning experiments.	<i>Angew. Chem. Int. Ed.</i> 2008 , <i>47</i> , 9245. <i>J. Am. Chem. Soc.</i> 2009 , <i>131</i> , 15887
2	Jaska, C.A.; Manners, I.	Amine-borane dehydrocoupling reaction beginning with $[\text{Rh}(1,5\text{-COD})\text{Cl}]_2$ at $25\text{ }^\circ\text{C}$. ^{12,17,21}	$\text{Rh}(0)_n$ nanoparticle catalysis is proposed based on TEM, UV-vis, kinetics, and $\text{Hg}(0)$ and quantitative kinetic poisoning experiments.	<i>J. Am. Chem. Soc.</i> 2004 , <i>126</i> , 9776.
	Linehan and coworkers		Rh_4 cluster catalysis is proposed based on <i>in operando</i> -XAFS and principal component analysis of the XAFS.	<i>J. Am. Chem. Soc.</i> 2007 , <i>129</i> , 11936
			<i>Needed studies to verify or to refute the hypothesis</i>	

			<i>for the true catalyst: Rate law of the reaction and quantitative kinetic poisoning experiments.</i>	
3	Finke and coworkers	Ziegler-type hydrogenation catalysts at 22 °C. ^{13,23,24,25}	The formation of Ir _{~4-15} clusters upon mixing the [(1,5-COD)Ir(μ-O ₂ C ₈ H ₁₅) ₂] pre-catalyst with AlEt ₃ before the cyclohexene hydrogenation: STEM, HR-TEM, XAFS, MALDI-MS, and kinetics.	<i>Inorg. Chem.</i> 2010 , 49, 8131
4	Finke and coworkers	Benzene hydrogenation reaction starting with [RhCp*Cl ₂] ₂ at 100 °C and 50 atm initial H ₂ pressure. ¹⁴	Ligated Rh ₄ clusters, with an average stoichiometry of Rh ₄ Cp* _{2.4} Cl ₄ H _c , catalysis via <i>in operando</i> -XAFS, kinetics, and quantitative kinetic poisoning experiments.	<i>J. Am. Chem. Soc.</i> 2011 , 133, 18889

Case Study 1. Formation of Ir₄/zeolite Y under Solid-Gas Phase Conditions as a Proposed Ethylene Hydrogenation Catalyst.

Supported Ir₄ clusters, such as Ir₄/zeolite, have been long known and employed as precatalysts or catalysts in the literature.^{15,16} Gates and coworkers have reported the formation of Ir₄/zeolite Y clusters, as the proposed true catalyst for solid-gas phase ethylene hydrogenations at 80 °C, via X-ray absorption fine structure (XAFS) and infrared (IR) spectroscopies when beginning with a well-defined [Ir(C₂H₄)₂]/zeolite Y complex.¹¹ Although physical characterization (via XAFS and IR) during the catalysis unequivocally identifies the formation of Ir₄ clusters as the only detectable species, the key kinetics and poisoning experiments required to identify the true catalyst are missing and thus one needed to verify, or refute, the Ir₄/zeolite Y catalysis hypothesis. Relevant collaborative studies with The Gates Group will be reported as part of this thesis, Chapter VII.

Case Study 2. The Amine-Borane Dehydrocoupling Catalysis Controversy: Rh(0)_n Nanoparticles or Rh₄ Clusters as the True Catalysts?

Manners and coworkers first reported¹⁷ amine-borane dehydrocoupling reactions starting with a [Rh(1,5-COD)Cl]₂ (1,5-COD= 1,5-cyclooctadiene) precatalyst at 25 °C. They proposed Rh(0)_n nanoparticles as the true catalyst of the system via the so-called 4-prong approach¹⁸ pioneered by our group and as outlined in the previous chapter. Specifically, (i) TEM investigation revealed the presence of Rh(0)_n nanoparticles when the dehydrocoupling reaction was over; (ii) UV-vis studies of the evolved catalyst showed a broad plasmon resonance signal similar to that of a well-defined Rh colloid; (iii) kinetics of H₂ formation via dehydrocoupling of amine-borane solution fits well to the 2-step mechanism,¹⁹ indicating the starting [Rh(1,5-COD)Cl]₂ complex is *not* the true catalyst but, instead, only a precatalyst; and (iv) consistent with (iii), the addition of fresh

amine-borane to the fully evolved catalyst yielded immediate dehydrocoupling activity without any induction period. In addition, (v) the catalyst is completely deactivated upon the addition of excess Hg(0); and (vi) 0.5 equiv of P(C₆H₅)₃ per equiv of total Rh addition substantially decrease the catalytic activity (by ~40% compared to without 0.5 equiv of P(C₆H₅)₃ addition, see Figure 4 elsewhere^{17b}). All these results are consistent with Rh(0)_n nanoparticles being the true catalyst.

However and in contrast, Linehan and coworkers reported *in operando*²⁰-XAFS spectroscopy of the aforementioned system revealing >98% of the soluble Rh mass during the catalysis is present as amine-borane-stabilized, Rh₄ subnanometer clusters.²¹ Principal component analysis (PCA) also confirmed that no more than 2% of a third component could possibly be present. Hence, an upper limit of <1-2% was placed on the possible amount of soluble Rh(0)_n present, if there is any.

Next, Linehan and coworkers also observed black precipitate formation during the reaction, which was shown to be linked Rh₄ clusters on the basis of the XAFS data. However, a dehydrocoupling reaction performed under O₂ led to the formation of bulk Rh(0)_n. This important result shows that *ex situ* analyses under O₂ hold the potential to yield very misleading results, at least for the rhodium catalyzed amine-borane dehydrocoupling reaction.

Linehan and coworkers concluded that the ligated Rh₄ clusters are the leading candidates for the true catalyst in the amine-borane dehydrocoupling reaction. Unfortunately, however, Linehan and coworkers reported *only* the evolution of the starting material, [Rh(1,5-COD)Cl]₂, into 98±2% Rh₄ clusters with unidentified <2% rhodium species which can be kinetically competent Rh(0)_n nanoparticles.¹⁴ In order to rule out the alternative hypothesis of XAFS undetectable, (<2%) but highly active rhodium species, one needs the rate law and quantitative kinetic poisoning experiments. Hence, the identity of the true catalyst in the amine-borane

dehydrocoupling reaction when beginning with $[\text{Rh}(1,5\text{-COD})\text{Cl}]_2$ became, and remains, controversial. Manners and coworkers still insist that the true catalyst is $\text{Rh}(0)_n$ nanoparticles²² while noting the lack of kinetic and other required work, vide supra, by Linehan and coworkers' report.^{12,21} Interestingly, the finding that only 0.5 equiv of $\text{P}(\text{C}_6\text{H}_5)_3$ per equiv of total Rh present poisons ~40% of the catalytic activity suggests that ≥ 1.25 equiv $\text{P}(\text{C}_6\text{H}_5)_3$ per equiv of total Rh present will be needed to fully poison the system. This, at present and tentatively, argues for a Rh_4 catalyst, especially given the results in Chapter V of this thesis. A collaborative Manners-Linehan-Finke groups study to complete the necessary poisoning and other studies, required to identify the true catalyst for this interesting and challenging system, has been agreed upon and is in progress.

Case Study 3. Evolution of Ir₄₋₁₅ Clusters from the Well-Defined $[(1,5\text{-COD})\text{Ir}(\mu\text{-O}_2\text{C}_8\text{H}_{15})]_2$ Precatalyst Plus AlEt_3 en route to $\text{Ir}(0)_{\sim 40-150}$ Ziegler Nanoclusters as the Most Active Catalyst.

Ziegler-type hydrogenation catalysts are formed from non-zerovalent group 8-10 transition metal precatalysts plus AlR_3 (R= alkyl) as the cocatalyst. Such catalyst recipes are used worldwide for industrial hydrogenation of styrenic block copolymers with a worldwide production of over 1.7×10^5 metric tons.²³ A critical review²³ of the Ziegler-type hydrogenation catalysts revealed that the nature and identity of the true Ziegler-type hydrogenation catalysts was lacking due to: (i) the multiple variables that these catalysts are sensitive to (such as metal-to-cocatalyst ratio, amount of water, and the order of addition), (ii) the employment of poorly defined transition-metal precursors, and (iii) the failure to use a state-of-the-art approach, such as the 5-prong method,²³ to identify the true catalyst.

Finke and coworkers approached the problem by first identifying and controlling the variables, vide supra, and synthesizing and characterizing the well-defined transition-metal complexes,

$[(1,5\text{-COD})\text{M}(\mu\text{-O}_2\text{C}_8\text{H}_{15})]_2$ where $\text{M} = \text{Ir}$ and Rh , as model Ziegler-hydrogenation precatalysts.²⁴ The results of an arsenal of different characterization techniques such as Z-contrast scanning transmission electron microscopy (STEM), high-resolution transmission electron microscopy (HR-TEM), XAFS spectroscopy, matrix assisted laser desorption ionization-mass spectroscopy (MALDI-MS) as well as cyclohexene hydrogenation kinetics and $\text{Hg}(0)$ poisoning experiments revealed that average of $\text{Ir}_{\sim 4-15}$ subnanometer clusters are formed first when $[(1,5\text{-COD})\text{Ir}(\mu\text{-O}_2\text{C}_8\text{H}_{15})]_2$ is mixed with AlEt_3 (i.e., before the hydrogenation reaction).¹³ However, post cyclohexene hydrogenation catalysis, average $\text{Ir}(0)_{\sim 40-150}$ “Ziegler nanoclusters” are formed and are most active, kinetically competent Ziegler-hydrogenation catalyst.¹³

The recent successful synthesis and complete characterization (via XRD, XAFS, MS, NMR, UV-vis, and IR) of previously unknown $[(1,5\text{-COD})\text{Ir}(\mu\text{-H})]_4$ complex has also been reported.²⁵ It is currently being used in The Finke Group to see what its catalysis is under Ziegler-type hydrogenation conditions with added AlEt_3 in hydrocarbon solvents.

Case Study 4. Solving the 30+ Years of Mystery: Identification of Rh_4 Clusters as the True Catalyst for Benzene Hydrogenation when Beginning with $[\text{RhCp}^\text{Cl}_2]_2$ at 100 °C and 50 atm Initial H_2 Pressure.*

The details of this study, as well as the previous investigations on the same system, are provided in Chapter V. The reader is therefore directed to Chapter V for those details.

Overall, then, and in conclusion:

- Subnanometer M_4 cluster catalysis is an evolving and increasingly important area, is of interest since M_4 clusters appear to be a meta-stable state poised between single metal homogeneous and nanoparticle heterogeneous catalysis.

- Importantly, the identification of subnanometer M_4 clusters as the true catalyst is challenging. The 5-prong approach outlined in the previous chapter needs to be utilized in this area, and will be done as part of this thesis.
- The identification of the true catalyst is important in all catalytic reactions, since all the important properties of a catalyst—the activity, selectivity, lifetime, recovery and regeneration, and poisoning behavior—depend on the nature of the true catalyst.

REFERENCES

- ¹ Johnson, B.F.G. *In Transition Metal Clusters*. Eds. Johnson, B.F.G. Wiley, Chichester, England, 1980, pp.2
- ² Muetterties, E.L. *Bull. Soc. Chim. Belg.* **1975**, *84*, 959.
- ³ Jahncke, M.; Süss-Fink, G. *In Catalysis by Di- and Polynuclear Metal Cluster Complexes*. Adams, R.D.; Cotton, F.A. Eds: Wiley-VCH: New York. 1998, pp.167.
- ⁴ See, for example; (a) Grunwaldt, J.-D.; Kappen, P.; Basini, L.; Clausen, B.S. *Catal. Lett.* **2002**, *78*, 13. (b) Stuntz, G.F.; Shapley, J.R.; Pierpont, C.G. *Inorg. Chem.* **1978**, *17*, 2596. (c) Kulzick, M.; Price, R.T.; Muetterties, E.L.; Day, V.W. *Organometallics* **1982**, *1*, 1256. (d) Day, V.W.; Day, R.O.; Kristoff, J.S.; Hirsekorn, F.J.; Muetterties, E.L. *J. Am. Chem. Soc.* **1975**, *97*, 2571. (e) Ryan, R.C.; Pittman, Jr. C.U.; O'Connor, J.P. *J. Am. Chem. Soc.* **1977**, *99*, 1986.
- ⁵ See, for example; Finocchiaro, S.; Salvini, A.; Frediani, P. *J. Organomet. Chem.* **1999**, *584*, 265.
- ⁶ See, for example; Moasser, B.; Gladfelter, W.L. *Inorg. Chim. Acta* **1996**, *242*, 125.
- ⁷ See, for example; Ingallina, P.; Donovan, R. J.; Clos, N.; Ojima, I. *Organometallics* **1990**, *9*, 3127.
- ⁸ See, for example; Yamazaki, H.; Hong, P.; Mise, T. *J. Org. Chem.* **1983**, *48*, 238.
- ⁹ See, for example; Demitras, G.C.; Muetterties, E.L. *J. Am. Chem. Soc.* **1977**, *99*, 2796.
- ¹⁰ See, for example; Fabrizi, G.; Bertozzi, S.; Pertici, P.; Lazzaroni, R.; *J. Mol. Cat.* **1990**, *58*, 75.

¹¹ (a) Uzun, A.; Gates, B. C. *Angew. Chem. Int. Ed.* **2008**, *47*, 9245. (b) Uzun, A.; Gates, B.C. *J. Am. Chem. Soc.* **2009**, *131*, 15887.

¹² (a) Chen, Y.; Fulton, J.L.; Autrey, T.; Linehan, J.C. *J. Am. Chem. Soc.* **2005**, *127*, 3254. (b) Szymczak, N.K.; Chen, Y.; Balasubramanian, M.; Autrey, T.; Fulton, J.L.; Linehan, J.C. *J. Am. Chem. Soc.* **2007**, *129*, 11936.

¹³ Alley, W.M.; Hamdemir, I.K.; Wang, Q.; Frenkel, A.I.; Li, L.; Yang, J.C.; Menard, L.D.; Nuzzo, R.G.; Özkar, S.; Johnson, K.A.; Finke, R.G. *Inorg. Chem.* **2010**, *49*, 8131.

¹⁴ Bayram, E.; Linehan, J.C.; Fulton, J.L.; Roberts, J.A.S.; Szymczak, N.K.; Smurthwaite, T.D.; Özkar, S.; Balasubramanian, M.; Finke, R.G. *J. Am. Chem. Soc.* **2011**, *133*, 18889.

¹⁵ Xu, Z.; Xiao, F.-S.; Purnell, S. K.; Alexeev, O.; Kawi, S.; Deutsch, S. E.; Gates, B.C. *Nature* **1994**, *372*, 346.

¹⁶ Alexeev, O.; Gates, B.C. *Top. Catal.* **2000**, *10*, 273.

¹⁷ (a) Jaska, C.A.; Temple, K.; Lough, A.J.; Manners, I. *J. Am. Chem. Soc.* **2003**, *125*, 9424. (b) Jaska, C.A.; Manners, I. *J. Am. Chem. Soc.* **2004**, *126*, 9776.

¹⁸ Lin, Y.; Finke, R.G. *Inorg. Chem.* **1994**, *33*, 4891.

¹⁹ Watzky, M.A.; Finke, R.G. *J. Am. Chem. Soc.* **1997**, *119*, 10382.

²⁰ *In operando* spectroscopy refers to any technique in which the catalyst is present in the reaction solvent at the operating temperature and pressure and also under the working conditions of the reactants and resultant products of that operating catalytic system: Tinnemans, S.J.; Mesu, J.G.; Kervinen, K.; Visser, T.; Nijhuis, T.A.; Beale, A.M.; Keller, D.E.; van der Eerden, A.M.J.; Weckhuysen, B.M. *Cat. Today* **2006**, *113*, 3.

²¹ Although the initial study¹² suggested an equilibrium between Rh₄ and Rh₆ clusters, and the true catalyst was suggested to be Rh₄₋₆ clusters, later *ab initio* molecular dynamics calculations^{21a} suggest that the equilibrium is actually between tetrahedral and butterfly

shaped Rh₄ clusters; see Figure 3 elsewhere.^{21a} (a) Rousseau, R.; Schenter, G.K.; Fulton, J.L.; Linehan, J.C.; Engelhard, M.H.; Autrey, T. *J. Am. Chem. Soc.* **2009**, *131*, 10516.

²² Staubitz, A.; Robertson, A.P.M.; Sloan, M.E.; Manners, I. *Chem. Rev.* **2010**, *110*, 4023.

²³ Alley, W.M.; Hamdemir, I.K.; Johnson, K.A.; Finke, R.G. *J. Mol. Catal. A: Chem* **2010**, *315*, 1.

²⁴ (a) Alley, W.M.; Girard, C.W.; Özkar, S.; Finke, R.G. *Inorg. Chem.* **2009**, *48*, 1114. (b) Yih, K.-H.; Alley, W.M.; Finke, R.G. *Organometallics* **2011**, *30*, 5068.

²⁵ Yih, K.-H.; Hamdemir, I.K.; Mondloch, J.E.; Bayram, E.; Özkar, S.; Vasic, R.; Frenkel, A.I.; Anderson, O.P.; Finke, R.G. *Inorg. Chem.* **2012**, *51*, 3186.

CHAPTER IV

IN SITU FORMED “WEAKLY LIGATED/LABILE LIGAND” Ir(0) NANOPARTICLES AND AGGREGATES AS CATALYSTS FOR THE COMPLETE HYDROGENATION OF NEAT BENZENE AT ROOM TEMPERATURE AND MILD PRESSURES

This dissertation chapter contains the manuscript of a paper published in *Langmuir* **2010**, *26*, 12455-12464 by co-authors (Zahmakıran, M.; Özkar, S.; Finke, R.G.). This chapter presents the identification of the “weakly ligated/labile ligand” Ir(0) nanoparticles and aggregates as the true catalyst for neat benzene hydrogenation at 22 °C and 40 psig initial H₂ pressure.

The experimental work was designed in consultation with Professor Richard G. Finke and performed by first author Ercan Bayram, except for the final section of the paper where Ir(0)_n nanoparticles were supported on zeolite Y to obtain a more stable and more active catalysts, syntheses performed by Mehmet Zahmakıran. The manuscript was produced via 14 versions with the rough drafts being written by Ercan Bayram (with the input by Mehmet Zahmakıran on his aforementioned part), and detailed editing by Professors Saim Özkar and Richard G. Finke.

Overview

“Weakly ligated/labile ligand” nanoparticles, that is nanoparticles where only weakly coordinated ligands plus the desired catalytic reactants are present, are of fundamental interest. Described herein is a catalyst system for benzene hydrogenation to cyclohexane consisting of “weakly ligated/labile ligand” Ir(0) nanoparticles and aggregates plus dry-HCl formed in-situ from commercially available [(1,5-COD)IrCl]₂ plus 40 ± 1 psig (~2.7 atm) H₂ at 22 ± 0.1 °C. Multiple control and other experiments reveal the following points: (i) that this catalyst system is quite active with a TOF (turnover frequency) of 25 h⁻¹ and TTO (total turnovers) of 5250; (ii) that the BF₄⁻ and PF₆⁻ iridium salt precursors, [(1,5-COD)Ir(CH₃CN)₂]BF₄ and [(1,5-COD)Ir(CH₃CN)₂]PF₆, yield inferior catalysts; (iii) that iridium-black with or without added, preformed HCl cannot achieve the TOF of 25 h⁻¹ of the in-situ formed Ir(0)/dry-HCl catalyst. However and importantly, CS₂ poisoning experiments yield the same activity per active iridium atom for both the Ir(0)/dry-HCl and Ir-black/no-HCl catalysts (12.5 h⁻¹ Ir⁻¹), but reveal that the *Ir(0)/dry-HCl system is 10-fold more dispersed compared to the Ir(0)-black catalyst*. The simple but important and key result is that “weakly ligated/labile ligand” Ir(0) nanoparticles and aggregates have been made in-situ as demonstrated by the fact that they have identical, per exposed Ir(0) activity within experimental error to Ir(0) black *and* that they have no possible ligands other than those desired for the catalysis (benzene and H₂) plus the at best poor ligand HCl. As expected, the in-situ catalyst is poorly stabilized, exhibiting only 60% of its initial activity in a second run of benzene hydrogenation and resulting in bulk metal precipitation. However, stabilization of the Ir(0) nanoparticles with a ca. 2-fold higher catalytic activity and somewhat longer lifetime for the complete hydrogenation of benzene was accomplished by supporting the Ir(0) nanoparticles onto zeolite-Y (TOF of 47 h⁻¹ and 8600 TTO under otherwise

identical conditions). Also reported is the interesting result that Cl^- (present as Proton SpongeTM H^+Cl^-) completely poisons benzene hydrogenation catalysis, but not the easier cyclohexene hydrogenation catalysis under otherwise the same conditions, results that suggest different active sites for these ostensibly related hydrogenation reaction. The results suggest that synthetic routes to “weakly ligated/labile ligand” nanoparticles exhibiting improved catalytic performance is an important goal worthy of additional effort.

Introduction

“Weakly ligated/labile ligand” nanoparticles^{1,2,3,4,5,6,7,8} are of interest to the nanoparticle catalysis community since their surfaces should be readily available for catalysis following only the dissociation of weakly coordinated ligands⁹ or solvent.^{3,10,11} In a previous publication,¹¹ we reported an easily prepared, highly active and selective “weakly ligated/labile ligand” nanoparticle catalyst system for neat-acetone hydrogenation consisting of iridium(0) plus dry-HCl formed in-situ from the H_2 reduction of commercially available 1,5-cyclooctadienechloroiridium(I) dimer, $[(1,5\text{-COD})\text{IrCl}]_2$. This Ir(0)/dry-HCl catalyst system is a superior catalyst for acetone hydrogenation at low temperature and pressure in terms of its activity (22 ± 0.1 °C and 40 ± 1 psig H_2 pressure with an estimated TOF of 1.9 s^{-1}), selectivity (95% 2-propanol, 5% diisopropyl ether), and total catalyst lifetime (16400 TTOs). These results suggested that it would be of interest to employ this easily formed, highly active Ir(0)/dry-HCl catalyst system for the solventless reduction of other challenging hydrogenations such as benzene hydrogenation.

The complete hydrogenation of aromatics is of interest^{12,13} for a number of reasons, including the growing demand for cleaner-burning, low-aromatic-content diesel fuels (that thereby minimize powerful carcinogens¹⁴ in diesel exhaust particles that contribute to asthma or nasal

allergies¹⁵). Benzene hydrogenation to cyclohexane is also important, cyclohexane being a key intermediate in the production of the nylon precursor adipic acid.¹⁶ However, benzene hydrogenation is notably difficult compared to simple olefin hydrogenation¹⁷ due to the loss of the resonance stabilization energy during benzene reduction and prior to the rate-determining transition state.¹⁸ Consequently, benzene hydrogenation has historically required higher temperatures and H₂ pressures (i.e., ≥ 100 °C and ~ 50 atm H₂).¹⁹ Confirming this, only 17 studies that we have been able to find report the complete hydrogenation of benzene to cyclohexane at temperatures ≤ 25 °C (*see* Table SI-A1 in Supporting Information).²⁰ Among those 17 studies, only 6 articles^{20b,c,f,j,o,q} report neat benzene hydrogenation, the conditions that will be employed herein. The reported neat-benzene hydrogenation catalyst systems also tend to involve multi-step, sometime laborious catalyst preparation procedures.

Hence, still of interest is the complete hydrogenation of neat benzene (i.e., solventless, green conditions²¹) via a highly active, long-lived, readily available catalyst that operates under mild conditions, (≤ 25 °C and ≤ 10 atm H₂ pressure). Also desirable is clear documentation of the catalyst turnover frequency and total turnover number, as well as determination of the important, but too infrequently measured, percentage of active catalyst sites via catalyst poisoning studies (e.g., with CS₂).¹⁸

Herein, we report that in-situ reduction of [(1,5-COD)IrCl]₂ under 40 ± 1 psig (~ 2.7 atm) initial H₂ pressure at 22 ± 0.1 °C forms Ir(0)/dry-HCl as highly active catalyst for neat-benzene hydrogenation with 100% conversion to cyclohexane. The in-situ co-production of dry-HCl is relevant to the catalytic activity as demonstrated by multiple control experiments such as i) scavenging in-situ formed H⁺ via Proton SpongeTM, and ii) comparing the catalytic activity of two other iridium precursors (i.e., [(1,5-COD)Ir(CH₃CN)₂]BF₄ and [(1,5-COD)Ir(CH₃CN)₂]PF₆)

under otherwise identical conditions. A comparison to iridium-black, employed as a benzene hydrogenation catalyst under otherwise identical conditions,²² reveals a 10-fold lower activity (TOF of 2.5 h⁻¹ for iridium-black vs 25 h⁻¹ for Ir(0)/dry-HCl), but CS₂ poisoning studies indicate that ca. 2% of total iridium atoms are catalytically active when starting with [(1,5-COD)IrCl]₂, but only 0.2% when starting with iridium-black (both assuming a 1:1 CS₂:Ir poisoning stoichiometry). Hence, the catalytic activity in each case is the same per exposed Ir(0)—results that also demonstrate the value of such active-site determination studies via quantitative poisoning experiments. The high activity and good lifetime, 25 ≤ TOF ≤ 1250 h⁻¹ and 5250 ≤ TTO ≤ 262 500, of the Ir(0)/dry-HCl catalyst system is consistent with the expected “weakly ligated/labile ligand” nature of the Ir(0) nanoparticles and aggregates where only the possible ligands are benzene, H₂ (i.e., and hydrides), and the weak to non-ligand HCl.

Experimental

Materials and General Considerations. All commercially obtained compounds were used as received unless indicated otherwise. Benzene (anhydrous, 99.8%), diethyl ether (≥99.9%), CH₂Cl₂ (anhydrous, ≥99.8%), Proton Sponge™ (1,8-bis(dimethylamino)naphthalene, 99%), and CS₂ (anhydrous, ≥99%) were purchased from Aldrich Chemicals and transferred into a Vacuum Atmosphere nitrogen atmosphere drybox. CD₂Cl₂ (Cambridge Isotope Laboratories) was purchased in 1 mL glass ampoules which were then transferred into the drybox where NMR sample preparations were performed. [(1,5-COD)IrCl]₂ and iridium-black (99.9%, 30-60 m²/gr) were purchased from Strem Chemicals. Sodium zeolite-Y (Na₅₆Y, Si/Al = 2.5) was purchased from Zeolyst Inc. and slurried with 0.1 M NaCl solution to remove cation defect sites, washed until free of chloride and calcined in dry oxygen at 500 °C for 12 h before use. Unless otherwise stated all studies were performed under oxygen- and moisture-free conditions using a Vacuum

Atmospheres N₂ drybox (always <5 ppm O₂, and typically <1 ppm O₂, as monitored by a Vacuum Atmospheres O₂ level monitor). ¹H-NMR spectra were taken on a Varian INOVA-300 instrument with 300.115 MHz for ¹H. Gas Chromatography (GC) measurements were performed using a Hewlett-Packard 5890 series II GC with an MSD 5970 B. The GC was equipped with a 30 m (0.25 mm i.d., 0,25 μm film thickness) Supelco SPB-1 column and with an ionizing voltage of 70 eV. The GC parameters were as follows: initial temperature, 50 °C; initial time, 3 min; solvent delay, 2 min; temperature ramp, 10 °C/min; final temperature, 270 °C; final time, 5 min; injector port temperature, 280 °C; detector temperature, 290 °C; injection volume, 0.2 μL. The iridium content of the Ir(0)/zeolite-Y sample was determined by ICP-OES analysis (Leeman-DRE) after each sample was completely dissolved in the mixture of HNO₃:HCl with a 1:3 ratio (theoretical Ir: 1%, found Ir: 1%). Powder X-ray diffraction (XRD) patterns of Ir(0)/zeolite-Y samples were recorded with Rigaku X-ray Diffractometer (Model, Miniflex) with Cu K (30 kV, 15 mA, λ = 1.54051 Å) radiation at room temperature.

Hydrogenation Apparatus. All the hydrogenation reactions were carried out on the previously described, custom-built pressurized hydrogenation apparatus which allows monitoring the H₂ pressure decrease accompanying hydrogenations (± 0.01 psig) via a computer interface (LabView ver. 8.2) in real-time.^{23,24,25} A Fischer-Porter (F-P) bottle was connected via its Swagelock TFE-sealed Quick Connects to a hydrogenation line and Omega D1512 10V A/D converter with RS-232 connection to a computer. The hydrogen (>99.5) was purchased from Airgas and scrubbed via a Trigon Moisture Trap and a Trigon Technologies Oxygen/Moisture Trap to remove O₂ and H₂O followed by a Trigon Technologies High Capacity Indicating Oxygen Trap.

Standard Conditions Procedure for the Complete Benzene Hydrogenation Experiments

Starting with [(1,5-COD)IrCl]₂. To start, 17.5 mg (0.052 mmol in iridium) of the [(1,5-COD)IrCl]₂ precatalyst was weighed in a 2 dram glass vial and then dissolved in 1.0 mL (11.2 mmol) of benzene added via a 5.0 mL gastight syringe; a clear, orange solution 52 mM in iridium resulted. The solution was then transferred via a disposable polyethylene pipette into a new 22 × 175 mm Pyrex culture tube containing a new 5/16 × 5/8 in. Teflon-coated stir bar. The culture tube was then sealed inside the F-P pressure bottle and brought outside the drybox. The F-P bottle was placed into a constant temperature circulating bath at 22 ± 0.1 °C, and attached via Swagelock TFE-sealed Quick-Connects to the hydrogenation line (which had already been evacuated for at least 30 min to remove any trace oxygen and water present, then refilled with purified H₂ at 40 ± 1 psig). Stirring was started (at 600 rpm) and the F-P bottle was then purged 15 times with hydrogen (15 s per purge) and t = 0 was started. When the hydrogen uptake ceased, the F-P bottle was disconnected from the hydrogenation line, remaining H₂ pressure was released, and transferred back into the drybox, where a 9 in. glass Pasteur pipette was used to withdraw a ca. 0.05 mL aliquot from the culture tube. This aliquot was then added to 1 mL of CD₂Cl₂ in an individual glass ampoule, mixed under agitation using the Pasteur pipette, and then transferred into an NMR sample tube which was subsequently brought out of the drybox after sealing for ¹H-NMR investigation. The NMR analysis showed the complete reduction of benzene (7.26 ppm, m) to cyclohexane (1.44 ppm, s). None of the partially hydrogenated benzene reduction product, cyclohexene, was observed.

X-Ray Photoelectron Spectroscopy (XPS) Analyses. At the end of the benzene hydrogenation reaction, the F-P bottle was vented and the solution was brought to dryness under vacuum to yield a gray solid. Some of that solid was then coated onto a XPS sample holder and

subsequently sealed in a desiccator under the N₂ atmosphere of the drybox. The desiccator-enclosed sample was then removed from the drybox for analysis via a Physical Electronics (PHI) Model 5800 XPS system equipped with a monochromator (Al K α source, $h\nu = 1486.8$ eV; system pressure $\leq 5 \times 10^{-9}$ Torr) and a hemispherical analyzer to detect the ejected photons; XPS analysis was accomplished with the expert assistance of Pat McCurdy at Central Instrument Facility of Colorado State University, Department of Chemistry. To minimize exposure of the sample to air, the desiccator was opened next to the instrument antechamber and the sample holder was mounted immediately followed by closing and evacuating the antechamber. The binding energies were compared to the literature values.²⁶

Transmission Electron Microscopy (TEM) Analyses. (i) Ir(0)/dry-HCl system: the final form of the hydrogenation reaction solution is not homogeneous; instead, a brown solution with black precipitate forms, so that the TEM images obtained as follows cannot be 100% representative of the whole medium. However, to obtain an idea about the particles present *in solution*, TEM samples were harvested after 4 h of a Standard Conditions benzene hydrogenation, and then at the end of this same reaction (i.e., after 8.7 ± 0.1 h). TEM samples were prepared as follows: the F-P bottle was detached from the hydrogenation line after 4 h of the reaction via its quick connects, vented, and brought back into the drybox. The solution was transferred with a disposable polyethylene pipette into a clean, 5 mL glass vial. TEM samples were prepared by dipping the SiO-TEM grid into the solution for 3 seconds. The F-P bottle was then resealed after transferring the solution back into the Pyrex culture tube in it, brought out of the drybox, reconnected to the line and pressurized to 40 ± 1 psig with H₂. At this point, collection of pressure versus time data was continued (ignoring the ~ 1 h gap required for the procedure). The same TEM preparation procedure was repeated at the end of the reaction, that is,

after 8.7 ± 0.1 h. The resultant TEM grids were then placed separately in a screw-capped glass vials, were sealed and then were shipped to Clemson University for TEM analysis via the expert assistance of Dr. JoAn Hudson and her staff. TEM images were obtained with a Hitachi H7000 instrument operating at 120 keV. (ii) Ir(0)/zeolite-Y system: when the otherwise Standard Conditions benzene hydrogenation reaction was complete (now after 4.7 ± 0.1 h for this faster catalyst), the F-P bottle was detached from the hydrogenation line via its quick connects, vented, and brought back into the drybox. The Pyrex culture tube inside F-P bottle was transferred into a schlenk tube and then brought to dryness under vacuum, yielding a gray solid. A small amount of the powdered sample was placed on a copper grid. Samples were examined at magnification between 100 and 400K by using JEM-2010F microscope (JEOL) operating at 200 keV.

Control Experiments of Benzene Hydrogenation Starting with [(1,5-COD)IrCl]₂ Plus 1.0 or 0.02 equiv of Proton Sponge™ per equiv of Ir. Two separate control experiments were performed starting with 17.5 mg (0.052 mmol in iridium) [(1,5-COD)IrCl]₂ in 1.0 mL (11.2 mmol) of benzene, but now plus 1.0 or 0.02 equiv of Proton Sponge™ (0.052 or 1.04×10^{-4} mmol, respectively) per equiv of iridium under the Standard Conditions of 22 ± 0.1 °C and 40 ± 1 psig initial H₂ pressure. The results are described in the Results and Discussion section.

Control Experiment of Cyclohexene Hydrogenation under Standard Conditions Starting with [(1,5-COD)IrCl]₂ in the presence of 1 equiv of Proton Sponge™ per equiv of Ir. A cyclohexene control hydrogenation experiment was performed starting with 17.5 mg (0.052 mmol in iridium) [(1,5-COD)IrCl]₂ in 1.0 mL (11.2 mmol) of benzene and 0.5 mL (4.9 mmol) cyclohexene plus 1 equiv of Proton Sponge™ (0.052 mmol) under the Standard Conditions of 22 ± 0.1 °C and 40 ± 1 psig initial H₂ pressure. The results are described in the Results and Discussion section.

Synthesis and Characterization of [(1,5-COD)Ir(CH₃CN)₂][X] (X: BF₄ and PF₆). These complexes were synthesized and characterized according to the literature procedure.²⁷ 2.02 g of [(1,5-COD)IrCl]₂ (3.01 mmol) was dissolved in 42 mL of CH₂Cl₂. Upon the addition of 10 mL of CH₃CN, the dark red solution turned bright yellow. Then, 6.01 mmol of AgX (where X represents BF₄ for [(1,5-COD)Ir(CH₃CN)₂]BF₄ and PF₆ for [(1,5-COD)Ir(CH₃CN)₂]PF₆) was added to precipitate AgCl. The obtained solution was filtered into 200 mL of diethyl ether; yellow microcrystals resulted of [(1,5-COD)Ir(CH₃CN)₂][X], where X: BF₄ or PF₆. The resultant solution was then filtered, washed with 2 × 10 mL diethyl ether, and dried under vacuum for 12 h (80% yield of [(1,5-COD)Ir(CH₃CN)₂]BF₄ as a yellow solid; 81% yield of [(1,5-COD)Ir(CH₃CN)₂]PF₆ as a yellow solid). ¹H-NMR data were compared to the literature²⁷ (in parentheses) to confirm the identity and purity of the complexes: 4.3 ppm, s (4.27 ppm, s); 2.5 ppm, s (2.53 ppm, s); 2.3 ppm, m (2.29 ppm, m); 1.8 ppm, m (1.78 ppm, m).

Control Experiments for Standard Conditions Benzene Hydrogenation Starting with [(1,5-COD)Ir(CH₃CN)₂]BF₄ and [(1,5-COD)Ir(CH₃CN)₂]PF₆. Two separate Standard Conditions benzene hydrogenation experiments were performed, but now using the two different iridium precursors [(1,5-COD)Ir(CH₃CN)₂]BF₄ and [(1,5-COD)Ir(CH₃CN)₂]PF₆ in place of [(1,5-COD)IrCl]₂. The results are described in the Results and Discussion section.

Control Experiments with Commercial Iridium-Black. Control experiments were performed by following the Standard Conditions, but now using commercial iridium-black in place of [(1,5-COD)IrCl]₂. The results are described in the Results and Discussion section.

Catalyst Lifetime Experiments. Catalyst lifetime experiments were performed by following the Standard Conditions for the Ir(0)/dry-HCl and for Ir(0)/zeolite-Y catalyst, but with (i) 1.2 mg (3.6 μmol in iridium) of [(1,5-COD)IrCl]₂ precursor in 3.0 mL (33.6 mmol) of benzene

corresponding to a maximum possible 9333 TTOs, and (ii) 1.75 mg (5.25 μmol in iridium) of [(1,5-COD)IrCl]₂ precursor and 48 mg zeolite-Y in 5.0 mL (56 mmol) of benzene corresponding to a maximum possible 10667 TTOs. The results are described in the Results and Discussion section.

CS₂ Poisoning Experiments. These experiments were each started as if they were a Standard Conditions benzene hydrogenation experiment. For each poisoning trial below (i.e., for each different equivs of CS₂ added), a fresh Standard Conditions benzene hydrogenation was started and allowed to proceed for 5 h while pressure versus time data were collected. The F-P bottle was then vented, taken into the drybox, opened, and the desired amount of CS₂ was added. After the addition of CS₂, the F-P bottle was resealed, brought out of the drybox, reconnected to the line and pressurized to 40 ± 1 psig with H₂. At this point, collection of pressure versus time data was continued (ignoring the ~ 1 h gap required for the procedure). For example, for the Ir(0)/dry-HCl system, 0.1 equiv CS₂ with respect to the total iridium present was added and found to poison the previous catalytic activity completely. In the next experiment, the amount of CS₂ added was lowered to 0.01 equiv; this in turn did not poison the catalyst completely. The third experiment employed 0.03 equiv of CS₂, and that did completely cease the catalytic activity. Hence, ca. 0.02 equiv of CS₂ was deemed sufficient to poison completely the catalytic activity.

Control Experiment for Benzene Hydrogenation Showing That Transferring to the Drybox, and Opening the F-P Bottle, and then Restarting the Reaction Does Not Cause a Detectable Loss of Activity. This experiment was performed to ensure that the loss of activity seen in the CS₂ poisoning experiment is due to the added CS₂, and not some other aspect of the necessary manipulations cited above in the CS₂ poisoning experiments. This control experiment was started as if it was a Standard Conditions benzene hydrogenation experiment. Pressure

versus time data were collected for 5 h. Then the F-P bottle was vented, taken into the drybox, and opened. The F-P bottle was then resealed, brought out of the drybox, reconnected to the line and pressurized to 40 ± 1 psig with H_2 . At this point, collection of pressure versus time data was continued (again ignoring the ~ 1 h gap required for the procedure). No detectable loss of activity due to the above transfer procedure was observed in this control experiment.

Catalyst Redispersibility Experiments. These experiments were each started as if they were Standard Conditions benzene hydrogenation experiment. After complete hydrogenation of benzene, the F-P bottle was vented and the solution was brought to dryness under vacuum to yield a gray solid for both the Ir(0)/dry-HCl and Ir(0)/zeolite-Y catalysts. In two separate experiments these gray residues were redispersed in 1.0 mL (11.2 mmol) of benzene, repressurized to 40 ± 1 psig with H_2 , purged 15 times (15 s per purge), and the collection of pressure versus time data was restarted. The results are described in the Results and Discussion section.

Curve-fitting trials of the Hydrogen Uptake Data. Curve-fitting trials for concentration vs time data to the previously established 2-step²⁸ or 4-step²⁹ nanoparticle and agglomerated nanoparticle formation mechanisms were performed using non-linear least squares fitting in Origin ver. 7.0 or MacKinetics, respectively.

Procedure for the Complete Hydrogenation of Neat Benzene Starting with [(1,5-COD)IrCl]₂ plus Zeolite-Y (Na₅₆Y, Si/Al: 2.5). In a 2 dram glass vial, 17.5 mg (0.052 mmol in iridium) of the precatalyst [(1,5-COD)IrCl]₂ was weighed and then dissolved in 1.0 mL (11.2 mmol) of benzene added via a 5.0 mL gastight syringe to yield a clear, orange solution; this solution was then transferred via a disposable polyethylene pipette into a new 22 × 175 mm Pyrex culture tube containing a new 5/16 × 5/8 in. Teflon-coated stir bar. Next, 480 mg zeolite-Y

(corresponding to 1.0 % wt Ir on zeolite-Y) was added into this solution and mixed for half an hour. Then, the hydrogenation experiment was performed in the same way as described previously in the section “Standard Conditions Procedure for the Complete Benzene Hydrogenation Experiments Starting with [(1,5-COD)IrCl]₂”.

Results and Discussion

Product Characterization and Balanced Stoichiometry for the Complete Hydrogenation of Benzene Starting with [(1,5-COD)IrCl]₂ as Precatalyst under Standard Conditions.

Figure 4.1 shows a typical benzene loss vs time plot for the complete hydrogenation of neat benzene (1.0 mL, 11.2 mmol) starting with the [(1,5-COD)IrCl]₂ (17.5 mg, 0.052 mmol Ir) precatalyst at 22 ± 0.1 °C and 40 ± 1 psig (~2.7 atm) initial H₂, what we will refer to as “Standard Conditions”. The initial orange color of the solution due to the [(1,5-COD)IrCl]₂ precatalyst darkens within 30 min of the initiation of the reaction by the addition of H₂ pressure, and that dark color remains throughout the entire reaction. Complete hydrogenation of benzene was achieved after 8.7 ± 0.1 h as indicated by the cessation of H₂ uptake and the production of cyclohexane (100%) as the sole product and confirmed by ¹H-NMR as detailed in the Experimental Section. This particular kinetic curve given in Figure 4.1 is not well fit by either our 2- or 4-step mechanisms of nanoparticle and agglomerated nanoparticle formation^{28,29} details of which are given in the Supporting Information for the interested reader (Figures SI-A1 and SI-A2).

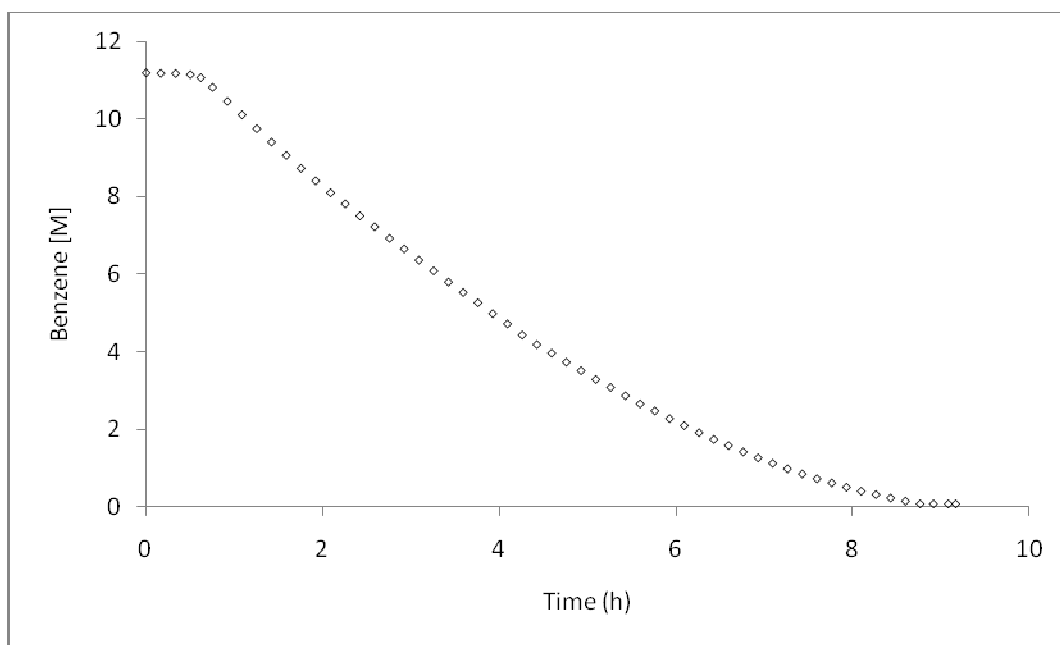


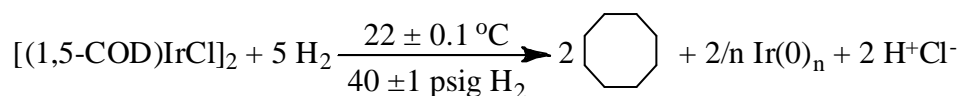
Figure 4.1. Typical benzene loss vs. time plot for the catalytic hydrogenation of benzene starting with 17.5 mg of [(1,5-COD)IrCl]₂ (0.052 mmol Ir) in 1.0 mL (11.2 mmol) benzene at 22 ± 0.1 °C with an initial H₂ pressure of 40 ± 1 psig (~2.7 atm). After an induction period of 0.7 ± 0.1 h, the hydrogenation starts with an initial rate of 2.0 ± 0.3 M benzene/h. Complete hydrogenation of benzene into cyclohexane was achieved in 8.7 ± 0.1 h as confirmed by ¹H-NMR analysis.

The balanced stoichiometry of the formation of Ir(0)/dry-HCl from [(1,5-COD)IrCl]₂ and concomitant benzene hydrogenation under Standard Conditions is given in Scheme 4.1: the reduction of 1 equiv of [(1,5-COD)IrCl]₂ requires 5 equiv of H₂ and produces 2/n equiv of Ir(0)_n plus 2 equiv of HCl by mass balance.^{24b} The evolution of 2 equiv of cyclooctane was confirmed by GC. The formation of Ir(0) was confirmed by XPS³⁰ on the vacuum-dried solid gray catalyst residue collected after the hydrogenation of benzene was complete (i.e., after 8.7 ± 0.1 h). The darkening of the solution within 30 mins following the addition of H₂ pressure is consistent with the formation of Ir(0) nanoparticles,³¹ and confirming evidence for those nanoparticles was obtained by ex-situ TEM, Figure 4.2. The TEM images were taken at two different, key stages of the reaction: after four hours of reaction, Figure 4.2(a), and at the end of the reaction (after 8.7

± 0.1 h), Figure 4.2(b). The close inspection of these images reveals smaller, average diameter <10 nm nanoparticles present after 4 h of reaction, but then larger, average diameter >20 nm, nanoparticles present at the end of the reaction—that is, that agglomeration of the Ir(0) nanoparticles to larger particles occurs as the reaction proceeds.

Scheme 4.1. Balanced stoichiometry for the formation of Ir(0)/dry-HCl from the precursor [(1,5-COD)IrCl]₂ and subsequent benzene hydrogenation under Standard Conditions.

Catalyst Formation



Neat Benzene Hydrogenation Catalysis

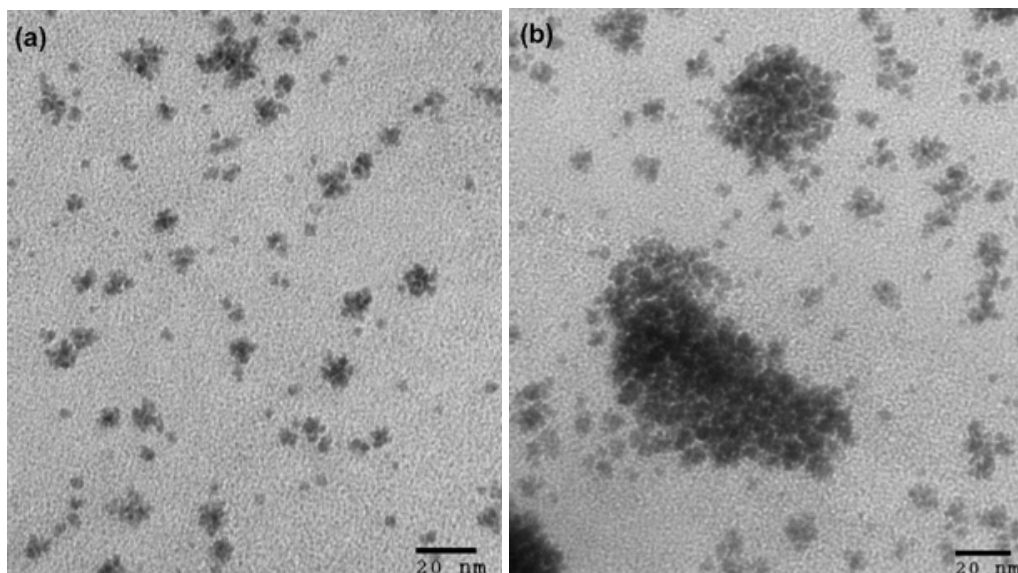
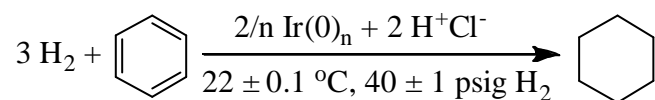


Figure 4.2. TEM images of the solution fraction of the heterogeneous reaction at different key stages of the reaction confirming the agglomeration of the Ir(0) nanoparticles in the solution fraction: (a) TEM image after 4 h of reaction exhibiting an average diameter <10 nm, and (b)

TEM image of the resultant, final solution once benzene hydrogenation is complete (after 8.7 ± 0.1 h) showing an increased average diameter of >20 nm.

Experiments Demonstrating the Requirement for the in-situ Formation of dry-HCl for the Observed Catalytic Activity. As mass balance requires and the balanced stoichiometry in Scheme 4.1 indicated, one equiv of HCl is produced in-situ per one equiv of Ir(I) reduced by H_2 .^{24b} Control experiments were done (vide infra) and reveal that the in-situ formation of dry-HCl is a required component of the observed, high catalytic activity reported herein. Specifically, 1.0 equiv of Proton SpongeTM (1,8-bis(dimethylamino)naphthalene)³² per equiv of iridium was added to an otherwise Standard Conditions benzene hydrogenation to learn the effects of removing the H^+ (Proton SpongeTM is a strongly basic, conjugate acid aqueous $pK_a = 12.3$, weakly coordinating, scavenger of H^+ that has been shown to be valuable in nanoparticle syntheses^{24b}). *No detectable hydrogen uptake* was observed in the presence of 1.0 equiv of Proton SpongeTM, even after more than 10 h. Immediate darkening of the initially orange reaction solution upon the application of hydrogen pressure indicates that Ir(0) nanoparticles were still formed,³¹ albeit ones significantly less catalytically active in the presence of the resultant 1.0 equiv Proton SpongeTM• H^+Cl^- that can serve as an iridium nanoparticle ligand, Scheme 4.2. As a further control to confirm that a (less active, more stable) nanoparticle catalyst is formed when 1.0 equiv Proton SpongeTM is added, the same experiment was repeated, except now with just one change: the much more easily reduced substrate, cyclohexene (0.5 mL), also added. H_2 uptake now occurred, but ceased right after the required stoichiometric amount of H_2 needed (~ 14 psig H_2) to convert (only) the cyclohexene into cyclohexane. No benzene hydrogenation was observed (1H -NMR was used to confirm that the initial amount of benzene still remained while the complete conversion of cyclohexene into cyclohexane had occurred).

This cyclohexene (only) hydrogenation curve is fit roughly ($R^2 = 0.997$) to the 2-step mechanism of nanoparticle nucleation and autocatalytic growth,²⁸ Figure 4.3. TEM investigation of the resultant product once the cyclohexene hydrogenation was complete reveals Ir(0) nanoparticles with >10 nm in diameter, Figure 4.4. The finding that Proton Sponge™•H⁺Cl⁻ poisons room temperature benzene reduction catalysis, but not cyclohexene hydrogenation catalysis, *is of some interest in its own right and is suggestive of either a different requirement for HCl in these two ostensibly related hydrogenation reactions or possible different active sites for these two reactions.*

Scheme 4.2. Stoichiometry for the experiment in which the H⁺ of HCl is scavenged via 1.0 equiv of Proton Sponge™ (PS™) to yield more stable, but less catalytically active, Ir(0) nanoparticles.

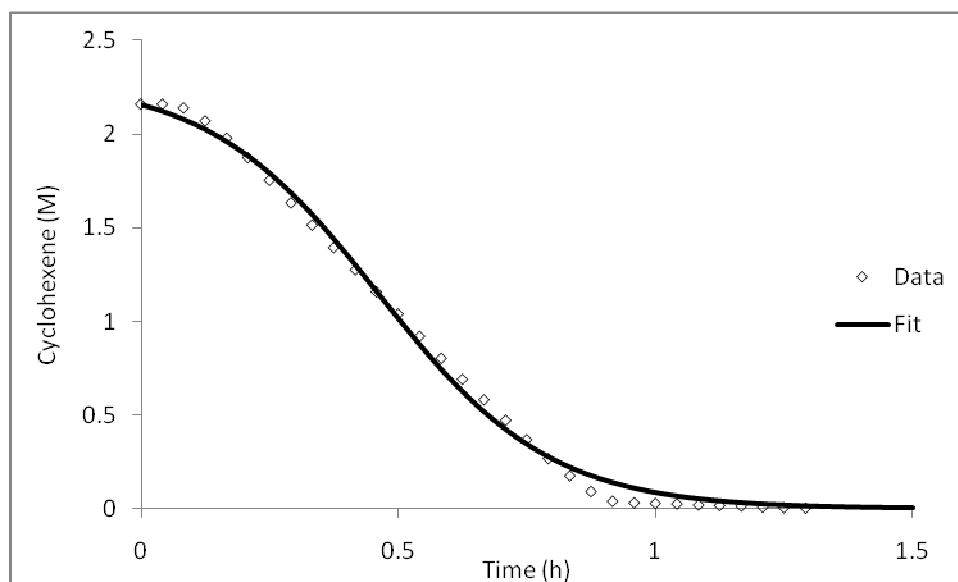
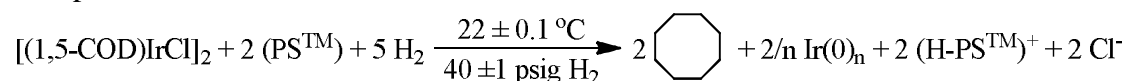


Figure 4.3. Cyclohexene hydrogenation curve (\diamond) and approximate fit to 2-step mechanism of nanoparticle formation²⁸ (—) obtained post the addition of 1.0 equiv of Proton Sponge™ plus 0.5 mL of cyclohexene under otherwise Standard Conditions. The fit is only approximate in this case

($R^2 = 0.997$), not unexpectedly since agglomerated nanoparticles and bulk metal are among the products. The resultant rate constants are $k_1 = 0.352 \text{ h}^{-1}$ and $k_{2corr} = 249 \text{ M}^{-1} \text{ h}^{-1}$ (k_2 being corrected as is proper by the stoichiometric factor of ~ 95 ; see elsewhere for the reasons for, and details of, this mathematically required correction factor when the evolution of the catalyst is being followed by the cyclohexene hydrogenation reporter reaction method²⁸).

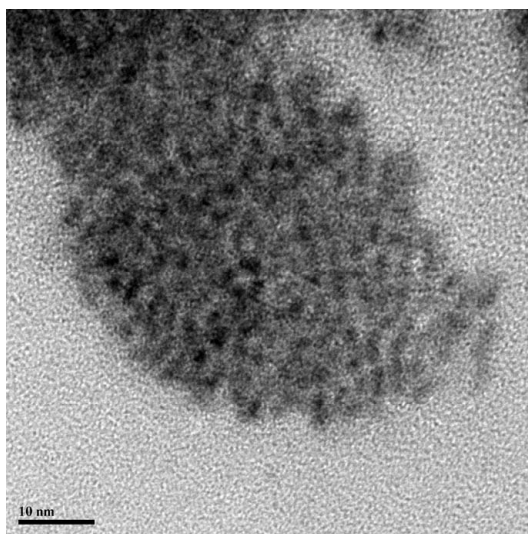


Figure 4.4. TEM image of the resultant nanoparticles after cyclohexene hydrogenation was completed. The presence of large Ir(0) nanoparticles with $>10 \text{ nm}$ in diameter indicates agglomerated nanoparticles and bulk metal are among the products.

In an attempt to see if more stable, yet still active iridium nanoparticles could be formed via the addition of <1.0 equiv Proton SpongeTM, the addition of 0.02 equiv was tried (the 0.02 equiv being picked since it matches the number of active iridium atoms found by CS_2 poisoning experiments, vide infra). Interestingly, even just 0.02 equivs of Proton SpongeTM poisons the activity, Figure 4.5.

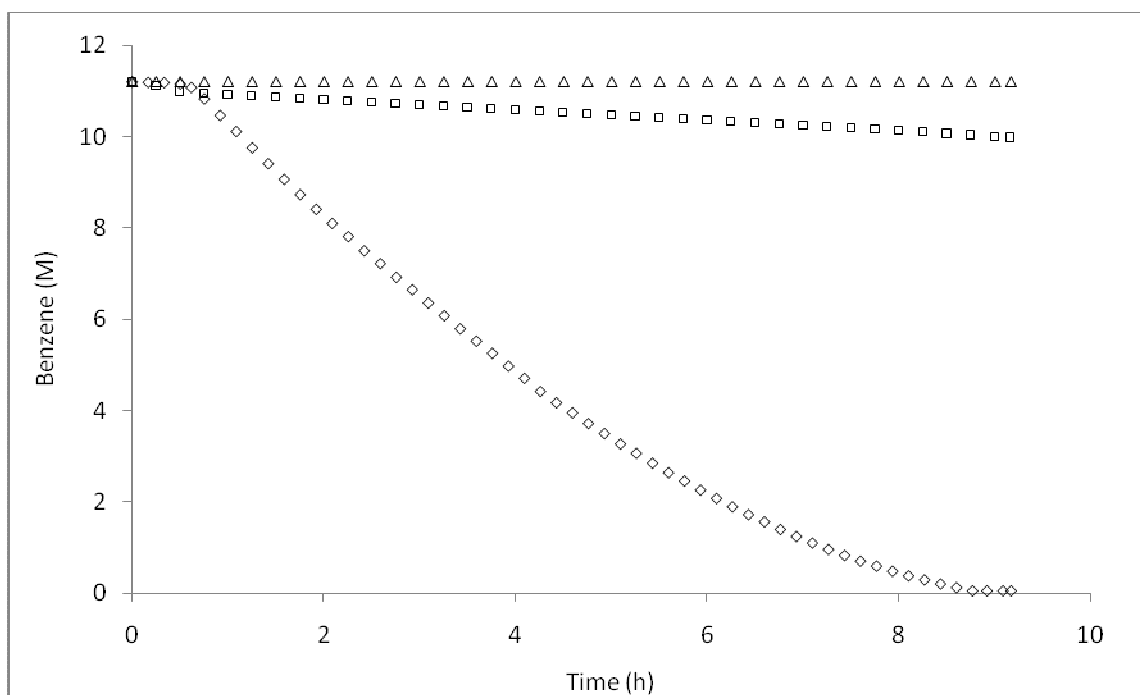


Figure 4.5. Standard Conditions complete benzene hydrogenation i) without (◇), ii) with 0.02 equiv (□), and iii) with 1.0 equiv (Δ) of Proton SpongeTM addition. Even just 0.02 equiv of Proton SpongeTM (~ 1.0 equiv per *active* iridium, vide infra) yields negligible activity in comparison to the experiment without Proton SpongeTM.

Very interestingly, however, replacing Cl⁻ by PF₆⁻ or BF₄⁻ does *not* yield a better catalyst as one might have guessed. Instead, these salts yield inferior, totally inactive systems. When the iridium precursors [(1,5-COD)Ir(CH₃CN)₂]PF₆ (that should yield HPF₆ under H₂) and [(1,5-COD)Ir(CH₃CN)₂]BF₄ (that should yield HBF₄ under H₂) were employed separately in an otherwise Standard Conditions benzene hydrogenation experiments (i.e., 0.052 mmol iridium concentration in 1.0 mL benzene at 22 ± 0.1 °C and initial H₂ pressure of 40 ± 1 psig), neither of the non-Cl⁻ containing, non-HCl generating precatalysts yielded *any catalytic activity* whatsoever, Figure 4.6. Both [(1,5-COD)Ir(CH₃CN)₂]PF₆ and [(1,5-COD)Ir(CH₃CN)₂]BF₄ do, however, yield black precipitates of bulk iridium metal after ~9 h along with a clear (and thus largely Ir(0) nanoparticle-plus aggregate-free) solution. The inactivity of catalysts formed from

the PF_6^- or BF_4^- salts of the iridium precursors is, however, not completely unexpected since we have previously seen that even these traditionally weakly coordinating anions PF_6^- and BF_4^- can coordinate well to at least Ir(0) nanoparticle surfaces.³ *The implication is that Cl binds H^+ in preference to the Ir(0) surface, while the opposite is true for BF_4^- and PF_6^- .*³³ *Restated, the Cl precursor is superior in yielding weakly ligated/labile ligand nanoparticles plus aggregates as benzene hydrogenation catalysts than are the PF_6^- and BF_4^- precatalysts.*

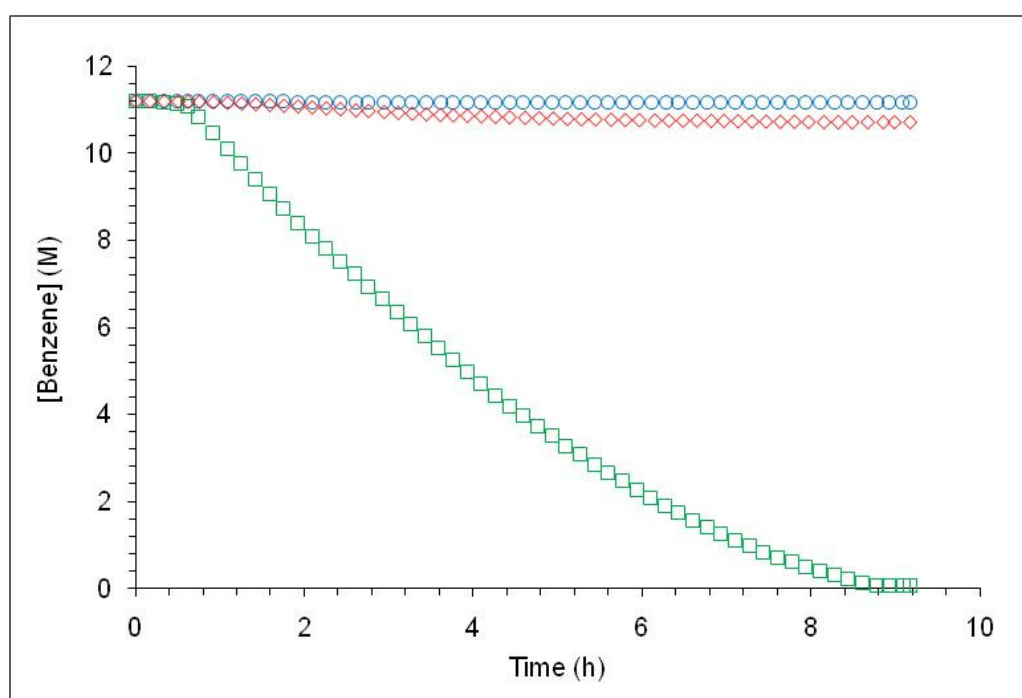


Figure 4.6. Comparison of hydrogenation activities of three different iridium precursors for complete benzene hydrogenation: $[(1,5\text{-COD})\text{IrCl}]_2$ (\square), $[(1,5\text{-COD})\text{Ir}(\text{CH}_3\text{CN})_2]\text{BF}_4$ (\circ), and $[(1,5\text{-COD})\text{Ir}(\text{CH}_3\text{CN})_2]\text{PF}_6$ (\diamond). Each experiment was performed under otherwise identical following conditions: 0.052 mmol iridium in 1.0 mL benzene (11.2 mmol) at 22 ± 0.1 °C and 40 ± 1 psig initial H_2 pressure. In the cases of the $[(1,5\text{-COD})\text{Ir}(\text{CH}_3\text{CN})_2]\text{BF}_4$ and $[(1,5\text{-COD})\text{Ir}(\text{CH}_3\text{CN})_2]\text{PF}_6$ precursors, catalytically inactive, poisoned bulk Ir(0) are observed.

Catalyst Lifetime Demonstration for Ir(0)/dry-HCl System in the Complete Hydrogenation of Benzene. A catalyst lifetime experiment reveals 5250 TTOs of complete

benzene hydrogenation over 320 h. The initial clear-yellow solution darkens as the iridium(0) nanoparticles are first generated, followed by the formation of a precipitate of bulk iridium(0) metal (via XPS³⁰) which becomes visible after a few hours, eventually yielding a clear, colorless (i.e., Ir(0) nanoparticle free) solution. The average TOF during the 320 h total catalyst lifetime, and 5250 TTOs, is 16.4 h^{-1} , before complete deactivation by aggregation into bulk metal occurs. The bulk Ir(0) metal product is of course the thermodynamic sink of the system, one readily formed here since there is little DLVO (Derjaguin-Landau-Verwey-Overbeek)³⁴ or other stabilization present for the initially formed Ir(0) nanoparticles, especially with Cl^- largely tied up as weakly to non-coordinating HCl.

Redispersibility of the Ir(0)/dry-HCl Catalyst System under Standard Conditions. Since aggregated Ir(0) is formed as catalysis proceeds, one would expect less than 100% catalytic activity in a second cycle/re-use of the in-situ formed Ir(0)/dry-HCl catalyst system. In addition, the volatile HCl should be lost in isolating the catalyst. As expected, only some (60%) of the previous initial catalytic activity is retained in a second, Standard Conditions benzene hydrogenation.

Control Experiments with Iridium-Black and CS_2 Poisoning Experiments Allowing the Comparison of the Activity per Exposed Ir(0) of the In-Situ Ir(0)/dry-HCl System. Iridium-black was examined as a neat-benzene hydrogenation catalyst and in the absence of HCl;²² an average TOF of 2.5 h^{-1} under otherwise Standard Conditions was seen, that is, 10-fold lower than the TOF of 25 h^{-1} for the in-situ Ir(0)/dry-HCl system, Table 4.1. CS_2 poisoning experiments³⁵ uncovered the primary source of the difference, ca. 0.02 equiv of CS_2 per iridium is sufficient to completely poison the benzene hydrogenation for the in-situ Ir(0)/dry-HCl system whereas only ca. 0.002 equiv of CS_2 is necessary for the Ir-black/no-HCl system. Hence, *the in-situ formation*

of the Ir(0)/dry-HCl system produced a 10-fold more dispersed catalyst, Table 4.1. As a simple control to check the CS₂ poisoning work, a Standard Conditions benzene hydrogenation with 10 times more iridium-black (i.e., using 0.520 mmol iridium vs 0.052 mmol iridium for Standard Conditions) was performed. As the above poisoning results predict, that experiment exhibited the same overall catalytic activity as the 0.052 mmol Ir(0)/dry-HCl system, showing an average turnover frequency of 25 h⁻¹, Table 4.1.

Table 4.1. Comparison of iridium catalysts' activity and percentage of active iridium atoms determined by CS₂ poisoning experiments under otherwise Standard Conditions.

<i>Catalyst System</i>	<i>Iridium (mmol)</i>	<i>Average Activity (TOF, h⁻¹)</i>	<i>Active Iridium Atom Percentage (%) via CS₂ Poisoning</i>	<i>Average Activity per Active Iridium Atom (h⁻¹Ir⁻¹)</i>
Ir(0)/dry-HCl	0.052	25	2	12.5
Iridium-black	0.052	2.5	0.2	12.5
Iridium-black	0.520	25	0.2	12.5

The CS₂ poisoning experiments, along with those using Proton SpongeTM and those with the HCl, HPF₆ and HBF₄ generating precatalyst salts above, reveal that the Ir(0)/dry-HCl catalyst system (i) provides a 10-fold more highly dispersed, weakly ligated/labile ligand nanoparticle plus aggregates catalyst, one where Cl⁻ is largely unavailable as a ligand for Ir(0) since it is tied up as HCl and where the only other ligands are benzene, H₂ and hydrides formed from H₂.

Two important findings here, then, are that: (a) Cl⁻ containing precursor systems that generate HCl in-situ are preferred, weakly ligated/labile ligand nanoparticle and aggregate catalyst systems; and (b) that the active catalyst that results is indistinguishable from surface Ir(0) of commercial iridium-black, except that it is formed in-situ in a 10-fold higher dispersion.

Catalyst Activity Comparison of Ir(0)/dry-HCl System with the Prior Highest Activity Catalysts. The CS₂ poisoning experiments allow a comparison of the catalytic activity to the prior best catalysts. Employing 1:1 CS₂:Ir poisoning stoichiometry assumption yields an estimated per-active site TOF of 1250 h⁻¹ and TTOs of 262 500 for the Ir(0)/dry-HCl catalyst system (The use of a 1:1 CS₂:Ir poisoning stoichiometry provides the most conservative, least favorable estimate as CS₂ is known to poison 7 or more active sites in some cases³¹). The highest TOF values previously reported for the complete hydrogenation of neat benzene at ≤25 °C and ≤10 atm are intrazeolite ruthenium(0) nanoparticles with a TOF (uncorrected for active sites) of 1040 h⁻¹ and TTOs (also uncorrected) of 2420.^{20o} The second most active catalyst system is that reported by Wai and coworkers with 1038 ≤ TOF ≤ 2414 h⁻¹,^{20q} Table 4.2. Hence and overall, the Ir(0)/dry-HCl catalyst system has comparable TOF and superior TTO values, without any need for laborious catalyst preparation steps, in comparison to the prior best two catalyst systems, Table 4.2.³⁶

Table 4.2. Comparison of the catalytic activity, lifetime and catalyst preparation steps for the present Ir(0)/dry-HCl catalyst system with the prior two best catalyst systems identified from an extensive literature search of benzene hydrogenation at room temperature or lower conditions (≤25 °C and ≤10 atm H₂ pressure). The complete table of the 17 prior, most relevant literature studies is provided in the Supporting Information for the interested reader, Table SI-A1.³⁶

<i>Authors</i>	<i>Catalyst System</i>	<i>Activity (TOF, h⁻¹)</i>	<i>Lifetime (TTO)</i>	<i>Catalyst Preparation Steps</i>	<i>Ref</i>
Özkar and coworkers ^(a)	Neat benzene at 22 °C and 2.7 atm H ₂	1040	2420	Ion exchange followed by borohydride reduction of Ru(III) to Ru(0) within the cages of zeolite	[20o]
Wai and coworkers	Neat benzene at 20 °C and 10 atm H ₂	1038 ≤ TOF ≤ 2414 ^(b)	Not reported	Sonochemical, synthesis of Rh nanoparticles on carbon nanotubes	[20q]

Finke and coworkers	Neat benzene at 22 °C and 40 psig (~2.7 atm) H ₂	$25 \leq \text{TOF} \leq 1250^{(c)}$	$5250 \leq \text{TTO} \leq 262500^{(c)}$	One-pot use of [(1,5-COD)IrCl] ₂ as a precatalyst	This study
---------------------	---	--------------------------------------	--	--	------------

^(a)The activity and lifetime values in this report is not corrected for the number of exposed surface atoms, that is, the values given are lower limits. ^(b)The lower limit TOF (of 1038 h⁻¹) was defined as the number of molecules reacted per unit weight of catalyst per unit time. The upper limit TOF of 2414 h⁻¹ was calculated from dispersion values evaluated from the mean size of Rh nanoparticles via TEM images.³⁷ ^(c)The TOF and TTO values reported herein are the lowest limit (i.e., considering all the iridium atoms are active catalysts) and then the estimated upper limit calculated from the CS₂ poisoning experiments and assuming a 1:1 CS₂:Ir poisoning stoichiometry; see the main text for details.

Supporting Ir(0) Nanoparticles on Zeolite-Y to Obtain More Stable and More Active Catalyst. The observed agglomerated Ir(0) nanoparticles and resultant bulk metal after extensive catalytic cycles make apparent the relatively low level of nanoparticle stabilization in these weakly ligated/labile ligand nanoparticles and aggregates. Restated, the weakness of weakly ligated/labile ligand nanoparticles in *solution-based* catalysis is just this, the lack of stabilization in solution of the nanoparticles. However, supporting the Ir(0) nanoparticles on microporous and macroporous materials (e.g., zeolite, Al₂O₃, TiO₂, etc.), then testing their activity and lifetime for benzene hydrogenation under the same mild temperature conditions, is expected to yield an improved catalyst lifetime.

To test this hypothesis, [(1,5-COD)IrCl]₂ plus zeolite-Y (Na₅₆Y, Si/Al: 2.5) was prepared in-situ as described in the Experimental Section. This precatalyst was then used for in-situ generation of the Ir(0)/HCl catalyst during neat-benzene hydrogenation to cyclohexane at 22 ± 0.1 °C and 40 ± 1 psig (~2.7 atm) initial H₂ pressure. The initial orange color of the suspension ([[(1,5-COD)IrCl]₂ plus zeolite-Y powders) darkens within 30 min of the initiation of the reaction with H₂ pressure; TEM analysis confirms the implied and expected formation of zeolite-supported Ir(0) nanoparticles, Figure 4.7. After an induction period of 0.3 ± 0.1 h, hydrogenation

starts with an initial rate of 2.6 ± 0.3 M benzene/h and the complete hydrogenation of benzene into cyclohexane (100%) is achieved after 4.7 ± 0.1 h as confirmed by $^1\text{H-NMR}$ analysis. Significantly, a smooth sigmoidal curve for the evolution of the catalyst and catalytic activity is now observed, along with an excellent ($R^2 = 0.999$) fit to the 2-step mechanism of nanoparticle formation,²⁸ Figure 4.8, with rate constants $k_1 = 0.081 \pm 0.002 \text{ h}^{-1}$ and $k_{2corr} = 22.8 \pm 0.5 \text{ M}^{-1} \text{ h}^{-1}$. The minimalistic nanoparticle formation kinetic scheme and the correspondent iridium/zeolite species are given in Scheme 4.3. The ability to follow in real time, even if indirectly, the formation of a supported heterogeneous catalyst in contact with solution is not trivial and of considerable interest by itself; hence such kinetics and mechanism of the formation of supported heterogeneous catalysts is being vigorously pursued in separate studies in our laboratories.³⁸

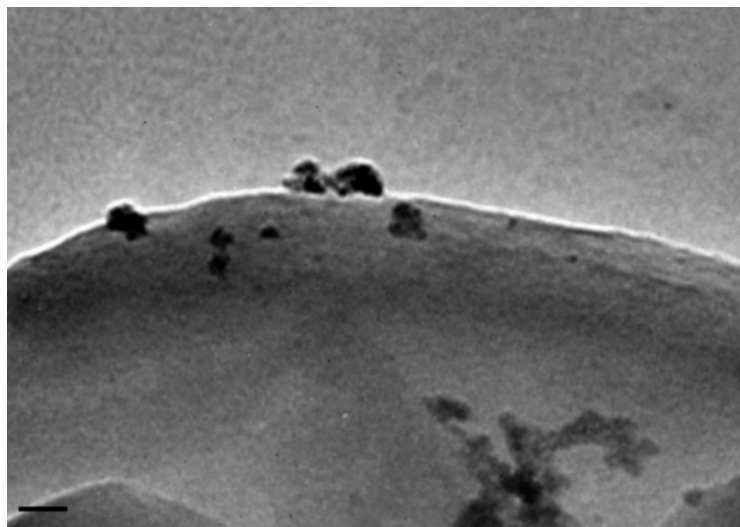


Figure 4.7. TEM image of zeolite-supported iridium(0) nanoparticles taken at the end of the hydrogenation of 1.0 mL neat benzene starting with 17.5 mg of $[(1,5\text{-COD})\text{IrCl}]_2$ precatalyst (0.052 mmol Ir) plus 480 mg zeolite-Y at 22 ± 0.1 °C with an initial H_2 pressure of 40 ± 1 psig (~ 2.7 atm). Scale bar corresponds to 25 nm.

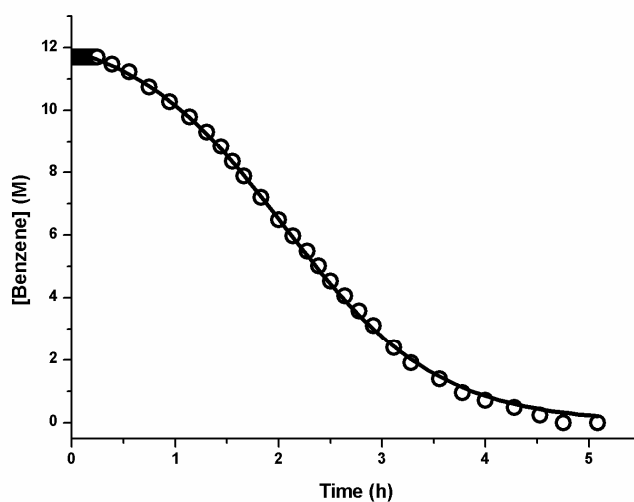
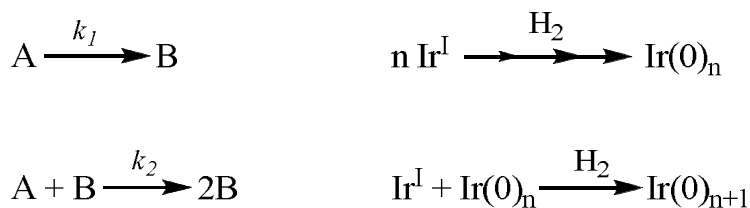


Figure 4.8. Data (\circ) and fit (—) for the catalytic hydrogenation of benzene starting with 17.5 mg [(1,5-COD)IrCl]₂ (0.052 mmol Ir) plus 480 mg zeolite-Y (Ir theoretical: 1%, Ir found: 1%) in 1.0 mL benzene at 22 ± 0.1 °C and 40 ± 1 psig (~ 2.7 atm) initial H₂ pressure. Following 0.3 ± 0.1 h of induction period, the hydrogenation rate increases in sigmoidal curve, which is well fit by the slow, continuous nucleation Ir(I) \rightarrow Ir(0) (rate constant, k_1), then autocatalytic surface growth, Ir(I) + Ir(0) \rightarrow 2 Ir(0) (rate constant, k_2). This observed sigmoidal curve fits well ($R^2 = 0.999$) to a 2-step nanoparticle formation mechanism²⁸ with rate constants $k_1 = 0.081 \pm 0.002$ h⁻¹ and $k_{2corr} = 22.8 \pm 0.5$ M⁻¹ h⁻¹.

Scheme 4.3. The minimalistic, 2-step nanoparticle nucleation then autocatalytic surface growth mechanism and its implied more detailed steps (right) for [(1,5-COD)IrCl]₂ precatalyst plus zeolite-Y (i.e., A below) system en route to the zeolite-Y supported Ir(0) nanoparticles (i.e., B below) under H₂.



The catalytic activity of the zeolite supported iridium(0) nanoparticles is increased almost 2-fold to a TOF of 47 h⁻¹ (vs 25 h⁻¹ for the unsupported Ir(0)/dry-HCl catalyst system), while the

TTO also increased some to 8600 TTOs over 232 h before deactivation (vs 5250 over 320 hrs for the unsupported Ir(0)/dry-HCl catalyst).

In a separate experiment, it was also shown that the vacuum-dried gray powder form of the resultant Ir(0)/zeolite-Y exhibited 89% of its initial activity in a second run of benzene hydrogenation.

Conclusions

The primary findings of the present work are:

- (i) That the “weakly ligated/labile ligand” nanoparticle plus aggregates concept has been explored in benzene hydrogenation starting with a [(1,5-COD)IrCl]₂ that evolves under H₂ to a Ir(0)/dry-HCl system that is quite active for the 100% reduction of neat benzene to cyclohexane at 22 ± 0.1 °C and 40 ± 1 psig (~2.7 atm) of initial H₂ pressure;
- (ii) That the CS₂-active site corrected, per Ir(0) benzene hydrogenation catalytic activity (TOF) and lifetime (TTOs) are at the high end of what has been observed at room temperature and mild pressures in comparison to the prior literature, 25 ≤ TOF ≤ 1250 h⁻¹ and 5250 ≤ TTO ≤ 262 500;
- (iii) That the 10-fold higher activity of the [(1,5-COD)IrCl]₂ plus H₂ system compared to Ir-black/no-HCl catalyst is due to the 10-fold higher dispersion of the in-situ formed Ir(0)/HCl catalyst. The number of active sites in this more highly dispersed catalyst is still just 0.02 equiv (2%) out of the total Ir present (and if one uses a 1:1 CS₂:Ir stoichiometry for the poisoning; the real number of active sites is possibly ≥7 fold higher³¹);

- (iv) That, significantly, what one can properly call weakly ligated/labile ligand Ir(0) nanoparticles and aggregates have been made in-situ as demonstrated by the fact that they have identical, per exposed Ir(0) activity within experimental error to Ir(0) black *and* that they have no possible ligands other than those desired for the catalysis plus the at best poor ligand HCl. Further consistent with the weakly ligated/labile ligand nanoparticle concept is that the iridium complexes [(1,5-COD)Ir(CH₃CN)₂]BF₄ and [(1,5-COD)Ir(CH₃CN)₂]PF₆, employed as precatalysts under otherwise identical conditions yield negligible benzene hydrogenation activity compared to the Cl⁻ containing, [(1,5-COD)IrCl]₂ precatalyst. The implication is that BF₄⁻ and PF₆⁻ prefer the Ir(0) surface rather than H⁺, where as Cl⁻ prefers H⁺ leading to a more active Ir(0) catalyst. That is, Cl⁻ is a preferred ligand over BF₄⁻ and PF₆⁻ in the presence of H⁺ for at least the present weakly ligated/labile ligand nanoparticle and aggregates catalysts.
- (v) That even 0.02 equivalents of Cl⁻ (Cl⁻ formed from the HCl plus Proton SpongeTM to give Proton SpongeTM•H⁺Cl⁻) poisons the room temperature benzene hydrogenation catalysis by the weakly ligated/labile ligand nanoparticles and their aggregates. Restated, H⁺ is a key component of the present, weakly ligated/labile ligand nanoparticles plus aggregates system.
- (vi) That the weakness of the weakly ligated/labile ligand nanoparticles, however, is their expected poor stabilization due to the lack of stabilizing ligands. Hence, aggregation and the formation of bulk metal, and a catalyst that yields only 60% of its initial activity in a second cycle benzene hydrogenation.
- (vii) That one can, however, generate the Ir(0)/dry-HCl catalyst in-situ from supported [(1,5-COD)IrCl]₂ on zeolite-Y. The resultant Ir(0) nanoparticles are more stable and

exhibit modest improvements in the catalyst activity (2-fold increase) and lifetime (1.6 fold increase) under otherwise identical conditions.

- (viii) That both Ir(0)/dry-HCl and Ir(0)/zeolite-Y catalyst systems are also relatively “green” in that they satisfy 9 out of 12 proposed principles of green chemistry.²¹ The Ir(0)/zeolite-Y heterogeneous catalyst is of course isolable, bottleable and reusable as is the case with other supported-nanoparticle heterogeneous catalysts, and finally
- (ix) That Proton SpongeTM•H⁺Cl⁻ poisons room temperature benzene, but not cyclohexene, catalysis is of interest and implies either a different requirement for H⁺ in these two, otherwise ostensibly related, types of hydrogenation reactions or, possibly, different active sites for these two hydrogenations.

This paper is our third exploring the weakly ligated/labile ligand nanoparticle catalysts hypothesis.^{3,11} Additional studies of this hypothesis are in progress and will be reported in due course.^{7,38}

Acknowledgments

This work was supported by the Department of Energy, Office of Basic Sciences, via DOE Grant SE-FG02-03ER15453. Partial support by Turkish Academy of Sciences (to S. Özkar) is also gratefully acknowledged.

Supporting Information Available. Literature table of 17 studies reporting the complete hydrogenation of benzene under room temperature conditions and mild pressures (≤ 25 °C and ≤ 10 atm H₂ pressure). Attempted fits of the kinetic data in Figure 4.1 to either a 2- or 4-step mechanisms of nanoparticle and agglomerated nanoparticle formation, plus brief discussion of the results. This material is available free of charge via the Internet at <http://pubs.acs.org>.

REFERENCES

¹ (a) The nomenclature “nanoparticle” is used herein rather than “nanocluster”. Although as Schmid and Fenske have noted there is at present no “sharp discrimination”^{1b} between these two terms, there is an evolving nomenclature where nanocluster is preferred when the composition and the structure of the species are precisely defined whereas nanoparticle is more appropriate when a size distribution is present.^{1b} However, reports exist where “nanoparticle” has been used to designate very precisely defined species.^{1c,d} (b) Schmid, G.; Fenske, D. *Phil. Trans. R. Soc. A* **2010**, *368*, 1207; (c) Jadzinsky, P.D.; Calero, G.; Ackerson, C.J.; Bushnell, D.A.; Kornberg, R.D. *Science* **2007**, *318*, 430; (d) Heaven, M.W.; Dass, A.; White, P.S.; Holt, K.M.; Murray, R.W. *J. Am. Chem. Soc.* **2008**, *130*, 3754.

² Ott, L.S.; Finke, R.G. *Coord. Chem. Rev.* **2007**, *251*, 1075; see especially sections 4.1 and 4.2 and references therein to the work of others on what we have termed the “weakly ligated/labile ligand” nanoparticles problem.

³ Ott, L.S.; Finke, R.G. *Inorg. Chem.* **2006**, *45*, 8382; see the references therein to putatively “solvent-only stabilized nanoparticles”. Also of interest is footnote 32 therein, reproduced here: “The ‘naked nanoparticle problem’, perhaps more accurately called the ‘ligand-labile nanoparticle problem’ is the need for efficient, high yield syntheses of metastable nanoparticles that have relatively easily removed ligands so that they can be used for low-temperature syntheses of novel heterogeneous catalysts or other applications of clean, ideally naked-surface nanoparticles.”

⁴ Korall, B.; Bönnehan, H. *Angew. Chem. Int. Ed.* **1992**, *31*, 1490.

⁵ More recently, Evanoff and coworkers^{5a} reported “essentially naked” Ag nanoparticles with a large H₂O solvation cage which encapsulates the Ag nanoparticles. In a later paper,^{5b} the stability of the Ag nanoparticles were attributed to electrostatic repulsion afforded by the low ionic strength solution (Ag⁺ and OH⁻). (a) Chumanov, G.; Evanoff, D.D. *J. Phys. Chem. B* **2004**, *108*, 13948. (b) Evanoff, D.D.; Chumanov, G. *Chem. Phys. Chem.* **2005**, *6*, 1221.

⁶ Raabe, I.; Krossing, I. *Angew. Chem. Int. Ed.* **2004**, *43*, 2066.

⁷ Mondloch, J.E.; Özkar, S.; Finke, R.G. *manuscript in preparation*. As part of this mini-review, a fuller survey of the literature related to “naked nanoparticles”, “solvent-only stabilized nanoparticles”,^{2,3} and “weakly ligated/labile ligand nanoparticles”³ is planned.

⁸ (a) Meisel and coworkers^{8b} find that a small amount of Ag⁺ is present on the surface of Ag nanoparticles, which in turn are negatively charged overall via adsorbed OH⁻ anions. (b) Merga, G.; Wilson, R.; Lynn, G.; Milosavljevic, B.H.; Meisel, D. *J. Phys. Chem. C* **2007**, *111*, 12220.

⁹ Strauss, S.H. *Chem. Rev.* **1993**, *93*, 927. Of interest here is the parallel between the development of the “weakly coordinating/labile ligand” nanocluster problem to the earlier “weakly coordinating anion” problem reviewed by S. H. Strauss.

¹⁰ Noteworthy here, however, is that even metal-alkane bond dissociation energies are $\sim 10 \pm 3$ kcal/mol, so that such putatively “naked” nanoparticles in even an alkane solvent would really be better labeled “weakly ligated/labile ligand” nanoparticles.^{10(a-c)} (a) Yang, G.K.; Peters, K.S.; Vaida, V. *Chem. Phys. Lett.* **1986**, *125*, 566. (b) Simon, J.D.; Xie, X. *J. Phys. Chem.* **1989**, *93*, 291. (c) Morse, J.M., Jr.; Parker, G.H.; Burkey, T.J. *Organometallics* **1989**, *8*, 2471.

¹¹ Özkar, S.; Finke, R.G. *J. Am. Chem. Soc.* **2005**, *127*, 4800.

¹² Widegren, J.A.; Finke, R. G. *Inorg. Chem.* **2002**, *41*, 1558.

¹³ Schulz, J.; Patin, H.; Roucoux, A. *Chem. Rev.* **2002**, *102*, 3757.

¹⁴ Enya, T.; Suzuki, H.; Watanabe, T.; Hirayama, T.; Hisamatsu, Y. *Environ. Sci. Technol.* **1997**, *31*, 2772.

¹⁵ (a) Casillas, A.M.; Hiura, T.; Li, N.; Nel, A.E. *Ann. Allergy, Asthma, Immunol.* **1999**, *83*, 624; (b) Nal, A.; Diaz-Sanchez, D.; Ng, D.; Hiura, T.; Saxon, A.J. *J. Allergy Clin. Immunol.* **1998**, *102*, 539.

¹⁶ Arpe, H.J.; Weissermel, K. *Industrial Organic Chemistry*, 4th Ed.; Wiley-VCH: New York, 2003.

¹⁷ (a) March, J. *Advanced Organic Chemistry: Reactions, Mechanisms, and Structure*, 4th Ed.; Wiley-Interscience: New York, 1992; (b) Fessenden, R.J.; Fessenden, J.S. *Organic Chemistry*, 5th Ed.; Brooks/Cole Publishing Company: Pacific Grove, 1993.

¹⁸ Widegren, J.A.; Finke, R.G. *J. Mol. Cat. A: Chemical* **2003**, *191*, 187.

¹⁹ Augustine, R.L. *Heterogeneous Catalysis for the Synthetic Chemistry*, Marcel Dekker: New York, 1996.

²⁰ (a) Januszkiewicz, K.R.; Alper, H. *Organometallics* **1983**, *2*, 1055; (b) Seeberger, M.H.; Jones, R.A. *J. Chem. Soc. Chem. Comm.* **1985**, *6*, 373; (c) Duan, Z.; Sylwester, A.P.; Hampden-Smith, M.J. *Chem. Mater.* **1992**, *4*, 1146; (d) Schulz, J.; Patin, H.; Roucoux, A. *Chem. Comm.* **1999**, 535; (e) Schulz, J.; Patin, H.; Roucoux, A. *Chem. Eur. Jour.* **2000**, *6*, 618; (f) Nicholas, J.P.; Ahn, H.; Marks, T.J. *J. Am. Chem. Soc.* **2003**, *125*, 4325; (g) Schulz, J.; Patin, H.; Roucoux, A. *Adv. Synth. Catal.* **2003**, *345*, 222; (h) Mevellec, V.; Ramirez, E.; Phillippot, K.; Chaudret, B.; Roucoux, A. *Adv. Synth. Catal.* **2004**, *346*, 72; (i) Park, I.S.; Kwon, M.S.; Kim, N.; Lee, J.S.; Kang, K.Y.; Park, J. *Chem. Comm.* **2005**, 5667; (j) Zhang, J.; Xie, Z.; Liu, Z.; Wu, W.; Han, B.; Huang, J.; Jiang, T. *Catalysis Letters* **2005**, *103*, 59; (k) Roucoux, A.; Phillippot, K.; Payen, E.; Granger, P.; Dujardin, C.; Nowicki, A.; Mevellec, V. *New J. Chem.* **2006**, *30*, 1214; (l) Nowicki, A.; Zhong, Y.; Leger, B.; Rolland, J. P.; Bricout, H.; Monflier, E.; Roucoux, A. *Chem. Comm.* **2006**, 296; (m) Nowicki, A.; Le Boulaire, V.; Roucoux, A. *Adv. Synth. Catal.* **2007**, *349*, 2326; (n) Park, I.S.; Kwon, M.S.; Lee, J.S.; Kang, K.Y.; Park, J. *Adv. Synth. Catal.* **2007**, *349*, 2039; (o) Zahmakıran, M.; Özkar, S. *Langmuir*, **2008**, *24*, 7065. (p) Hubert, C.; Denicourt-Nowicki, A.; Guégan, J.-P.; Roucoux, A. *Dalton Trans.* **2009**, 7356. (q) Pan, H.-B.; Wai, C.M. *J. Phys. Chem. C* **2009**, *113*, 19782.

²¹ Poliakoff, M.; Fitzpatrick, J.M.; Farren, T. R.; Anastas, P. T. *Science* **2002**, *297*, 807.

²² Attempts to mimic the in-situ Ir(0)/dry-HCl catalyst system, by employing iridium-black as the catalyst while adding preformed dry-HCl in benzene, failed. Specifically, independently prepared HCl(g), generated by reacting NaCl with H₂SO₄, was bubbled into 10 mL of fresh benzene (at ~20 °C and ~1 atm for ~30 mins) to obtain saturated benzene/dry-HCl stock solution (the solubility of HCl in benzene is 0.039 mol HCl per mol of benzene at 20 °C^{22a}). This stock solution was then diluted with fresh benzene to obtain the same amount of dry-HCl as is present when starting with [(1,5-COD)IrCl]₂, namely 0.052 mmol HCl was added to the Ir(0) black catalyst. However, due to the necessary experimental protocol involving flushing the apparatus with H₂ to begin the benzene hydrogenation reaction, the HCl was partially removed from the apparatus, resulting in irreproducible results with a TOF of 0 to ~10 h⁻¹. Hence, these experiments were abandoned. (a) Hydrogen Chloride. *Kirk-Othmer Encyclopedia of Chemical Technology*; Wiley & Sons: New York, 2004; Vol. 13, pp 808-837.

²³ Lin, Y.; Finke, R.G. *J. Am. Chem. Soc.* **1994**, *116*, 8335.

²⁴ (a) Özkar, S.; Finke, R.G. *J. Am. Chem. Soc.* **2002**, *124*, 5796; (b) Özkar, S.; Finke, R.G. *Langmuir* **2002**, *18*, 7653.

²⁵ Lin, Y.; Finke, R.G. *Inorg. Chem.* **1994**, *33*, 4891.

²⁶ Moulder, J.F.; Stickle, W.F.; Sobol, P.E.; Bomben, K.D. *Handbook of X-ray Photoelectron Spectroscopy*, Physical Electronics Inc.: Eden Prairie, MN, 1995.

²⁷ Day, V.W.; Klemperer, W.G.; Main, D.G. *Inorg. Chem.* **1990**, *29*, 2345.

²⁸ (a) Watzky, M.A.; Finke, R.G. *J. Am. Chem. Soc.* **1997**, *119*, 10382, and references therein; (b) Watzky, M.A.; Finke, R.G. *Chem. Mater.* **1997**, *9*, 3083; (c) Aiken III, J.D.; Finke, R.G. *J. Am. Chem. Soc.* **1998**, *120*, 9545 and references therein; (d). Widegren, J.A.; Aiken III, J.D.; Özkar, S.; Finke, R.G. *Chem. Mater.* **2001**, *13*, 312 and references therein.

²⁹ (a) Besson, C.; Finney, E.E.; Finke, R.G. *J. Am. Chem. Soc.* **2005**, *127*, 8179; (b) Besson, C.; Finney, E.E.; Finke, R.G. *Chem. Mater.* **2005**, *17*, 4925; (c) Finney, E. E.; Finke, R. G. *Chem. Mater.*, **2008**, *20*, 1956.

³⁰ The resultant XPS binding energies were compared to the literature²⁶ (in parentheses). The results confirm that the solid is Ir(0): 577 eV (4p_{1/2}, 578 eV), 494 eV (4p_{3/2}, 495 eV), 311 eV (4d_{3/2}, 312 eV), 298 eV (4d_{5/2}, 297 eV), 64 eV (4f_{5/2}, 64 eV), 61 eV (4f_{7/2}, 61 eV).

³¹ Widegren, J.A.; Finke, R.G. *J. Mol. Cat. A: Chemical* **2003**, *198*, 317.

³² Brzezinski, B.; Schroeder, G.; Grech, E.; Malarski, Z.; Sobczyk, L. *J. Mol. Soc. Perkin Trans.* **1991**, *2*, 1643.

³³ To determine any effect of CH₃CN (present in the other two iridium precursors along with BF₄ or PF₆) a control experiment was performed. Specifically, the addition of even 5 equivs (per iridium) of CH₃CN to a Standard Conditions benzene hydrogenation with [(1,5-COD)IrCl]₂ yielded the same catalytic activity within the experimental error as Standard Conditions benzene hydrogenation with [(1,5-COD)IrCl]₂. The implication is that it is not the CH₃CN, but rather the PF₆⁻ or BF₄⁻, that is the catalyst poison.

³⁴ DLVO theory^{34a} was developed to describe the stabilization of colloids in 1940s and relies on the Coulombic repulsion between anions and coordinatively unsaturated electrophilic surface of colloids. Further details of the theory, its application to transition metal nanoparticles stability, and implications of DLVO stabilization of nanoparticles are well reviewed for the interested reader.^{2,3,34b} (a) Verwey, E.J.W.; Overbeek, J.T.G. *Theory of the Stability of Lyophilic Colloids*, 2nd Ed.; Dover Publications: Mineola, New York, 1999; (b) Ott, L.S.; Cline, M.L.; Finke, R.G. *J. Nanosci. Nanotech.* **2007**, *7*, 2400.

³⁵ Hornstein, B.J.; Aiken, J.D.; Finke, R.G. *Inorg. Chem.* **2002**, *41*, 1625.

³⁶ (a) One of us (S.Ö.) wishes to point out that in a recent publication^{36b} some wording and information in Table S-1 of that publication^{36b} was adapted, inadvertently without proper referencing^{36b} to the present paper, from the literature search first done in 2007 as part of the present work and as summarized in Table SI-1 herein (i.e., and not the other way around, as it might appear since that *J. Am. Chem. Soc.* paper^{36b} appeared first). (b) Zahmakıran, M.; Tonbul, Y.; Özkar, S. *J. Am. Chem. Soc.* **2010**, *132*, 6541.

³⁷ Boudart, M. *Chem. Rev.* **1995**, *95*, 661.

³⁸ (a) Mondloch, J. E.; Yan, X.; Finke, R. G. *J. Am. Chem. Soc.* **2009**, *131*, 6389; (b) Mondloch, J.E.; Wang, Q.; Frenkel, A.I.; Finke, R.G. *J. Am. Chem. Soc.* **2010**, *132*, 9701.

APPENDIX-A

SUPPORTING INFORMATION FOR:

IN-SITU FORMED “WEAKLY LIGATED/LABILE LIGAND IRIDIUM(0)
NANOPARTICLES AND AGGREGATES AS CATALYSTS FOR THE COMPLETE
HYDROGENATION OF NEAT BENZENE AT ROOM TEMPERATURE AND MILD
PRESSURES

The Literature on the Complete Hydrogenation of Neat Benzene under Mild Conditions

(defined here as ≤ 25 °C and ≤ 10 atm H₂ pressure)

Table SI-A1. The top 17 catalysts in terms of the measurable shown in the table from a SciFinder search of “benzene hydrogenation” (>1900 citations) refined by “benzene hydrogenation at room temperature” (~90 hits), with those 17 studies arranged chronologically. Each study resulted in the complete reduction of benzene into (100%) cyclohexane.

Entry	Authors	Catalyst Precursor/ Catalyst	Conditions	TTO ^(a) (TOF) ^(b)	Ref
1	Alper and coworkers (1983)	[RhCl(1,5-hexadiene)] ₂	20 °C, 1 atm H ₂ pressure, biphasic (benzene/H ₂ O)	Not demonstrated	[1a]
2	Jones and coworkers (1985)	[Rh(COD)Cl] ₂	25 °C, 1 atm H ₂ pressure, monophasic (benzene)	Not demonstrated (16)	[1b]
3	Hamptden-Smith and coworkers (1992)	[Rh(COD)H] ₄	Room Temperature, H ₂ bubbling, monophasic (benzene)	Not demonstrated	[1c]
4	Roucoux and coworkers (1999)	RhCl ₃ •3H ₂ O	20 °C, 1 atm H ₂ pressure, biphasic (benzene/H ₂ O)	Not demonstrated (19) ^(c)	[1d]
5	Roucoux and coworkers (2000)	RhCl ₃ •3H ₂ O	20 °C, 1 atm H ₂ pressure, biphasic (benzene/H ₂ O)	Not demonstrated (30) ^(c)	[1e]
6	Marks and coworkers (2003)	[(Cp*)Zr(CH ₃) ₂] on sulfated alumina	25 °C, 1 atm H ₂ pressure, monophasic (benzene)	Not demonstrated (960)	[1f]
7	Roucoux and coworkers (2003)	RhCl ₃ •3H ₂ O	20 °C, 1 atm H ₂ pressure, biphasic (benzene/H ₂ O)	100 (28) ^(c)	[1g]
8	Chaudret and coworkers (2004)	IrCl ₃	25 °C, 40 bar H ₂ pressure, biphasic (benzene/H ₂ O)	Not demonstrated (125) ^(c)	[1h]
9	Park and coworkers (2005)	RhCl ₃ •3H ₂ O	22 °C, 1 atm H ₂ pressure, monophasic (benzene/hexane mixture)	Not demonstrated (200) ^(c)	[1i]
10	Jiang and coworkers (2005)	RuCl ₃ •3H ₂ O	20 °C, 3 MPa H ₂ pressure, monophasic (benzene)	Not demonstrated (268)	[1j]
11	Roucoux and coworkers	RhCl ₃ •3H ₂ O	20 °C, 1 atm H ₂ pressure, triphasic	Not demonstrated	[1k]

	(2006)		(H ₂ O/benzene/silica)	(38) ^(c)	
12	Roucoux and coworkers (2006)	RuCl ₃	20 °C, 1 bar H ₂ pressure, biphasic (benzene/H ₂ O)	Not demonstrated (8) ^(c)	[1l]
13	Roucoux and coworkers (2007)	RuCl ₃	20 °C, 30 bar H ₂ pressure, biphasic (benzene/H ₂ O)	Not demonstrated (200) ^(c)	[1m]
14	Park and coworkers (2007)	Rh/AlO(OH)	Room temperature, 1 atm H ₂ pressure, monophasic (<i>n</i> -hexane/benzene)	Not demonstrated (690)	[1n]
15	Özkar and coworkers (2008)	Intrazeolite Ru(0) nanoparticles	22 °C, 40 psig H ₂ pressure, monophasic	2420 (1040)	[1o]
16	Roucoux and coworkers (2009)	Polyhydroxylated ammonium chloride stabilized Rh(0) nanoparticles	Room temperature, 1 bar H ₂ pressure, biphasic (benzene/H ₂ O)	Not demonstrated (100) ^(c)	[1p]
17	Wai and coworkers (2009)	Carbon nanotube supported Rh nanoparticles	Room temperature, 10 atm H ₂ pressure, monophasic	Not demonstrated (1038 ≤ TOF ≤ 2414)	[1q]

^(a) TTO (Total Turnover Number), TOF × time. In no case was the actual number of active sites determined; however, in Marks' study (entry 6) the actual number of active sites is known with some certainty (virtually 100% active sites), and in Wai's study (entry 17) the lower limit TOF of 1038 is given by the number of molecules reacted per *unit weight of catalyst* per unit time. The upper limit TOF of 2414 is was calculated from dispersion values evaluated from the mean size of Rh nanoparticles via TEM images.² ^(b) TOF (Turnover frequency), (moles of product)/((moles of total catalyst loading)×time), where available. ^(c) TOFs were reported as moles of H₂ per moles of catalyst per hour. However, so that they can be directly compared, those reported values were converted into moles of benzene per moles of catalyst per hour by dividing the H₂ loss by 3 since 3 equivs of H₂ molecules are required to completely hydrogenate 1.0 equiv of benzene.

Trials Attempting to Fit the Kinetics of a Standard Conditions Hydrogenation of Benzene Starting with [(1,5-COD)IrCl]₂.

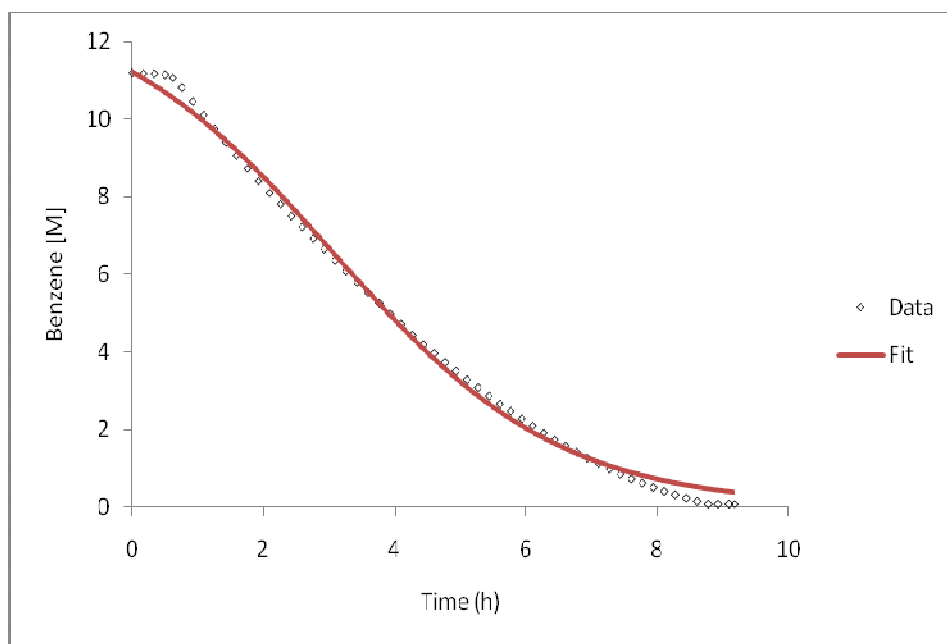


Figure SI-A1. Attempts to fit the kinetic curve in Figure 1 to the 2-step mechanism³ yielded a poor fit ($R^2 = 0.996$) not unexpectedly since aggregated iridium is the final product (i.e., and since the 2-step mechanism describes the formation of stable nanoparticles), $k_1 \approx 0.09 \text{ h}^{-1}$; $k_{2\text{corr}} \approx 9.5 \text{ h}^{-1} \text{ M}^{-1}$.

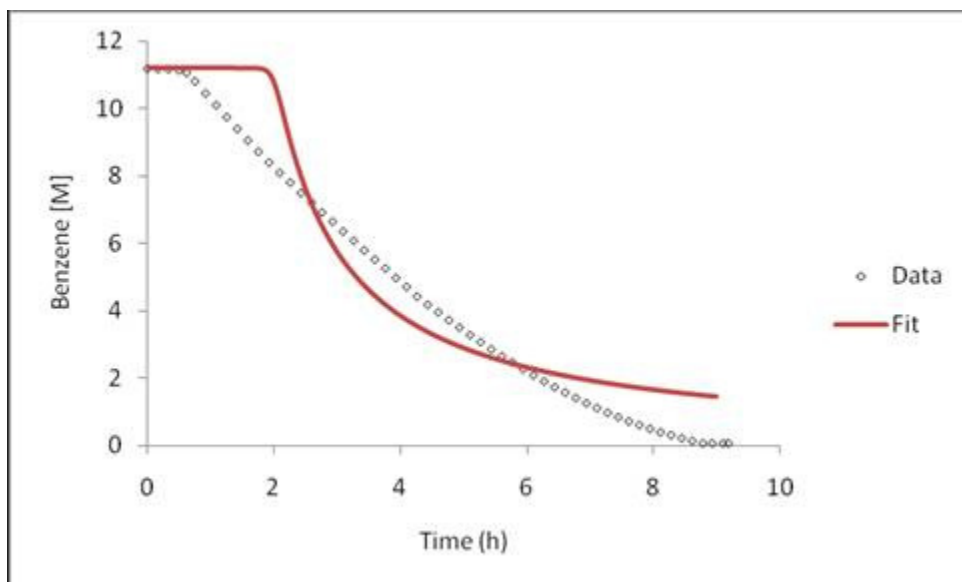


Figure SI-A2. Demonstration of the failed attempt (*residual*= 0.21098) to fit the kinetic curve in Figure 1 to the 4-step mechanism of transition-metal nanoparticle formation via nucleation, autocatalytic surface growth, bimolecular agglomeration, and autocatalytic agglomeration.⁴ The failure is not well understood but could be due: (i) to the failure of *benzene* hydrogenation as a reporter reaction (i.e., and since it is slow compared to cyclohexene hydrogenation⁵). However, the good fits seen to supported nanoparticle formation using benzene as the reporter reaction (Figure 8, main text) argues against this explanation. Hence, a more likely explanation is that the failed fits (ii) reflect the fact that significant higher aggregates/bulk metal are being formed as the final products in the present case, while the 4-step mechanism just describes up to “second generation aggregates” labeled as “C” elsewhere.⁴ In any event the ability to describe the kinetics and mechanism of the formation of the aggregated nanoparticles/bulk metal in the present case is not a focus of the present work, nor thought to be particularly important for the present work. Rather, it is included here primarily to document a case where the 4-step mechanism of nanoparticle formation is unable to fit the observed benzene reporter reaction^{3,4} kinetic data.

REFERENCES

¹ (a) Januszkiewicz, K.R.; Alper, H. *Organometallics* **1983**, *2*, 1055; (b) Seeberger, M.H.; Jones, R.A. *J. Chem. Soc. Chem. Comm.* **1985**, *6*, 373; (c) Duan, Z.; Sylwester, A.P.; Hampden-Smith, M.J. *Chem. Mater.* **1992**, *4*, 1146; (d) Schulz, J.; Patin, H.; Roucoux, A. *Chem. Comm.* **1999**, 535; (e) Schulz, J.; Patin, H.; Roucoux, A. *Chem. Eur. Jour.* **2000**, *6*, 618; (f) Nicholas, J.P.; Ahn, H.; Marks, T.J. *J. Am. Chem. Soc.* **2003**, *125*, 4325; (g) Schulz, J.; Patin, H.; Roucoux, A. *Adv. Synth. Catal.* **2003**, *345*, 222; (h) Mevellec, V.; Ramirez, E.; Phillippot, K.; Chaudret, B.; Roucoux, A. *Adv. Synth. Catal.* **2004**, *346*, 72; (i) Park, I.S.; Kwon, M.S.; Kim, N.; Lee, J.S.; Kang, K.Y.; Park, J. *Chem. Comm.* **2005**, 5667; (j) Zhang, J.; Xie, Z.; Liu, Z.; Wu, W.; Han, B.; Huang, J.; Jiang, T. *Catalysis Letters* **2005**, *103*, 59; (k) Roucoux, A.; Phillippot, K.; Payen, E.; Granger, P.; Dujardin, C.; Nowicki, A.; Mevellec, V. *New J. Chem.* **2006**, *30*, 1214; (l) Nowicki, A.; Zhong, Y.; Leger, B.; Rolland, J. P.; Bricout, H.; Monflier, E.; Roucoux, A. *Chem. Comm.* **2006**, 296; (m) Nowicki, A.; Le Boulaire, V.; Roucoux, A. *Adv. Synth. Catal.* **2007**, *349*, 2326; (n) Park, I.S.; Kwon, M.S.; Lee, J.S.; Kang, K.Y.; Park, J. *Adv. Synth. Catal.* **2007**, *349*, 2039; (o) Zahmakiran, M.; Özkar, S. *Langmuir*, **2008**, *24*, 7065. (p) Hubert, C.; Denicourt-Nowicki, A.; Guégan, J.-P.; Roucoux, A. *Dalton Trans.* **2009**, 7356. (q) Pan, H.-B.; Wai, C.M. *J. Phys. Chem. C* **2009**, *113*, 19782.

² Boudart, M. *Chem. Rev.* **1995**, *95*, 661.

³ (a) Watzky, M.A.; Finke, R.G. *J. Am. Chem. Soc.* **1997**, *119*, 10382, and references therein; (b) Watzky, M.A.; Finke, R.G. *Chem. Mater.* **1997**, *9*, 3083; (c) Aiken III, J.D.; Finke, R.G. *J. Am. Chem. Soc.* **1998**, *120*, 9545 and references therein; (d) Widegren, J.A.; Aiken III, J.D.; Özkar, S.; Finke, R.G. *Chem. Mater.* **2001**, *13*, 312 and references therein.

⁴ (a) Besson, C.; Finney, E.E.; Finke, R.G. *J. Am. Chem. Soc.* **2005**, *127*, 8179; (b) Besson, C.; Finney, E.E.; Finke, R.G. *Chem. Mater.* **2005**, *17*, 4925.

⁵ (a) March, J. *Advanced Organic Chemistry: Reactions, Mechanisms, and Structure*, 4th Ed.; Wiley-Interscience: New York, 1992; (b) Fessenden, R.J.; Fessenden, J.S. *Organic Chemistry*, 5th Ed.; Brooks/Cole Publishing Company: Pacific Grove, 1993.

CHAPTER V

IS IT HOMOGENEOUS OR HETEROGENEOUS CATALYSIS DERIVED FROM [RhCp*Cl₂]₂? *IN OPERANDO* XAFS, KINETIC, AND CRUCIAL KINETIC POISONING EVIDENCE FOR SUBNANOMETER Rh₄ CLUSTER-BASED BENZENE HYDROGENATION CATALYSIS

This dissertation chapter contains a paper published in *Journal of the American Chemical Society* **2011**, *133*, 18889-18902 with co-authors (Linehan, J.C.; Fulton, J.L.; Roberts, J.A.S.; Szymczak, N.K.; Smurthwaite, T.D.; Özkar, S.; Balasubramanian, M.; Finke, R.G.). This chapter presents the identification of the subnanometer Rh₄ clusters as true catalyst for benzene hydrogenation at 100 °C and 50 atm initial H₂ pressure via *in operando* XAFS, kinetic, and kinetic quantitative poisoning experiments.

All the experiments were performed by first author Ercan Bayram except the *in operando* XAFS studies which were done by our collaborators Dr. John C. Linehan and coworkers at Pacific Northwest National Laboratory (PNNL). Those co-authors also wrote the *in operando* XAFS section of the manuscript, notably all the XAFS data analyses and interpretations.

The drafts of the complete manuscript were written by Ercan Bayram with the aid of John C. Linehan and John L. Fulton for XAFS analysis. The final manuscript on this classic, challenging system was prepared via ca. 23 versions over a >12 month period via extensive editing by mainly Professor Richard G. Finke.

Overview

Determining the true, kinetically dominant catalytically active species, in the classic benzene hydrogenation system pioneered by Maitlis and co-workers 34 years ago starting with $[\text{RhCp}^*\text{Cl}_2]_2$ ($\text{Cp}^* = [\eta^5\text{-C}_5(\text{CH}_3)_5]$), has proven to be one of the most challenging case studies in the quest to distinguish single-metal-based “homogeneous” from polymetallic, “heterogeneous” catalysis. The reason, this study will show, is the previous failure to use the proper combination of (i) *in operando* spectroscopy to determine the dominant form(s) of the precatalyst’s mass under catalysis (i.e., operating) conditions, plus then and crucially also (ii) the previous lack of the necessary kinetic studies, catalysis being a “wholly kinetic phenomenon” as J. Halpern long ago noted. An important contribution from this study will be to reveal the power of quantitative kinetic poisoning experiments for distinguishing single-metal, or in the present case subnanometer Rh_4 cluster-based catalysis from larger, polymetallic $\text{Rh}(0)_n$ nanoparticle catalysis, at least under favorable conditions. The combined *in operando*-XAFS (X-ray absorption fine structure) spectroscopy and kinetic evidences provide a compelling case for Rh_4 -based, with average stoichiometry “ $\text{Rh}_4\text{Cp}^*_{2.4}\text{Cl}_4\text{H}_c$ ”, benzene hydrogenation catalysis in 2-propanol with added Et_3N and at 100 °C and 50 atm initial H_2 pressure. The results also reveal, however, that if even ca. 1.4% of the total soluble $\text{Rh}(0)_n$ had formed nanoparticles, then those $\text{Rh}(0)_n$ nanoparticles would have been able to account for all the observed benzene hydrogenation catalytic rate (using commercial, ca. 2 nm, polyethyleneglycol-dodecylether hydrosol stabilized $\text{Rh}(0)_n$ nanoparticles as a model system). The results—especially the poisoning methodology developed and employed—are of significant, broader interest since determining the nature of the true catalyst continues to be a central, often vexing issue in any and all catalytic reactions. The results are also of fundamental interest in that they add to a growing body of evidence indicating

that certain, appropriately ligated, coordinatively unsaturated, subnanometer M_4 transition-metal clusters can be relatively robust catalysts. Also demonstrated herein is that Rh_4 clusters are poisoned by $Hg(0)$, demonstrating for the first time that the classic $Hg(0)$ poisoning test of “homogeneous” vs “heterogeneous” catalysts cannot distinguish Rh_4 -based subnanometer catalysts from $Rh(0)_n$ nanoparticle catalysts, at least for the present examples of these two specific, Rh-based catalysts.

Introduction

Distinguishing catalysis by a discrete metal complex “homogeneous” catalyst from multiple metal “heterogeneous” nanoparticle catalyst¹ remains a challenging problem in catalytic science.^{2,3} It is also a forefront topic in catalysis since key catalytic properties—including selectivity, activity, stability, catalytic lifetime, poisoning as well as catalyst recovery and regeneration—are inherently different for homogeneous and heterogeneous catalysts.² The problem of the “identification of the true catalyst” is made more intriguing, as well as compounded in complexity, by the recent findings that subnanometer clusters, such as M_4 species, can be active catalysts.^{4,5,6,7}

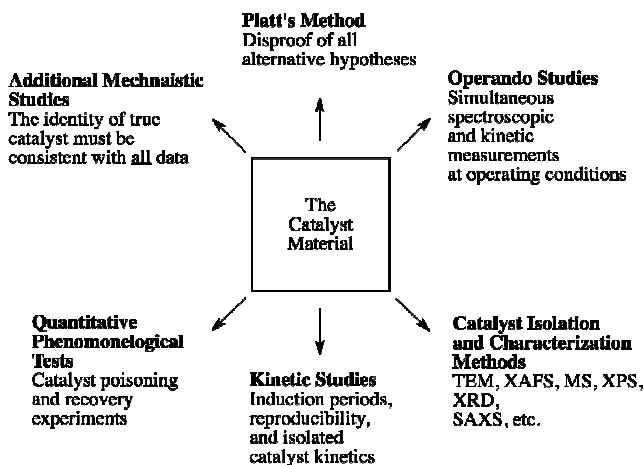
Those of us at Colorado State University (CSU) entered the arena of “is it homogeneous or heterogeneous catalysis?” in the pre-1990s with the then generally unsolved problem of how to best and most efficiently approach distinguishing these two types of catalysis; work that resulted in the discovery of polyoxoanion-stabilized $Ir(0)_n$ nanoparticles^{8,9}—plus a more general approach then was available in 1994 for distinguishing homogeneous vs heterogeneous catalysts.⁸ At its most basic level, the underlying conceptual basis¹⁰ of that 1994 approach *is still the essence of the required approach today*: (i) determining in where the precatalyst mass resides *during*

catalysis (i.e., in what species or forms), and then necessarily (ii) performing kinetic studies—including quantitative catalyst poisoning studies as the present work will make apparent—since “catalysis is a wholly kinetic phenomenon”,¹⁰ at least when starting from favorable reaction thermodynamics. That 1994 methodology, developed via 3rd row transition metals that tend to form TEM-beam stable nanoparticles (from 3rd row metal precatalysts that are also often TEM-beam stable), has been updated recently^{6,11} by the addition of *in operando*¹² spectroscopic studies that are required for a detailed, correct picture of “what is the evolved form(s) the precatalyst mass” under operating conditions, Scheme 5.1. Other notable parts of Scheme 5.1 include: (i) a necessary focus throughout the research on the disproof of multiple alternative hypotheses,¹³ (ii) the idea that *no single experiment can convincingly determine the true nature of the catalyst*,^{2,14,15} and again (iii) the required kinetic studies. Although already part of Scheme 5.1 since 1994,⁸ the present work reveals clearly (iv) the power of *quantitative kinetic poisoning experiments*^{2,14,16,17} for distinguishing nanoparticle catalysts (where only a fraction of the total metal atoms in a nanoparticle are on the surface, resulting in poison/M ratios < 1) from single metal or M₄ catalysts (where 1 or more equivs of poison are expected to be required, poison/M ratios > 1). Another key part of Scheme 5.1 is (v) that the correct description of the catalyst should be able to explain all observations and have predictive value. Aiding the experimental distinction of homogenous vs nanoparticle heterogeneous catalysts is the early review of that topic in 2003 by one of our groups,² and a series of subsequent reviews probing the nature of the true palladium catalysts employed for Heck,^{18,19,20,21} Suzuki,¹⁸ C-C coupling,²² and hydrogenation²² reactions.

Also relevant to the present study is the literature of arene hydrogenation,^{2,14,23} including the issue of homogeneous vs heterogeneous catalysis therein,^{2,14} arene reduction being a topic

important to industry.²⁴ Interesting historically here is that benzene reduction was originally interpreted as a “telltale sign”¹⁴ of heterogeneous catalysis, benzene hydrogenation often requiring harsher reaction conditions of ≥ 100 °C and ≥ 50 atm.²⁵

Scheme 5.1. An updated approach to distinguish single-metal homogeneous catalysis from polymetallic heterogeneous catalysis.¹¹ Reprinted with permission.



A now classic “is it homogeneous or heterogeneous catalysis?” problem, identified in our 2003 review,² is Maitlis and coworkers’ pioneering study of benzene hydrogenation catalysis beginning with $[\text{RhCp}^*\text{Cl}_2]_2$ at 50 °C and 50 atm H_2 pressure.²⁶ In 1977 the catalytically active species was suggested to be homogeneous on the basis of light scattering experiment—showing the absence of metal particles—and the apparent²⁷ lack of an observable metal precipitate at the end of the reaction. However, the light scattering results appeared to depend on the reaction vessel, and small amounts of metal precipitate were occasionally observed (see the Supporting Information elsewhere²⁷ for additional details and discussion of the early light-scattering experiments). In addition, other authors reported the formation of dark colored reaction solution, 1-2 h induction periods, and the formation of metallic precipitates using this same (pre)catalyst

under the same conditions (i.e., 50 °C and 50 atm H₂ pressure).²⁸ Unfortunately, no kinetic studies were reported as part of the 1977 work,²⁶ meaning that the true benzene reduction catalyst has remained unknown since that time.²⁶

Also relevant to what follows is the report that green colored solutions of [RhCp*H]₄[X]₂ (where X: Cl, PF₆, BF₄) are “relatively poor hydrogenation catalysts”²⁹ in organic solvents such as acetone or alcohols due, apparently, to a high degree of steric shielding of the Rh centers by the Cp* ligands.²⁹ In short, identifying the benzene hydrogenation catalysis when beginning with [RhCp*Cl₂]₂ has remained as a significant, central mechanistic challenge to the more general problem of “is it homogeneous or heterogeneous catalysis?”

In 2003, the Colorado State subgroup of our team recognized this challenge² and began reinvestigations of the catalytically active species in benzene reduction²⁷ at 50 atm H₂ beginning with [RhCp*Cl₂]₂, but at 100 °C where more convenient rates are present. (The reduction of benzene at 50 °C beginning with [RhCp*Cl₂]₂ takes ~21 days to go to completion, while at 100 °C, the reaction is completed in a much more convenient, ≥80-fold faster, ~6 h period.) A 2005 paper²⁷ resulted from that work demonstrating an induction period and overall sigmoidal kinetics (see Figure 3 in that 2005 paper²⁷), kinetics reproduced herein, Figure 5.1. Those sigmoidal kinetic curves are well-fit by the 2-step mechanism of nucleation and autocatalytic growth developed by one of us,³⁰ A → B with rate constant k_1 , then A+B → 2B with rate constant k_2 , where A = [RhCp*Cl₂]₂ and B = the catalytically active species. The kinetics are unequivocal in revealing that the starting complex A = [RhCp*Cl₂]₂ is *not* the catalyst but, instead, is a *precatalyst* en route to the catalytically active species, “B”. In other words, those previously missing kinetics and net, overall reaction stoichiometry, A→B, demonstrate that B must form before catalysis ensues. The next question became—and still is—“what is B?”

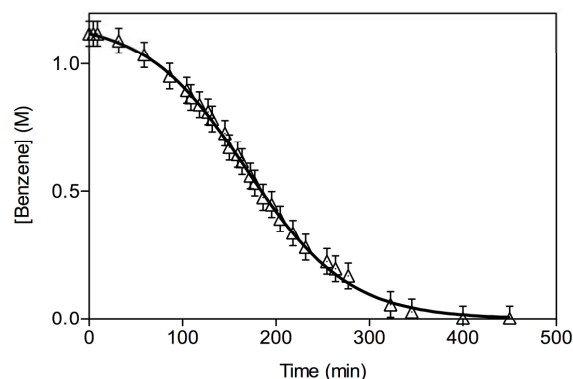


Figure 5.1. Data (\triangle) and curve fit (—) for a typical benzene hydrogenation reaction starting with $[\text{RhCp}^*\text{Cl}_2]_2$ in 2-propanol with added Et_3N at 100 °C and 50 atm initial H_2 pressure. The observed sigmoidal curve is well fit ($R^2 = 0.999$) by the 2-step mechanism $\text{A} \rightarrow \text{B}$, $\text{A} + \text{B} \rightarrow 2\text{B}$, with rate constants $k_1 = 7.1 \times 10^{-2} \text{ h}^{-1}$, and $k_2 = 2.1 \times 10^2 \text{ M}^{-1}\text{h}^{-1}$. This repeat experiment was performed as part of the present study to test the kinetic reproducibility of the system. The results reproduce our previously published data²⁷ of $k_1 = 1.9 \times 10^{-2} \text{ h}^{-1}$, and $k_2 = 2.6 \times 10^2 \text{ M}^{-1}\text{h}^{-1}$ within experimental error, given the $\sim 10^{1.2}$ range historically seen in the k_1 nucleation rate constant.³¹

A short summary of the evidence for “B” prior to the present study follows next, as that evidence, and the traps and pitfalls in interpreting it, are important both in order to appreciate what follows and so that the broader community can understand the pitfalls, as well as fully capture the key insights, from this challenging case study. Central here en route to deducing the correct answer as to the true catalyst is a complete, balanced stoichiometry for the precatalyst-to-catalyst conversion reaction (i.e., for $\text{A} (= [\text{RhCp}^*\text{Cl}_2]_2) \rightarrow \text{B}$ in the above kinetic formulation of the problem). That is, and in the end, the answer as to “what is B?” could be as simple—or as complex, *vide infra*—as determining the product(s) *under the precise reaction conditions*, that is, *in operando*, *vide infra*.

The 2005 study reported that a black, Rh-containing precipitate is formed at the end of the reaction, a result verified herein by both CSU and Pacific Northwest National Laboratory

(PNNL) groups, *vide infra*. *Ex situ* XPS analysis as part of the 2005 study identified that product as Rh(0),²⁷ seemingly providing strong evidence for “B = Rh(0)” —albeit *ex situ* evidence. A control experiment filtrating the resultant solution using a 0.2 μm nylon syringe filter argued against bulk, low-surface-area Rh(0)_n as the catalytically active species since any filterable precipitate did not provide a kinetically competent rate of benzene hydrogenation.²⁷ Complete poisoning of the catalyst was observed upon the addition of ~ 300 equiv Hg(0) per equiv of rhodium —again *suggestive, but not definitive*, evidence for of polymetallic, heterogeneous nanoparticle catalysis (i.e., given the problems and ambiguities in interpreting Hg(0) poisoning experiments as discussed elsewhere,² and as will be apparent from the Hg(0) poisoning results herein). *Ex situ* TEM investigation in 2005 of the resultant catalyst solution dried on a TEM grid revealed the presence of 1.9 ± 0.5 nm, albeit poorly formed/somewhat “smeared” appearing, Rh(0)_n nanoparticles. Significantly, TEM control experiments further revealed that just the [RhCp*Cl₂]₂ precatalyst (diluted in 2-propanol, benzene, and triethylamine, then placed on a TEM grid) yielded similar, smeared-appearing, 1.7 ± 0.3 nm Rh(0)_n nanoparticles. Hence, the TEM evidence for Rh(0)_n nanoparticles as a result of the catalytic reaction was, at best, rendered equivocal. In the end, the evidence that B = Rh(0) came back to the black, *ex situ* XPS characterized, Rh(0) product. And, since there was no other precedented hypothesis at the time that could explain the available data, it seemed like a safe conclusion that the [RhCp*Cl₂]₂ evolved at 100 °C and 50 atm H₂ pressure to [Rh(0)_n·(ClEt₃NH⁺)_m] nanoparticles as the most probable true catalyst,²⁷ a conclusion reinvestigated herein and shown to be in error.

In the meantime, studies at PNNL were focused on amine-borane dehydrocoupling prototype reactions starting with a [Rh(1,5-COD)Cl]₂ (COD: cyclooctadiene) precatalyst.⁴ That work re-examined prior studies interpreted as Rh(0)_n nanoparticle catalysis of amine-borane

dehydrocoupling.³² Significantly, *in operando*-XAFS spectroscopy revealed that >98% of the soluble Rh mass during the catalysis is present as amine-borane-stabilized, Rh₄ subnanometer clusters.^{4,33} Importantly, principal component analysis (PCA) confirmed that no more than 2% of a third component could possibly be present in the *in operando* reaction cell constructed for the measurements. An upper limit of <1-2% was placed on the possible amount of soluble Rh(0)_n present (in comparison to authentic Rh(0) metal examined as a control and XAFS standard).

Next, in what are very important observations relevant to the present studies, a black precipitate formed in the later stages of the reaction (and which gives rise to a clear solution plus the black precipitate after 72 hours) was shown by XAFS *not* to be the anticipated Rh(0)_n nanoparticles. Instead, that black precipitate was proposed to be *linked Rh₄ clusters* on the basis of the XAFS data. In a second, significant observation a dehydrocoupling reaction done *under O₂* led to the formation of a precipitate exhibiting the XAFS of—surprisingly—bulk Rh(0)_n, formed apparently via some sort of still ill-understood *oxidation-induced, metal-reduction* reaction. This result shows that *ex situ* analyses of black precipitates in air in at least the Rh/amine-borane system have considerable potential to yield very misleading results. In further studies directly relevant to the present work, four other Rh precursors were shown to evolve *under the amine-borane dehydrocoupling reaction conditions* (but not the benzene reduction conditions herein) to analogous ligand-stabilized Rh₄ clusters, including [RhCp*Cl₂]₂, the precatalyst of the present benzene hydrogenation investigations.

The 2007 PNNL study concluded that the Rh₄ clusters are the leading true catalyst candidates for the amine-borane dehydrocoupling reaction.⁴ Unfortunately, the needed rate law, poisoning and other kinetic studies required to support or definitively refute the “Rh₄ subnanometer cluster catalysis hypothesis” in the amine-borane dehydrocoupling reaction have not yet been

performed.⁴ Hence, the identity of the true catalyst in the amine-borane dehydrocoupling reaction became, and remains, controversial. The authors of the first study using the $[\text{Rh}(1,5\text{-COD})\text{Cl}]_2$ precatalyst for amine-borane dehydrocoupling still prefer their original conclusion, namely that the true catalyst is $\text{Rh}(0)_n$ nanoparticles.³⁴ Those authors note the lack of kinetic work in the second study,⁴ and point out that in air—where $\text{Rh}(0)_n$ has been shown to form in the PNNL study⁴—a drastically shortened induction period is observed. That case history re-teaches the lesson from Halpern, namely that “catalysis is a wholly kinetic phenomenon”,¹⁰ again at least once favorable reaction thermodynamics are in place. Restated, one cannot possibly learn the identity of the true catalyst, *for any catalytic reaction*, without employing the necessary kinetic studies. As we will see herein, this includes the appropriate kinetic poisoning experiments in some cases, such as the present, and when polymetallic species are among the possible catalysts.

However, the PNNL work⁴ proved central to—and indeed gave rise to—the present work by supplying the previously missing alternative hypothesis investigated herein: that ligated Rh_{-4} clusters are actually the true catalysts for benzene hydrogenation beginning with $[\text{RhCp}^*\text{Cl}_2]_2$ in 2-propanol with added Et_3N at 100 °C and 50 atm H_2 . Hence, herein the CSU and PNNL groups have joined forces to try to answer unequivocally the question of the true, kinetically dominant catalyst in the classic Maitlis benzene hydrogenation system beginning with $[\text{RhCp}^*\text{Cl}_2]_2$ and 50 atm initial H_2 pressure at 100 °C. It is the required studies which are reported next.

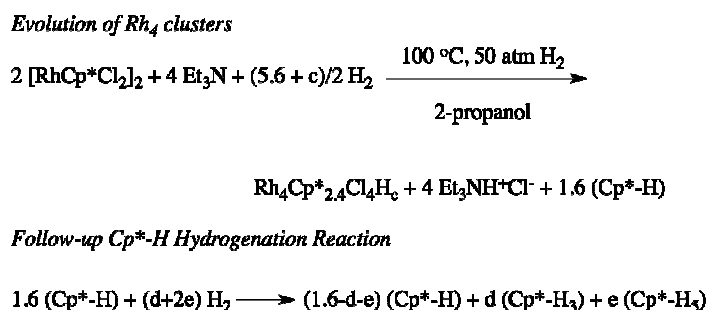
Results and Discussion

Controls Repeating Key Experiments, Product Observations and Construction of a Working Catalyst Evolution Stoichiometry. To start, controls repeating the hydrogenation of benzene, starting with $[\text{RhCp}^*\text{Cl}_2]_2$ at 100 °C and 50 atm initial H_2 pressure, were performed according to the 2005 procedure.²⁷ Also repeated were $\text{Hg}(0)$ poisoning and GC-MS

investigation of the amount of hydrogenated Cp* released, initially as Cp*-H. These experiments were done to check the broad reproducibility of the catalyst evolution and resultant benzene hydrogenation system. Pleasingly, each of these repeat experiments yielded the same results as published previously²⁷ within experimental error. Specifically, (i) a sigmoidal benzene hydrogenation curve is again obtained (in seven repeat experiments throughout the course of these studies), kinetics that are nicely fit ($R^2 = 0.999$) to the 2-step mechanism of autocatalytic catalyst evolution,³⁰ data shown back in Figure 5.1; (ii) the addition of ~300 equiv of Hg(0) per Rh, after 1/3 of a Standard Conditions benzene hydrogenation reaction is finished, kills the catalytic activity completely (Figure SI-B1 of the Supporting Information) as previously observed;²⁷ and (iii) GC-MS investigation of the resultant solution reveals the release of free Cp*-H and its hydrogenation products, Cp*-H₃ and Cp*-H₅ at a level of ~42% of the initial Cp* present (Table SI-B1). The ~42% Cp* release results are identical within experimental error to those we previously reported, ~45%,²⁷ results which will also be fortified by a ca. 40% Cp* loss according to XAFS, vide infra. Interestingly, when one opens the Parr reactor after ~6 h *in the drybox*, (iv) one sees a dark green solution suggestive of the presence of a tetra-rhodium species²⁹ such as “Rh₄Cp*_{~2.4}Cl_bH_c”, where the Cp*_{~2.4} value has been set from the Cp* loss value of ca. 40%. A black precipitate, plus the formation of a black film on the walls of the glass liner, is also seen in the Parr reactor opened in the drybox (that black ppt previously believed to be Rh(0) from ex situ XPS,²⁷ but which *in operando*-XAFS will characterize as linked/agglomerated discrete, on average Rh₄ clusters, vide infra). Interestingly, (v) fast atom bombardment-mass spectroscopy (FAB-MS) investigation of the rhodium product right after the benzene hydrogenation is complete in ~6 h reveals a molecular ion peak at $m/z = 956$ attributable to fully Cp*-ligated [Rh₄Cp*₄H₄]⁺; that MS includes an excellent match to the calculated,

theoretical isotope distribution pattern for a Rh₄ cluster, Figure SI-B2 of the Supporting Information. Overall, a mixture of Rh₄Cp*_a species is implied, any mixture so long as the average “a” value is ca. 2.4, Rh₄Cp*_{2.4} (i.e., and after ca. 6 h, when the benzene hydrogenation is complete, Figure 5.1). Combined together, the GC-MS, FAB-MS (and upcoming XAFS) results allow the suggested, average Rh evolution stoichiometry given in Scheme 5.2 to be written. Worth emphasizing here is that the “Rh₄Cp*_{2.4}Cl₄H_c” written is *not* intended to indicate a single Rh₄ species; any mixture of Rh₄Cp*_aCl_bH_c that averages out to a = 2.4, b = 4 will account for the observed data.

Scheme 5.2. Average stoichiometry for the evolution of the [RhCp*Cl₂]₂ precatalyst into, on-average, Rh₄Cp*_{~2.4}Cl₄H_c clusters via GC-MS, FAB-MS and XAFS (vide infra), investigations.



As a control and in expectation that longer reaction times would yield higher levels of Cp* loss from the [RhCp*Cl₂]₂ precatalyst, the level of Cp* loss after ~11 h reaction time in the Parr reactor was measured by GC-MS (i.e., and in comparison to the ~6 h “standard time” in Figure 5.1, vide supra, when all the benzene, *but only ca. 16.3 atm of the initial 50 atm H₂*, has been consumed). As expected, additional Cp* was lost with the additional 5 h of reaction: ~73% Cp*

loss after 11 h vs ~42% after 6 h. This experiment reveals that the average stoichiometry in Scheme 5.2 applies to the 6 h reaction time post which the benzene hydrogenation is complete.

However, the formulation of even the average, $\text{Rh}_4\text{Cp}^*_{2.4}\text{Cl}_4\text{H}_c$, species present in solution after 6 h is still an important advance in addressing the true catalyst in this classic benzene hydrogenation catalysis system: it provides direct evidence for the hypothesis that “ $\text{Rh}_4\text{Cp}^*_{2.4}\text{Cl}_4\text{H}_c$ ” is the true catalyst (i.e., one or more of the species present that average to the stated, average molecular composition). The next order of business then became *in operando*-XAFS studies to verify the proposed stoichiometry and to see if ~100% of the Rh mass could be accounted for by just Rh_4 species.

Investigation of the $[\text{RhCp}^*\text{Cl}_2]_2$ Evolution Reaction via *In Operando*-XAFS. *In operando*-XAFS was employed to check and further reveal the average structural changes around rhodium atoms during the benzene hydrogenation and concomitant $[\text{RhCp}^*\text{Cl}_2]_2$ evolution reaction. This enabled us to observe the evolution of what proved to be ligated Rh_4 clusters in a way that is impossible via *ex situ* analytical methods.^{4,7}

In order to obtain the higher signal-to-noise ratio needed to search carefully for trace species (i.e., in particular any $\text{Rh}(0)_n$ nanoparticle formation, *vide infra*), 4-fold more $[\text{RhCp}^*\text{Cl}_2]_2$ was employed in the PNNL XAFS investigations compared to the CSU studies presented so far. Employing that 4-fold higher concentration of $[\text{RhCp}^*\text{Cl}_2]_2$ shortened the reaction time to a convenient, ca. ~1 h period (vs ~6 h under the CSU Standard Conditions, Figure 1). A control experiment was done showing that the XAFS results which follow are the same at the CSU conditions of one-fourth the concentration of $[\text{RhCp}^*\text{Cl}_2]_2$ (Figure SI-B3).

To begin, a stirred batch reactor for *in operando*-XAFS investigations was constructed from a stainless steel “tee” fittings (9/16 inch, HIP, Erie, PA) plus custom PEEK windows that allow

transmission of the X-ray beam, Figure 5.2. This continuously stirred, pressured reactor allowed the desired *in operando*-XAFS measurements.

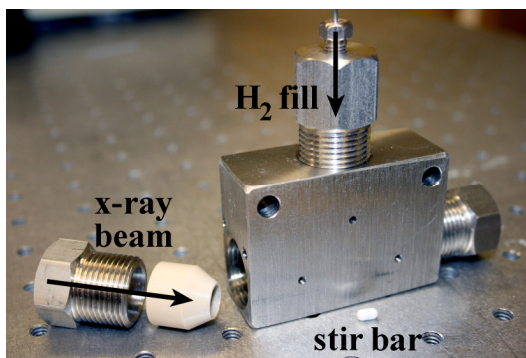


Figure 5.2. Continuously stirred reactor constructed and used for the *in operando*-XAFS investigations herein of benzene hydrogenation starting with $[\text{RhCp}^*\text{Cl}_2]_2$ at 100 °C and 50 atm initial H_2 pressure.

Figure 5.3 shows a time series of rhodium K-edge *in operando* X-ray absorption spectra of the benzene hydrogenation reaction accomplished with the cell shown in Figure 5.2. The primary feature of this raw-data spectrum is the presence of *three* distinct isosbestic points.³⁵ Those isosbestic points provide strong evidence that the starting material is being converted into primarily a single new rhodium species as the reaction proceeds.³⁵ The *in operando*-XAFS confirms the kinetics and the 2-step mechanism curve fits back in Figure 5.1: namely that $[\text{RhCp}^*\text{Cl}_2]_2$ is a *precursor* to the dominant form of rhodium in solution once catalysis ensues post the induction period, $\text{A} \rightarrow \text{B}$, necessary to begin to make that catalyst, “B”.

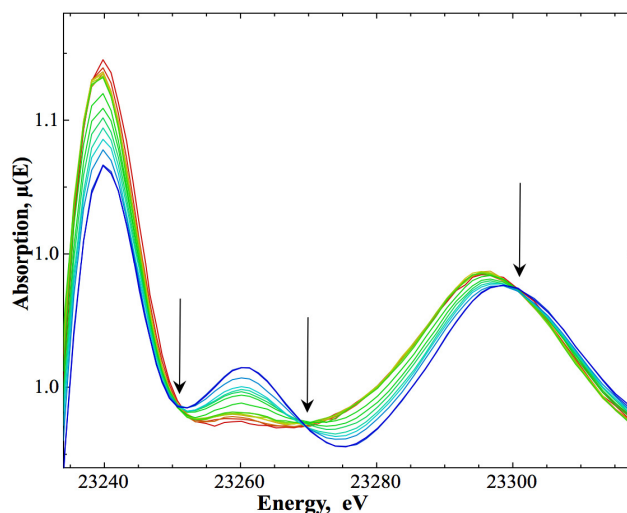


Figure 5.3. Series of time-dependent K-edge *in operando*-X-ray absorption spectra showing three distinct isosbestic points (indicated by the arrows) revealing that the precatalyst $[\text{RhCp}^*\text{Cl}_2]_2$ is evolving to primarily a single new form of rhodium during the catalysis.

Significantly, the new rhodium species, B, has a Rh-Rh bond length of ca. 2.7 Å as given in the radial structure plot (RSP) with increasing Rh-Rh interaction, Figure 5.4a. For comparison, the starting material, $[\text{RhCp}^*\text{Cl}_2]_2$, has a Rh-Rh distance of about 3.7 Å with no direct Rh-Rh bonding, Table 5.1. Figure 5.4a also shows the loss of the 1.8 Å feature, interpreted as the loss of Cp* and Cl ligands, a result consistent with the independent GC-MS results showing ca. 42% loss of Cp*. These features are summarized in Figure 5.4b which shows the time-dependence of the rhodium coordination number (CN) for nearby rhodium, chloride, and Cp* ligands derived from fitting the experimental data to FEFF8 theoretical standards,³⁶ all done as detailed previously.⁴ The *average* Rh-Rh CN increases quickly to ~3—that is, *to on average Rh₄ clusters*³⁷—concomitant with Rh-Cl and Rh-Cp* CNs decreasing on average to ~1 and ~0.6, respectively. This is a central and key result: *the hypothesis that Rh₄ clusters are the true catalyst is provided by the XAFS results.*

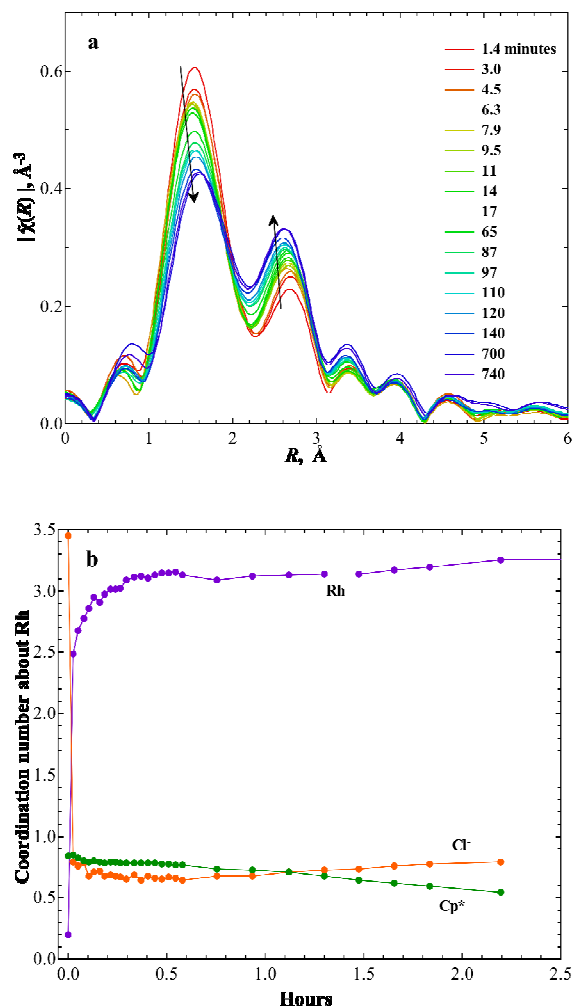


Figure 5.4. (a) Radial structure plot of the reaction progress showing an increase at around 2.7 \AA attributed to Rh-Rh formation and a decrease at around 1.8 \AA for Rh-Cp* and Rh-Cl interactions. (b) The coordination numbers for Rh, Cl and Cp* about Rh as a function of the reaction time derived from fitting the *in operando*-XAFS results to FEFF8 theoretical standards,³⁶ as detailed previously.⁴ Note that although the starting material has a Rh-Cl CN of 3 initially, an XAFS experimental Rh-Cl CN of ~3.5 is observed at the start of the reaction, revealing an initial ~17% experimental error in the Rh-Cl CN, one consistent with an expected XAFS uncertainty of $\pm 20\%$ for the CN.

As the reaction proceeds, the Rh-Cp* coordination number calculations from the XAFS data show a decreased CN around the new rhodium species while the Rh₄ core is maintained, Figure

5.4b. However, since XAFS analysis is not very sensitive to the light, third shell atoms around the Rh₄ core (e.g., C, O, Cl, etc.), one cannot obtain reliable information about the percentages of possible mixtures with the same Rh₄ core but different coordination numbers such as (but not limited to) Rh₄Cp*₄ or Rh₄Cp*₂. The only requirement is that the species present must average to a ca. 40% Cp* loss (i.e., or ca. 60% Cp* *retention* as found by XAFS, *vide infra*). The results in Figure 5.4 also reveal that the precatalyst transformation is largely accomplished within 0.5-1.0 hr, *under the 4-fold higher [RhCp*Cl₂]₂ starting concentrations*, so that the precatalyst evolution should be complete under ca. 4×(0.5-1.0) h = ca. 2-4 h under the 4-fold more dilute, CSU conditions (and assuming a first-order dependence on the concentration as will be shown to be the case, *vide infra*). Additional XAFS and other data will reveal additional hydrogenated Cp* loss at longer times, however, *vide supra*.

When the benzene hydrogenation was complete (as judged by the cessation of H₂ uptake and ¹H-NMR), XAFS parameters of the final solution were fit to FEFF8 theoretical standards.³⁶ Excellent fits to the experimental data were obtained, Figure 5.5. Table 5.1 provides the structural details of the Rh₄ clusters derived from these fits. Table 5.1 also includes the starting complex [RhCp*Cl₂]₂ for a comparison of CNs and bond lengths, and the control of comparing the XAFS results with the published crystal structure data of [RhCp*Cl₂]₂.³⁸ Noteworthy is that, in the new Rh species, there is no evidence, within the detection limits of XAFS, for any backscattering from either third or fourth rhodium shells. Restated, “no” (i.e., ≤2%) Rh(0)_n nanoparticles could be detected by *in operando*-XAFS.

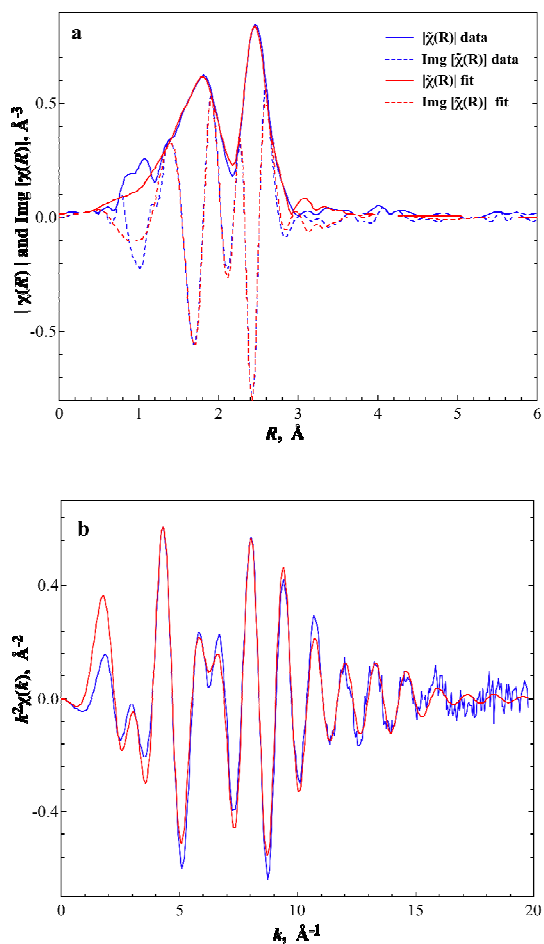


Figure 5.5. The k^2 -weighted (a) $|\tilde{\chi}(R)|$ vs $\text{Im}[\tilde{\chi}(R)]$ and (b) $k^2\tilde{\chi}(k)$ vs $\text{Im}[\tilde{\chi}(R)]$ plots for the Rh_4 clusters formed at the end of the complete benzene reduction. The experimental data, and the model fits³⁶ shown, reveal generally good agreement between the two.

The detailed analysis of XAFS data of the on-average Rh_4 cluster product shows that all the CNs are different than those for the $[\text{RhCp}^*\text{Cl}_2]_2$ starting material, Table 5.1. The most noticeable difference is the increase in the Rh-Rh CN from 1 to 2.9 ± 0.4 concomitant with a significant decrease in the Rh-Rh distance from the non-bonding value of 3.725 Å to a directly bonded Rh-Rh value of 2.714 Å . This change is similar to that found for the catalysis of dehydrocoupling of amine-borane complexes starting with $[\text{Rh}(1,5\text{-COD})\text{Cl}]_2$ precatalyst and in

which amine-borane stabilized Rh₄ clusters are formed.⁴ The relatively low Debye-Waller factor (0.0068 Å²), and the high quality of the *k*²-weighted fit, Figure 5.5, *suggest that all four rhodium atoms are equivalent in this cluster.* Consistently, all Rh-Rh bond lengths for the Rh₄ cluster are equal with 2.714 ± 0.004 Å, a value somewhat longer than the Rh-Rh distance of 2.68 Å in bulk metal,³⁹ but similar to that found previously⁴ for Rh₄ clusters of 2.734 ± 0.005 Å.⁴⁰

Each rhodium atom has an average CN of 1.3 ± 0.6 with Cl with a distance of 2.320 ± 0.029 Å. The Rh-Cp* contribution has a distance of 2.219 ± 0.012 Å with a CN of 0.6 ± 0.1. However, in the absence of a similar, literature structure with complete structural details that we could use as a model (i.e., no such structure was found from an extensive literature search), XAFS has limited ability to yield a more detailed picture for the ligand environment around Rh₄ clusters. The XAFS does reveal the presence of ligated Rh₄ clusters, their average Rh CNs, and that no additional Rh_x species are detectable.

Noteworthy here is that the XAFS and GC-MS Cp* evolution results agree rather well in terms of the average Cp* content of the resultant dominant form of rhodium present: the XAFS yielded a Rh-Cp* coordination number of 0.6 ± 0.1 (implying that the average Rh₄ cluster is ligated on average by 2.4 Cp* molecules), while the GC-MS reveals a ~42% Cp* loss from the starting material, equivalent to a ~58% (or 0.6 x 4 = 2.4) Cp* retention after 6 h of catalysis. In both cases a Rh₄Cp*_{2.4} formulation results as shown back in Scheme 5.2. With the 1:1 Rh:Cl ratio found on average by XAFS (i.e., Rh₄Cl₄), the resultant average Rh product becomes the “Rh₄Cp*_{2.4}Cl₄H_c” previously written in Scheme 5.2, with the caveat here that XAFS is unable to detect “H” ligands. Worth emphasizing again is that the formula “Rh₄Cp*_{2.4}Cl₄H_c” represents an *average* and *is not* intended to indicate a single Rh₄ species; any mixture of Rh₄Cp*_aCl_bH_c that averages out to *a* = 2.4, *b* = 4 is consistent with the XAFS and other data to this point.

Nevertheless, the significant result is that the hypothesis that “Rh₄Cp*_{2.4}Cl₄H_c” is the true catalyst (i.e., one or more of the species present that average to these values) is now fortified by direct, *in operando*-XAFS evidence.

Table 5.1. Results of the EXAFS analyses for [RhCp*Cl₂]₂ in solid state and the average Rh₄ clusters observed at the end of the hydrogenation reaction. In all cases the *k*²-weighting was used for the fit.

	EXAFS					XRD ³⁸
	Scatterer	CN	<i>R</i> , Å	² ×10 ³ , Å ²	ℳ ^a	<i>R</i> , Å
[RhCp*Cl ₂] ₂ in solid state (as boron nitride pellets)	Rh-Cp*	1	2.126 ± 0.006	3.0 ± 0.5	0.01	2.128
	Rh-Cp*CH ₃	1	3.218 ± 0.017	5.1 ± 2.0		3.252
	Rh-Cl	2+1 ^b	2.442 ± 0.015	5.0 ± 2.0		2.424
	Rh-Rh	1	3.725 ± 0.042	8.1 ± 2.9		3.719
Rh ₄ clusters formed in solution after the catalysis	Rh-Cp*	0.6 ± 0.1	2.219 ± 0.012	5.2 ± 1.7	0.02	
	Rh-Cp*CH ₃	0.6	3.282 ± 0.020	3.9 ± 2.1		
	Rh-Cl	1.3 ± 0.6	2.320 ± 0.029	12.8 ± 7.6		
	Rh-Rh	2.9 ± 0.4	2.714 ± 0.004	6.8 ± 0.6		

(a) Goodness of fit defined by a scaled sum of squares as described in FEFFIT.³⁶ (b) EXAFS is unable to resolve the two different Cl ligands of [RhCp*Cl₂]₂ (1 bridging + 2 terminal per Rh) so they were modeled as an average.

XAFS Insights Into the Amount of Soluble Rh as a Function of Time and the Nature of the Black Precipitate. Since the XAFS edge height is proportional to the total amount of soluble rhodium in the X-ray beam (i.e., and for a constant beam path-length as employed herein), edge

height provides a fairly precise ($\pm 2\%$) measure of the concentration of the soluble rhodium species, as detailed elsewhere.⁴ The features in Figure 5.6 show that until complete conversion of the benzene (in ~ 1 h, at the 4-fold higher concentrations used), the total amount of rhodium in solution via XAFS—identified as ligated Rh_4 clusters—*stays relatively constant at $98 \pm 2\%$* . After ~ 1 h, when three equivalents of H_2 were consumed per benzene (via pressure measurements simultaneous with the *in operando*-XAFS spectroscopy) and when ^1H -NMR confirmed that all the benzene had been hydrogenated to cyclohexane, *there is a marked reduction in the amount of soluble rhodium*. The solubility of the Rh_4 cluster is reduced presumably because either “ $\text{Rh}_4\text{Cp}^*_{2,4}\text{Cl}_4\text{H}_c$ ” clusters that are no longer benzene-ligated become insoluble in cyclohexane, or perhaps they H-bridge (if Rh-H are present in the Rh_4 clusters), or the Rh_4 otherwise forms a *black precipitate* at the end of the reaction. This is the same black precipitate observed in the 2005 study²⁷ and now, independently, in both the PNNL and the CSU studies. Recall that it was this black precipitate, and the ex situ XPS evidence that suggested it was “Rh(0)”, that ultimately misled the prior study into believing that the black product of the reaction was the then expected, black $\text{Rh}(0)_n$ nanoparticles.²⁷

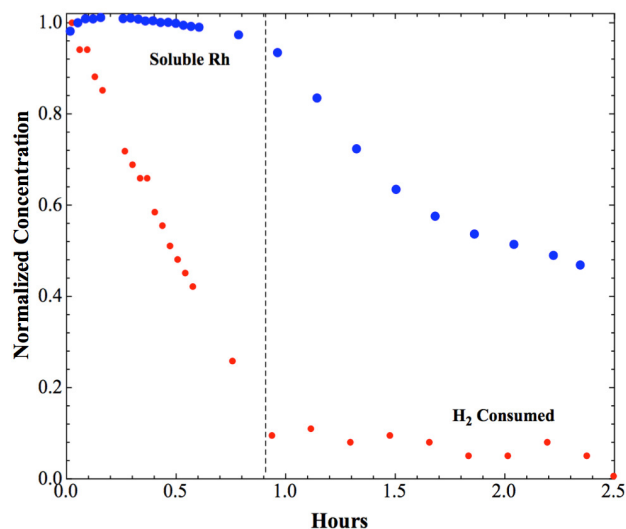


Figure 5.6. Normalized concentrations (via XAFS) of the ligated Rh₄ clusters and the H₂ pressure (measured simultaneously with the *in operando*-XAFS) during and after benzene hydrogenation at 100 °C and 50 atm H₂ beginning with the [RhCp*Cl₂]₂ precatalyst. The final product analysis via ¹H-NMR confirms that all the benzene initially present was converted into cyclohexane.

The experimental observations on the black precipitate are as follows: First and again, (i) a black precipitate is observed in both the CSU and PNNL investigations, at the end of the reaction starting with [RhCp*Cl₂]₂ at 100 °C and 50 atm initial H₂ pressure, as well as a black film formation (on the PEEK windows of the reactor for PNNL investigation or on the glass liner of the Parr reactor for the CSU investigations). (ii) XAFS characterization of the black precipitate and black film at PNNL (in the fluorescence mode due to the low level of the black film) under O₂-free conditions *showed the presence of Rh₄ clusters, but no metallic rhodium nanoparticles within the ±2% detection limits of XAFS.* (iii) However, upon exposure to air, *the black precipitate forms metallic rhodium by XAFS*—a crucial observation that explains the previous observation of Rh(0) via *ex situ* XPS that included exposure to air.²⁷ Additional control experiments performed at CSU reveal that (iv) when the benzene hydrogenation is completed (~6

h) and the Parr reactor cooled, *taken into the drybox* to avoid any significant O₂ exposure, and then opened, a dark-green (i.e., Rh₄-like²⁹) solution along with a black precipitate is observed (plus a black film formation on the walls of glass liner). Then, if 4 mL of fresh benzene are added to the reactor in the drybox, the reactor resealed and brought out of the drybox, and the Parr reactor reheated to 100 °C (without applying H₂ pressure) then quickly opened in a hood *with exposure to O₂/air*; immediate visual inspection of the resultant solution reveals that the *black precipitate had redissolved and a homogeneous, dark-green solution had formed*. This simple experiment confirms the XAFS derived absence of detectable, insoluble Rh(0)_n. This control further supports the XAFS conclusion that the black precipitate is *not* Rh(0)_n. However, if this dark-green solution is exposed to O₂/air in the hood, the solution becomes red-brown and again a black precipitate is formed within 5 min (Rh(0) by ex situ XPS,⁴¹ repeating the previous observation²⁷). Overall, this control experiment fortifies the XAFS finding of Rh(0) formation from Rh₄ clusters via oxidatively induced metal reduction following exposure to O₂/air.

Overall, the XAFS studies are definitive in revealing that the black precipitate is not Rh(0) but, instead, is composed of soluble, apparently linked Rh₄ clusters—ones that, surprisingly, are *reduced* to Rh(0) under ex situ analyses involving exposure to O₂/air. The details of this presently somewhat mysterious “oxidatively induced metal reduction” reaction remain to be established, however, including its full reaction stoichiometry and the details of its underlying mechanism. Nevertheless, this unexpected observation of Rh(0) formation under O₂ exposure (and, presumably, concomitant ligand oxidation as the source of the reducing equivalents) is an important result. This unexpected result highlights the enormous potential of ex situ, non-*in operando* methods to mislead one *completely* regarding the true products of at least this particular system and its reactions.

Resultant Two Main Hypotheses for the True Catalyst. The sigmoidal kinetics and $A \rightarrow B$, $A + B \rightarrow 2B$ curve fit, the GC-MS and now the XAFS results lead to the two main hypotheses for the true catalyst; hypotheses which will be the focus of the remaining parts of this paper, namely: (i) that one or more forms of the ligated, on average “ $\text{Rh}_4\text{Cp}^*_{2.4}\text{Cl}_4\text{H}_c$ ” subnanometer clusters that comprise $98 \pm 2\%$ of the Rh mass are the true catalyst; or (ii) that the *possibly* present, $\leq 2\%$ of other form(s) of XAFS undetectable Rh are the true catalyst, for example, the previously suggested $[\text{Rh}(0)_n \cdot (\text{ClEt}_3\text{NH}^+)_m]$ nanoparticles. Hence, kinetic experiments, the use of authentic $\text{Rh}(0)_n$ nanoparticles in control experiments, as well as what turned out to be key quantitative kinetic poisoning experiments with 1,10-phenanthroline were performed next en route to ruling out one or more of the above hypotheses.

Kinetic Experiments Determining the Reaction Order of the $\geq 98\%$ Rh_4 Species Present at the End of 6 h of Benzene Hydrogenation. By using predetermined amounts of initial $[\text{RhCp}^*\text{Cl}_2]_2$ to change the concentration of the final Rh_4 solutions, the kinetics of the dependence on the rhodium species *present at the end of the catalytic reaction* was investigated. A simple first-order dependence would indicate if Rh_4 —or any constant concentration, trace-level Rh species—is the true catalyst. Alternatively, some higher order or fractional order dependence would indicate aggregated Rh_4 clusters or fragmented Rh_4 clusters are the true catalyst, respectively. Specifically, four separate Standard Conditions benzene hydrogenation starting with different amounts of $[\text{RhCp}^*\text{Cl}_2]_2$ (62.5, 53.6, 44.3, or 27.2 mg) were performed. After the first benzene hydrogenation was completed, a subsequent benzene hydrogenation was started at the normal 100 °C and 50 atm initial H_2 pressure after the addition of 4 mL fresh benzene in the drybox, all as detailed in the Experimental section. The resultant benzene hydrogenation curves were then fit to a polynomial equation in order to obtain the initial rates.⁴²

These kinetic curves are provided in Figure SI-B4 of Supporting Information for the interested reader. One example curve, for an initial $[\text{RhCp}^*\text{Cl}_2]_2$ amount of 62.5 mg (0.101 mmol or 2.3 mM under the reaction conditions) is provided in Figure 5.7. Significantly, no induction period is seen indicating that no further evolution of the XAFS-observed $\geq 98\%$ Rh_4 (or the possible $\leq 2\%$ of other Rh species) is apparently necessary for catalysis.

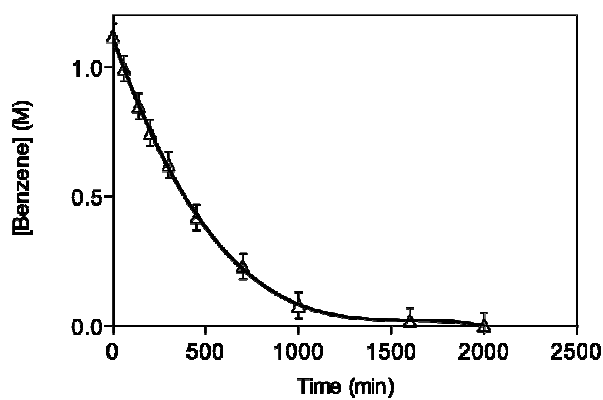


Figure 5.7. Benzene hydrogenation data (Δ) at 100 °C and 50 atm H_2 pressure employing the fully evolved catalyst initially started with 62.5 mg (0.101 mmol; 2.3 mM) $[\text{RhCp}^*\text{Cl}_2]_2$. A polynomial fit to the data (—) with the equation $y = -2.7 \times 10^{-10}x^3 + 1.3 \times 10^{-6}x^2 - 0.0023x + 1.115$ to the data yielded an initial rate of $\{-d[\text{Benzene}]/dt\}_{\text{in}} = 0.0023 \text{ M/min}$. An important feature of this kinetic curve is the lack of an induction period.

The initial rate values obtained from the series of experiments allowed construction of Figure 5.8 showing a clean, first-order dependence on the $[\text{Rh}]_{\text{Total}}$ (i.e., ostensibly on the $[\text{Rh}_4]^1$), $R^2 = 0.998$. As a control, the same data set was tried in a second-order and a half-order plots (i.e., the initial rate with respect to $\{[\text{Rh}]_{\text{Total}}\}^2$ and $\{[\text{Rh}]_{\text{Total}}\}^{1/2}$), but resulted in concave and convex curves, respectively, Figure SI-B5a-b), thereby confirming the better first-order fit.

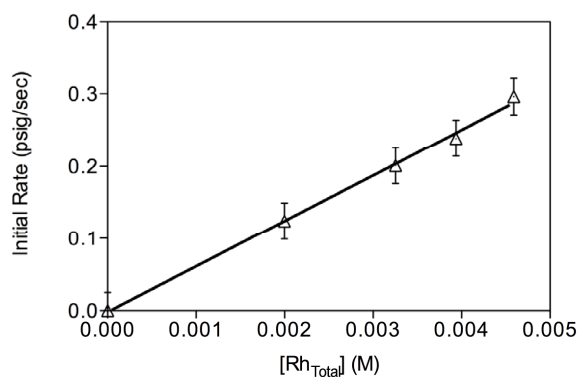


Figure 5.8. Plot revealing a clean first-order dependence ($R^2 = 0.998$) on the $[\text{Rh}]_{\text{Total}}$ formed at the end of an initial benzene hydrogenation reaction, conditions under which $98 \pm 2\%$ of the Rh is present as (average) Rh_4 subnanometer clusters.

The kinetic results are consistent with and supportive of the Rh_4 species present being the true catalyst. The results also rule out any higher order process or fragmentation where by the Rh_4 present would aggregate or fragment in either an irreversible step or a reversible, prior $K_{\text{eq}} \ll 1$ step. However, the kinetics alone do not rule out other, trace Rh species such as $\text{Rh}(0)_n$ nanoparticles as the true catalyst—since the concentration of any such, reproducibly present trace species present *would also change in a linear way in this experiment*. Restated, the kinetics do not rule out trace, (i.e., $\ll 2\%$) but potentially high activity, $\text{Rh}(0)_n$ nanoparticles as the true catalyst. Hence so that possibility was addressed next.

Benzene Hydrogenation Control Experiments at 100 °C and 50 atm Initial H_2 Pressure with Authentic $\text{Rh}(0)_n$ Nanoparticles as Model for Putative, XAFS-Undetectable, $\leq 2\%$ $\text{Rh}(0)_n$ Nanoparticles Possibly Present. Can Such $\text{Rh}(0)_n$ Nanoparticles Account for the Observed Catalytic Activity? Polyethyleneglycol-dodecylether hydrosol stabilized $\text{Rh}(0)_n$ nanoparticles that are ca. 2 nm and 9 wt-% Rh were employed as model $\text{Rh}(0)_n$ nanoparticles.

These Rh(0)_n nanoparticles were picked since they should be “weakly ligated/labile ligand”¹⁶ and thus *good catalytic activity* Rh(0)_n nanoparticles as an example and model. For such ca. 2 nm Rh(0)_n nanoparticles, ~40% of total rhodium atoms are on the surface according to a calculation using full shell, so-called “magic number” nanoparticles for this estimate.⁴³

Employing the Rh(0)_n nanoparticles in benzene hydrogenation under the normal Standard Conditions given in the Experimental section was accomplished as follows: 231±1 mg of polyethyleneglycol-dodecylether hydrosol stabilized Rh(0)_n nanoparticles (0.202 mmol Rh, the same mmols as when [RhCp*Cl₂]₂ was used as a precatalyst) were added to a mixture of 36 mL of 2-propanol plus 4 mL of benzene.⁴⁴ Figure 5.9 shows the resultant benzene hydrogenation curve. The authentic Rh(0)_n nanoparticles both (i) showed no induction period—consistent with their being an active catalyst, and (ii) *exhibited a superior, ca. 70 fold more active benzene hydrogenation catalyst activity* on an equivalent, per rhodium basis in comparison to starting with the catalyst evolved from [RhCp*Cl₂]₂ after 6 h. The benzene reduction reaction was complete in <15 min and showed an initial rate of $\{-d[\text{Benzene}]/dt\}_{\text{in}} = 0.1624 \text{ M/min}$ (vs a ~6 h total reaction time and initial rate of $\{-d[\text{Benzene}]/dt\}_{\text{in}} = 0.0023 \text{ M/min}$ from Figure 5.7). TEM analysis of the final product revealed intact, albeit somewhat agglomerated, 2-3 nm Rh(0)_n nanoparticles, Figure SI-B6.

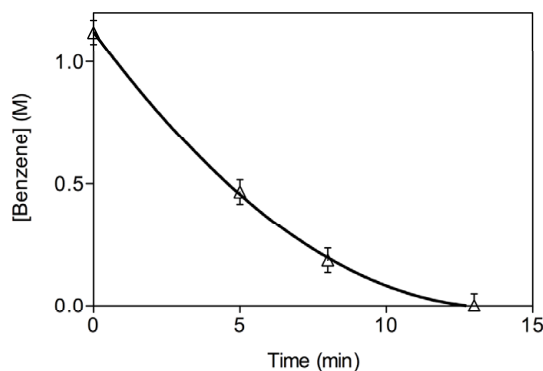


Figure 5.9. Benzene hydrogenation data (Δ) at 100 °C and 50 atm initial H_2 pressure employing polyethyleneglycol-dodecylether hydrosol stabilized $Rh(0)_n$ nanoparticles (231(\pm 1) mg, 0.202 mmol Rh, the same amount of total Rh used in the “Standard Conditions Benzene Hydrogenation beginning with $[RhCp^*Cl_2]_2$ ”). Also shown is a $y = 0.0058x^2 - 0.1624x + 1.1224$ polynomial fit (—) to the data.

The 70-fold greater reactivity allows the estimate that if even a mere $1/70 = \sim 1.4\%$ of the total Rh present initially in the $[RhCp^*Cl_2]_2$ precatalyst is present as $Rh(0)_n$ nanoparticles, then those trace $Rh(0)_n$ nanoparticles could account for all the observed catalytic activity (all assuming that the polyethyleneglycol-dodecylether hydrosol stabilized $Rh(0)_n$ nanoparticles are a reasonable model of the activity of the nanoparticles postulated to be present as an alternative hypothesis for the true catalyst⁴⁵). Significantly, $\sim 1.4\%$ is below the XAFS-undetectable upper limit of 2%. Just to check this result, one additional control was done of testing the activity of the model $Rh(0)_n$ nanoparticles at a 50-fold lower concentration (i.e., at a concentration equal to the 2% upper limit of other rhodium species that could be present). That experiment employed 4.04 μ mol, 4.6 mg of polyethyleneglycol-dodecylether hydrosol stabilized $Rh(0)_n$ nanoparticles and resulted in an initial rate of $\{-d[Benzene]/dt\}_{in} = 0.0032$ M/min, Figure SI-B7 of the Supporting Information. This initial rate of 0.0032 M/min is still ca. 1.6 fold faster than the rate of the $\geq 98\%$ Rh_4

solution, $\{-d[\text{Benzene}]/dt\}_{\text{in}} = 0.0023 \text{ M/min}$, Figure 5.7, *vide supra*. In short, trace, $\text{Rh}(0)_n$ nanoparticles present at a level of $\leq 2\%$ of the total Rh are a kinetically competent catalyst.

The next question then became: are such $\text{Rh}(0)_n$ nanoparticles actually present, and if so at what level? Or, is there another way to distinguish the two, still unrefuted hypotheses for the true catalyst: $\geq 98\%$ Rh_4 subnanometer clusters or putative $\leq 2\%$, trace $\text{Rh}(0)_n$ nanoparticles? To attempt to refute one of these still remaining hypotheses, quantitative poisoning experiments were designed next and, fortunately, proved definitive in our opinion.

1,10-Phenanthroline Quantitative Kinetic Poisoning Experiments. The one and only quantitative poison candidate known at present to work *both* for benzene reduction catalysts *and* under $\geq 100 \text{ }^\circ\text{C}$ and $\geq 50 \text{ atm H}_2$ pressure is 1,10-phenanthroline.⁴⁶ Previously, 0.5 equiv of 1,10-phenanthroline (per metal) was shown to completely halt the catalytic activity at $110 \text{ }^\circ\text{C}$ and 60 atm H_2 pressure of what was in the end proposed to be a $\text{Ru}(0)_n$ nanoparticle benzene hydrogenation catalyst.³

Quantitative 1,10-phenanthroline poisoning experiments were performed as detailed in the Experimental section. Specifically, the catalytic activities were tested as a function of the addition of 0.02, 0.5, 1.0, 2.0, 4.0, and 5.0 equivs (per total rhodium) of 1,10-phenanthroline (0.7, 18.2, 36.4, 72.8, 145.6, and 182 mg, respectively). The 1,10-phenanthroline was added to a fully evolved sample of catalyst post its ca. 6 h evolution. Significantly, when 0.02 or 0.5 equivs of 1,10-phenanthroline per Rh_{Total} were added, an initial rate of 0.0022 M/min was observed (Figures SI-B8a-b). That is, *the catalytic activity did not change within experimental error after the addition of 0.02 or 0.5 equivs of poison per Rh_{Total} present* (initial rate = 0.0023 M/min as was also seen in Figure 5.7). These results, while negative, argue against a $\text{Rh}(0)_n$ nanoparticle

catalyst, especially when the next set of experiments with higher, 1-5 equivalents of poison are considered.

Significantly, the addition of 1, 2, 4, and 5 equivs of 1,10-phenanthroline per Rh_{Total} did slow the initial catalytic activity, from $\{-d[\text{Benzene}]/dt\}_{\text{in}} = 0.0023 \text{ M/min}$ to $\{-d[\text{Benzene}]/dt\}_{\text{in}} = 0.0017, 0.0012, 0.0005, \text{ and } 0.0003 \text{ M/min}$, respectively, Figures SI-B8c-f. Figure 5.10 reveals that ~ 4.0 equiv of 1,10-phenanthroline per total Rh poisons most, ca. 75%, of the catalyst's activity.¹⁷ As is customary for such quantitative poisoning plots,^{17,47} an $x_{\text{intercept}}$ was calculated from a linear regression analysis of the linear portion of the relative rate vs equivs of 1,10-phenanthroline per Rh_{Total} , Figure 5.10. That plot yielded an $x_{\text{intercept}} = 4.0 \pm 0.4$, implying that the amount of poison required to totally poison the active catalyst is ≥ 4.0 equivs of 1,10-phenanthroline per Rh_{Total} . *These poisoning findings are consistent with and strongly supportive of the in operando-XAFS detected Rh_4 clusters being the true catalyst, especially in light of the control experiments of poisoning the authentic $\text{Rh}(0)_n$ nanoparticles discussed next where the $x_{\text{intercept}} = 0.12 \pm 0.02$.*

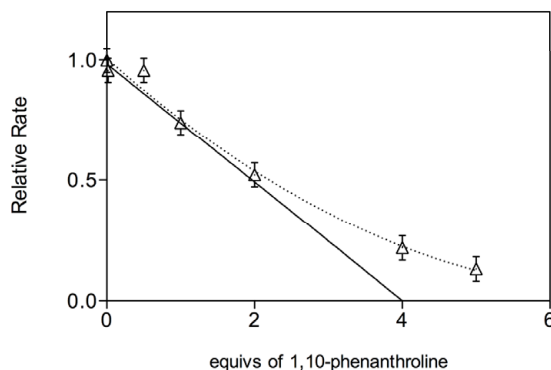


Figure 5.10. Plot of relative initial rate vs equivs of 1,10-phenanthroline per total Rh for the benzene hydrogenation starting with $98 \pm 2\%$ ligated Rh_4 clusters according to XAFS. The linear, extrapolated portion of the data yields $x_{\text{intercept}} = 4.0 \pm 0.4$.

Next, polyethyleneglycol-dodecylether hydrosol stabilized $\text{Rh}(0)_n$ nanoparticles were examined in 1,10-phenanthroline poisoning control experiments, all as detailed in the Experimental section, using 0.05, 0.1, 0.2, and 0.3 equivs of 1,10-phenanthroline per total rhodium, Figures SI-9Ba-d. As plot of the relative rates vs equivs of 1,10-phenanthroline per Rh_{Total} graph makes clear, Figure 5.11, these authentic $\text{Rh}(0)_n$ nanoparticles are poisoned by $\ll 1.0$ equivalent of poison. The $x_{\text{intercept}} = 0.12 \pm 0.02$, a value far smaller and unequivocally distinguishable from the $x_{\text{intercept}} = 4.0 \pm 0.4$ for the solution composed of $\geq 98\%$ of XAFS-detected, subnanometer Rh_4 clusters.

The combined poisoning studies make a very strong case that the on-average Rh_4 subnanometer clusters are the most active benzene hydrogenation catalyst present—that is, that one or more of the $\text{Rh}_4\text{Cp}^*_{2,4}\text{Cl}_4\text{H}_c$ species present *is the true benzene hydrogenation catalyst in the present system and under the 100 °C and 50 atm H_2 initial pressure conditions in 2-propanol and with added Et_3N* . The other insight remains, however, that had even 1.4% of the soluble Rh been in the form of $\text{Rh}(0)_n$ nanoparticles, then those nanoparticles would have been the most active catalyst (and if those nanoparticles had the activity of the model polyethyleneglycol-dodecylether hydrosol stabilized $\text{Rh}(0)_n$ nanoparticles).

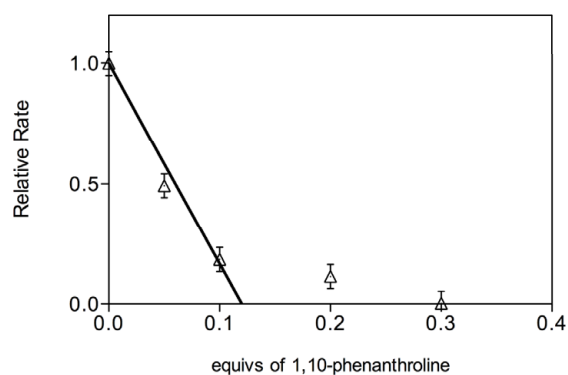


Figure 5.11. Plot of relative initial rate vs equivs of 1,10-phenanthroline per total Rh for benzene hydrogenation starting with polyethyleneglycol-dodecylether hydrosol stabilized $\text{Rh}(0)_n$ nanoparticles. The linear, extrapolated portion of the data yields $x_{\text{intercept}} = 0.12 \pm 0.02$.

Additional Insights From the 1,10-Phenanthroline Poisoning Studies. Even for the present data one can make a couple of additional, interesting interpretations: First, the $\text{Rh}(0)_n$ nanoparticles probably bind the 1,10-phenanthroline more tightly (just looking at the shapes of the two poisoning plots, the curve for Rh_4 being more convex and thus suggesting a weaker binding constant), a point that argues against the one alternative interpretations of the present poisoning data that we can see which would have required a much higher binding constant of the poison by the Rh_4 clusters.⁴⁸ Second, if one takes the 0.12 $x_{\text{intercept}}$ of the $\text{Rh}(0)_n$ poisoning plot and divides by the 0.4 fraction of Rh on the surface, one calculates that 0.12/0.4 or 0.3 equivalents of 1,10-phenanthroline per surface Rh are required to poison the $\text{Rh}(0)_n$ nanoparticles. Hence, a rather large fraction, ca. 30%, of the surface Rh of these specific polyethyleneglycol-dodecylether hydrosol stabilized $\text{Rh}(0)_n$ nanoparticles are active (or twice this, ca. 60%, if each 1,10-phenanthroline binds in a bidentate fashion, poisoning 2 sites). Additional quantitative model and mechanistic studies of the 1,10-phenanthroline poisoning studies are in progress, as

they have the potential to strengthen further⁴⁸ the results presented herein and to yield more precise values of the numbers of active sites for both the Rh₄ and Rh(0)_n catalysts.

One Additional Hg(0) Poisoning Experiment with the Now-Identified, Subnanometer Rh₄ Cluster-Based Catalyst. Since it has previously often—but incorrectly²—been believed that a Hg(0) poisoning experiment can definitively distinguish homogeneous vs heterogeneous catalysis, a Hg(0) poisoning experiment was repeated on a sample of catalyst post its ~6 h evolution and where the average form of the Rh catalyst is now known to be 98±2% Rh₄Cp*_{2.4}Cl₄H_c. Specifically, and as detailed in the Experimental section, the addition of ~300 equiv of Hg(0) (per rhodium) and fresh benzene (4 mL) to a previously fully active catalyst halted the catalyst activity *completely*, Figure 5.12. This experiment reveals for the first time that Hg(0) poisoning cannot distinguish M₄ from M(0)_n catalysis, at least when M = Rh and for the present benzene hydrogenation system. This finding supports and further fortifies the conclusion that the Hg(0) poisoning test “is not definitive and is not universally applicable.”² Hence, the Hg(0) test should be used and interpreted with considerable caution.

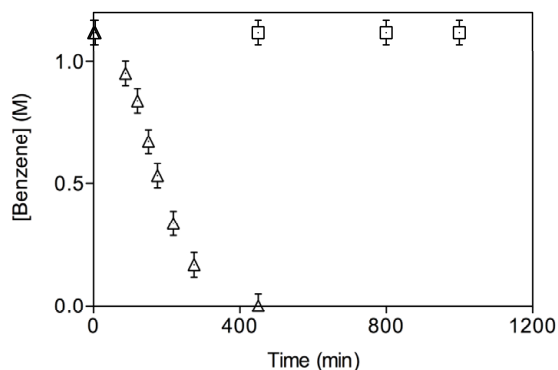


Figure 5.12. The addition of ~300 equiv of Hg(0) per total Rh plus good stirring poisoned completely (□, data) the catalytic activity of a solution of previously active (△, data) 98±2% Rh₄ clusters. The results indicate that Rh₄ benzene hydrogenation catalysis is fully poisoned by excess Hg(0).

Summary

(i) The bulk of the evidence—and particularly the combination of *in operando*-XAFS, kinetic and quantitative kinetic poisoning experiments—reveals that the true benzene hydrogenation catalyst, beginning with $[\text{RhCp}^*\text{Cl}_2]_2$ at 100 °C and 50 atm initial H_2 pressure in 2-propanol and with added Et_3N , is in all probability one or more of the Rh_4 subnanometer clusters of average formula $\text{Rh}_4\text{Cp}^*_{2.4}\text{Cl}_4\text{H}_c$.

(ii) The present studies, and the history of this classic system and the historical “is it single-metal homogeneous or polymetallic, nanoparticle heterogeneous catalysis?” question reveals that it is neither. Instead, appropriately ligand-stabilized subnanometer M_4 clusters can be the dominant catalyst in favorable situations and cases.

(iii) The results, and the history of this challenging “who is the true catalyst?” case study, reveals that one *must* use *in operando* spectroscopic methods, along with the appropriate kinetic and kinetic poisoning studies, to identify the true catalyst in at least this example. In one limiting view, this is nothing more—nor less—than what J. Halpern showed 30 years ago, albeit there for discrete, single-metal organometallic systems.¹⁰ Catalysis is a kinetic phenomenon.¹⁰

(iv) Ex situ TEM investigations, ex situ XPS studies in air, and $\text{Hg}(0)$ poisoning studies have each been shown to be ambiguous, if not highly misleading, when one is attempting to determine the true catalyst, at least in the present Rh catalysis system.

(v) Identifying the form of the bulk of the evolved precatalyst mass, even by the powerful *in operando*-XAFS studies herein that identify >98% of the starting Rh present as Rh_4 clusters, is insufficient to identify the true catalyst. That is, *in operando* spectroscopic studies are necessary,

but insufficient, for identifying the true catalyst. Kinetic investigations are a must. If even ~1.4% of the total Rh present had formed Rh(0)_n nanoparticles with activity as good or higher than that exhibited by the polyethyleneglycol-dodecylether hydrosol stabilized model Rh(0)_n nanoparticles, then those nanoparticles would have been the active catalyst.

(vi) And, finally, quantitative kinetic poisoning experiments are hereby added to the arsenal of the most important, if not necessary, experiments for distinguishing single-metal from M₄ from M(0)_n polymetallic catalysts—those kinetic poisoning studies being intrinsically “*in operando*”. It will be of interest to see if such poisoning studies can now resolve the controversy over the active catalyst—Rh₄ subnanometer clusters vs Rh(0)_n nanoparticles?—in the amine borane dehydrocoupling area. In addition, some of our (i.e., RGF and co-workers’) interests are focused on a more detailed analysis of nanoparticle kinetic poisoning studies due to the broad application and potential importance to nanoparticle catalysis that such studies promise to have.

Experimental

In what follows, all details refer to experiments done at CSU except for the *in operando*-XAFS, for which separate experimental details are reported.

Materials. Benzene (Aldrich, 99.8%, anhydrous, packaged under N₂), 2-propanol (Aldrich, 99.5%, anhydrous, packaged under N₂), and 1,10-phenanthroline (Aldrich, 99%) were transferred into the drybox and used as received. Elemental Hg(0) (Aldrich, 99.9995%) was brought into the drybox just before it was needed, and then removed after that, since Hg(0) will poison the oxygen-scavenging Cu catalyst of the drybox. Triethylamine (Aldrich, 99.5%, packaged under N₂) was stored in a refrigerator and used as received. Hydrogen gas (General Air, 99.5%) was used as received. Deuterated NMR solvents were purchased from Cambridge Isotope Laboratories, Inc. [RhCp*Cl₂]₂ (99%) and Rh colloid (polyethyleneglycol-dodecyl ether

hydrosol) (~9 wt%-Rh, ~2 nm Rh(0)_n nanoparticles) were purchased from Strem Chemicals, stored in the drybox, and used as received.

For the In Operando-XAFS: Benzene (Aldrich) was fractionally distilled twice from sodium, 2-propanol (Aldrich) was distilled from CaH₂, and triethylamine (Aldrich) was distilled from KOH. Reagent alcohol (Aldrich) and [RhCp*Cl₂]₂ (Strem Chemicals) were used as received.

General Procedures for Benzene Hydrogenation. All preparations and manipulations were performed under oxygen- and moisture-free conditions in a Vacuum Atmosphere N₂-drybox (<2 ppm of O₂ as continuously monitored by a Vacuum Atmosphere O₂-monitor), unless indicated otherwise. All benzene hydrogenations were performed in a Parr pressure reactor (model 4561) made of Monel 400 alloy. The reactor is equipped with a pressure gauge marked at intervals of 20 psig (~1.36 atm) and an automatic temperature controller (±3 °C). Additionally, the inside of the reactor contains a stainless steel (i.e., non-Monel) impeller, thermocouple, cooling loop, and dip tube; all these components are in contact with the reaction solution. A glass liner was used to avoid contacting the reaction solution with the rest of the reactor. The glass liner was dried overnight in a 160 °C drying oven before being transferred into the drybox. Pressurizing the reactor took about 1 min, and $t = 0$ was set once the reactor was fully pressurized. Pressure gauge readings vs time data were then collected and recorded.

Standard Conditions Benzene Hydrogenation with [RhCp*Cl₂]₂. In the drybox, 62.5 (±1) mg (0.101 mmol) of [RhCp*Cl₂]₂ was quantitatively transferred into an oven-dried glass liner with 36 mL of 2-propanol and 4.0 mL (44.8 mmol) of benzene, yielding a clear, orange solution with some undissolved [RhCp*Cl₂]₂ to start. Next, 0.41 mL (2.94 mmol) of Et₃N was added with a gas-tight syringe, and the glass liner was sealed in the reactor. The reactor was removed from the drybox, stirring was started at 600 rpm, equilibrated at 100 °C, and pressurized to 740

psig (50 atm) with H₂. Under these conditions complete conversion of benzene to cyclohexane corresponds to a pressure loss of about 240 psig, (~16.3 atm), see the calculation below. At the end of each hydrogenation reaction, and as a control to avoid attributing possible reactor leaks to hydrogenation activity, the percent conversion of benzene into cyclohexane was verified directly by ¹H-NMR analysis (via Varian INOVA-300 instrument with 300.115 MHz for ¹H). In those control experiments, the NMR sample was prepared by adding a drop of the final reaction solution into 1 mL CD₂Cl₂ and the resultant solution examined by ¹H-NMR for the singlet at 1.4 ppm for cyclohexane and also the absence of benzene singlet peak at 7.2 ppm. Seven repeats of this Standard Conditions experiments were performed, all of which showed hydrogen-uptake curves analogous to that given in Figure 5.1 within experimental error along with complete conversion of benzene into cyclohexane.

The pressure data were converted to benzene concentration data by a simple proportional relationship:²⁷ $[\text{benzene}] = [\text{benzene}]_{\text{initial}} \times (\text{pressure} - \text{pressure}_{\text{final}}) / (\text{pressure}_{\text{initial}} - \text{pressure}_{\text{final}})$. This treatment assumes that the pressure_{final} corresponds to complete conversion of benzene to cyclohexane, as verified experimentally by ¹H-NMR. The error bars shown for the benzene concentration assume an error of ±10 psig (~0.68 atm) in the pressure gauge reading. A variability of ±3 °C in the temperature control is also present with our Parr high-pressure apparatus.

Cleaning the Reactor between Benzene Hydrogenation Reactions, and the Control of Testing the Residual Hydrogenation Activity of the Reactor Itself. The possible non-negligible hydrogenation activity of the reactor components was prevented by careful cleaning as described below, followed by checking a blank solution (i.e., 36 mL of 2-propanol, 4.0 mL of benzene, and 0.41 mL of Et₃N with no added [RhCp*Cl₂]₂) for residual activity prior to each

catalytic run. Then, after a catalytic reaction, the Parr reactor parts in contact with the reaction solution were carefully cleaned by scrubbing with a steel wool pad and then rinsed with water, nitric acid, and distilled water. This cleaning procedure, and resultant control checking for residual activity, gave no measurable H₂ loss (0 psig) over 5 h in every case.

Hg(0) Poisoning Experiments. Two separate Hg(0) poisoning experiments were performed. For the first one, a “Standard Conditions Benzene Hydrogenation with [RhCp*Cl₂]₂” was started. Pressure vs time data were collected until the pressure had decreased to 660 psig (~44.6 atm), that is, until ca. one-third completion. Then the reactor was vented, cooled to room temperature, taken into the drybox, and opened. Next, 6.05 g Hg(0) (~300 equivs per Rh) were added to the reaction solution. The reactor was then resealed, brought out of the drybox, equilibrated at 100 °C, and repressurized to the prior 660 psig (~44.6 atm) with H₂. At this point the collection of pressure vs time data was resumed.

A separate “Standard Conditions Benzene Hydrogenation with [RhCp*Cl₂]₂” was started for the second Hg(0) poisoning experiment. When the reaction was completed—as judged by the cessation of H₂ uptake and by the ¹H-NMR of the product—the reactor was vented, cooled to room temperature, taken into the drybox, and opened. Next, 6.05 g Hg(0) (~300 equivs per Rh) and fresh benzene (4 mL) were added to the reaction solution. The reactor was then resealed, brought out of the drybox, equilibrated at 100 °C, and repressurized to the 740 psig (50 atm) with H₂. At this point the collection of pressure vs time data was started.

A control experiment (without the addition of Hg(0)) was performed to see if the procedure of releasing the remained H₂ pressure, cooling, opening the Parr reactor in the drybox, then resealing it, rewarming it and reapplying the H₂ pressure caused any loss in catalytic activity. No change in the catalytic activity was observed within the experimental error. Hence, any changes

in the catalytic activity must be due to the addition of Hg(0) (or 1,10-phenanthroline, *vide infra*) and not the physical procedure necessary to open up the Parr reactor, add Hg(0) (or add 1,10-phenanthroline, *vide infra*), and restart the reaction by repressurization with H₂ at 100 °C.

GC-MS Experiment Showing Cp* Ligand Loss from [RhCp*Cl₂]₂ via Observation of the Resultant Cp*-H and Its Hydrogenation Products. The details of this investigation are provided in the Supporting Information. The key result is that ~42% of released, partially hydrogenated Cp* products are observed, within experimental error of the ~45% detected previously.²⁷

Additionally, the same GC-MS procedure was employed when the reaction was allowed to proceed for ~11 h of prolonged reaction time (vs the ~6 h in Figure 5.1, *vide supra*). Quantification of the resultant by GC-MS analysis revealed additional Cp* loss as the reaction proceeds for an additional 5 h, ~73% Cp* loss after 11 h (vs ~42% after 6 h), Table SI-B1 of the Supporting Information.

Kinetic Investigation of the Rhodium Solution and Species Formed at the End of the Benzene Hydrogenation Reaction. A “Standard Conditions Benzene Hydrogenation with [RhCp*Cl₂]₂” was repeated four times, but starting with different initial amounts of [RhCp*Cl₂]₂ of 62.5, 53.5, 44.3, and 27.2 mg in the 4 separate experiments. In these 4 independent experiments, the following procedure was used at the completion of the benzene hydrogenation (as judged by the cessation of H₂ uptake and by ¹H-NMR of the product): the remaining H₂ pressure was released, the reactor was cooled, taken into the drybox, and opened. Then, 4.0 mL (44.8 mmol) of fresh benzene was added. The reactor was resealed and removed from the drybox, stirring was started at 600 rpm, equilibration to 100 °C accomplished, then, pressurized to 740 psig (50 atm) with H₂. At this point the collection of pressure vs time data was started.

The method of initial rates was used to analyze the kinetic data (see below for details). The hydrogenation curves for each trial, along with the polynomial equation and fit used to get the initial rates, are provided in the Supporting Information (Figure SI-B4).

Kinetic Data Treatment: Initial Rate Method. Initial rates were calculated from benzene concentration vs time or hydrogen pressure vs time data employing the initial rate method described elsewhere.⁴² Briefly, the obtained data were fit to a second- or a third-degree polynomial equation using Microsoft Excel 2008; the polynomial that fits best, as judged by the highest R^2 value, was used. Taking the derivative of the polynomial equation with respect to time, and evaluating it at $t = 0$, yields the initial rate (the coefficient of the second, initially t^1 term of the polynomial). For all initial rate calculations, the data, fit, and polynomial equation are provided in the Supporting Information. For all the initial rate determinations, the first ~25% of the data were also fit to a straight line as a check of the polynomial-determined initial rate; similar initial rates resulted in all cases. However, the initial rates obtained from the more rigorous procedure of the second- (or third-) order polynomial fits are what are reported in the Supporting Information.

Benzene Hydrogenation Starting with Polyethyleneglycol-dodecylether hydrosol Stabilized $\text{Rh}(0)_n$ Nanoparticles and Product Analysis via TEM. To start, 231 (± 1) mg (0.202 mmol total Rh, the same amount as in the case of “Standard Conditions Benzene Hydrogenation with $[\text{RhCp}^*\text{Cl}_2]_2$ ”) of polyethyleneglycol-dodecylether hydrosol stabilized Rh nanoparticles (ca. 2 nm, ~9 wt%-Rh) were transferred quantitatively into an oven-dried glass liner with 36 mL of 2-propanol and 4.0 mL (44.8 mmol) of benzene,⁴⁴ followed by sealing of the reactor. The reactor was removed from the drybox, stirring was started at 600 rpm, equilibrated at 100 °C, and

pressurized to 740 psig (50 atm) with H₂. The collection of pressure vs time data was then started.

A sample for NMR was prepared by adding a drop of the resultant solution into 1 mL CD₂Cl₂ in the drybox. The complete conversion of benzene into cyclohexane was verified directly by ¹H-NMR analysis by observing a singlet at 1.4 ppm for cyclohexane while also looking for the absence of singlet peak at 7.2 ppm for benzene.

A TEM sample was prepared in the drybox from the same, resultant solution. A 300 mesh Formvar-coated SiO₂ TEM grid was dipped into the sample solution for 5 sec and allowed to dry. The grid was then placed in a 2-dram vial and the TEM investigation was performed with JEOL 1400 instrument with 100 kV accelerating voltage. The TEM images of the resultant show the presence of somewhat agglomerated, 2-3 nm sized Rh(0)_n nanoparticles (Figure SI-B6).

The above procedure was repeated for 50-fold lower concentration of Rh(0)_n nanoparticles, corresponding to the upper limit of 2% of other possible rhodium species when starting with [RhCp*Cl₂]₂ under Standard Conditions. For this purpose, only the initial amount of polyethyleneglycol-dodecylether hydrosol stabilized Rh nanoparticles was changed to 4.6 mg (4.04 μmol) in a separate experiment (Figure SI-B7).

1,10-Phenanthroline Quantitative Poisoning Experiments for the Standard Conditions Benzene Hydrogenation with [RhCp*Cl₂]₂. For each quantitative poisoning experiments with 1,10-phenanthroline, a separate “Standard Conditions Benzene Hydrogenation with [RhCp*Cl₂]₂” was started. When the reaction was completed—its completion being judged by the cessation of H₂ uptake and by ¹H-NMR of the cyclohexane product—the reactor was vented, cooled to room temperature, taken into the drybox, and opened. Note that, from the XAFS results, 98±2% of the total Rh in solution at this time is ligated Rh₄ clusters with ≤2%

undetectable soluble Rh species. Next, 4 mL of fresh benzene plus a quantitative, predetermined amount of 1,10-phenanthroline were added to the solution; 0.02, 0.5, 1, 2, 4, and 5 equivs per total Rh (i.e., 0.7, 18.2, 36.4, 72.8, 145.6, and 182 mg, respectively). The reactor was then resealed, brought out of the drybox, equilibrated at 100 °C, and repressurized to 740 psig (50 atm) with H₂. At this point the collection of pressure vs time data was started.

The resultant poisoning data were then fit to a polynomial, as detailed previously, to obtain the initial rate for each experiment. The kinetic curves along with the polynomial fits are provided in the Supporting Information, Figure SI-B8.

1,10-Phenanthroline Quantitative Poisoning Experiments for Polyethyleneglycol-dodecylether Hydrosol Stabilized Rh(0)_n Nanoparticles. For each quantitative poisoning experiment using these authentic, commercial Rh(0)_n nanoparticles plus 1,10-phenanthroline, a separate “Benzene Hydrogenation Reaction Starting with Polyethyleneglycol-dodecylether hydrosol Stabilized Rh Nanoparticles” was performed, as detailed above, except with one change: a quantitative, predetermined amount of 1,10-phenanthroline was added to the initial solution. For this purpose, 0.05, 0.1, 0.2, and 0.3 equiv 1,10-phenanthroline (i.e., 1.8, 3.6, 7.2, and 10.8 mg, respectively) per total Rh was added for each separate poisoning experiment. The resultant hydrogenation curves for each trial were fit to a polynomial and the initial rate was calculated as detailed previously with the results shown in the Supporting Information, Figure SI-B9.

Standard Conditions Benzene Hydrogenation with [RhCp*Cl₂]₂: *In Operando*-XAFS Investigation Details. The same experimental procedure, data analysis, and fit methods were followed as detailed previously.⁴ The rhodium K-edge (23222 eV) XAFS spectra were collected in transmission mode on the bending magnet beamline (PNC-CAT, Sector 20) at the Advanced

Photon Source, Argonne National Laboratory. The bending magnet beamline was chosen, over the much higher flux insertion-device line, to minimize the potential for beam damage to the rhodium complexes. No evidence of beam-created photoelectron or other damage was observed during exposure of the rhodium complexes to the X-rays. Details of the XAFS beamline methods are given elsewhere.⁴ Portions of the Athena and Artemis programs were used for the analysis of XAFS data with theoretical standards calculated using FEFF8.³⁶ The XAFS $\chi(k)$ data were weighted by k^2 , and windowed between $2.0 < k < 19.0 \text{ \AA}^{-1}$ using a Hanning window with $dk = 1.0 \text{ \AA}^{-1}$. The fits were to both the real and imaginary parts of $\chi(R)$ in the region of $1.0 < R < 4.0 \text{ \AA}$. Five rhodium-containing standard compounds were previously used⁴ to establish the value of the core hole factor, $S_0^2 = 0.89$. S_0^2 has an associated uncertainty of about 15% that results in an approximate 15% uncertainty in the reported coordination number. Strategies for generating appropriate theoretical standards have been previously discussed.⁴

Catalysis reactions for the *in operando*-XAFS were conducted in a stirred reactor constructed from a stainless steel “tee” fittings (9/16 inch, HIP, Erie, PA) that was fit with custom PEEK windows to allow for transmission of the X-ray beam (Figure 5.2). The concentration of the $[\text{RhCp}^*\text{Cl}_2]_2$ complex used for XAFS measurements was, by design for better signal-to-noise (S/N), 4-fold higher than that used for the Standard Conditions experiments at CSU. The increased S/N ratio of the resultant XAFS data allowed differentiation of the noise from any possible, low concentration, $\text{Rh}(0)_n$ nanoparticles. A control showed that reducing the concentration 4-fold to the CSU Standard Conditions yielded the *identical* XAFS spectrum, but with poorer S/N ratio (Figure SI-B3), results that provide confidence in connecting the CSU and 4-fold higher concentration PNNL data.

In all XAFS experiments, the reactor was initially loaded with the reaction solution in a glove box containing 4% H₂ in helium, then sealed and removed from the box. Just prior to reaction, the helium was replaced by three pressurizations with H₂ to 20 bar. The cell was placed in the XAFS beam, heated to the set-point (i.e., 100 °C) using electrical-resistive heaters and a three-mode controller in ~5 min. The cell was then pressurized to 50 atm from a small H₂ reservoir while stirring with a Teflon-coated stir bar in order to initiate the reaction. The pressure inside the reactor was followed via Honeywell Atomic Pressure Transducer (Model TJE). For each set of experiments, a new reactor was used to avoid the possibility of contamination by metallic rhodium or rhodium complexes remaining from previous run.

Supporting Information Available. GC-MS investigation details and results of the hydrogenated Cp* products (Table SI-B1); Hg(0) poisoning when 1/3 of the reaction was completed (Figure SI-B1); GC-MS isotope distribution analysis of the resultant and comparison with the theoretical isotope distribution (Figure SI-B2); EXAFS comparison of the CSU vs PNNL Standard Conditions (Figure SI-B3); plots of hydrogenation reaction data and fits to a polynomial to calculate the order with respect to fully evolved Rh_{Total} catalyst (Figure SI-B4); initial rate with respect to [Rh_{Total}]² and [Rh_{Total}]^{1/2} concentrations graphs (Figure SI-B5); TEM of the Rh(0)_n nanoparticles at the end of the benzene hydrogenation reaction (Figure SI-B6); benzene hydrogenation curve, its polynomial fit and equation when starting with 50-fold lower concentration Rh(0)_n nanoparticles (Figure SI-B7); plots of hydrogenation reaction data and fits to a polynomial for 1,10-phenanthroline poisoning of Rh₄ clusters (Figure SI-B8); plots of hydrogenation reaction data and fits to a polynomial for 1,10-phenanthroline poisoning of authentic Rh(0)_n nanoparticles (Figure SI-B9). This material is free of charge via the Internet at <http://pubs.acs.org>.

Acknowledgments

This work was supported by the U.S. Department of Energy, Office of Basic Energy Sciences, Division of Chemical Sciences, Geosciences and Bioscience at PNNL and at Colorado State University (by DOE grant SE-FG02-03ER15453). A portion of the research described herein was performed at the W. R. Wiley Environmental Molecular Sciences Laboratory, a national scientific user facility sponsored by the U.S. Department of Energy's Office of Biological and Environmental Research and located at Pacific Northwest National Laboratory. PNNL is operated for the Department of Energy by Battelle. PNC/XOR facilities at the Advanced Photon Source, and research at these facilities, are supported by the US Department of Energy - Basic Energy Sciences, a major facilities access grant from NSERC, the University of Washington, Simon Fraser University, the Pacific Northwest National Laboratory and the Advanced Photon Source. Use of the Advanced Photon Source is also supported by the U. S. Department of Energy, Office of Science, Office of Basic Energy Sciences, under Contract DE-AC02-06CH11357. EB and RGF would like to thank Joseph E. Mondloch for valuable discussions and proofreading during the preparation of the manuscript and Shannon Riha for the help with the TEM investigation.

REFERENCES

- ¹ (a) Schwartz's more modern definition^{1b} of homogeneous vs heterogeneous catalysts is used herein (and in place of the older, historical definitions that equate "homogeneous" with soluble and "heterogeneous" with insoluble); see Figure 6 elsewhere.^{9b} That is, homogeneity or heterogeneity of the catalyst is defined and used herein according to the catalytically active site(s): a homogeneous catalyst has a single, uniform catalyst site, whereas a heterogeneous catalyst has more than one active sites. Hence, the catalytically active species uncovered herein, of Rh₄ clusters with the average stoichiometry of Rh₄Cp*_{2.4}Cl₄H_c, will be classified (admittedly a bit arbitrarily) as a homogeneous catalyst since a single active site per each Rh₄ cluster is expected given the presence of bulky Cp* and Cl⁻ (and possibly H⁺) ligands and since there is no evidence for more than a single active site within each Rh₄ cluster. This assignment should be considered tentative, especially since the evidence to follow will indicate the presence of more than one, on average Rh₄ cluster in the evolved, "homogeneous" Rh₄ catalyst. (b) Schwartz, J. *Acc. Chem. Res.* **1985**, *18*, 302.
- ² Widegren, J.A.; Finke, R.G. *J. Mol. Cat. A: Chem.* **2003**, *198*, 317.
- ³ Hagen, C.M.; Vieille-Petit, L.; Laurency, G.; Süß-Fink, G.; Finke, R.G. *Organometallics* **2005**, *24*, 1819.
- ⁴ (a) Fulton, J.L.; Linehan, J.C.; Autrey, T.; Balasubramanian, M.; Chen, Y.; Szymczak, N.K. *J. Am. Chem. Soc.* **2007**, *129*, 11936. (b) Rousseau, R.; Schenter, G.K.; Fulton, J.L.; Linehan, J.C.; Engelhard, M.H.; Autrey, T. *J. Am. Chem. Soc.* **2009**, *131*, 10516.
- ⁵ Alley, W.M.; Kayiran, I.K.; Wang, Q.; Frenkel, A.I.; Li, L.; Yang, J.C.; Menard, L.D.; Nuzzo, R.G.; Özkar, S.; Johnson, K.A.; Finke, R.G. *Inorg. Chem.* **2010**, *49*, 8131.
- ⁶ Alley, W.M.; Kayiran, I.K.; Wang, Q.; Frenkel, A.I.; Li, L.; Yang, J.C.; Menard, L.D.; Nuzzo, R.G.; Özkar, S.; Yih, K.-H.; Johnson, K.A.; Finke, R.G. *Langmuir* **2011**, *27*, 6279.
- ⁷ (a) Uzun, A.; Gates, B.C. *Angew. Chem. Int. Ed.* **2008**, *47*, 9245. (b) Uzun, A.; Gates, B.C. *J. Am. Chem. Soc.* **2009**, *131*, 15887.
- ⁸ Lin, Y.; Finke, R.G. *Inorg. Chem.* **1994**, *33*, 4891.

⁹ (a) Lin, Y.; Finke, R.G. *J. Am. Chem. Soc.* **1994**, *116*, 8335. (b) Aiken III, J.D.; Lin, Y.; Finke, R.G. *J. Mol. Cat. A: Chem.* **1996**, *114*, 29. (c) Weiner, H.; Trovarelli, A.; Finke, R.G. *J. Mol. Cat. A: Chem.* **2003**, *191*, 253. (d) Hornstein, B.J.; Finke, R.G. *Chem. Mater.* **2003**, *15*, 899.

¹⁰ Noteworthy here is that much of the basis for this underlying approach, for distinguishing homogeneous from heterogeneous catalysts, can in essence be traced back to seminal kinetic and mechanistic studies by J. Halpern and co-workers, even though distinguishing polymetallic from monometallic catalysts was not part of the following work: (a) Halpern, J. *Inorg. Chim. Acta* **1981**, *50*, 11. (b) Halpern, J.; Okamoto, T.; Zakhariyev, A. *J. Mol. Cat.* **1977**, *2*, 65. (c) Landis, C.R.; Halpern, J. *J. Am. Chem. Soc.* **1987**, *109*, 1746.

¹¹ Alley, W.M.; Hamdemir, I.K.; Johnson, K.A.; Finke, R.G. *J. Mol. Cat. A: Chem.* **2010**, *315*, 1.

¹² *In operando* spectroscopy as used herein refers to any technique in which the catalyst is present in the reaction solvent at the *operating temperature and pressure* and also under the *working conditions of the reactants and resultant products* of that operating catalytic system: Tinnemans, S.J.; Mesu, J.G.; Kervinen, K.; Visser, T.; Nijhuis, T.A.; Beale, A.M.; Keller, D.E.; van der Eerden, A.M.J.; Weckhuysen, B.M. *Catal. Today* **2006**, *113*, 3.

¹³ Platt, J.R. *Science* **1964**, *146*, 347.

¹⁴ Widegren, J.A.; Finke, R.G. *J. Mol. Cat. A: Chem.* **2003**, *191*, 187.

¹⁵ Gómez, M.; Favier, I.; Metal Nanoparticles Dispersed in Solution: Tests to Identify the Catalyst Nature. In *Metal Nanoclusters in Catalysis and Materials Science: The Issue of Size Control*. Eds. Corain, B.; Schmid, G.; Toshima, N.; Elsevier, 2008; Ch. 31 pp. 427-436.

¹⁶ Bayram, E.; Zahmakıran, M.; Özkar, S.; Finke, R.G. *Langmuir* **2010**, *26*, 12455.

¹⁷ Hornstein, B.J.; Aiken III, J.D.; Finke, R.G. *Inorg. Chem.* **2002**, *41*, 1625.

¹⁸ Phan, N.T.S.; Sluys, M.V.D.; Jones, C.W. *Adv. Synth. Catal.* **2006**, *348*, 609.

¹⁹ de Vries, J.G. *Dalton Trans.* **2006**, 421.

- ²⁰ Huang, L.; Ang, T.P.; Wang, Z.; Tan, J.; Chen, J.; Wong, P.K. *Inorg. Chem.* **2011**, *50*, 2094.
- ²¹ Reimann, S.; Stötzel, J.; Frahm, R.; Kleist, W.; Grunwaldt, J.-D.; Baiker, A. *J. Am. Chem. Soc.* **2011**, *133*, 3921.
- ²² Durand, J.; Teuma, E.; Gómez, M. *Eur. J. Inorg. Chem.* **2008**, 3577.
- ²³ Dyson, P.J. *Dalton Trans.* **2003**, 2964.
- ²⁴ Arpe, H.J.; Weissermel, K.; *Industrial Organic Chemistry*, 4th edition; Wiley-VCH: New York, 2003.
- ²⁵ Schulz, J.; Patin, H.; Roucoux, A. *Chem. Rev.* **2002**, *102*, 3757.
- ²⁶ Russell, M.J.; White, C.; Maitlis, P.M. *J. Chem. Soc. Chem. Commun.* **1977**, 427.
- ²⁷ Hagen, C.M.; Widegren, J.A.; Maitlis, P.M.; Finke, R.G. *J. Am. Chem. Soc.* **2005**, *127*, 4423.
- ²⁸ Collman, J.P.; Kosydar, K.M.; Bressan, M.; Lamanna, W.; Garrett, T. *J. Am. Chem. Soc.* **1984**, *106*, 2569.
- ²⁹ (a) Espinet, P.; Bailey, P.M.; Piraino, P.; Maitlis, P.M. *Inorg. Chem.* **1979**, *18*, 2706. (b) Maitlis, P.M. *Acc. Chem. Res.* **1978**, *11*, 301.
- ³⁰ (a) Watzky, M.A.; Finke, R.G. *J. Am. Chem. Soc.* **1997**, *119*, 10382, and references therein; (b) Watzky, M.A.; Finke, R.G. *Chem. Mater.* **1997**, *9*, 3083; (c) Aiken III, J.D.; Finke, R.G. *J. Am. Chem. Soc.* **1998**, *120*, 9545 and references therein; (d). Widegren, J.A.; Aiken III, J.D.; Özkar, S.; Finke, R.G. *Chem. Mater.* **2001**, *13*, 312 and references therein.
- ³¹ Widegren, J.A.; Bennett, M.A.; Finke, R.G. *J. Am. Chem. Soc.* **2003**, *125*, 10301.
- ³² (a) Jaska, C.A.; Temple, K.; Lough, A.J.; Manners, I. *J. Am. Chem. Soc.* **2003**, *125*, 9424. (b) Jaska, C.A.; Manners, I. *J. Am. Chem. Soc.* **2004**, *126*, 9776.

³³ Although the initial study^{4a} suggested an equilibrium between Rh₄ and Rh₆ clusters, and the true catalyst was suggested to be Rh₄₋₆ clusters, later *ab initio* molecular dynamics calculations^{4b} suggest that the equilibrium is actually between tetrahedral and butterfly shaped Rh₄ clusters; see Figure 3 elsewhere.^{4a}

³⁴ Staubitz, A.; Robertson, A.P.M.; Sloan, M.E.; Manners, I. *Chem. Rev.* **2010**, *110*, 4023.

³⁵ Senior, W.A.; Verrall, R.E. *J. Phys. Chem.* **1969**, *73*, 4242

³⁶ Stern, E.A.; Newille, M.; Ravel, B.; Yacoby, Y. *Physica B* **1995**, *208&209*, 117.

³⁷ For low coordination numbers (<6), accurate measurements for the first coordination shell are possible with small uncertainties by XAFS. When coordination numbers approach 12, the precision of the size measurement greatly diminishes.^{4,37a} (a) Frenkel, A.I.; Hills, C.W.; Nuzzo, R.G. *J. Phys. Chem. B* **2001**, *105*, 12689.

³⁸ Churchil, M.R.; Julis, S.A.; Rotella, F.J. *Inorg. Chem.* **1977**, *16*, 1137.

³⁹ Farrugia, L.J. *J. Cluster Sci.* **2000**, *11*, 39.

⁴⁰ Maitlis and coworkers found two different Rh-Rh bond lengths for [RhCp*H]₄[BF₄]₂ (2.610 Å and 2.829 Å) in which four hydrides are face bridging.^{40a} This observation was explained via two different oxidation states of the rhodium atoms in the Rh₄ cluster (i.e., two Rh^{II} and two Rh^{III} per Rh₄ cluster). Our XAFS investigation shows that all Rh-Rh *average* bond lengths are equal; hence, any hydride ligands present would have to be consistent with this fact (e.g., four face-bridging hydrides or something else that makes the average Rh-Rh bond lengths equal). (a) Ricci, J.S.; Koetzle, T.F.; Goodfellow, R.J.; Espinet, P.; Maitlis, P.M. *Inorg. Chem.* **1984**, *23*, 1828.

⁴¹ XPS analysis was performed using a Physical Electronics 5800 spectrometer equipped with a hemispherical analyzer and using monochromatic Al-K radiation (1486.6 eV, the X-ray tube working at 15 kV and 350 W) and a pass energy of 23.5 eV. The obtained binding energies are consistent with the metallic rhodium binding energies^{41a} (given in paranthesis): 307.03 eV (307.0 eV) for Rh-3d_{5/2} and 311.7 eV (312.0 eV) for Rh-3d_{3/2}. (a) Moulder, J. F.; Stickle, W. F.; Sobol, P. E.; Bomben, K. D.; *Handbook of X-ray Photoelectron Spectroscopy*; Physical Electronics, Inc.: Eden Prairie, MN, 1995.

⁴² Wilkins, R.G. *Kinetics and Mechanisms of Reactions of Transition Metal Complexes*, 2nd ed.; VCH: New York, 1991.

⁴³ The number of metal atoms, y , per n th shell, in full shell “magic number” nanoparticles is given by the equation $y = 10n^2 + 2$ ($n > 0$). See: Schmid, G. *Endeavour* **1990**, *14*, 172.

⁴⁴ The stoichiometry for the “Standard Conditions benzene hydrogenation with $[\text{RhCp}^*\text{Cl}_2]_2$ ” requires the use of excess (~15 equiv per total Rh) of Et_3N to scavenge the formed HCl from the precursor, $[\text{RhCp}^*\text{Cl}_2]_2$. Because the experiments starting with the authentic, preformed $\text{Rh}(0)_n$ nanoparticles do not evolve HCl, no Et_3N was added for those benzene hydrogenation reactions. In addition, a separate control experiment with the authentic $\text{Rh}(0)_n$ nanoparticles (in which 14 equiv (per total Rh) of Et_3N plus 1 equiv (per total Rh) of $\text{Et}_3\text{N}^+\text{Cl}^-$ was added) yielded the same activity within experimental error as when Et_3N plus $\text{Et}_3\text{N}^+\text{Cl}^-$ were absent. The normal amount of 2-propanol (36 mL) and benzene (4 mL) as in the case of starting with $[\text{RhCp}^*\text{Cl}_2]_2$ were used in these experiments.

⁴⁵ Of interest here is how the “Catch 22” issue noted in our 1994 paper⁸ (see Figure 4 elsewhere⁸) again appears in the present study. As Figure 4 elsewhere emphasizes,⁸ what one ideally needs when attempting to identify the true catalyst in any reaction are authentic samples of each of the possible, proposed true catalysts for use in control experiments to determine everything from their relative catalytic activities, spectroscopic properties to their stabilities, solubilities, whether they can be removed by filtration or centrifugation, and so on. *But*, the problem is that these are often the same (putative; unknown) catalyst(s) that one is trying to identify in the first place and for the first time! A specific example here is the need, ideally, in the present studies for the putative $\text{Rh}(0)_n$ nanoparticles that *could* be present in the current system, nanoparticles that would then have a previously unknown set of surface ligands made up from the possible Cp^* , Cl, H, benzene, Et_3N and other possible ligands present in the system. Such a catalyst does not exist in the literature. That fact, however, does not mean it has not been made in the current benzene hydrogenation system and at a level $\leq 2\%$. The reader interested in solving more difficult cases of “what is the true catalyst?” will want to study Figure 4 elsewhere and the “Catch 22” implication noted therein.

⁴⁶ Noteworthy here is that poisoning experiments, with ligands such as CS_2 , PPh_3 , and thiophene, are not expected to be useful in cases such as the present higher temperature benzene reduction catalysis since their exothermic binding and insufficiently strong binding constants tend to cause these ligands to dissociate above 50 °C.² That said, it should be possible to find and develop other, polydentate poisons analogous to 1,10-phenanthroline as needed for future quantitative poisoning studies aimed at distinguishing single metal from polymetallic catalysts.

⁴⁷ Maxted, E.B. *Adv. Catal.* **1951**, 3, 129.

⁴⁸ The one alternative hypothesis that we can think of is that *if* the 1,10-phenanthroline binding constant of the Rh₄ clusters was orders of magnitude larger than the binding constant of the Rh(0)_n nanoparticles, *then* it would be conceivable that all the added 1,10-phenanthroline poison could be bound first by the Rh₄ clusters, with no poisoning reaching the (in this case hypothesized, true) Rh(0)_n catalyst until the 1,10-phenanthroline binding capacity of the Rh₄ clusters had been saturated. While both less consistent with the observed binding curves (as argued in the text) as well as physically unlikely, we believe, this possibility is being investigated via a more detailed, quantitative model and mechanistic analysis of the poisoning data designed to uncover the relative 1,10-phenanthroline binding constants of the Rh₄ and Rh(0)_n catalysts. A preliminary quantitative analysis as part of that work supports what the curves themselves already suggest, namely, that if anything, the 1,10-phenanthroline binding constant for the Rh₄ appears to be smaller, not larger, than that for the Rh(0)_n nanoparticles .

APPENDIX-B

SUPPORTING INFORMATION FOR:

IS IT HOMOGENEOUS OR HETEROGENEOUS CATALYSIS DERIVED FROM
[RhCp*Cl₂]₂? *IN-OPERANDO* XAFS, KINETIC AND CRUCIAL KINETIC POISONING
EVIDENCE FOR SUBNANOMETER Rh₄ CLUSTER-BASED BENZENE
HYDROGENATION CATALYSIS

GC-MS Experiment Showing Cp* Ligand Loss from [RhCp*Cl₂]₂ via Observation of the Resultant Cp*-H and Its Hydrogenation Products. Two separate GC-MS samples were analyzed: the first sample was prepared after performing a “Standard Conditions Benzene Hydrogenation with [RhCp*Cl₂]₂” as detailed in the Experimental section of the main text. When the reduction of benzene was complete in ~6 h (via cessation of H₂ uptake and as judged by ¹H-NMR), the reactor was cooled to room temperature, then taken into a drybox and opened. The solution was filtered twice through (two separate) small silica plugs, and then placed in a separate capped amber vial for GC-MS analysis. The second sample was prepared via the same procedure but with a longer reaction time, 11 h. The only difference between two measurement is the ratio of Cp* hydrogenated products by GC-MS: ca. 42% after ~6 h of reaction, ca. 73% after 11 h of reaction.

The GC-MS analyses were performed as detailed previously:¹ The GC-MS standard of 1,2,3,4,5-pentamethyl-1,3-cyclopentadiene was prepared using 31 μL (0.202 mmol) of 1,2,3,4,5-pentamethyl-1,3-cyclopentadiene (Aldrich 95%) in 4.0 mL (44.8 mmol) benzene, 0.41 ml (2.94 mmol) triethylamine, and 36 mL 2-propanol under red light due to the light sensitivity of 1,2,3,4,5-pentamethyl-1,3-cyclopentadiene. After mixing the solution, aliquot was placed in a capped amber vial. Also, benzene, cyclohexane, 2-propanol, and triethylamine were individually placed in a capped vial for GC-MS measurements to confirm that impurities in the substrate, solvent, or base did not cause the observed GC-MS peaks in the GC-MS standard of 1,2,3,4,5-pentamethyl-1,3-cyclopentadiene.

Agilent 6890 GC and Agilent 5973N Mass Selective Detector were employed for the measurement. A SPBTM-1 capillary column (30 m x 0.25 mm x 0.25 μm film thickness) was used for GC. The mass spectrometry data was collected after electron ionization at 70 eV and

signals were given in m/z with relative intensity (%) in brackets (Table SI-B1). The percent yields were determined by quantization of the hydrogenated products of Cp* using the “effective carbon number” (ECN) method.²

Table SI-B1. GC-MS data. The hydrogenated products of Cp* are listed in the order of their retention times. The percentages shown in brackets (%) are relative peak intensities vs. the base peak. The in situ formation of triisopropyl borate,^{3,4,5} formed from the reaction of 2-propanol (solvent) and boron (in the glassware), was also observed in the reaction sample as previously reported^{3,4,5} (at 10 mins with a base peak of 45).

Entry	Sample	Time (min)	M ⁺ (%)	Fragmentation Peaks (%) [Assigned Cation Composition]				
	Standard							
1	1,2,3,4,5-pentamethyl-1,3-cyclopentadiene	15.4	136 (61)	121 (100) [M-CH ₃]	105 (45) [M-C ₂ H ₇]	91 (21) [M-C ₃ H ₉]	79 (16) [M-C ₄ H ₉]	
	Reaction Sample							
2	1,2,3,4,5-pentamethyl-cyclopentane	10.5	140 (20)	125 (10) [M-CH ₃]	84 (100) [M-C ₄ H ₈]	69 (88) [M-C ₅ H ₁₁]	55 (19) [M-C ₆ H ₁₃]	41 (19) [M-C ₇ H ₁₅]
3	1,2,3,4,5-pentamethyl-cyclopentane	12.5	140 (5)	123 (5) [M-CH ₅]	84 (100) [M-C ₄ H ₈]	69 (56) [M-C ₅ H ₁₁]	55 (15) [M-C ₆ H ₁₃]	41 (15) [M-C ₇ H ₁₅]
4	1,2,3,4,5-pentamethyl-cyclopentane	12.8	140 (4)	123 (4) [M-CH ₅]	84 (100) [M-C ₄ H ₈]	69 (58) [M-C ₅ H ₁₁]	55 (15) [M-C ₆ H ₁₃]	41 (15) [M-C ₇ H ₁₅]
5	1,2,3,4,5-pentamethyl-cyclopentene	14.0	138 (23)	123 (100) [M-CH ₃]	95 (7) [M-C ₃ H ₇]	91 (9) [M-C ₅ H ₁₁]	81 (32) [M-C ₄ H ₉]	67 (16) [M-C ₅ H ₁₁]
6	1,2,3,4,5-pentamethyl-1,3-cyclopentadiene	14.6	136 (70)	121 (100) [M-CH ₃]	105 (38) [M-C ₂ H ₇]	91 (22) [M-C ₃ H ₉]	77 (15) [M-C ₄ H ₁₁]	45 (32) [M-C ₇ H ₇]
7	1,2,3,4,5-pentamethyl-cyclopentane	16.1	140 (1)	123 (3) [M-CH ₅]	84 (100) [M-C ₄ H ₈]	69 (88) [M-C ₅ H ₁₁]	55 (18) [M-C ₆ H ₁₃]	41 (11) [M-C ₇ H ₁₅]

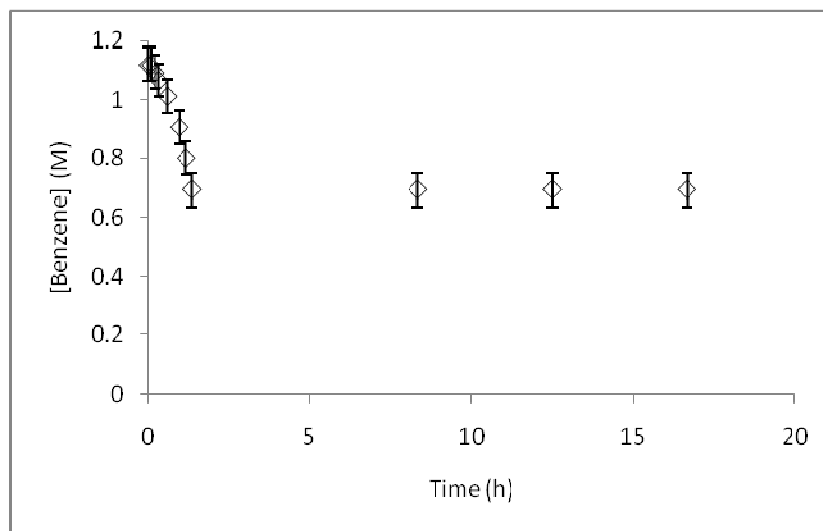
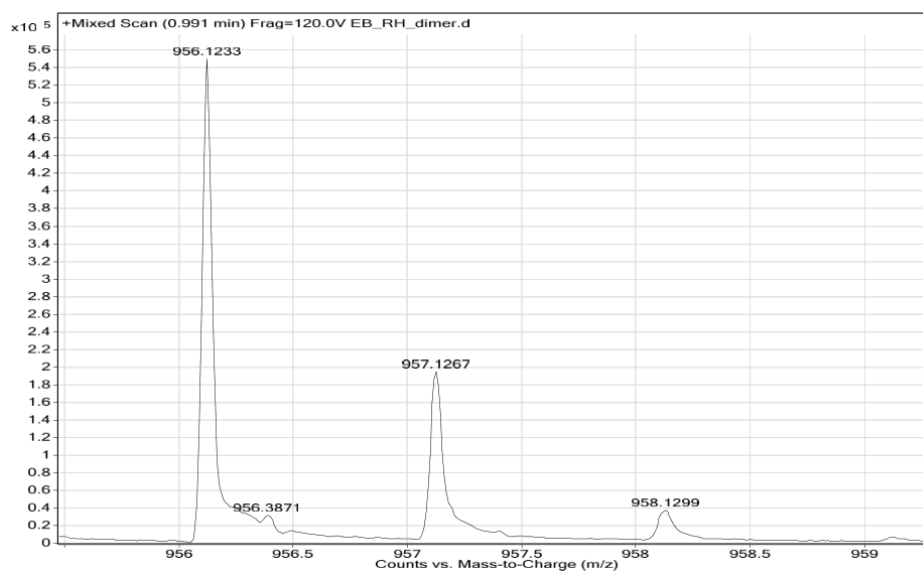


Figure SI-B1. Plot of benzene concentration vs time for a Hg(0) poisoning experiment. A Standard Conditions benzene hydrogenation with $[\text{RhCp}^*\text{Cl}_2]_2$ was started and allowed to proceed to 1/3 completion (i.e., ~2 h). At that point, ~300 equivs of Hg(0) per equiv of Rh was added, and the reaction was resumed by repressurizing with H_2 plus vigorous stirring, as detailed in the Experimental section. As the data reveal, the Hg(0) completely halted the catalytic activity over the 15 h the reaction was monitored.



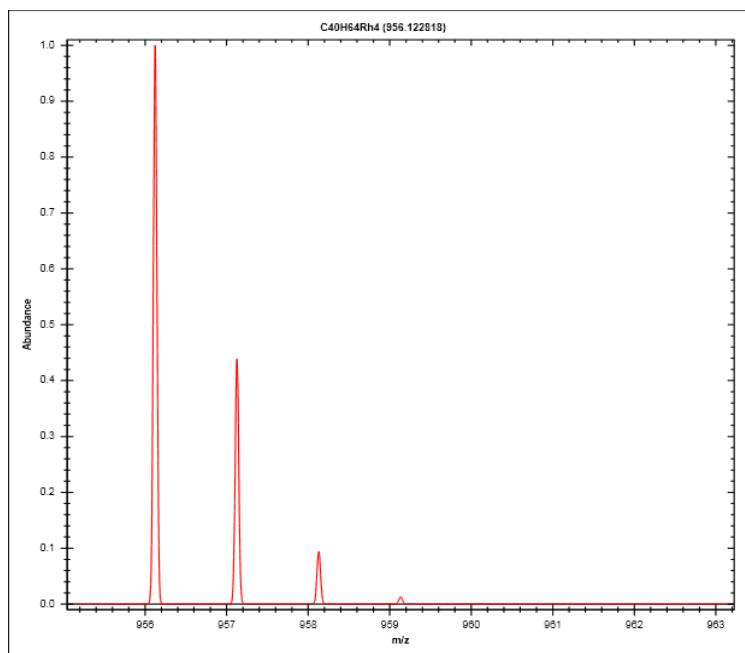


Figure SI-B2. The FAB-MS investigation of the rhodium product solution post the complete reduction of benzene after ~6 h revealed a molecular ion peak at $m/z = 956$ (top) attributable to fully, four Cp*-ligated $[\text{Rh}_4\text{Cp}^*_4\text{H}_4]^+$ with an excellent match to the calculated, theoretical isotope distribution pattern for $[\text{Rh}_4\text{Cp}^*_4\text{H}_4]^+$ (bottom spectrum in comparison to the top spectrum). Observed isotope distribution and ratios to the base peak at 956.1233 (given in parenthesis) are: 956.1233 (100); 957.1267 (44); 958.1299 (9.5); 959.1331 (1.3). Simulated isotope distribution of $[\text{Rh}_4\text{Cp}^*_4\text{H}_4]^+$ and ratios to the base peak at 956.1228 (given in parenthesis) are: 956.1228 (100); 957.1262 (44); 958.1296 (9.45); 959.1330 (1.3). The other, small signals at 960 and 962 (not shown) have very low ratios compared to the base peak, 0.13 and 0.01, respectively.

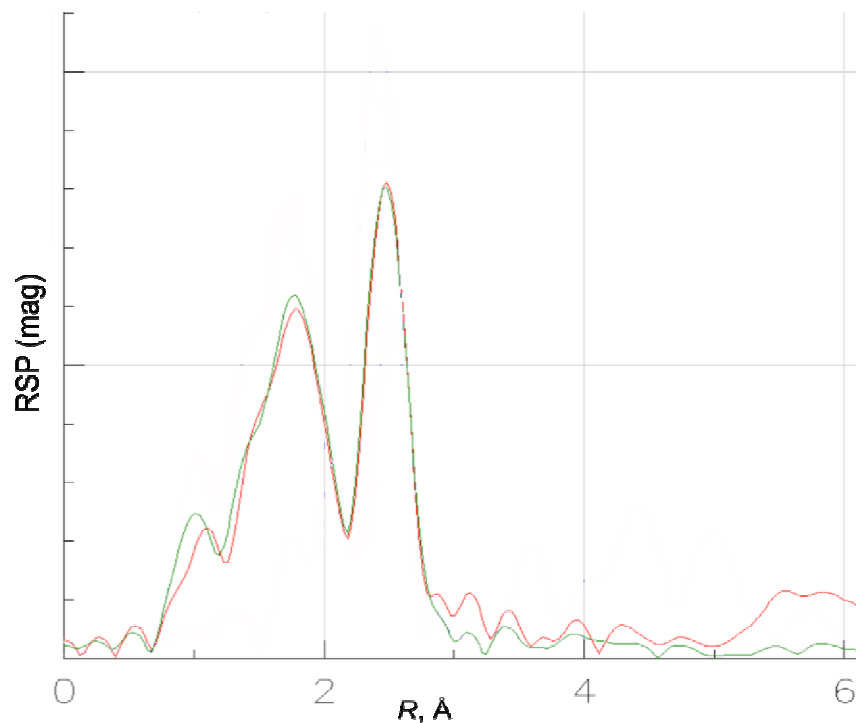
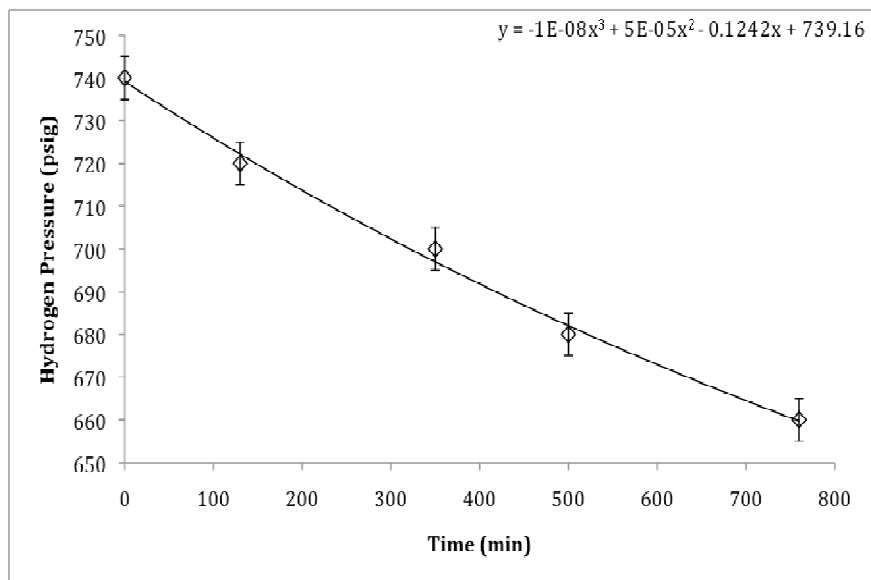
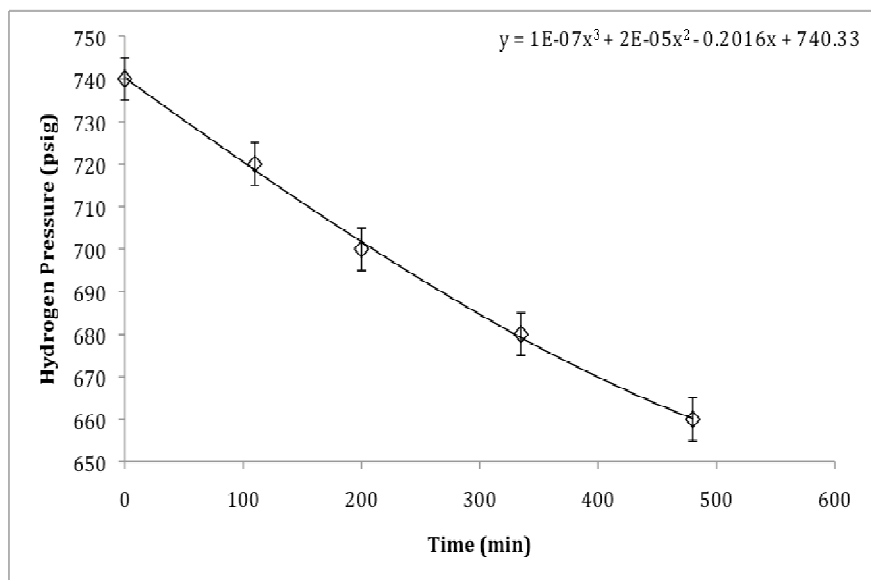


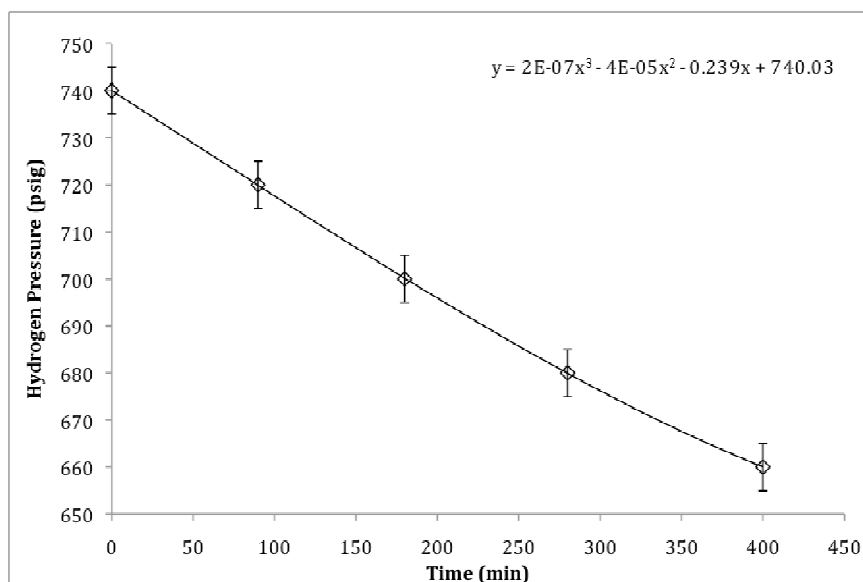
Figure SI-B3. In order to obtain the higher signal-to-noise needed to search carefully for trace species, 4-fold more $[\text{RhCp}^*\text{Cl}_2]_2$ was employed in the PNNL XAFS investigations compared to the CSU studies. However, both investigations yielded *identical* EXAFS spectrum (PNNL: 4-fold higher concentration conditions: green line; CSU concentration conditions: red line) other than the expected higher signal-to-noise at the 4-fold higher $[\text{RhCp}^*\text{Cl}_2]_2$ concentration. Note that $\text{Rh}(0)_n$ nanoparticles are not apparent in the $>3\text{\AA}$ region where they would have appeared if detectable.



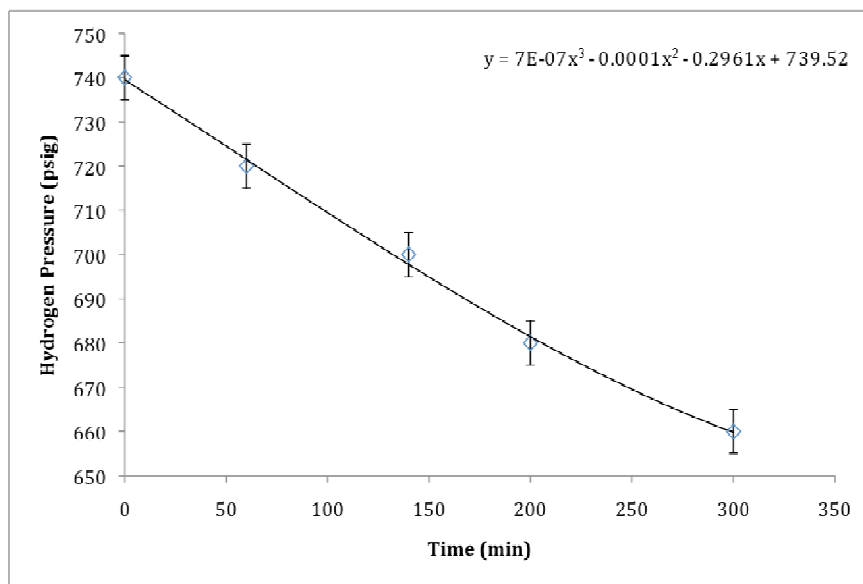
(a)



(b)



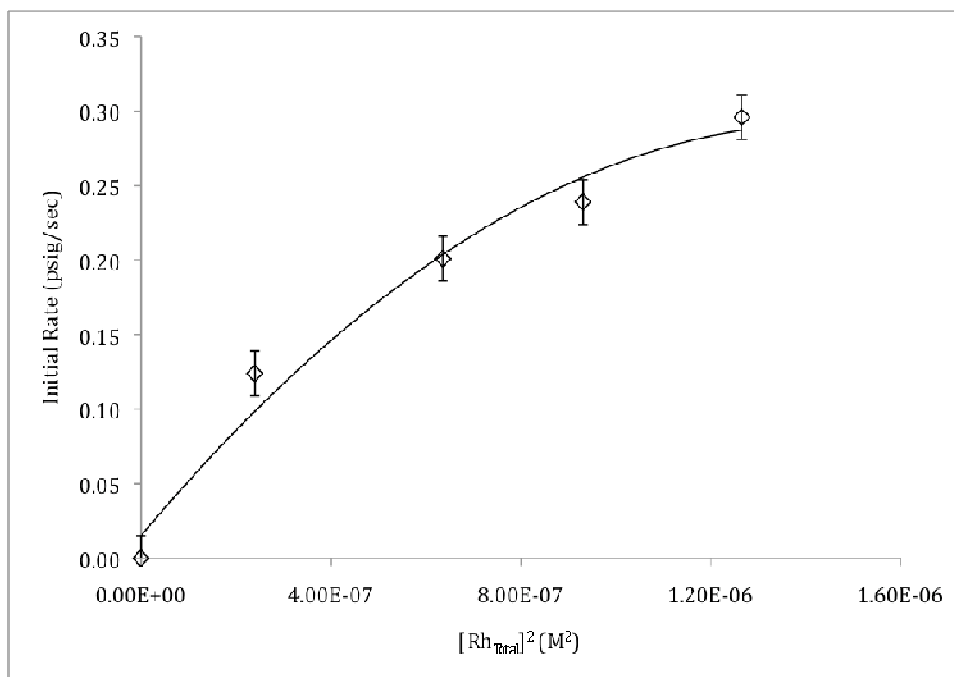
(c)



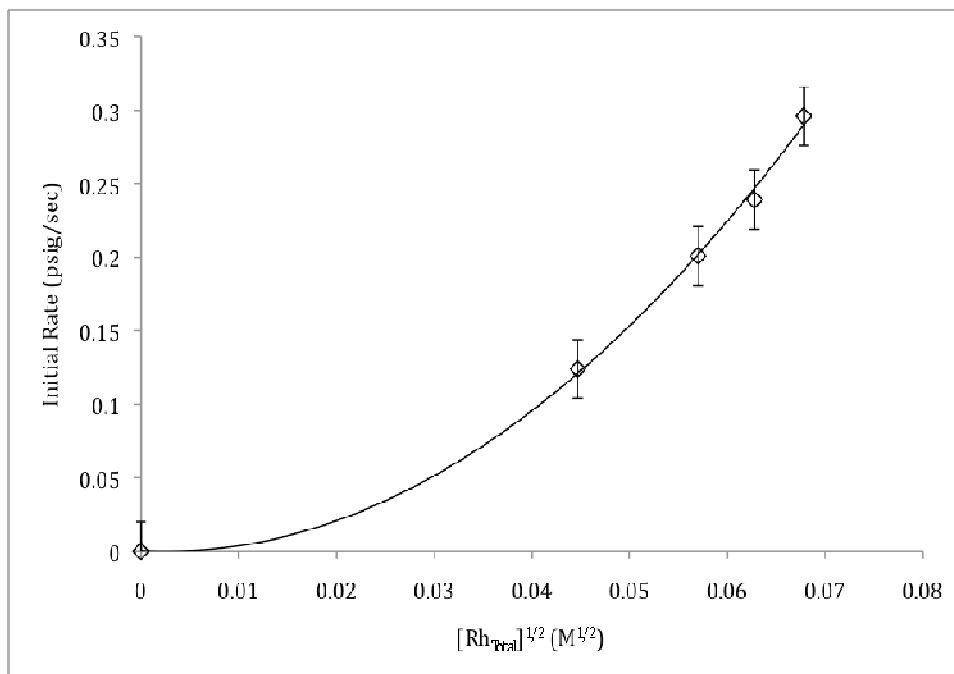
(d)

Figure SI-B4. Plots of benzene hydrogenation data (\diamond) and their 3rd degree polynomial fit (—) with the equation provided within each graph. A “Standard Conditions Benzene Hydrogenation with $[\text{RhCp}^*\text{Cl}_2]_2$ ” was repeated four times, but starting with different initial amounts of $[\text{RhCp}^*\text{Cl}_2]_2$ of (a) 27.2, (b) 44.3, (c) 53.5, (d) 62.5 mg. In these 4 separate experiments, the following procedure was used at the end of the benzene hydrogenation: the remaining H_2 pressure was released, the reactor was cooled, taken into the drybox, and opened. Then, 4.0 mL

(44.8 mmol) of fresh benzene was added. The reactor was resealed and removed from the drybox, stirring was started at 600 rpm, equilibrated at 100 °C, and pressurized to 740 psig (50 atm) with H₂. At this point the collection of pressure vs time data was started. The method of initial rates was used to analyze the kinetic data as detailed in the main text. Briefly, the derivative of the fitted polynomial equation for each experiment was evaluated at $t = 0$, yielding the initial rate for that experiment from the coefficient of the second, t^1 term of the polynomial.



(a)



(b)

Figure SI-B5. Initial rate with respect to (a) $[\text{Rh}_{\text{Total}}]^2$ and (b) $[\text{Rh}_{\text{Total}}]^{1/2}$ yielding a concave and convex non-linear curves, respectively. The non-linearity of these plots argues against second- and half-order dependences in the $[\text{Rh}_{\text{Total}}]$, respectively.

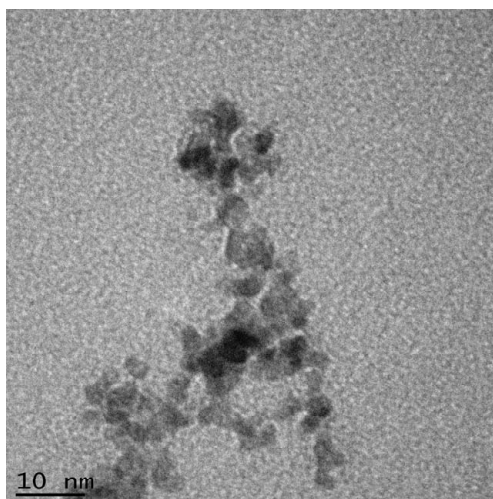


Figure SI-B6. TEM of a grid dipped into the product solution in the drybox post the complete hydrogenation of benzene starting with ca. 2 nm authentic, polyethyleneglycol-dodecylether

hydrosol stabilized $\text{Rh}(0)_n$ nanoparticles. The above image shows somewhat agglomerated, 2-3 nm $\text{Rh}(0)_n$ nanoparticles.

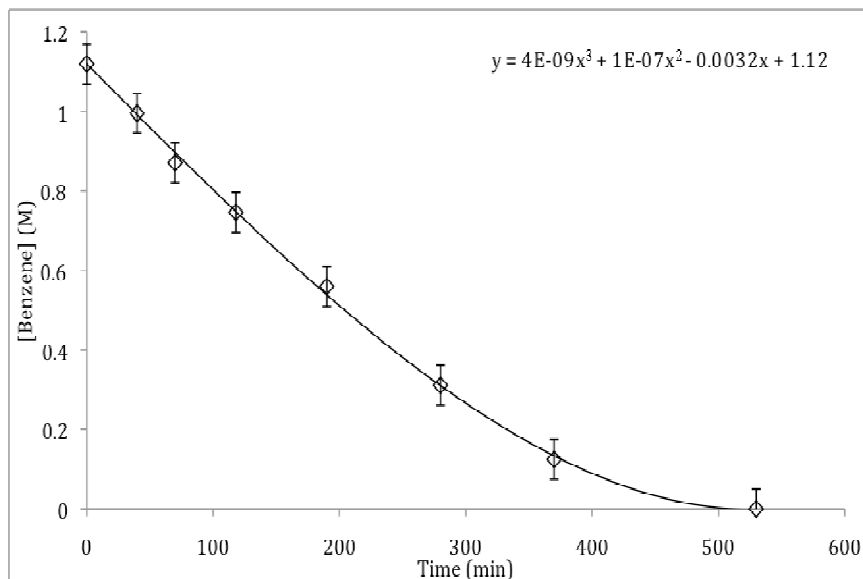
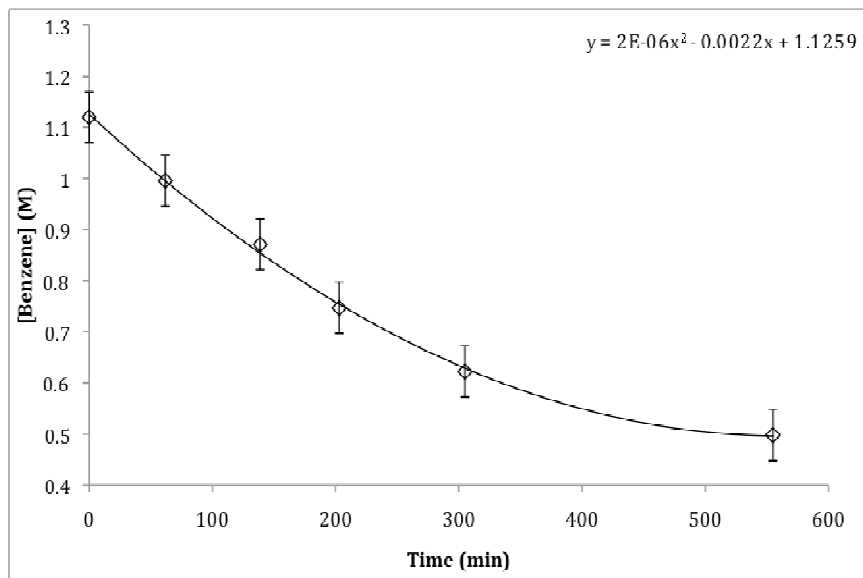
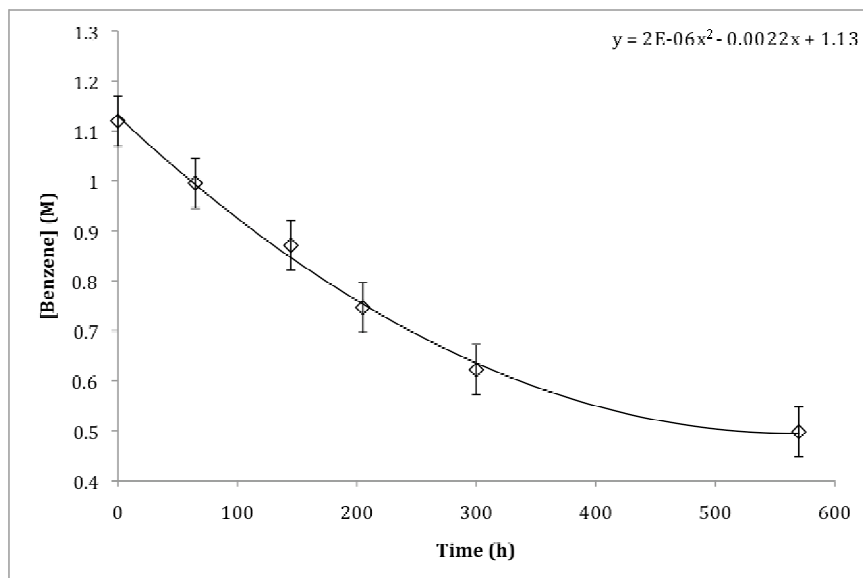


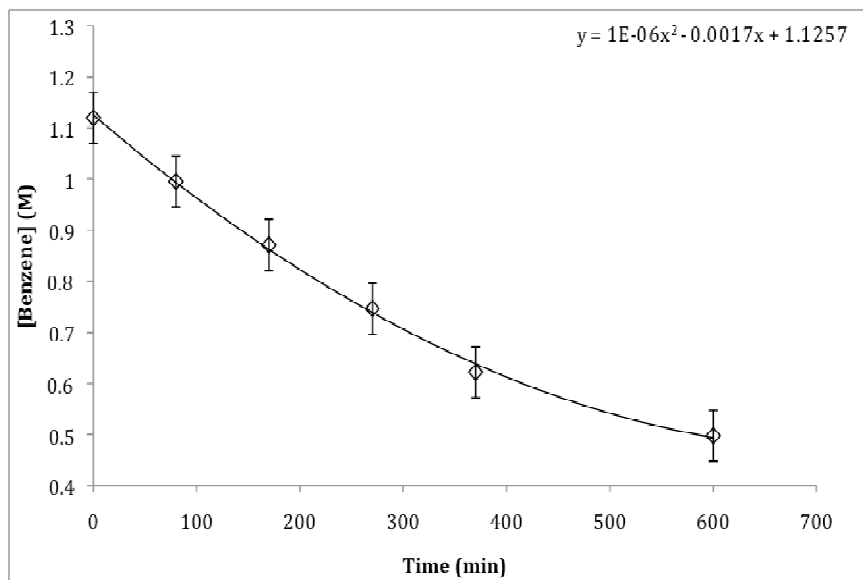
Figure SI-B7. Benzene hydrogenation starting with polyethyleneglycol-dodecylether hydrosol stabilized $\text{Rh}(0)_n$ nanoparticles in an amount corresponding to just 2% of the total rhodium present (i.e., $4.04 \mu\text{mol}$, 4.6 mg of polyethyleneglycol-dodecylether hydrosol stabilized $\text{Rh}(0)_n$ nanoparticles) under otherwise “Standard Conditions”. The polynomial fit (—) of the data (\diamond) yielded an initial rate of $\{-d[\text{Benzene}]/dt\}_{\text{in}} = 0.0032 \text{ M/min}$, that is ~ 1.6 fold faster than the initial rate of $\{-d[\text{Benzene}]/dt\}_{\text{in}} = 0.0023 \text{ M/min}$ for the $98 \pm 2\%$ solution of Rh_4 clusters.



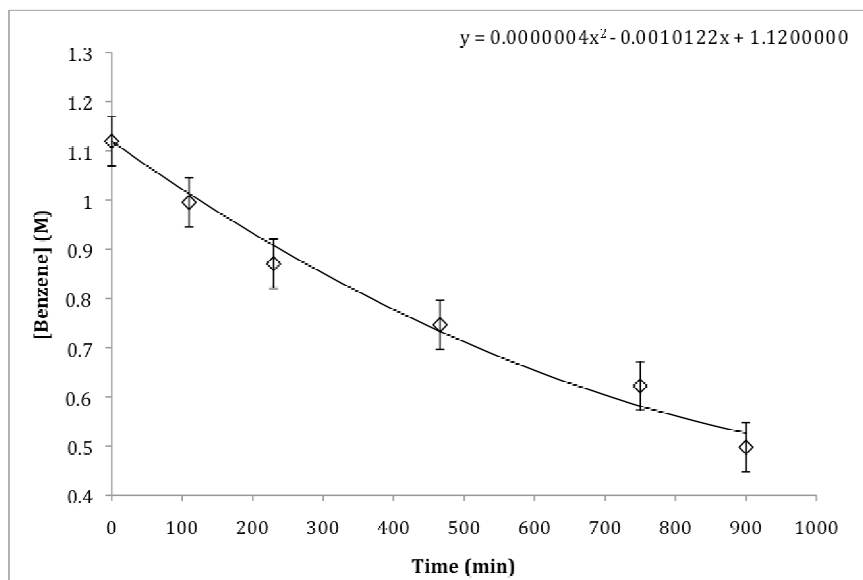
(a)



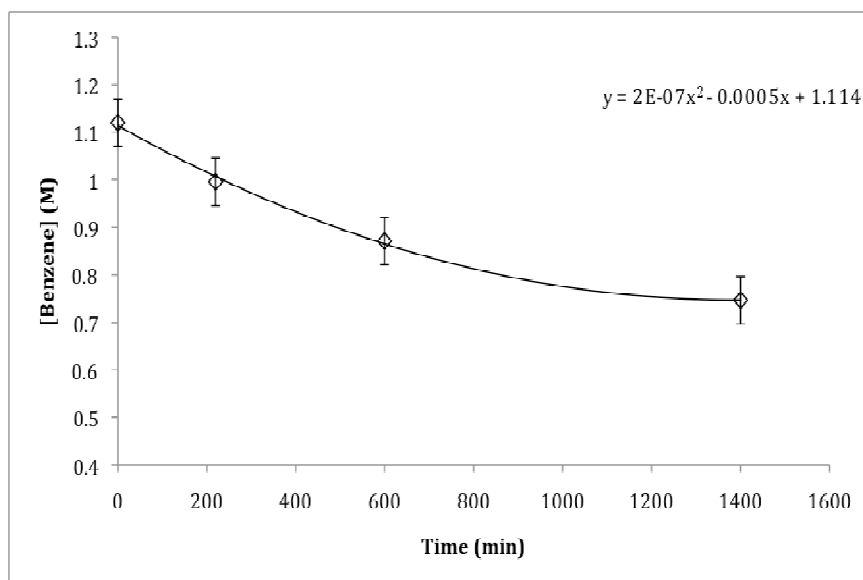
(b)



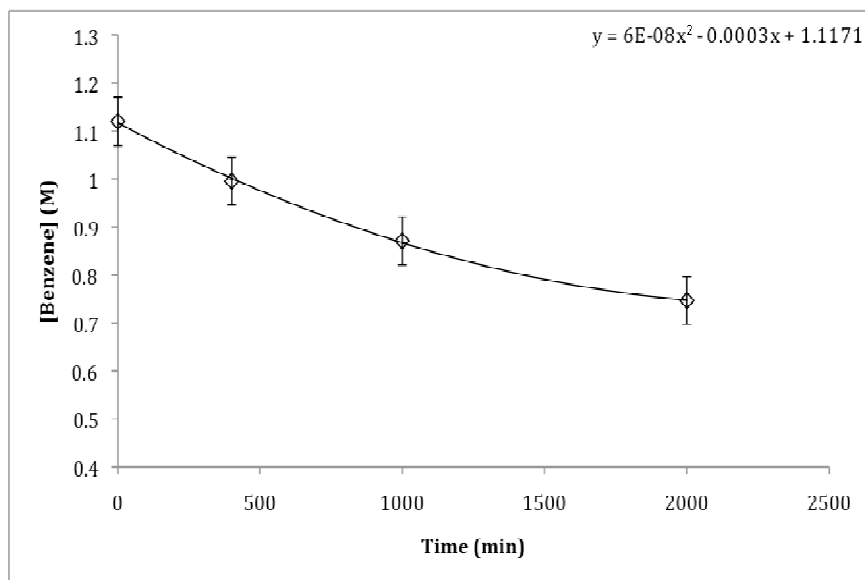
(c)



(d)



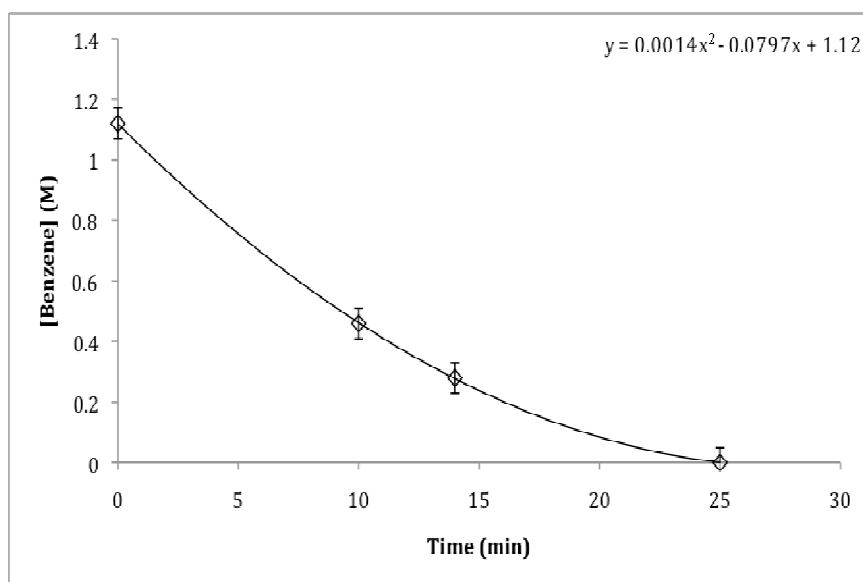
(e)



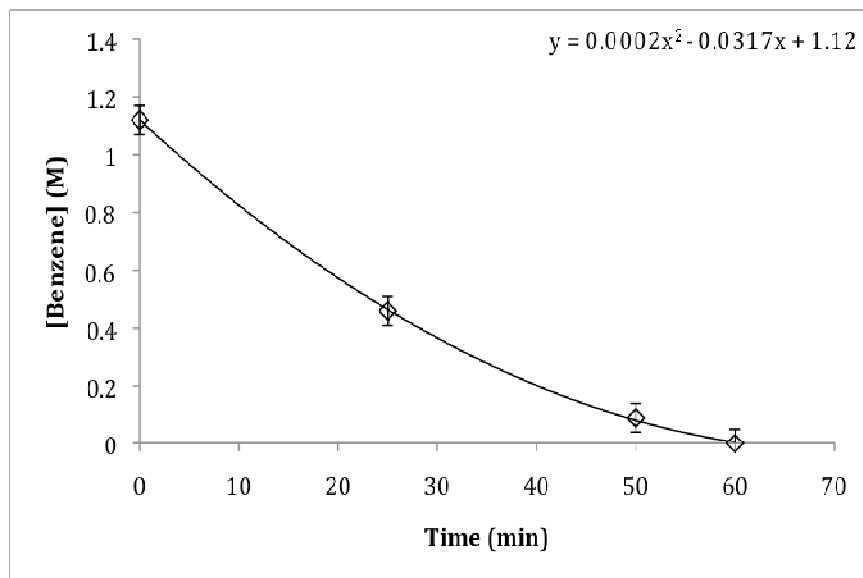
(f)

Figure SI-B8. Plots of benzene hydrogenation poisoning reaction data (\diamond) with 1,10-phenanthroline and their 2nd degree polynomial fit (—) with the equation provided within each graph. For each quantitative poisoning experiments with 1,10-phenanthroline, a separate “Standard Conditions Benzene Hydrogenation with $[\text{RhCp}^*\text{Cl}_2]_2$ ” was started. When the reaction was completed the reactor was vented, cooled to room temperature, taken into the drybox, and opened (at this time, $98 \pm 2\%$ of the total Rh in solution is, on-average, ligated Rh_4 clusters with

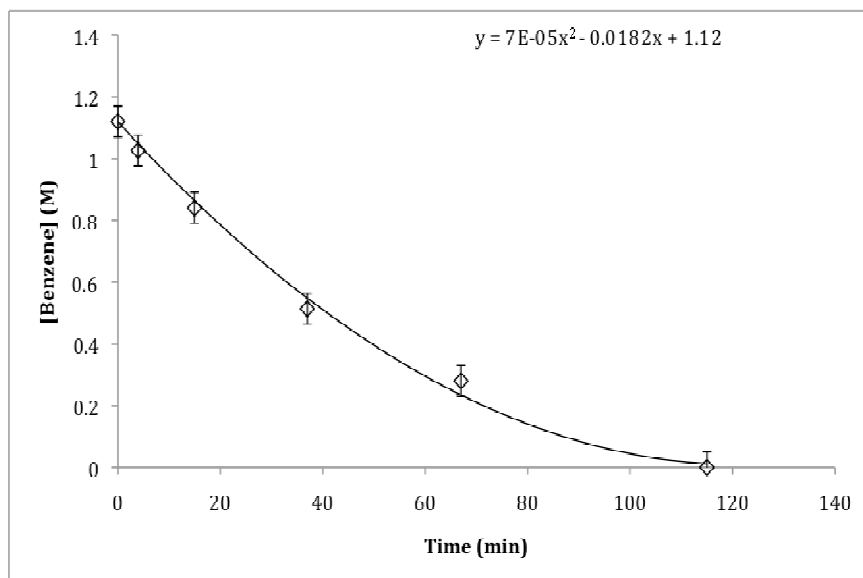
$\leq 2\%$ undetected soluble Rh species via XAFS). Next, a quantitative, predetermined amount of 1,10-phenanthroline was added to the solution; (a) 0.02, (b) 0.5, (c) 1, (d) 2, (e) 4, and (f) 5 equivs per total Rh (i.e., 0.7, 18.2, 36.4, 72.8, 145.6, and 182 mg, respectively). The reactor was then resealed, brought out of the drybox, equilibrated at 100 °C, and repressurized to 740 psig (50 atm) with H₂. At this point the collection of pressure vs time data was started and the corresponding hydrogenation plots are given above in the order of (a) 0.02, (b) 0.5, (c) 1, (d) 2, (e) 4, and (f) 5 equivs 1,10-phenanthroline added per total Rh (i.e., 0.0, 0.7, 18.2, 36.4, 72.8, 145.6, and 182 mg, respectively). The method of initial rates was used to analyze the kinetic data as detailed in the main text. Briefly, the derivative of the fitted polynomial equation for each experiment was evaluated at $t = 0$, yielding the initial rate for that experiment from the coefficient of the second, t^1 term of the polynomial.



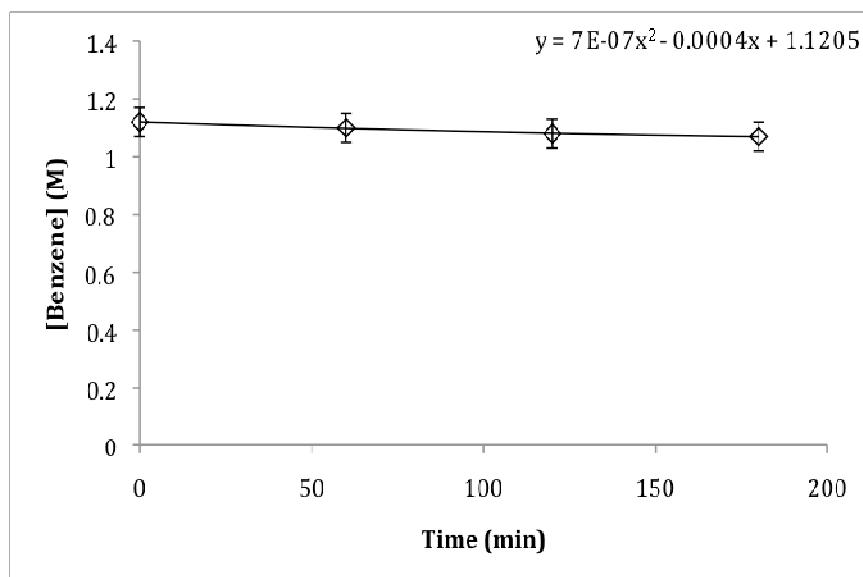
(a)



(b)



(c)



(d)

Figure SI-B9. Plots of benzene hydrogenation poisoning reaction data (\diamond) with 1,10-phenanthroline and their 2nd degree polynomial fit (—) with the equation provided within the graph. For each quantitative poisoning experiment with 1,10-phenanthroline, a separate “Benzene Hydrogenation Reaction Starting with Polyethyleneglycol-dodecylether hydrosol Stabilized Rh(0)_n Nanoparticles” was performed, as detailed in the main text Experimental section, except for one change: a quantitative, predetermined amount of 1,10-phenanthroline was added to the initial solution. Specifically, (a) 0.05, (b) 0.1, (c) 0.2, and (d) 0.3 equivs 1,10-phenanthroline (i.e., 1.8, 3.6, 7.2, and 10.8 mg, respectively) per total Rh was added in the separate poisoning experiments. The method of initial rates was used to analyze the kinetic data as detailed in the main text. Briefly, the derivative of the fitted polynomial equation for each experiment was evaluated at $t = 0$, yielding the initial rate for that experiment from the coefficient of the second, t^1 term of the polynomial.

REFERENCES

¹ Hagen, C.M.; Widegren, J.A.; Maitlis, P.M.; Finke, R.G. *J. Am. Chem. Soc.* **2005**, *127*, 4423.

² For details, see: Grob, R.L.; Editor *Modern Practice of Gas Chromatography, Third Edition*, 1995.

³ Swain, C.G.; Okamoto, Y. *J. Am. Chem. Soc.* **1970**, *92*, 3409.

⁴ Sancier, K.M. *J. Phys. Chem.* **1957**, *61*, 1127.

⁵ Porter, R.P. *J. Phys. Chem.* **1957**, *61*, 1260.

CHAPTER VI

A MONONUCLEAR ZEOLITE-SUPPORTED IRIIDIUM CATALYST: KINETIC, SPECTROSCOPIC, ELECTRON MICROSCOPIC, AND SIZE-SELECTIVE POISONING EVIDENCE FOR AN ATOMICALLY DISPERSED TRUE CATALYST AT 22 °C

This dissertation chapter presents a manuscript submitted for publication with co-authors Lu, J.; Aydin, C.; Uzun, A.; Browning, N.D.; Gates, B.C.; Finke, R.G. This chapter presents the identification of a mononuclear, atomically dispersed, zeolite-supported iridium catalyst via kinetic, post-catalysis XAFS, post-catalysis HAADF-STEM, and size-selective and quantitative phosphorus-based poisoning evidence.

All the experiments were performed by first author Ercan Bayram except the synthesis and characterization of the starting material ($[\text{Ir}(\text{C}_2\text{H}_4)_2/\text{zeolite Y}]$), and post-catalysis XAFS and post-catalysis HAADF-STEM investigations which were done by our collaborators Professor Bruce C. Gates and coworkers at University of California, Davis (UCD). Those co-authors also wrote the XAFS and HAADF-STEM sections of the manuscript, specifically all the XAFS data analyses and interpretations as well as diffusion-limitation calculations according to Thiele model.

The drafts of the complete manuscript were written by Ercan Bayram with the aid of Jing Lu, Ceren Aydin, and Alper Uzun for XAFS and HAADF-STEM analyses and interpretations. The

final manuscript on this system was prepared via 24 versions via editing by Professors Bruce C. Gates and Richard G. Finke.

Overview

This work addresses the question of what is the true catalyst when beginning with a site-isolated, atomically dispersed precatalyst for the prototype catalytic reaction of cyclohexene hydrogenation in the presence of cyclohexane solvent: is the atomically dispersed nature of the zeolite-supported, $[\text{Ir}(\text{C}_2\text{H}_4)_2]/\text{zeolite Y}$ precatalyst retained, or are possible alternatives including Ir_4 clusters and subnanometer or larger, $\text{Ir}(0)_n$, nanoparticle catalysts formed, for example? Determining the true catalyst in a given catalyst system is a forefront topic in catalysis because the activity, selectivity, stability, lifetime, recovery, regeneration, and poisoning all depend on the identity of the true catalyst. Reported herein are kinetic, post-catalysis extended X-ray absorption fine structure (EXAFS) spectra, post-catalysis high-angle annular dark-field scanning transmission electron microscopy (HAADF-STEM) images, size-selective $\text{P}(\text{C}_6\text{H}_{11})_3$ and $\text{P}(\text{OCH}_3)_3$, as well as quantitative $\text{P}(\text{OCH}_3)_3$ -based kinetic poisoning evidence that the true cyclohexene hydrogenation catalyst, when beginning with site-isolated $[\text{Ir}(\text{C}_2\text{H}_4)_2]/\text{zeolite Y}$ in contact with cyclohexene plus cyclohexane solution at 22 °C, is a supported mononuclear species, $[\text{Ir}_1]/\text{zeolite Y}$, in which the single-metal-atom nature of the precatalyst is retained with no detectable leaching of catalytically active iridium species into the reactant solution. Overall, this study (i) provides compelling evidence that the use of a site-isolated $[\text{Ir}(\text{C}_2\text{H}_4)_2]/\text{zeolite Y}$ precatalyst allows a site-isolated $[\text{Ir}_1]/\text{zeolite Y}$ hydrogenation catalyst to be retained even when in contact with solution, at least at 22 °C; (ii) allows a comparison of the current solid-solution catalyst system to our prior studies examining $[\text{Ir}(\text{C}_2\text{H}_4)_2]/\text{zeolite Y}$ in solid-gas-phase ethylene hydrogenation catalysis at room temperature; and (iii) develops and illustrates the necessary methodology—namely, the use of multiple, complementary physical methods plus the necessary kinetic, size-selective poisoning, and quantitative kinetic poisoning studies—needed to identify

the true catalyst in this and related systems. This study (iv) also is, to our knowledge, the first example presenting compelling evidence fully supporting the identification of an atomically dispersed, supported transition-metal species (in the present case, mononuclear $[\text{Ir}_1]/\text{zeolite Y}$) as the true catalyst, in the present case in a reaction performed in contact with a liquid phase.

Introduction

Identification of the true, catalytically active species in a given catalytic system is a forefront research topic in catalysis.^{1,2,3,4,5,6} Knowledge of the precise nature of the true catalyst is a central issue in modern chemical catalysis since the nature of the catalyst—to be distinguished from the form of the precatalyst—determines the catalytic activity, selectivity, stability as well as the recovery, regeneration, and poisoning properties of the actual catalyst. Knowledge of the true catalyst is also essential for obtaining strong, composition-of-matter patents. However, the true catalyst may be a minority component of the species formed from the precatalyst and, therefore, can be challenging to identify.¹

Among the simplest of supported catalysts are those consisting of mononuclear metal complexes on oxides or zeolites; they are an important class of industrial catalyst, finding application for olefin polymerization (Cr/SiO_2 , for example⁷) and for olefin epoxidation (silicalite with Ti in the framework providing the catalytic sites⁸). The topic of catalysis by supported mononuclear metal complexes, even complexes of noble metals, has drawn wide recent attention since researchers have come to recognize that they offer previously unanticipated catalytic properties,^{9,10,11} for example, for the water-gas shift reaction.^{12,13}

Subtle control of the catalytic properties of supported metal complexes can be exerted when the complexes are converted into small clusters and, further, into metal nanoparticles. For example, mononuclear iridium complexes can be reversibly converted into Ir_4 clusters by

treatment in H₂ at 80 °C,¹⁴ and under more severe conditions (i.e., at 400 °C for 8 h under 1 bar H₂), these clusters are converted into 1-nm-diameter nanoparticles.¹⁵ The catalytic activity for ethylene hydrogenation increases markedly with increasing nuclearity of the supported species.¹⁵

In recent work at the University of California, Davis (UCD), one of our groups focused on structural characterization of well-defined, mononuclear iridium species supported on a zeolite, notably [Ir(C₂H₄)₂]/zeolite Y.^{16,17} Extended X-ray absorption fine structure (EXAFS) and infrared (IR) spectroscopies were employed to show^{14,18} that a mononuclear zeolite Y-supported iridium complex, abbreviated as Ir₁/zeolite Y, is the only detectable form of iridium produced from the precatalyst during ethylene hydrogenation at 25 °C in ethylene-H₂ mixtures in a plug-flow reactor. Hence, mononuclear Ir₁/zeolite Y was proposed as the leading candidate for the catalytically active species (i.e., appropriately ligated and as opposed to higher-nuclearity species).¹⁸ Remaining to be performed, however, were the needed kinetic and other studies to verify or refute the mononuclear Ir₁/zeolite Y hypothesis for the true catalyst in that gas-solid reaction system. Of note here as well is that that work was done without the benefit of atomic-resolution electron microscopy and that EXAFS spectra provide *average* structural information with substantial errors in metal–metal coordination numbers, *vide infra*, so that it remains possible that undetected minority species are actually the kinetically dominant catalyst.

Work at Colorado State University (CSU) includes a long history of investigations addressing the question of “Who is the true catalyst?” as well as the related question of “Is the catalysis homogeneous or heterogeneous?”^{1,2,3,19,20,21,22} For example, recently CSU work addressed²³ the question of the true benzene hydrogenation catalyst at 100 °C and 50 atm (ca. 740 psig) initial H₂ partial pressure when beginning with [RhCp*Cl₂]₂ as the precatalyst. In that study, *in-operando* EXAFS spectra showed that 98 ± 2% of the total, initial rhodium mass from the [RhCp*Cl₂]₂

transforms into ligated Rh₄ clusters (with the average formula of Rh₄Cp*_{2.4}Cl₄H_c) as the *only* ($\pm 2\%$) detectable rhodium species. In the end, quantitative 1,10-phenanthroline poisoning studies with both model, polyethyleneglycol-dodecyl ether hydrosol-stabilized Rh(0)_n nanoparticles (poisoned by 0.12 ± 0.02 equiv of 1,10-phenanthroline per total equiv of Rh present) and the Rh₄ clusters (poisoned by 4.0 ± 0.4 equiv of 1,10-phenanthroline per total equiv of Rh present) provided a very strong case that the *in-operando* EXAFS-observed Rh₄ clusters are indeed the true, catalytically active species of the benzene hydrogenation system. This conclusion followed even though control experiments with the model, 2–3 nm diameter Rh(0)_n nanoparticles revealed that if even 1.4% of the total Rh mass had evolved to such Rh(0)_n nanoparticles, then they would have been kinetically competent to carry 100% of the observed catalytic activity. This example illustrates, again, the well-known fact that trace species formed under the reaction conditions can be highly active catalysts.

In the work reported herein, we combine the complementary approaches of the UCD and the CSU research groups to answer the question of (i) “who is the true catalyst?” when beginning with the site-isolated, [Ir(C₂H₄)₂]/zeolite Y precatalyst, but now during the prototype catalytic reaction of cyclohexene hydrogenation, *in contact with cyclohexane solution* in a batch reactor, at 22 °C. Additional questions addressed in this work include: (ii) what are the dominant forms of the catalyst evolving from the solid [Ir(C₂H₄)₂]/zeolite Y in contact with solution, and does the presence of the liquid phase change that speciation when compared to our previously reported investigation of the gas-solid reaction, *vide supra*?¹⁸ (iii) Are, as expected, a synergistic combination of spectroscopy and microscopy, accompanied by kinetics as well as quantitative catalyst poisoning experiments, mandatory en route to identification of the true catalyst or catalysts?²³ In addition, (iv) it is of some interest to link the information about the working

catalyst determined by kinetics with the information available from post-catalysis *ex situ* EXAFS and HAADF-STEM methodologies employed herein? Do they tend to support or contradict each other?

One other premise of the work reported herein is that investigations of the formation of supported catalytic species, in contact with solution, may help transfer the synthetic and mechanistic insights that have emerged from investigations of nanoparticle formation *in contact with solution*^{24,25,26,27} to the synthesis of improved *supported* nanoparticle catalysts. We regard [Ir(C₂H₄)₂]/zeolite Y as an especially valuable starting material in this endeavor because of the monometallic nature and structural uniformity of [Ir(C₂H₄)₂]/zeolite Y, as well as the wealth of data now available characterizing its reactivity, albeit to date only in gas-solid reactions.^{18,28,29} Now, by investigating the reactivity of [Ir(C₂H₄)₂]/zeolite Y in contact with solution, we have the first opportunity²⁴ to examine and compare gaseous vs liquid environments for reactions, *vide infra*, for this well-characterized, site-isolated, atomically dispersed, zeolite Y-supported precatalyst system.

Hence, herein we present our collaborative investigation of the true cyclohexene hydrogenation catalyst when beginning with [Ir(C₂H₄)₂]/zeolite Y in contact with cyclohexane solution at 22 ± 0.1 °C and 40 ± 1 psig initial H₂ partial pressure. The key studies consist of (i) kinetics, (ii) post-catalysis EXAFS spectroscopy and HAADF-STEM, and (iii) size-selective poisoning experiments with P(C₆H₁₁)₃ and P(OCH₃)₃, and then (iv) quantitative kinetic poisoning experiments with P(OCH₃)₃. Overall, the results argue, we believe compellingly, for a mononuclear [Ir₁]/zeolite Y catalyst as opposed to possible higher-nuclearity species and catalysts.

In what follows, we first present the experimental details, as those details are important in order to be able to understand the studies which follow, which were performed at four different locations: UCD, CSU, and two synchrotrons, Brookhaven National Laboratory and Stanford Synchrotron Radiation Lightsource.

Experimental Methods and Data Analysis

Materials and General Considerations. *Precatalyst Syntheses at UCD.* Precatalyst syntheses and handling were performed with the exclusion of moisture and air. The highly dealuminated HY zeolite (DAY zeolite) (Zeolyst International, CBV760), with a Si:Al atomic ratio of approximately 30, was calcined in O₂ at 500 °C for 4 h and evacuated for 16 h at 500 °C. After calcination, the zeolite was isolated and stored in an argon-filled drybox (MBraun, with an H₂O concentration <0.5 ppm and an O₂ concentration <5 ppm as monitored by VAC monitors equipped with LM-H₂O-A and LM-O₂-A alarms). *n*-Pentane (Fisher, 99%) was dried and purified by column chromatography (Grubbs apparatus, MBraun SPS) in the presence of argon.

Cyclohexene Hydrogenation and Poisoning Experiments at CSU. Unless indicated otherwise, all manipulations were performed under N₂ in a Vacuum Atmospheres drybox. Oxygen concentrations were continuously maintained in the drybox at ≤5 ppm, monitored by a Vacuum Atmospheres O₂ monitor. Unless noted otherwise, all solvents, compounds, and other materials mentioned below were stored in the drybox. Cyclohexane (99.5%, anhydrous), P(OCH₃)₃ (≥99.999%), and P(C₆H₁₁)₃ were purchased from Aldrich and used as received. Cyclohexene (99%, inhibitor free) was distilled over sodium metal under argon or purified in a MicroSolv solvent purification system (Innovative Technology) equipped with an activated –Al₂O₃ column under N₂. H₂ gas was purchased from General Air (>99.5%) and was passed through a Trigon Moisture Trap and a Trigon Technologies Oxygen/Moisture Trap to remove O₂ and H₂O

followed by a Trigon Technologies High Capacity Indicating Oxygen Trap. The conversion of cyclohexene to cyclohexane was verified by ^1H -NMR spectra of a sample prepared by adding a drop of the resultant product solution into 1 mL CD_2Cl_2 (Cambridge Isotope Laboratories) and examined with a Varian INOVA-300 instrument, 300.115 MHz for ^1H (cyclohexene: 5.5 ppm (m), 2 ppm (m), 1.6 ppm (m); cyclohexane: 1.4 ppm (s)).

Sample Transport Between UCD and CSU. The exclusion of air/ O_2 was maintained by careful handling of the samples in an argon or N_2 atmosphere drybox. That is, the samples to be shipped to either CSU (for cyclohexene hydrogenation and poisoning experiments) or to UCD (for HAADF-STEM analysis and for preparation for transport to a synchrotron for EXAFS spectroscopy) were prepared in the drybox. The samples were placed into a stainless-steel Swagelok vacuum tube, the ends were clamped together, sealed with O-rings, and shipped to the other laboratory or to the synchrotron, where the vacuum tube was opened in a drybox and prepared for the reactions or analyses, vide infra.

Synthesis and Characterization of $[\text{Ir}(\text{C}_2\text{H}_4)_2]/\text{Zeolite Y}$ containing 1 wt% Iridium.

$[\text{Ir}(\text{C}_2\text{H}_4)_2(\text{acac})]$ (acac = $\text{CH}_3\text{COCH}_2\text{COCH}_3$) was synthesized and characterized at UCD as described elsewhere³⁰ and slurried in dried *n*-pentane at ice temperature with the calcined zeolite powder in a Schlenk flask. The stirred slurry was warmed to room temperature and, after one day, the solvent was removed by evacuation over another day. The resultant solid, $[\text{Ir}(\text{C}_2\text{H}_4)_2]/\text{zeolite Y}$, containing 1 wt% iridium, was characterized¹⁶ by EXAFS, IR, and NMR spectroscopies and was stored in an argon-filled drybox.

Catalytic Hydrogenation Apparatus. All the hydrogenation reactions at CSU were carried out with the previously described, custom-built pressurized hydrogenation apparatus that allows monitoring of the pressure in real time (± 0.01 psig) as H_2 is consumed during the cyclohexene

hydrogenation reactions. The apparatus consists of a Fischer-Porter (F-P) bottle connected via its Swagelok TFE-sealed Quick Connects to a hydrogenation line and an Omega D1512 10V A/D converter with an RS-232 connection to a PC interface via LabView ver. 8.2.^{31,32,33} Once the pressure-transducer H₂ uptake data were obtained, the data were converted to cyclohexene loss data via the known 1:1 H₂:cyclohexene stoichiometry.¹⁹

Procedure for Cyclohexene Hydrogenation Reaction under Standard Conditions Starting with [Ir(C₂H₄)₂]/Zeolite Y. To begin with, at CSU inside the drybox, 25 ± 1 mg of [Ir(C₂H₄)₂]/zeolite Y (1 wt% Ir) was weighed in a 2-dram glass vial and then transferred into a new 22 × 175 mm Pyrex culture tube containing a new 5/16 × 5/8-in. Teflon-coated stir bar. Cyclohexane (2.5 mL) and cyclohexene (0.5 mL) were added via separate gastight syringes. The culture tube was sealed inside the F-P pressure bottle and brought outside of the drybox. The F-P bottle was placed into a constant-temperature circulating bath at 22 ± 0.1 °C and attached via Swagelok TFE-sealed Quick-Connects to the hydrogenation line (which had already been evacuated for at least 30 min to remove trace oxygen and water), then refilled with purified H₂ at 40 ± 1 psig (ca. 2.7 atm). Stirring at 600 rpm was started, the F-P bottle was then purged 10 times with H₂ (5 s in between purges), and the reaction was started and $t = 0$ designated. The foregoing statement defines the Standard Conditions cyclohexene hydrogenation reaction experiment.

When the H₂ uptake ceased according to the PC interfaced monitoring, the F-P bottle was disconnected from the hydrogenation line, the remaining H₂ pressure was released, and the F-P bottle was transferred back into the drybox. The resultant solution in the culture tube was transferred into a new 20-mL scintillation vial with a new 5/16 × 5/8-in. Teflon-coated stir bar and dried under vacuum for 8 h. This sample was sealed in a stainless-steel Swagelok-equipped

vacuum tube sealed with O-rings, brought out of the drybox, and shipped to UCD for characterization investigations.

The above Standard Conditions cyclohexene hydrogenation reaction was repeated five times, yielding the same initial rates and total reaction times within $\pm 10\%$.

A test for H₂ gas-to-solution, mass-transfer limitations (MTL) was performed by changing the stirring speed (450, 600, and 1000 rpm) for a Standard Conditions cyclohexene hydrogenation reaction, similar to tests for MTL performed previously.²¹ Specifically, a Standard Conditions cyclohexene hydrogenation reaction yielded the same initial H₂ uptake rates within $\pm 10\%$ experimental error when stirred at 450, 600, or 1000 rpm (see the Supporting Information for the data). This result indicates negligible H₂ gas-to-solution MTLs in the work reported herein.

A check was also made to see if there is any diffusion limitation within the pores of the catalyst. Calculations according to the Thiele model³⁴ were performed and indicate that there is a negligible diffusion resistance within the catalyst pores (the Thiele modulus is approximately 1, see the Supporting Information). Consequently, the rates of the catalytic reaction are without significant diffusion limitations, and report on the underlying, intrinsic chemistry. Details of the calculations are given in the Supporting Information.

Kinetic Data Treatment: Initial Rate Method. Initial rates were calculated from either the H₂ partial pressure (psig) loss vs time (h) or cyclohexene concentration (M) vs time (h) data by employing the initial rate method described elsewhere.³⁵ The resultant data were fit to a third-degree polynomial equation via GraphPad Prism software (version 5 for Mac OS X, GraphPad Software, San Diego, California USA, www.graphpad.com) with $R^2 > 0.990$. Then, the derivative of the third-degree polynomial was taken at time $t = 0$ yielding the initial rate (the t^1 term of the polynomial).³⁵

Experiments Demonstrating First-Order Dependence on the Starting Ir Complex, [Ir(C₂H₄)₂]/Zeolite Y, and Zero-Order Dependences on [Cyclohexene] and [H₂]. The details of these experiments at CSU are provided in the Supporting Information. Briefly, zero-order dependencies were observed for both [cyclohexene] and the H₂ partial pressure. Because the initial rate was found to be proportional to the mass of catalyst, the intrapore diffusion resistance is negligible as judged by a Thiele modulus calculation (see the Supporting Information), and since the evidence which follows is that the catalyst is atomically dispersed, the turnover frequencies (TOFs) are reported in a per-Ir atom form.

Subsequent Cyclohexene Hydrogenation. The details of this experiment are provided in the Supporting Information. Briefly, the total reaction times and initial rates were compared for an initial cyclohexene hydrogenation run and a subsequent cyclohexene hydrogenation run using that same catalyst solution but just adding more cyclohexene: ca. 12 h and $-\{d[\text{cyclohexene}]/dt\}_{\text{initial}} = 0.30 \text{ M/h}$ for the first run vs. ca. 14 h and $-\{d[\text{cyclohexene}]/dt\}_{\text{initial}} = 0.25 \text{ M/h}$ for the second run. The comparison indicates a small, ca. 16% catalyst deactivation between the first and second runs, as discussed further in the Results and Discussion section.

X-ray Absorption Spectroscopy. The X-ray absorption spectra were recorded at X-ray beamline X18-B of the National Synchrotron Light Source (NSLS) at Brookhaven National Laboratory (BNL) and at beamline 4-1 of the Stanford Synchrotron Radiation Lightsource (SSRL). The storage ring electron energy and ring current were ~3 GeV and 200–300 mA, respectively. Si(111) and Si(220) double-crystal monochromators were used at BNL and SSRL, respectively. Each monochromator was detuned to 80% of maximum intensity to reduce the interference of higher harmonics in the X-ray beam.

To minimize the exposure to air and moisture, each powder sample was placed in a glass vial and sealed with Parafilm inside the argon-filled drybox. Each glass vial was placed into a stainless-steel Swagelok-equipped vacuum tube sealed with O-rings for transfer to the synchrotron. The mass of each sample (approximately 0.3 g) was chosen to give an absorbance between 1.5 and 3.0 calculated at 50 eV above the Ir L_{III} edge (11215 eV). In an N₂-filled glovebox at the synchrotron, each sample was pressed into a wafer and mounted in a cell for transmission spectroscopy³⁶ and maintained under vacuum (at a pressure of 10⁻⁷ kPa) at liquid-nitrogen temperature during the data collection. X-ray intensity data were collected in transmission mode by use of ion chambers mounted on each end of the sample cell.

EXAFS Data Analysis. The X-ray absorption edge energy was calibrated with the measured signal of a platinum foil (scanned simultaneously with the sample) at the Pt L_{III} edge, which was taken to be the inflection point at 11564 eV. The data were normalized by dividing the absorption intensity by the height of the absorption edge.

Analysis of the EXAFS data was carried out with the software ATHENA of the IFEFFIT^{37,38} package and the software XDAP developed by Vaarkamp et al.³⁹ Each spectrum that was analyzed was the average of four spectra. ATHENA was used for edge calibration and deglitching. XDAP was used for background removal, normalization, and conversion of the data into an EXAFS (χ) file. A “difference-file” technique for shell isolation was applied with XDAP for determination of optimized fit parameters. A second-order polynomial was fit to the data in the pre-edge region and subtracted from the entire spectrum in each analysis. The functional that was minimized, and the function used to model the data, are given elsewhere.⁴⁰ The background was subtracted by using cubic spline routines. Reference backscattering phase shifts were calculated with the software FEFF7⁴¹ from crystallographic data. Ir(C₂H₄)₂(acac)³⁰ was used as

the reference for Ir–O_{support}, Ir–C, Ir–O_{long}, and Ir–C_{long} (the latter two being Ir–O and Ir–C contributions at distances longer than bonding distances); Ir–Al alloy⁴² was used for Ir–Al contributions, and iridium metal⁴² was used for Ir–Ir and Ir–Ir 2nd contributions. Iterative fitting was done in R (distance) space with the Fourier-transformed χ data until optimum agreement was attained between the calculated k^0 -, k^1 -, k^2 -, and k^3 -weighted EXAFS data and each postulated model (k is the wave vector). The number of parameters used in the fitting was always less than the statistically justified number, computed with the Nyquist theorem:⁴³ $n = (2\Delta k\Delta r/\pi) + 1$, where Δk and Δr are the k and r ranges used in the fitting, respectively, and r is the interatomic distance.

For each analysis of EXAFS data characterizing the sample, several candidate models were investigated that were selected on the basis of the expected and plausible contributions. We emphasize that attempts were made to include Ir–Ir contributions in each model to test for the presence/absence of iridium clusters. Each candidate model was compared with the data and evaluated on the basis of the goodness of fit for each individual shell and overall. The estimated errors in the reported coordination numbers and bond distances are $\pm 20\%$ and ± 0.02 Å, respectively. Details of all the EXAFS data analyses and fitting for each model are provided in the Supporting Information.

HAADF-STEM: Sample Handling, Instrumentation, and Analysis. To minimize the exposure to air and moisture, powder samples (prepared at UCD or shipped from CSU in a stainless-steel Swagelok vacuum tube, vide supra) were loaded onto a lacey carbon, 300-mesh copper grid (Ted-Pella) in the argon-filled drybox. The grid was packed in an Eppendorf tube and sealed with Parafilm inside the drybox. Each Eppendorf tube was placed into a stainless-steel Swagelok vacuum tube sealed with O-rings for transfer to the microscope facility. There, an

argon-filled glovebag (Glas-Col) was purged five times with ultra-high-purity argon (Praxair, Grade 5.0), and the TEM grid was loaded onto the TEM holder under the blanket of flowing argon in the glovebag. The TEM holder was then inserted into the microscope under flowing argon, with a time of possible exposure to air of <5 s. Prior to imaging of a sample, the aberration corrector was aligned with a Pt/Ir-on-hole-carbon standard sample (SPI Supplies) until atomic resolution of the metal particles was achieved and the lattice spacings of the metals were confirmed.

Images of the samples were obtained with a JEOL JEM-2100F electron microscope at UCD. The microscope was equipped with a field emission gun (FEG), operating at 200 kV, with a CEOS hexapole probe (STEM) aberration corrector. An HAADF detector with a collection semi-angle of 75–200 mrad and a probe convergence semi-angle of 17.1 mrad was used to capture the images. To minimize the artifacts in the images caused by beam damage, the microscope was aligned for one region of the sample, and then the beam was shifted to a neighboring region for a quick image acquisition: 5 s for a 512×512 pixel size.

Poisoning Experiments with Phosphine and Phosphite. *Size-selective poisoning studies using $P(OCH_3)_3$ and $P(C_6H_{11})_3$:* At CSU, two aforementioned cyclohexene hydrogenation reactions beginning with $[Ir(C_2H_4)_2]/zeolite\ Y$ were repeated at $22 \pm 0.1\ ^\circ C$, with one change: in two separate experiments, one equivalent of $P(OCH_3)_3$ or $P(C_6H_{11})_3$ per equiv of total iridium present (1.3×10^{-6} mol) was added to the initial reaction solutions in the separate experiments. For the $P(OCH_3)_3$ poisoning experiment, 0.15 μL of $P(OCH_3)_3$ was added via a 1- μL syringe to the initial 2.5 mL of cyclohexane plus 0.5 mL of cyclohexene solution mixed with 25 ± 1 mg of $[Ir(C_2H_4)_2]/zeolite\ Y$. For the $P(C_6H_{11})_3$ poisoning experiment, a stock solution was prepared by dissolving 0.4 mg of $P(C_6H_{11})_3$ in 10 mL of cyclohexane. Then, 0.1 mL of this stock solution

(i.e., 1 equiv of $P(C_6H_{11})_3$ per mol of Ir present) was added via a 1 mL syringe to the initial 2.5 mL of cyclohexane along with 0.5 mL of cyclohexene solution, all mixed with 25 ± 1 mg of $[Ir(C_2H_4)_2]/zeolite$ Y. Each size-selective poisoning experiment was repeated three times, yielding the same values of the initial reaction rate within $\pm 10\%$.

Quantitative $P(OCH_3)_3$ Poisoning Experiments: Three separate experiments were carried out at CSU as described in the aforementioned Standard Conditions reaction starting with $[Ir(C_2H_4)_2]/zeolite$ Y, except that a prechosen amount of $P(OCH_3)_3$ poison was added as follows. Specifically, a Standard Conditions reaction was started at 22 ± 0.1 °C; after 5 h, the F-P bottle was removed from the line, vented, and taken into the drybox where, then, one of 0.1, 0.4, or 0.7 equiv (1.3×10^{-7} , 5.2×10^{-7} , 9.1×10^{-7} mol, respectively) of $P(OCH_3)_3$ per equiv of total Ir were added in 3 separate, but otherwise identical, experiments. The addition of $P(OCH_3)_3$ was accomplished using a stock solution prepared by adding 0.15 μ L of $P(OCH_3)_3$ to 0.1 mL of fresh cyclohexane via a 1- μ L syringe. Then, 0.01, 0.04, and 0.07 mL (or, equally, 10, 40, and 70 μ L via 100 μ L syringe, respectively) of this stock solution was added to the F-P bottle that had been brought back into the drybox for the respective 0.1, 0.4, and 0.7 equiv of $P(OCH_3)_3$ poisoning experiments. (For each trial, a new stock solution was prepared.) The F-P bottle was then resealed, taken out of the drybox, and reconnected to the hydrogenation line. Stirring at 600 rpm was restarted, the F-P bottle was then again purged 10 times with H_2 (5 s in between purges), and then refilled with 40 ± 1 psig of H_2 . At this point, collection of pressure versus time data was continued (ignoring the ~ 1 h gap required for the procedure). Each quantitative poisoning experiment with $P(OCH_3)_3$ was repeated three times, yielding the same values of the initial reaction rate within $\pm 10\%$.

An additional control experiment, repeating the same procedure but without added $\text{P}(\text{OCH}_3)_3$, showed no change in the catalytic activity. Hence, the observed decrease in catalytic activity upon addition of $\text{P}(\text{OCH}_3)_3$ is inferred to have been caused by the addition of $\text{P}(\text{OCH}_3)_3$ and not any aspect of the ~1 h procedure required for that addition.

Results and Discussion

Synthesis, Characterization, and Structure of the $[\text{Ir}(\text{C}_2\text{H}_4)_2]/\text{Zeolite Y}$ Precatalyst. The $[\text{Ir}(\text{C}_2\text{H}_4)_2]/\text{zeolite Y}$ precatalyst was synthesized as detailed previously¹⁶ and as summarized in the Experimental section. Briefly, $[\text{Ir}(\text{C}_2\text{H}_4)_2(\text{acac})]^{30}$ was slurried with highly dealuminated zeolite Y (Si/Al atomic ratio = 30) to form $[\text{Ir}(\text{C}_2\text{H}_4)_2]/\text{zeolite Y}$. The iridium in this well-defined supported complex has been shown to incorporate two π -bonded ethylene ligands and two Ir–O bonds to the zeolite, Figure 6.1.¹⁶ The individual iridium complexes are site-isolated and well-separated from each other, with the loading corresponding to approximately 1 Ir atom per 12 zeolite supercages; the zeolite incorporates approximately one Al site per supercage.¹⁶

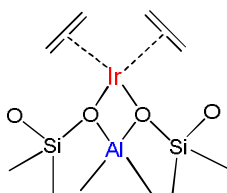


Figure 6.1. Schematic representation of the structure of $[\text{Ir}(\text{C}_2\text{H}_4)_2]/\text{zeolite Y}$ prepared by the reaction of $[\text{Ir}(\text{C}_2\text{H}_4)_2(\text{acac})]$ with highly dealuminated (Si/Al = 30) zeolite Y.¹⁶ Each Ir atom is π -bonded to two ethylene ligands and anchored to the support by two Ir–O bonds.

Kinetics of Cyclohexene Hydrogenation Reaction Starting with $[\text{Ir}(\text{C}_2\text{H}_4)_2]/\text{Zeolite Y}$ in Contact with Cyclohexane Solvent at 22 °C and 40 psig Initial H_2 Partial Pressure.

Cyclohexene hydrogenation as a prototypical test reaction^{19,25,26,31,32} was performed in the

presence of cyclohexane solvent. A slurry consisting of 25 ± 1 mg of $[\text{Ir}(\text{C}_2\text{H}_4)_2]/\text{zeolite Y}$ in cyclohexene (0.5 mL) plus cyclohexane (2.5 mL) was stirred (600 rpm) at 22 ± 0.1 °C and 40 ± 1 psig initial H_2 partial pressure. The progress of the reaction was monitored by the pressure loss via a PC-interfaced pressure transducer reporting precise, ± 0.01 psig, pressure data. The hydrogenation reaction in the batch reactor started immediately, *without a detectable induction period*, and took ~ 12 h to go to completion, Figure 6.2. The cyclohexane end product and 100% reaction (i.e., the lack of detectable starting cyclohexene) were confirmed by $^1\text{H-NMR}$ spectra of an aliquot of the liquid product. Four repetitions of the experiment yielded data indistinguishable within $\pm 10\%$ from those shown in Figure 6.22. The reaction slurry retained its pale-dirty-gray color throughout the reaction; no darkening—a characteristic of metal nanoparticle formation¹—was observed. The absence of an induction period and the lack of a color change or darkening of the solution are consistent with the hypothesis that the starting mononuclear iridium complex anchored to zeolite Y is the true catalyst—with one or more of the ethylene ligands in the $[\text{Ir}(\text{C}_2\text{H}_4)_2]/\text{zeolite Y}$ precatalyst presumably being replaced by cyclohexene and/or hydrogen, *vide infra*.

In the presence of an excess of cyclohexene reactant over catalyst and at a constant initial H_2 pressure, the initial rate of the reaction, $\{-d[\text{H}_2]/dt\}_{\text{initial}}$, is proportional to the mass of precatalyst (as shown in Supporting Information, Figure SI-C1a). The initial rate at constant initial (total) precatalyst was then used, in a series of experiments varying the concentration of cyclohexene (at constant initial H_2 partial pressure) and varying the initial H_2 partial pressure (at constant $[\text{cyclohexene}]_{\text{initial}}$), to determine the reaction orders in the initial $[\text{cyclohexene}]$ and in the initial H_2 partial pressure, respectively. The initial rate data reveal zero-order dependencies on both the $[\text{cyclohexene}]_{\text{initial}}$ and on the $\{\text{H}_2 \text{ partial pressure}\}_{\text{initial}}$. Specifically, the data from a Standard

Conditions cyclohexene provide an initial rate value, $\{-d[\text{cyclohexene}]/dt\}_{\text{initial}}$ of $0.30 \text{ M}\cdot\text{hr}^{-1}$, that yields a rate constant of $k_{\text{obs}} = 1 \times 10^{-5} \text{ mol} \times (\text{g of catalyst} \times \text{s})^{-1}$ for 25 mg of $[\text{Ir}(\text{C}_2\text{H}_4)_2]/\text{zeolite Y}$ catalyst, corresponding to a $\text{TOF}_{\text{initial}} = 0.20 \pm 0.03 \text{ molecules} \times (\text{Ir atom} \times \text{s})^{-1}$.⁴⁴ A footnote summarizes why the kinetic plots are concave up, reflecting changes from the initial zero-order dependencies on $[\text{cyclohexene}]$ and the $\{\text{H}_2 \text{ partial pressure}\}$ as the reactants are consumed in the batch reactor.⁴⁵

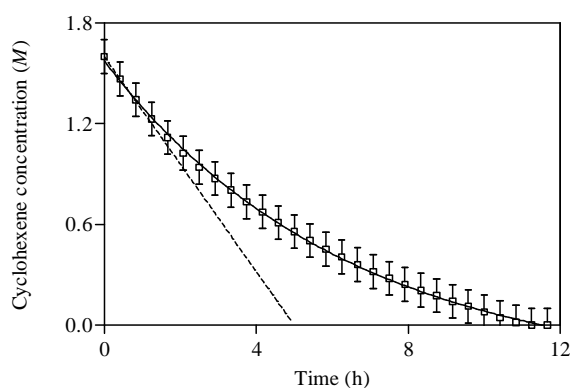


Figure 6.2. Hydrogenation of cyclohexene in presence of cyclohexane solvent under the Standard Conditions ($22 \pm 0.1 \text{ }^\circ\text{C}$ and $40 \pm 1 \text{ psig}$ initial H_2 partial pressure) and starting with 25 mg (1 wt% Ir) $[\text{Ir}(\text{C}_2\text{H}_4)_2]/\text{zeolite Y}$ (\square). The tangential initial rate,⁴⁵ $\{-d[\text{cyclohexene}]/dt\}_{\text{initial}} = 0.30 \text{ M/h}$, is determined from a 3rd order polynomial fit (—) with $R^2 = 0.999$. This corresponds to a per Ir atom initial rate of $3.2 \times 10^{-25} \text{ mol} \times (\text{Ir atoms} \times \text{s})^{-1}$. The observed rate constant is then $k_{\text{obs}} = 1 \times 10^{-5} \text{ mol} \times (\text{g of catalyst} \times \text{s})^{-1}$ for the 25 mg of $[\text{Ir}(\text{C}_2\text{H}_4)_2]/\text{zeolite Y}$ catalyst, corresponding to $\text{TOF}_{\text{initial}} = 0.20 \pm 0.03 \text{ molecules} \times (\text{Ir atom} \times \text{s})^{-1}$. For clarity, only one of every ten data points collected and fit is shown.

A second, repeat cyclohexene hydrogenation reaction was performed with the catalyst slurry produced by the first run, as detailed in the Supporting Information. Briefly, once the first, Standard Conditions cyclohexene hydrogenation was completed (via H_2 uptake cessation and ^1H -NMR analysis), the F-P bottle and its reaction solution were transported back into the drybox, 0.5 mL of fresh cyclohexene added, the F-P bottle removed from the drybox and reattached to

the hydrogen line, and a second, repeat cyclohexene hydrogenation run started. The plot of the cyclohexene loss is given in the Supporting Information (Figure SI-C2b); it reveals: (i) no induction period; (ii) no darkening of the reaction solution; and (iii) an initial rate – $\{d[\text{cyclohexene}]/dt\}_{\text{initial}} = 0.25 \text{ M/h}$ (Figure SI-C2b) that is 16% below that of the first run – $\{d[\text{cyclohexene}]/dt\}_{\text{initial}} = 0.30 \text{ M/h}$ (Figures 6.2 and SI-C2a), with a total reaction time of 14 h, slightly longer than the total reaction time of the first run of 12 h.⁴⁶ The lack of an induction period (during which a new catalyst could have been formed) is consistent with the hypothesis that a mononuclear Ir₁/zeolite Y species is the true catalyst.

The data to this point are consistent with the hypothesis that a mononuclear iridium species is the true catalyst. However, an alternative hypothesis not yet disproven is that larger iridium species, such as Ir₄ sub-nanometer clusters,¹⁴ or larger Ir_n nanoparticles, could have formed so quickly that no induction period would be evident, an interpretation that also requires those putative Ir₄ or larger Ir_n be active catalysts (as they are for ethylene hydrogenation¹⁵). Hence, EXAFS spectroscopy and HAADF-STEM were employed to characterize the nuclearity of the post-catalysis iridium species.

Post-Kinetics EXAFS Analysis of the Resultant Iridium Species and their Comparison to the Starting Material, [Ir(C₂H₄)₂]/Zeolite Y. After a Standard Conditions cyclohexene hydrogenation reaction, the resultant sample was dried under vacuum for 8 h in a drybox and transported in the absence of air and moisture as detailed in the Experimental section for characterization by EXAFS spectroscopy and HAADF-STEM.⁴⁷

The details of the EXAFS data fitting are provided in the Supporting Information. The best-fit model yielded the most realistic coordination numbers for iridium with excellent fits, as illustrated by the comparisons shown in Figure 6.3. The best-fit model representing the data,

Table 6.1, shows no detectable Ir–Ir contribution; that is, the Ir–Ir coordination number is indistinguishable from zero as expected for an Ir₁ catalyst. Coordination numbers (CN) of 4.9 and 3.6 were found for the Ir–C and Ir–C_{long} contributions, respectively, indicating the presence of hydrocarbons bonded to the iridium. The EXAFS data are not sufficient to determine the identities of these ligands, but they are consistent with the expected ligands including cyclohexene, ethylene, ethyl, or a combination of these, as just one plausible set of possibilities.⁴⁸ The EXAFS data show no detectable changes in the metal–support Ir–O_{zeolite} and Ir–Al contributions (i.e., no detectable change in their respective CNs). This result, and the lack of detectable Ir–Ir interactions, are completely consistent with the kinetic data, *vide supra*, as well as the hypothesis that mononuclear Ir₁/zeolite Y is the true catalyst. In other words, a close comparison of the EXAFS data for the post catalysis product with that of the [Ir(C₂H₄)₂]/zeolite Y starting material,⁴⁹ Table 6.1, is fully supportive of the inference that the true cyclohexene hydrogenation catalyst is the Ir₁/zeolite Y site shown in Figure 6.1, but with a different ligand environment around iridium as expected for the catalyst in the presence of a solution of cyclohexene, cyclohexane, and H₂.⁴⁸

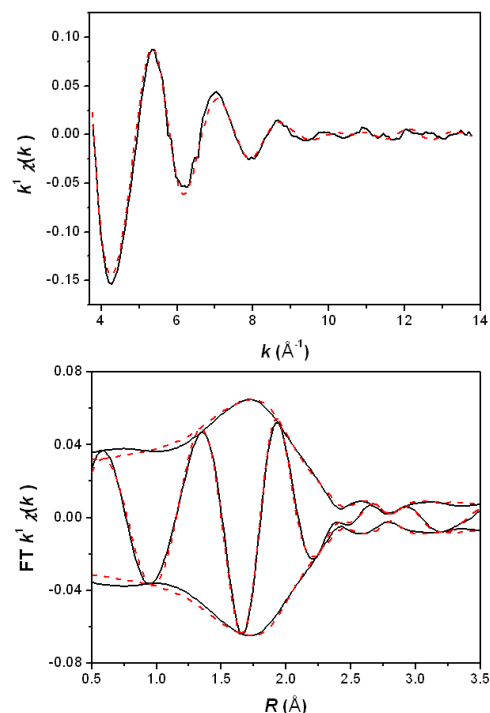


Figure 6.3. EXAFS analysis of the post-catalysis iridium species. *Top:* k^1 -weighted EXAFS function, χ (solid line), and sum of the calculated contributions (dashed line). *Bottom:* k^1 -weighted imaginary part and magnitude of the Fourier transform of the data (solid line) and sum of the calculated contributions (dashed line). Both EXAFS function and the Fourier transform show excellent fits. See the main text for a discussion of the results and the Supporting Information for a more in-depth analysis comparing three models (Models I-II-III) en route to the selection of Model I.

Table 6.1. Summary of the EXAFS data at the Ir L_{III} edge characterizing the starting complex, $[\text{Ir}(\text{C}_2\text{H}_4)_2]/\text{zeolite Y}$,⁴⁹ and the post-catalysis iridium species (resulting in a best-fit Model I; see the Supporting Information for details).

Sample	EXAFS parameters				
	Absorber – backscatter pair	N	R (Å)	$10^3 \times \Delta\sigma^2$ (Å ²)	ΔE_0 (eV)
$[\text{Ir}(\text{C}_2\text{H}_4)_2]/\text{zeolite Y}^{\text{a}}$	Ir- $\text{O}_{\text{zeolite}}$	2.0	2.12	13	-5.1
	Ir-C	4.1	2.10	10	-2.2
	Ir-Al	1.1	3.02	6.8	-7.9
	Ir-Ir	$_{\text{b}}$	$_{\text{b}}$	$_{\text{b}}$	$_{\text{b}}$
Post-catalysis iridium sample	Ir- $\text{O}_{\text{zeolite}}$	2.1	2.18	5.4	-8.0
	Ir-C	4.9	2.09	11	-6.6
	Ir-Al	1.1	3.01	0.6	-2.2

Ir-C _{long}	3.6	2.98	1.0	-6.7
Ir-Ir	_{-b}	_{-b}	_{-b}	_{-b}

Notation: N, coordination number; R, distance between absorber and backscatterer atoms; $\Delta\sigma^2$, variance in the absorber-backscatterer distance; ΔE_0 , inner potential correction. Error bounds (accuracies) characterizing the structural parameters are estimated to be as follows: N, $\pm 20\%$; R, $\pm 0.02 \text{ \AA}$; $\Delta\sigma^2$, $\pm 20\%$; and ΔE_0 , $\pm 20\%$. [a] See the details elsewhere.⁴⁹ [b] Contribution not detected.

Post-Kinetics HAADF-STEM Analysis of the Resultant Iridium Species and Comparison with Starting Material, [Ir(C₂H₄)₂]/Zeolite Y. The same post-catalysis iridium sample, as well as the starting supported iridium complex [Ir(C₂H₄)₂]/zeolite Y, were imaged with HAADF-STEM. Strikingly, the atomic-resolution images show the presence of isolated Ir atoms (a few are circled in the images for clarity). No iridium clusters or larger iridium nanoparticles are detectable in either the images of the initial [Ir(C₂H₄)₂]/zeolite Y or in the post-catalysis sample, Figure 6.4. Thus, the images demonstrate the presence of solely mononuclear iridium species.

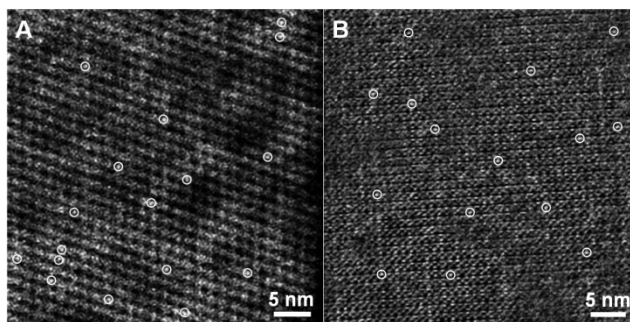


Figure 6.4. HAADF-STEM images of (A) initially prepared [Ir(C₂H₄)₂]/zeolite Y, and (B) the post-catalysis sample/product. Bright features are the site-isolated, single Ir atoms supported in the zeolite Y. A few single Ir atoms are circled for clarity.

Overall, the post-catalysis HAADF-STEM results are in agreement with the post-catalysis EXAFS spectra—as well as all the other results presented so far—in supporting the inference of mononuclear Ir₁/zeolite Y as the true catalyst. The kinetic poisoning data provided in the next

section provide additional, very strong if not compelling evidence for both an Ir₁ catalyst, as well as for its intrazeolitic pore location.

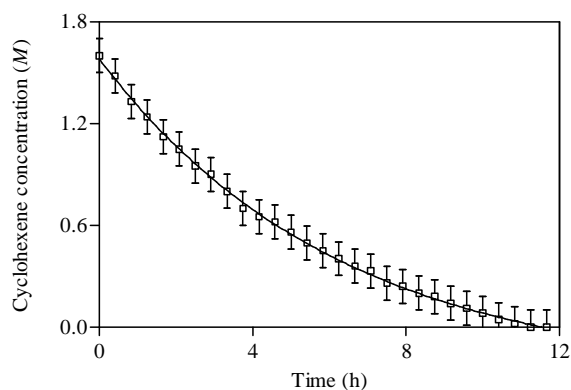
Size-Selective Poisoning Experiments with the Bulky Phosphine, P(C₆H₁₁)₃, and the Smaller Phosphite, P(OCH₃)₃. One additional, alternative hypothesis for the true catalyst not yet disproven is that small amounts of iridium might have leached from the zeolite into solution. If, for example, even 1% of the total iridium had been extracted into solution but was 1000-fold more active catalytically than the zeolite-bound Ir₁, then that leached species in this hypothetical example would be responsible for ~90% of the observed catalytic reaction rate.

Hence, to test this leached Ir alternative hypothesis for the true catalyst, the size-selective properties of the zeolite were exploited in quantitative catalyst poisoning experiments. These potential ligands were chosen for their ability to bond strongly to iridium and, thereby, poison the catalyst *if* they can access the catalyst.¹ Relevant here is that P(C₆H₁₁)₃, with its three bulky cyclohexyl groups, has a diameter of ~10 Å,⁵⁰ and a cone angle of 170°,⁵¹ and is therefore too large to enter the supercages of zeolite Y via the pore apertures, which have relatively small diameters of 7.4 Å.⁵² In contrast, P(OCH₃)₃, with its three methoxy groups, has a diameter of ~5 Å,⁵⁰ and a cone angle of 107°,⁵¹ so that P(OCH₃)₃ can pass through the zeolite pores.

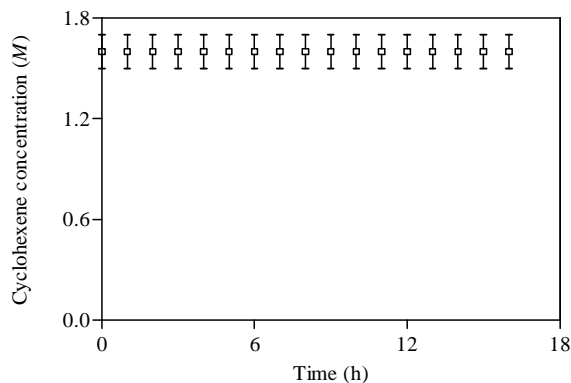
Experimentally and under our Standard Conditions for cyclohexene hydrogenation at 22 ± 0.1 °C and 40 ± 1 psig initial H₂ partial pressure, the addition of 1.0 equiv of P(C₆H₁₁)₃ per equiv of total iridium present *did not affect the catalytic activity* within experimental error. The cyclohexene hydrogenation activity started immediately without an observable induction period, and again the catalytic reaction was completed in ~12 h, Figure 6.5a, as confirmed by ¹H-NMR spectra of the liquid product. The TOF_{initial} is the same within error (TOF_{initial} = 0.18 ± 0.03

molecules \times (Ir atom \times s)⁻¹ for 1.0 equiv of P(C₆H₁₁)₃ per mole of iridium vs TOF_{initial} = 0.20 \pm 0.03 molecules \times (Ir atom \times s)⁻¹ without P(C₆H₁₁)₃).

Whereas the non-poisoning by P(C₆H₁₁)₃ is by itself a negative result, in dramatic contrast, the addition of 1.0 equiv of P(OCH₃)₃ per equiv of total iridium led to a *complete deactivation* of the catalyst for more than 15 h, after which point the experiment was stopped, Figure 6.5b. Taken together, the results of the size-selective poisoning experiments with phosphorus-containing compounds—the smaller (P(OCH₃)₃) being a poison and the larger (P(C₆H₁₁)₃) not being a poison—provide *prima facie* evidence that all of the detectable catalytically active iridium is confined within the zeolite pores. These results also demonstrate the advantage of using a zeolite as a catalyst support when the goal is to identify the catalytically active species—size-selective poisoning experiments are then available to assist in identification and location of the catalyst.⁵³



(a)



(b)

Figure 6.5. Cyclohexene hydrogenation kinetics at 22 ± 0.1 °C: (a) After the addition of 1 equiv (per mole of iridium) of $P(C_6H_{11})_3$ (\square); the polynomial fit (—), $R^2 = 0.999$, yields an initial rate of $\{-d[\text{cyclohexene}]/dt\}_{\text{initial}} = 0.28$ M/h, so within experimental error of the initial rate of 0.30 M/h seen in Figure 6.2. For clarity, only one of every 10 data points is shown. (b) A separate experiment showing the complete inactivation of the catalysis following the addition of 1 equiv of $P(OCH_3)_3$ (per mole of iridium), all under the otherwise identical Standard Conditions. For clarity, only one of every 20 data points is shown in Figure 6.5b. These selective poisoning experiments provide strong evidence that all of the detectable catalysis occurs in the zeolite Y pores.

Quantitative $P(OCH_3)_3$ Poisoning Experiments. Although the hypothesis that a supported mononuclear iridium species, $Ir_1/\text{zeolite Y}$, is the true catalyst is consistent with all the data presented so far, one more reasonable alternative hypothesis which has not yet been ruled out is that fast formation of higher-nuclearity iridium species (such as Ir_4 clusters or larger Ir_n nanoparticles) occurs in the supercages of the zeolite. In this alternative hypothesis for the true catalyst, the hypothetical cluster or nanoparticle species are not observable by EXAFS spectroscopy or even HAADF-STEM, because (according to this alternative hypothesis) they constitute $\leq 10\%$ of the iridium (and were somehow missed—highly unlikely in our experience given the atomic resolution HAADF-STEM results), but are postulated to be much more active catalysts than the Ir_1 species, all at 22 °C.

Hence, *quantitative poisoning experiments* with $\text{P}(\text{OCH}_3)_3$ were performed to check this alternative hypothesis, as summarized in detail in the Experimental section. Briefly, three separate experiments were initiated at 22 ± 0.1 °C and 40 ± 1 psig initial H_2 partial pressure. After 5 h, 0.1, 0.4, and 0.7 equiv of $\text{P}(\text{OCH}_3)_3$ (per equiv of total iridium) were added, respectively, to the reactor in the three separate experiments. The increased $\text{P}(\text{OCH}_3)_3$ poison concentration gradually slowed down the catalytic reaction, as shown in Figure 6.6, and 1.0 equiv of $\text{P}(\text{OCH}_3)_3$ per mole of iridium again poisoned the catalyst completely as previously observed, *vide supra*. Specifically, the reaction takes 14, 23, and 60 h to completion upon the addition of 0.1, 0.4, and 0.7 equiv of $\text{P}(\text{OCH}_3)_3$ per equiv of iridium respectively, compared to ca. 12 h without any added $\text{P}(\text{OCH}_3)_3$, Figure 6.2.

The key result from Figure 6.6 is that ~ 1.0 equiv of poison, $\text{P}(\text{OCH}_3)_3$, per total iridium is required to deactivate the catalyst completely, *as expected for an Ir_1 catalyst*. Crucial here is that the required ~ 1.0 equiv of poison is quite distinct from the expectation for multinuclear metal catalysts, the specific case of at least previous Ir_n nanoparticle catalysts⁵⁴ requiring only $\ll 1$ equiv (often 0.1–0.3 equiv) of poison per total equiv of metal present for complete deactivation. This result is as expected since only a fraction of the metal atoms are exposed and catalytically active,⁵⁵ with for example only $\sim 40\%$ of the atoms of for example an ~ 3 -nm, $\text{Ir}(\text{O})_{\sim 900}$ nanoparticle being on the surface of the nanoparticle and thus even accessible. These quantitative poisoning experiments, along with all the other evidence presented to this point, provide extremely strong if not now compelling evidence that the mononuclear nature of the $[\text{Ir}(\text{C}_2\text{H}_4)_2]/\text{zeolite Y}$ precatalyst is retained in a kinetically dominant, $\text{Ir}_1/\text{zeolite Y}$ catalyst.

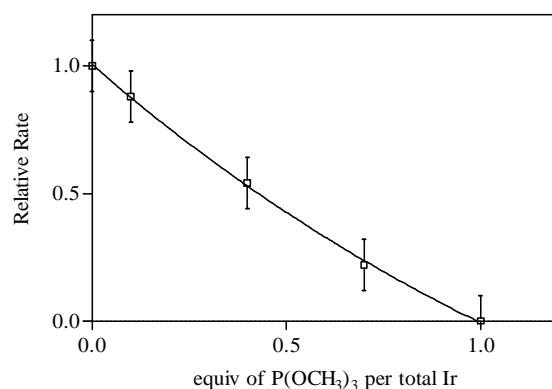


Figure 6.6. Results of quantitative poisoning experiments with $\text{P}(\text{OCH}_3)_3$ at 22 ± 0.1 °C under a Standard Conditions cyclohexene hydrogenation beginning with $[\text{Ir}(\text{C}_2\text{H}_4)_2]/\text{zeolite Y}$. A gradual decrease in the activity was observed as a function of added equivalents of $\text{P}(\text{OCH}_3)_3$ per equivalent of iridium: 14, 23, and 60 h to completion upon the addition of 0.1, 0.4, and 0.7 equiv of $\text{P}(\text{OCH}_3)_3$ per equiv of iridium, respectively, compared to ~12 h without any added $\text{P}(\text{OCH}_3)_3$ (Figure 6.2). Overall, 1 equiv of $\text{P}(\text{OCH}_3)_3$ per equiv of total iridium present completely inhibits the catalytic activity.

Summary

In summary, all the available evidence—in our view the combination of the needed evidence—is strongly supportive of the inference that a mononuclear iridium complex supported within the supercages of the zeolite, $[\text{Ir}_1]/\text{zeolite Y}$, is the true catalytically active species for hydrogenation of cyclohexene at 22 ± 0.1 °C and 40 ± 1 psig initial H_2 partial pressure. This strong inference is supported by five lines of consistent, highly supportive evidence: (i) the lack of an observable induction period (i.e., the lack of a period during which higher-nuclearity iridium species could have been formed) and the lack of darkening of the reaction solution (which could have indicated the formation of nanoparticles); (ii) the post-catalysis, ex-situ EXAFS analysis of the resultant iridium species which showed no detectable Ir–Ir contributions, but was fully consistent with and supportive of mononuclear $\text{Ir}_1/\text{zeolite Y}$; (iii) the post-catalysis, ex-situ HAADF-STEM analysis that detected only atomically dispersed Ir_1 on the zeolite Y; (iv) the results of the size-selective

poisoning experiments, which are consistent only with catalysis by intra-zeolite Ir, and lastly but importantly (v) the results of the quantitative $\text{P}(\text{OCH}_3)_3$ poisoning experiments that argue very strongly if not compellingly for a mononuclear Ir_1 catalyst, as opposed to Ir cluster (e.g., Ir_4) or Ir_n nanoparticle catalysts, for example.

The above evidence for a zeolite-supported mononuclear iridium catalyst for cyclohexene hydrogenation in the presence of cyclohexane closely parallels the characterization of a mononuclear, zeolite-supported Ir_1 complex as the dominant species present under gas-phase ethylene and H_2 at 25 °C and 1 atm (ca. 15 psig).¹⁸ The mononuclear species were inferred to be the catalytically active species in the latter case because there was spectroscopic evidence of them, plus no evidence for iridium clusters such as the Ir_4 that was observed to form at a higher temperature, 80 °C.¹⁸ In short, all the available evidence points to a consistent, clear picture of zeolite-supported Ir_1 as catalyst for either gas-solid¹⁸ or liquid-solid hydrogenation of olefins, at least at mild temperatures of 22–25 °C. That is, the presence or absence of liquid-phase cyclohexene and cyclohexane does not alter the catalytically active site at 22–25 °C.

Overall, a well-characterized, site-isolated, atomically dispersed $[\text{Ir}(\text{C}_2\text{H}_4)_2]/\text{zeolite Y}$ precatalyst has been shown to evolve into an active catalyst in which strong if not compelling evidence has been collected supporting the hypothesis that the true catalyst at 22–25 °C retains its atomic dispersion, $\text{Ir}_1/\text{zeolite Y}$. This is to our knowledge the first such example for which all the required evidence, to support a compelling case for atomic dispersion of a zeolite-supported transition metal species as the true catalyst, in the present case in contact with solution phase, has been obtained.^{9,11,12,13}

In work in progress, we raised the temperature ca. 50 °C and investigated the present system under otherwise identical conditions, but at 72 °C. There we do detect higher-nuclearity species

(a control, effectively, demonstrating that we would have detected them had they been formed under the 22 °C conditions examined herein). Experiments are in progress to identify the kinetically dominant catalyst(s) at 72 °C. Those studies also promise to yield insights into the sintering of an initially atomically dispersed (pre)catalyst, so that we are working to bring those interesting results to a publishable conclusion.

Supporting Information. Experimental details and plots of kinetic experiments varying the $[\text{Ir}(\text{C}_2\text{H}_4)_2]/\text{zeolite Y}$, cyclohexene, and H_2 amounts and determining the corresponding initial rate changes in order to determine the order of reaction in each of those reactants as well as the control varying the stirring rate; Experimental details, data, and fit to third-degree polynomial of a second, repeat cyclohexene hydrogenation using the product solution plus its comparison to the first run; Details of the EXAFS data analyses with the fits of the candidate models; Calculation of the Thiele modulus. This material is available free of charge via the Internet at <http://pubs.acs.org>.

Acknowledgments

This work was supported by the Department of Energy (DOE) Grant FG02-87ER15600 (J.L.), Grant DE- FG02-03ER15453 (to R.G.F. at CSU), Grant DE-FG02-03ER46057 (C.A.) and the University of California Lab Fee Program. A.U. was supported by a fellowship from Chevron. We gratefully acknowledge beam time and support of the DOE Division of Materials Sciences for its role in the operation and development of beamline X-18B at the National Synchrotron Light Source and beamline 4-1 at the Stanford Synchrotron Radiation Lightsource. We also thank Saim Özkar for valuable discussions leading to the size-selective catalyst poisoning experiments.

REFERENCES

- ¹ Widegren, J. A.; Finke, R. G. *J. Mol. Catal. A: Chem.* **2003**, 198, 317-341.
- ² Phan, N. T. S.; Sluys, M. V. D.; Jones, C. W. *Adv. Synth. Catal.* **2006**, 348, 609-679.
- ³ Crabtree, R. H. *Chem. Rev.* **2012**, 112, 1536-1554.
- ⁴ Alley, W.M.; Hamdemir, I.K.; Johnson, K. A.; Finke, R. G. *J. Mol. Catal. A: Chem.* **2010**, 315, 1-27.
- ⁵ Dyson, P. J. *Dalton Trans.* **2003**, 2964-2974.
- ⁶ de Vries, J. G. *Dalton Trans.* **2006**, 421-429.
- ⁷ McDaniel, M. P. *Adv. Catal.* **2010**, 53, 123-606.
- ⁸ Ratnasamy, P.; Srinivas, D.; Knözinger, H. *Adv. Catal.* **2004**, 48, 1-169.
- ⁹ Qiao, B.; Wang, A.; Yang, X.; Allard, L. F.; Jiang, Z.; Cui, Y.; Liu, J.; Li, J.; Zhang, T. *Nat. Chem.* **2011**, 3, 634-641.
- ¹⁰ Lu, J.; Aydin, C.; Browning, N. D.; Gates, B. C. *Angew. Chem. Int. Ed.* **2012**, 51, 5842-5846.
- ¹¹ Kyriakou, G.; Boucher, M. B.; April D. Jewell, A. D.; Lewis, E. A.; Lawton, T. J.; Baber, A. E.; Tierney, H. L.; Flytzani-Stephanopoulos, M.; Sykes, E. C. H. *Science* **2012**, 335, 1209-1212.

- ¹² Flytzani-Stephanopoulos, M.; Gates, B. C. *Ann. Rev. Chem. Biomol. Eng.* **2012**, 3, 545-574.
- ¹³ Zhai, Y.; Pierre, D.; Si, R.; Deng, W.; Ferrin, P.; Nilekar, A. U.; Peng, G.; Herron, J. A.; Bell, D. C.; Saltsburg, H.; Mavrikakis, M.; Flytzani-Stephanopoulos, M. *Science* **2010**, 329, 1633-1636.
- ¹⁴ Uzun, A.; Gates, B. C. *Angew. Chem., Int. Ed.* **2008**, 47, 9245-9248.
- ¹⁵ Aydin, C.; Lu, J.; Browning, N. D.; Gates, B. C. *Angew. Chem. Int. Ed.* **2012**, 51, 5929-5934.
- ¹⁶ Uzun, A.; Bhirud, V. A.; Kletnieks, P. W.; Haw, J. F.; Gates, B. C. *J. Phys. Chem. C* **2007**, 111, 15064-15073.
- ¹⁷ Ortalan, V.; Uzun, A.; Gates, B.C.; Browning, N.D. *Nat. Nanotech.* **2010**, 5, 506-510.
- ¹⁸ Uzun, A.; Gates, B. C. *J. Am. Chem. Soc.* **2009**, 131, 15887-15894.
- ¹⁹ Watzky, M. A.; Finke, R. G. *J. Am. Chem. Soc.* **1997**, 119, 10382-10400.
- ²⁰ Watzky, M. A.; Finke, R. G. *Chem. Mater.* **1997**, 9, 3083-3095.
- ²¹ Aiken III, J. D.; Finke, R. G. *J. Am. Chem. Soc.* **1998**, 120, 9545-9554.
- ²² Widegren, J. A.; Aiken III, J. D.; Özkar, S.; Finke, R. G. *Chem. Mater.* **2001**, 13, 312-324.
- ²³ Bayram, E.; Linehan, J. C.; Fulton, J.L.; Roberts, J. A. S.; Szymczak, N. K.; Smurthwaite, T. D.; Özkar, S.; Balasubramanian, M.; Finke, R. G. *J. Am. Chem. Soc.* **2011**, 133, 18889-18902.

- ²⁴ Mondloch, J. E.; Bayram, E.; Finke, R. G. *J. Mol. Catal. A: Chem.* **2012**, 355, 1-38.
- ²⁵ Mondloch, J. E.; Wang, Q.; Frenkel, A. I.; Finke, R. G. *J. Am. Chem. Soc.* **2010**, 132, 9701-9714.
- ²⁶ Mondloch, J. E.; Finke, R. G. *J. Am. Chem. Soc.* **2011**, 133, 7744-7756.
- ²⁷ Mondloch, J. E.; Finke, R. G. *ACS Catal.* **2012**, 2, 298-305.
- ²⁸ Lu, J.; Serna, P.; Aydin, C.; Browning, N. D.; Gates, B. C. *J. Am. Chem. Soc.* **2011**, 133, 16186-16195.
- ²⁹ Lu, J.; Aydin, C.; Browning, N. D.; Gates, B. C. *J. Am. Chem. Soc.* **2012**, 134, 5022-5025.
- ³⁰ Bhirud, V. A.; Uzun, A.; Kletnieks, P. W.; Craciun, R.; Haw, J. F.; Dixon, D. A.; Olmstead, M. M.; Gates, B. C. *J. Organomet. Chem.* **2007**, 692, 2107-2113.
- ³¹ Lin, Y.; Finke, R. G. *J. Am. Chem. Soc.* **1994**, 116, 8335-8353.
- ³² Özkar, S.; Finke, R. G. *J. Am. Chem. Soc.* **2002**, 124, 5796-5810.
- ³³ Özkar, S.; Finke, R. G. *Langmuir* **2002**, 18, 7653-7662.
- ³⁴ Bird, R. B.; Stewart, W. E.; Lightfoot, E. N. In *Transport Phenomena*; Wiley: New York, 2002.
- ³⁵ Wilkins, R. G. In *Kinetics and Mechanisms of Reactions of Transition Metal Complexes*, 2nd ed.; VCH: New York, 1991.

- ³⁶ Jentoft, M.; Deutsch, S. E.; Gates, B. C. *Rev. Sci. Instrum.* **1996**, 67, 2111-2113.
- ³⁷ Newville, M.; Ravel, B.; Haskel, D.; Rehr, J. J.; Stern, E. A.; Yacoby, Y. *Physica B* **1995**, 208/209, 154-156.
- ³⁸ Newville, M. *J. Synchrotron Rad.* **2001**, 8, 96-100.
- ³⁹ Vaarkamp, M.; Linders, J. C.; Koningsberger, D. C. *Physica B* **1995**, 209, 159-160.
- ⁴⁰ Koningsberger, D. C.; Mojet, B. L.; van Dorssen, G. E.; Ramaker, D. E. *Top. Catal.* **2000**, 10, 143-155.
- ⁴¹ Zabinsky, S. E.; Rehr, J. J.; Ankudinov, A.; Albers, R. C.; Eller, M. J. *Phys. Rev. B.* **1995**, 52, 2995-3009.
- ⁴² Pearson, W. B.; Calvert, L. D.; Villars, P. In *Pearson's Handbook of Crystallographic Data for Intermetallic Phases*; American Society for Metals: Metals Park, OH, 1985.
- ⁴³ Lytle, F. W.; Sayers, D. E.; Stern, E. A. *Physica B* **1989**, 158, 701-722.
- ⁴⁴ For comparison, the initial TOF for *ethylene* hydrogenation with the catalyst formed from the same precatalyst, but in a solid-gas phase reaction, is the ca. 3.5 fold larger value of $0.71 \text{ molecules} \times (\text{Ir atom} \times \text{s})^{-1}$, in the latter case for a feed of C_2H_4 and H_2 at partial pressures of 333 and 666 mbar, respectively, all at 25 °C and atmospheric pressure.¹⁴
- ⁴⁵ The plot in Figure 6.2 (and the others in the Supporting Information) are concave up: the reaction is zero order in the *initial* cyclohexene concentration and the *initial* partial pressure of H_2 , and if these reaction orders pertained over the whole conversion range, the plot would have been linear. The curvature is explained by the increasing orders of reaction as the reactants are

depleted and presumably the catalyst is no longer saturated with reactant-derived ligands. (i) First, recall that we are monitoring the H₂ pressure loss, so that even though the reaction begins with a zero-order dependence on the initial partial H₂ pressure, at some point in the reaction the H₂ partial pressure-dependence must transition to something more like first order, so that the decreasing H₂ partial pressure as the reaction proceeds can contribute to a decrease of the observed rate and the concave-up plot (and even though the H₂ consumed under our Standard Conditions corresponds to a change in H₂ partial pressure from 40 to 25 psig (corresponding to a change in absolute pressure from about 55 to 40 psia). (ii) Second, the cyclohexene was completely used up during the reaction, so analogous to the above case for H₂, the dependence of the rate on cyclohexene concentration must transition from an initial zero-order dependence to something more like first order later in the reaction. In short, the above reasons explain why initial rate kinetics have been deliberately and solely used throughout this work.

⁴⁶ A control experiment of adding 0.5 mL fresh cyclohexene without bringing the F-P bottle into the drybox (i.e., adding 0.5 mL fresh cyclohexene to the solution at the end of first run under flowing H₂ gas) yielded the same initial rate within experimental error as the experiment given in the main text in which 0.5 mL of cyclohexene were added after detaching the F-P bottle, taking it into the drybox, adding the cyclohexene there, and removing the F-P reactor from the drybox, reattaching it to the hydrogen line, and starting the second cyclohexene hydrogenation. In short, that added manipulation and removing the H₂ from the catalyst does not lead to the observed slightly lower initial rate in the second hydrogenation run.

⁴⁷ We recently noted²³ the general importance of *in-operando* spectroscopy to identify where and in what form the precatalyst mass resides. However, *ex-situ* EXAFS experiments (and inherently *ex situ* HAADF-STEM) were employed in this work, in significant part since samples had to be shipped between laboratories to take advantage of the specialized equipment in each laboratory. This is one advantage of the third-row Ir system, where greater Ir-support bond energies appear to make it relatively stable to *ex-situ* conditions and analyses. In addition, to minimize possible contamination from air/O₂, the catalysts were prepared and handled meticulously to exclude air/O₂ during the transfers between laboratories (as detailed in the Experimental section). The EXAFS data would have indicated any inadvertent oxidation of the iridium resulting from the handling; none was observed.

⁴⁸ Assignment of the contribution from hydrocarbon ligands on the basis of EXAFS spectroscopy is not straightforward, in part because of the possible presence of hydrocarbon rings which can be tilted and bent on top of the Ir atoms, causing the Ir-C and/or Ir-C_{long} contributions to be counted twice in some cases.

- ⁴⁹ Lu, J.; Serna, P.; Gates, B. C. *ACS Catal.* **2011**, 1, 1549-1561.
- ⁵⁰ Davies, J. A.; Dutremez, S.; Pinkerton, A. A. *Inorg. Chem.* **1991**, 30, 2380-2387.
- ⁵¹ Tolman, C. A. *Chem. Rev.* **1977**, 77, 313-348.
- ⁵² Breck, D. W. In *Zeolite Molecular Sieves*; Krieger: Malabar, FL, 1984.
- ⁵³ Zahmakıran, M.; Tonbul, Y.; Özkar, S. *J. Am. Chem. Soc.* **2010**, 132, 6541-6549.
- ⁵⁴ Hornstein, B. J.; Aiken III, J. D.; Finke, R. G. *Inorg. Chem.* **2002**, 41, 1625-1638.
- ⁵⁵ Bayram, E.; Zahmakıran, M.; Özkar, S.; Finke, R.G. *Langmuir* **2010**, 26, 12455-12464.

APPENDIX-C

SUPPORTING INFORMATION FOR:

A MONONUCLEAR ZEOLITE-SUPPORTED IRIDIUM CATALYST: KINETIC,
SPECTROSCOPIC, ELECTRON MICROSCOPIC, AND SIZE-SELECTIVE POISONING
EVIDENCE FOR AN ATOMICALLY DISPERSED TRUE CATALYST AT 22 °C

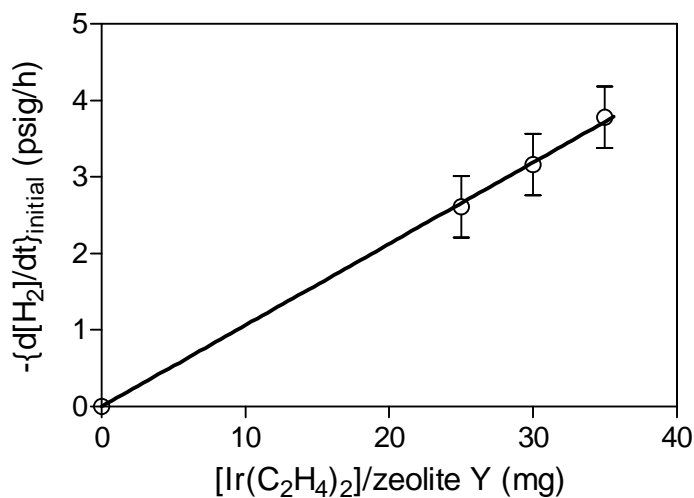
Experiments Demonstrating (i) First-Order Dependence on the Starting Ir Complex Amount of $\{[\text{Ir}(\text{C}_2\text{H}_4)_2]/\text{Zeolite Y}\}$, (ii) Zero-Order Dependences on $[\text{Cyclohexene}]$ and H_2 Pressure, and (iii) the Stirring Rate Independence Testing for Mass Transfer Limitations. A Standard Conditions cyclohexene hydrogenation at 22 ± 0.1 °C and 40 ± 1 psig initial H_2 partial pressure, beginning with 25 ± 1 mg of $[\text{Ir}(\text{C}_2\text{H}_4)_2]/\text{zeolite Y}$ in 2.5 mL cyclohexane plus 0.5 mL cyclohexene, yields an initial rate of 2.6 ± 0.4 psig/h. In order to calculate the order of reaction with respect to the amount of $\{[\text{Ir}(\text{C}_2\text{H}_4)_2]/\text{zeolite Y}\}$, the aforementioned cyclohexene hydrogenation reaction was repeated in two separate experiments, but with two different starting iridium amounts than 25 mg. That is, 30 and 35 mg (± 1 mg) $\{(\text{Ir}(\text{C}_2\text{H}_4)_2)/\text{zeolite Y}\}$ were used in two additional, separate experiments yielding initial rates of 3.2 ± 0.4 and 3.8 ± 0.4 psig/h, respectively (average of two repeats of each different Ir amount). Initial rate vs initial amount of $\{[\text{Ir}(\text{C}_2\text{H}_4)_2]/\text{zeolite Y}\}$ plot (including 0,0 point) shows a first-order dependence on the initial amount of $\{[\text{Ir}(\text{C}_2\text{H}_4)_2]/\text{zeolite Y}\}$, Figure SI-C1(a).

Then, in order to study the dependence of the rate law with respect to the $[\text{cyclohexene}]_{\text{initial}}$, a cyclohexene hydrogenation reaction was repeated, but with two different initial cyclohexene amounts than the Standard Conditions 0.5 mL. Specifically, 0.25 and 1.0 mL of cyclohexene were employed in two separate experiments (plus 2.75 and 2 mL of cyclohexane, respectively, so that the initial total volume was 3 mL in both cases). The resultant initial rates were 2.6 ± 0.4 and 2.9 ± 0.4 psig/h, respectively (average of two repeats of each $[\text{cyclohexene}]_{\text{initial}}$ value). The initial rates are the same within 10% error showing a zero-order dependence on the initial cyclohexene concentration, Figure SI-C1(b).

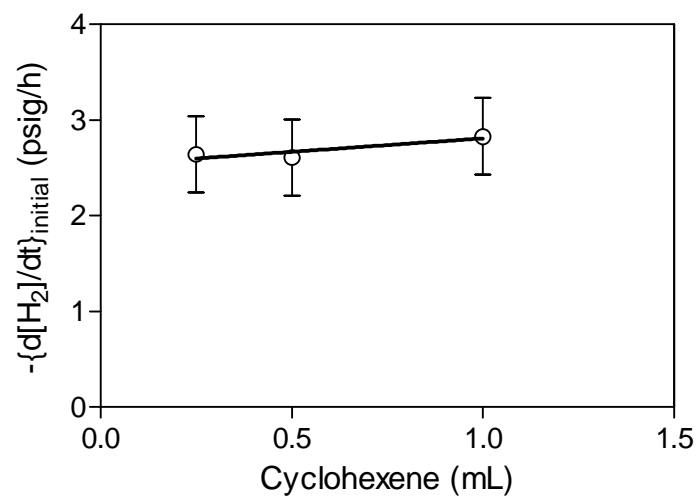
Next, the order of reaction with respect to the initial H_2 pressure was studied by repeating a cyclohexene reaction, but with two different initial H_2 partial pressures other than the Standard

Conditions 40 psig. Specifically, 45 and 50 psig of initial H_2 pressure were employed in two separate experiments. The resulting initial rates were 2.6 ± 0.4 and 2.6 ± 0.4 psig/h, respectively (average of two repeats of each different H_2 partial pressure), the same within 10% error demonstrating a zero-order dependence on the initial H_2 partial pressure, Figure SI-C1(c).

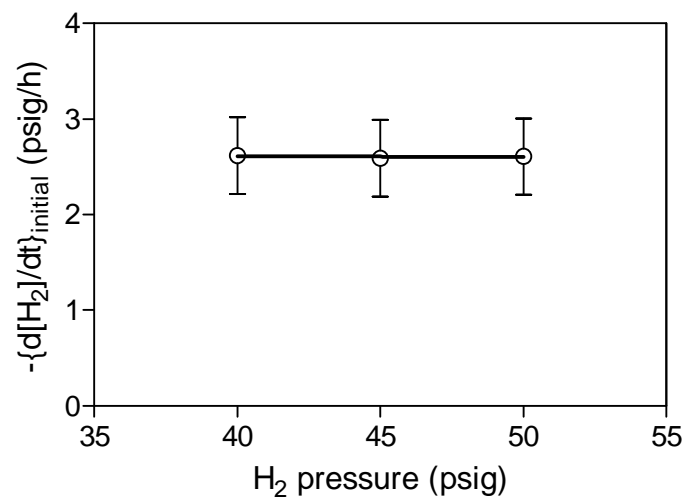
Finally, in order to test H_2 gas-to-solution mass-transfer limitations (MTLs), two separate Standard Conditions cyclohexene hydrogenations were performed in which the only difference was the stirring speed, specifically 450 rpm, 600 rpm, and 1000 rpm. These three experiments yielded initial rates of 2.4 ± 0.4 , 2.6 ± 0.4 , and 2.6 ± 0.4 psig/h, respectively (average of two repeats of each different stirring speed). The results, Figure SI-C1(d), are the same within 10% error, thereby demonstrating negligible H_2 gas-to-solution MTLs.



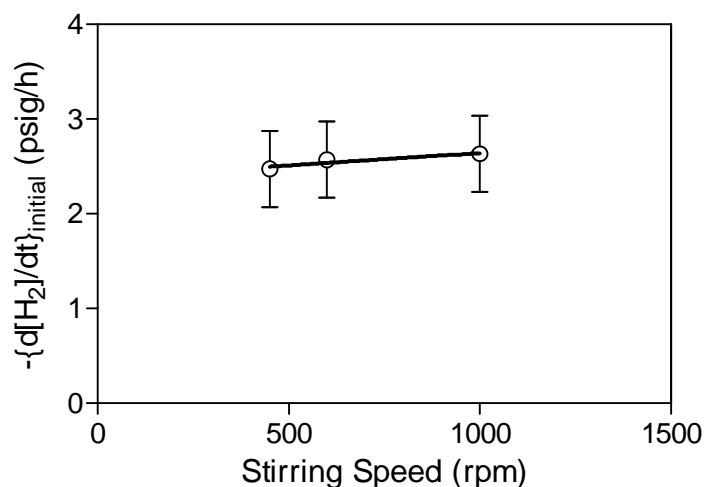
(a)



(b)



(c)



(d)

Figure SI-C1. The plots of the kinetics experiments demonstrating (a) a first-order dependence of the starting Ir complex, $[\text{Ir}(\text{C}_2\text{H}_4)_2]/\text{zeolite Y}$, zero-order dependences on (b) [cyclohexene] and (c) the H_2 pressure, and (d) negligible H_2 gas-to-solution MTL.

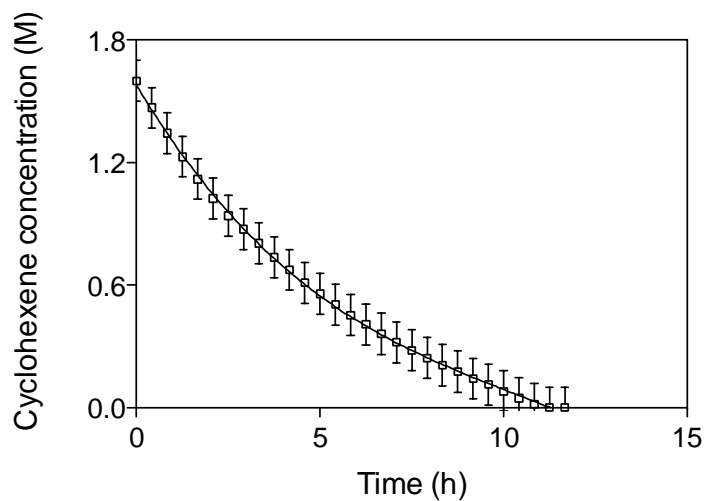
A Second, Repeat Cyclohexene Hydrogenation Using the Product Solution from a First

Run. When the Standard Conditions cyclohexene hydrogenation was completed post beginning with 25 ± 1 mg $\{[\text{Ir}(\text{C}_2\text{H}_4)_2]/\text{zeolite Y}\}$ in 2.5 mL cyclohexane plus 0.5 mL cyclohexene at 22 ± 0.1 °C and 40 ± 1 psig initial H_2 partial pressure (complete as judged by the cessation of any H_2 uptake and by $^1\text{H-NMR}$ of the product solution showing no remaining cyclohexene), the remaining H_2 pressure in the F-P bottle was vented, taken into the drybox, and opened. Then, 0.5 mL of fresh cyclohexene was added, the F-P bottle was resealed, and taken out of the drybox. The F-P bottle was placed into a constant-temperature circulating bath at 22 ± 0.1 °C and attached via Swagelok TFE-sealed Quick-Connects to the hydrogenation line (which had already been evacuated for at least 30 min to remove any trace oxygen and water), then refilled with

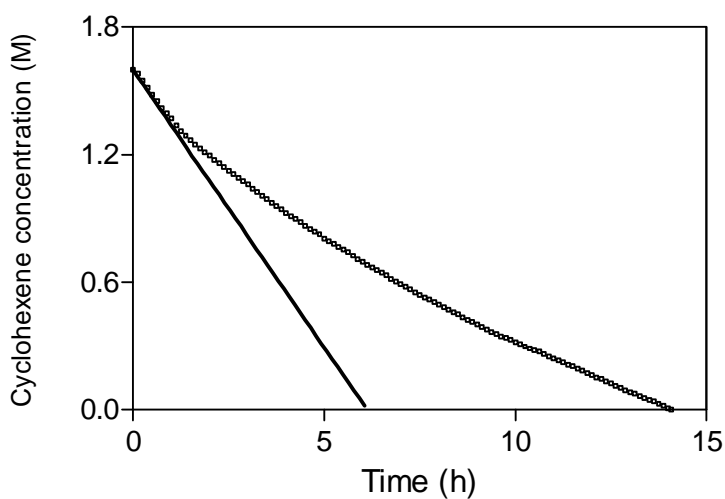
purified H₂ at 40 ± 1 psig (~2.7 atm). Stirring at 600 rpm was restarted, and the F-P bottle was then purged 10 times with H₂ (5 s in between purges), and the reaction was started with a designation of $t = 0$.

When the H₂ uptake ceased, the F-P bottle was disconnected from the hydrogenation line, the remaining H₂ pressure was released, and the F-P bottle was transferred back into the drybox to prepare a ¹H-NMR sample to confirm the complete reduction of cyclohexene.

The cyclohexene hydrogenation data obtained for the first run was then fit to a third-degree polynomial equation via GraphPad Prism software (version 5 for Mac OS X, GraphPad Software, San Diego California USA, www.graphpad.com). The derivative of the third-degree polynomial was then evaluated at $t=0$ to yield the initial rate (the coefficient of the initially t^1 term of the polynomial).¹ The close inspection of the second, subsequent run reveals that an initially linear hydrogenation activity is seen followed by a slowing, convex curvature hydrogenation plot (the error bars on each point have been removed intentionally to show more clearly these two kinetic regimes and the initial, tangential line). Hence, in this case an initial tangential line was drawn through the initial, linear data points to calculate the initial rate (i.e., and instead of the otherwise usual polynomial fitting). Overall, the total reaction time for the first run is ca. 12 h with an initial rate of $-\{d[\text{cyclohexene}]/dt\}_{\text{initial}} = 0.30 \pm 0.05$ M/h, Figure SI-C2(a), while that of subsequent run is ca. 14 h with an initial rate of $-\{d[\text{cyclohexene}]/dt\}_{\text{initial}} = 0.25 \pm 0.05$ M/h, Figure SI-C2(b).



(a)



(b)

Figure SI-C2. (a) Standard Conditions cyclohexene hydrogenation (i.e., first run) beginning with $[\text{Ir}(\text{C}_2\text{H}_4)_2]/\text{zeolite Y}$ at 22 °C and 40 psig initial H_2 partial pressure data (\square) and the third-degree polynomial fit (—) to the equation $[\text{Cyclohexene}] = 1.6 - 0.30t + 0.024t^2 - 0.0008t^3$ with $R^2 = 0.999$; then (b) the subsequent run data (\square) and the tangential line (—) drawn to the initial linear portion of data, $[\text{Cyclohexene}] = -0.25t + 1.6$.

Details of the EXAFS Data Analysis and the Methods for Selection Between Models I, II and III. Described below, are the detailed analyses carried out on the EXAFS data. Different combinations of plausible absorber-back-scatterer contributions (Ir-O_{support}, Ir-C, Ir-Al, Ir-C_{long}, Ir-O_{long}, and Ir-Ir) were fitted initially, which led to a narrowed list of candidate models on the basis of the goodness-of-fit and the overall fit, in both k space and R space. The detailed fitting parameter of the final candidate models of each sample are summarized in Table SI-C1 and the corresponding fits for each model analysis are given in Figure SI-C1.

In order to further examine the fitting parameters and to compare candidate models, a difference-file technique was applied using the software XDAP,² in which calculated XAFS contribution from each individual Ir-back scatter was compared with the data in R space (calculated from subtracting all the other calculated Ir-back scatter contributions from the experimental overall contributions). The best model should give not only good overall fits in both k range and R range, but should also fits well in all individual contributions.

We emphasize that the contributions are very weak for those Ir-back scatters with distances that are longer than bonding distances, and it was difficult to distinguish one from another (e.g. between Ir-C_{long} and Ir-O_{long}). Thus those contributions are assigned only tentatively, and the errors characterizing those shells are greater than those stated below for other shells.

Table SI-C1. Summary of EXAFS fit parameters characterizing the post-catalysis iridium species.

Model	Absorber – backscatter pair	N	R (Å)	$10^3 \times \Delta\sigma^2$ (Å²)	ΔE_0 (eV)	k-range	R-range	Error in EXAFS function [b]	Goodness of fit^[c]
I (best fit)	Ir–O _{zeolite}	2.1	2.18	5.4	-8.0	3.79– 13.75	0.5– 3.5	0.0009	4.0
	Ir–C	4.9	2.09	11	-6.6				
	Ir–Al	1.1	3.01	0.6	-2.2				
	Ir–C _{long}	3.6	2.98	1.0	-6.7				
II	Ir–O _{zeolite}	3.9	2.16	9.4	-6.1				
	Ir–C	6.3	2.08	15	-8.0				
	Ir–Al	1.6	3.06	6.0	-4.0				
	Ir–O _{long}	5.1	2.94	7.8	-6.2				
III	Ir–O _{zeolite}	1.0	2.19	3.8	-7.9				
	Ir–C	6.3	2.12	12	-5.7				
	Ir–Al	2.1	2.92	15	-3.8				

[a] Notation: O_{support}, oxygen from support; O_{long}, oxygen from support in a distance longer than bonding distance; N, coordination number; R, distance between absorber and backscatterer atoms; $\Delta\sigma^2$, Debye-Waller factor; ΔE_0 , Inner potential correction. Error bounds (accuracies) characterizing the structural parameters, obtained by EXAFS spectroscopy are estimated to be as follows: N, $\pm 20\%$; R, $\pm 0.02\text{Å}$; $\Delta\sigma^2$, $\pm 20\%$; and ΔE_0 , $\pm 20\%$. [b] The error in the data was calculated as the root mean square of the value obtained from the subtraction of smoothed χ data from the background-subtracted experimental χ values. [c] Goodness of fit values were calculated with the software XDAP, as follows:

$$\text{goodness of fit} = \frac{\sum_{i=1}^{\text{NPTS}} \left(\frac{\chi_{\text{exp},i} - \chi_{\text{model},i}}{\sigma_{\text{exp},i}} \right)^2}{\text{NPTS}(-N_{\text{free}})}$$

χ_{exp} are the model and experimental EXAFS values, respectively; σ_{exp} is the error in the experimental results; v is the number of independent data points in the fit range; and NPTS is the actual number of data points in the fit range; N_{free} is the number of free parameters. [d] Number of statistically justified parameters was calculated by the Nyquist theorem as follows: number of justified parameters = $n = (2\Delta k \Delta R / \pi) + 2$, where Δk and ΔR are the k- and R- ranges used the fitting.

Comparison of Three Models. All three models (I-III) indicate that the zeolite supported iridium sample is a mononuclear complexes with hydrocarbon ligands plus bonding to the zeolite-support oxygen atoms. We emphasize that attempts were made to include Ir-Ir contributions in all the models (to test the presence of Ir clusters), but no Ir-Ir contributions could be found (in all k weightings). The final three candidate models were selected on the basis of

goodness-of-fit and overall fit in both k and R space. Both model I and model II provide good individual shell fits for all contributions. However, we reject model II because the coordination number for Ir-O_{support} and Ir-C contributions are unrealistically high (i.e. breaking the 18 e⁻ rule for the supported Ir complex). In addition, the coordination number for Ir-Al contribution in model II is also unrealistically high for the zeolite with Si/Al atomic ratio of 30 : 1. We reject model III because the very poor individual shell fit for the Ir-Al contribution, and a relatively poor overall fit in R space compared to model I and II. Thus, of the three models, model I was selected.

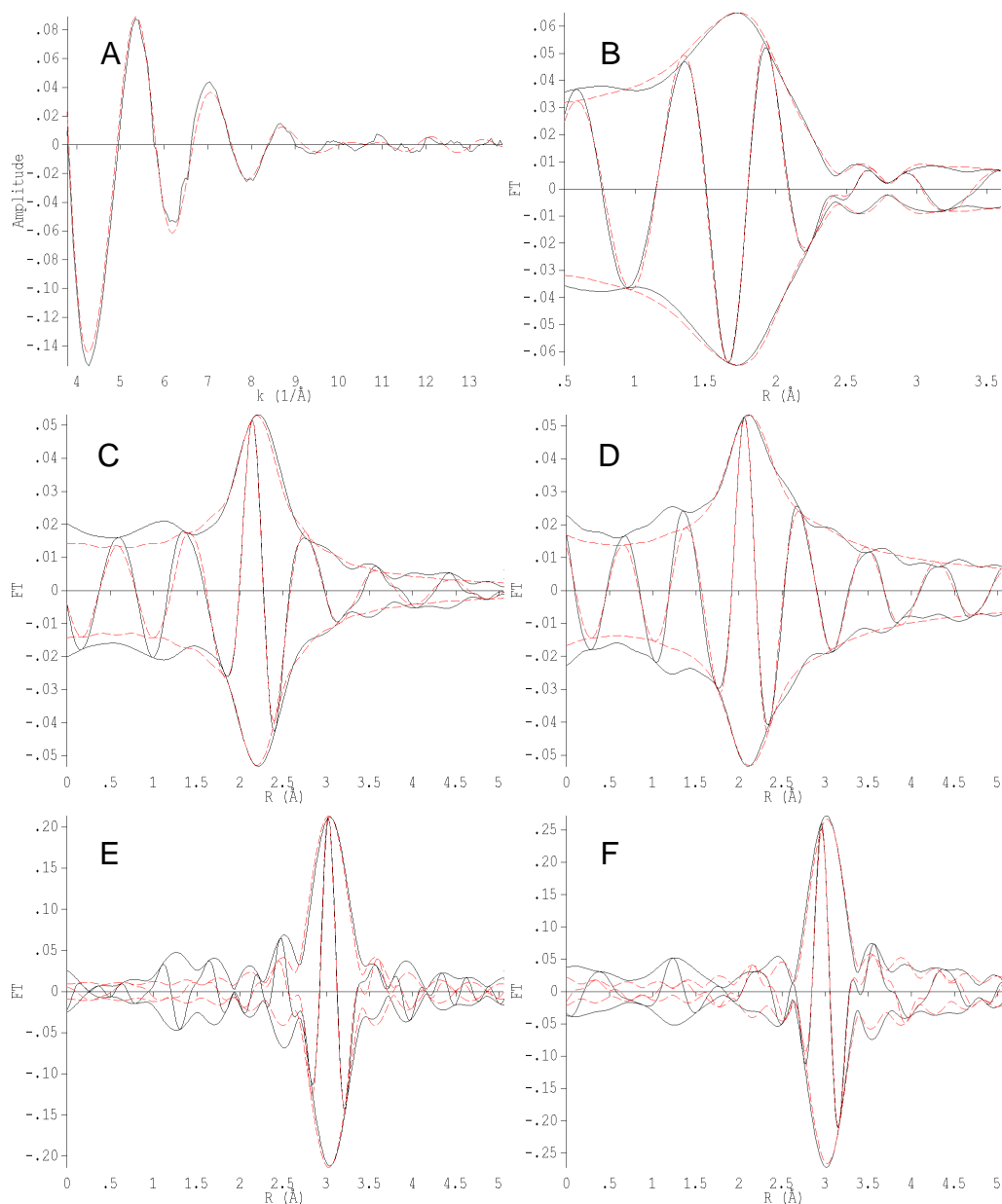


Figure SI-C3. EXAFS data characterizing the dealuminated Zeolite Y-supported iridium complex after cyclohexene hydrogenation at 22 °C. Fitting for Model I: (A) k^1 -weighted EXAFS function, $k^1(\chi)$ (solid line) and sum of the calculated contributions (dashed line); (B) k^1 -weighted imaginary part and magnitude of the Fourier transform of the data (solid line) and sum of the calculated contributions (dashed line); (C) k^1 -weighted, phase-corrected, imaginary part and magnitude of the Fourier transform of the data (solid line) and calculated contributions (dashed line) of Ir-O_{support} shell; (D) k^1 -weighted, phase-corrected, imaginary part and magnitude of the Fourier transform of the data (solid line) and calculated contributions (dashed line) of Ir-C shell; (E) k^2 -weighted, phase-corrected, imaginary part and magnitude of the Fourier transform of the data (solid line) and calculated contributions (dashed line) of Ir-Al shell; (F) k^2 -weighted, phase-corrected, imaginary part and magnitude of the Fourier transform of the data (solid line) and calculated contributions (dashed line) of Ir-C_{long} shell.

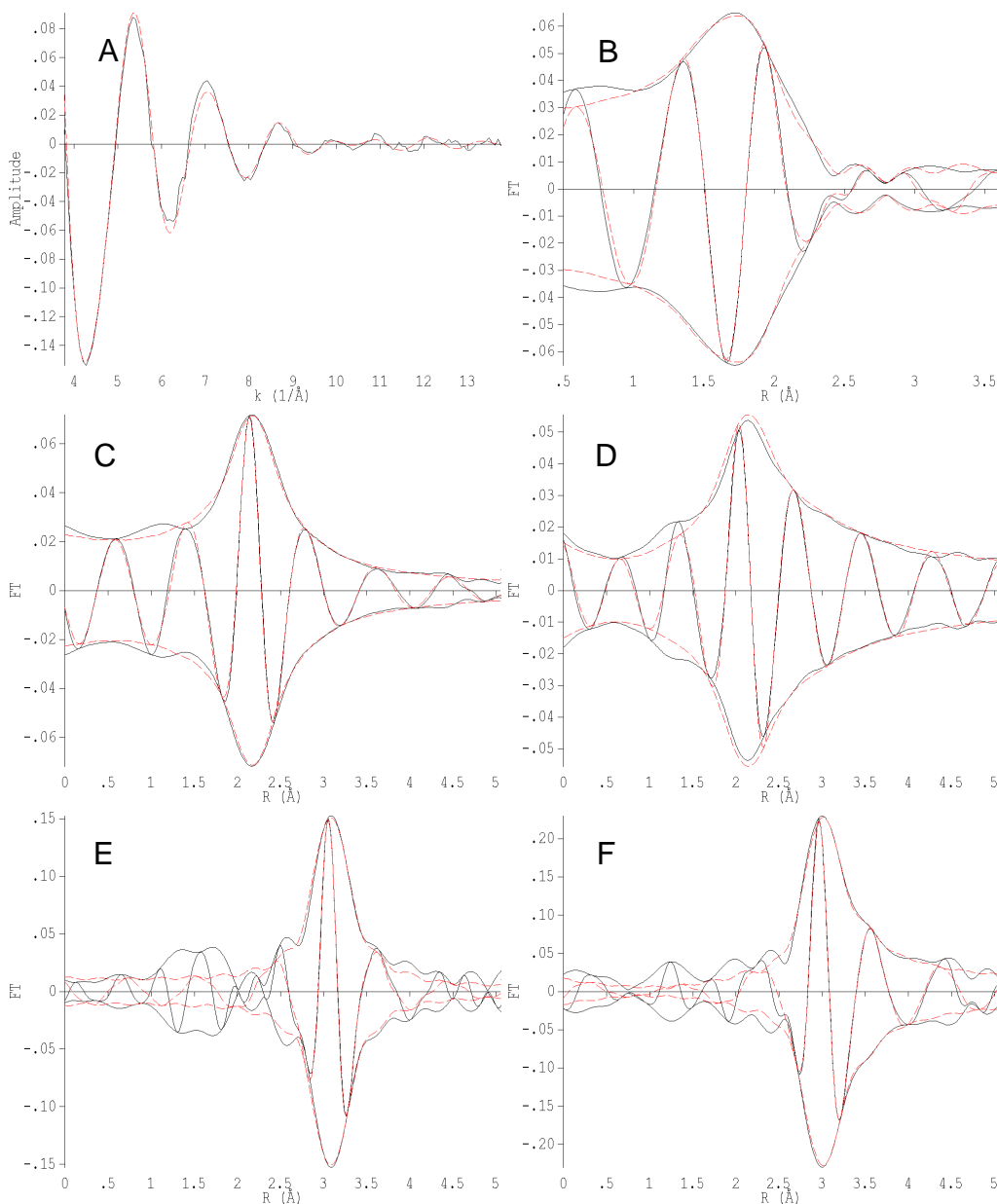


Figure SI-C4. EXAFS data characterizing the dealuminated Zeolite Y-supported iridium complex after cyclohexene hydrogenation at 22 °C. Fitting for Model II: (A) k^1 -weighted EXAFS function, $k^1(\chi)$ (solid line) and sum of the calculated contributions (dashed line); (B) k^1 -weighted imaginary part and magnitude of the Fourier transform of the data (solid line) and sum of the calculated contributions (dashed line); (C) k^1 -weighted, phase-corrected, imaginary part and magnitude of the Fourier transform of the data (solid line) and calculated contributions (dashed line) of Ir-O_{support} shell; (D) k^1 -weighted, phase-corrected, imaginary part and magnitude of the Fourier transform of the data (solid line) and calculated contributions (dashed line) of Ir-C shell; (E) k^2 -weighted, phase-corrected, imaginary part and magnitude of the Fourier transform of the data (solid line) and calculated contributions (dashed line) of Ir-Al shell; (F) k^2 -weighted, phase-corrected, imaginary part and magnitude of the Fourier transform of the data (solid line) and calculated contributions (dashed line) of Ir-O_{long} shell.

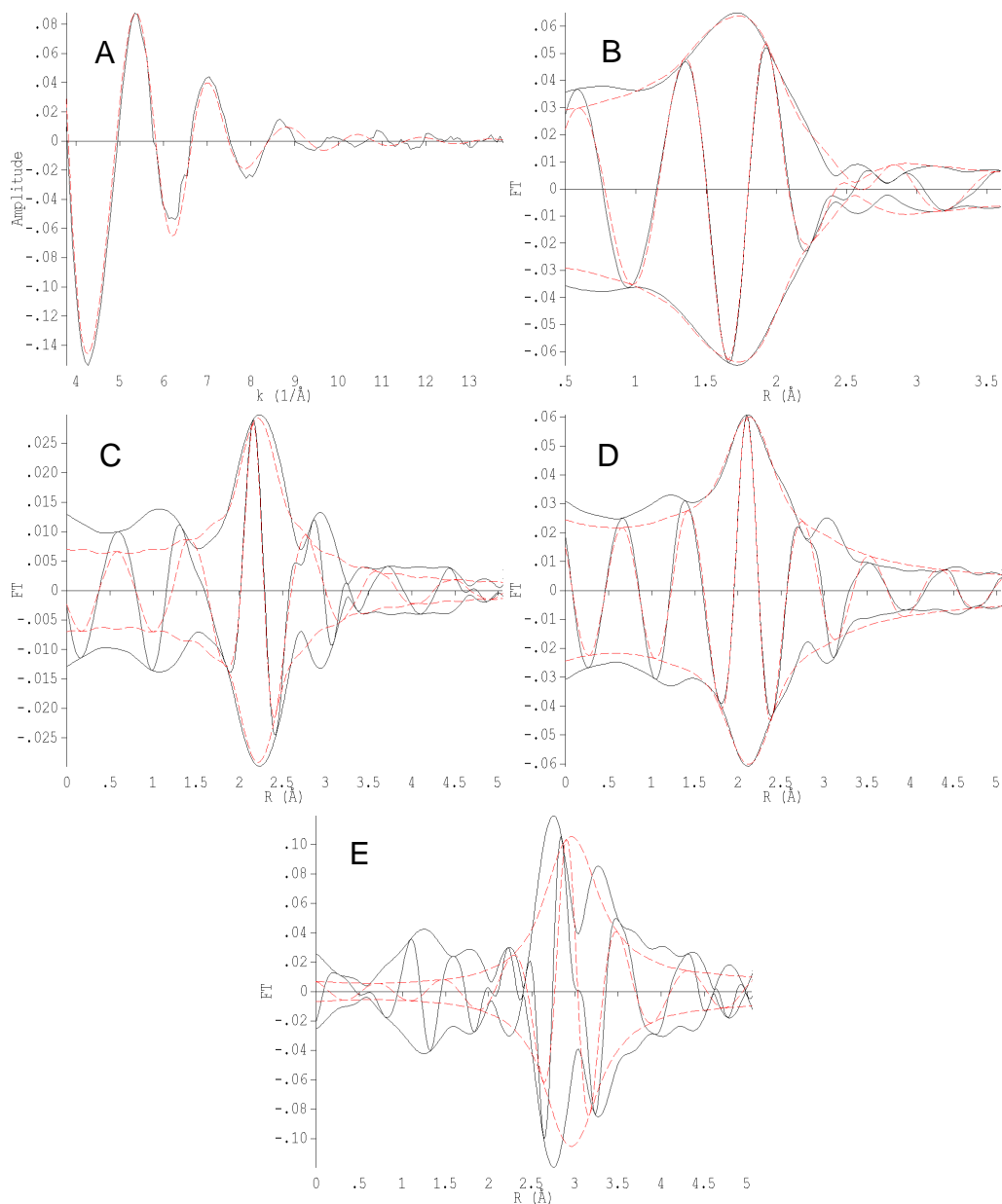


Figure SI-C5. EXAFS data characterizing the dealuminated Zeolite Y-supported iridium complex after cyclohexene hydrogenation at 22 °C. Fitting for Model III: (A) k^1 -weighted EXAFS function, $k^1(\chi)$ (solid line) and sum of the calculated contributions (dashed line); (B) k^1 -weighted imaginary part and magnitude of the Fourier transform of the data (solid line) and sum of the calculated contributions (dashed line); (C) k^1 -weighted, phase-corrected, imaginary part and magnitude of the Fourier transform of the data (solid line) and calculated contributions (dashed line) of Ir-O_{support} shell; (D) k^1 -weighted, phase-corrected, imaginary part and magnitude of the Fourier transform of the data (solid line) and calculated contributions (dashed line) of Ir-C shell; (E) k^2 -weighted, phase-corrected, imaginary part and magnitude of the Fourier transform of the data (solid line) and calculated contributions (dashed line) of Ir-Al shell.

Calculation of Thiele Modulus. To check if our system is diffusion- or chemical reaction-limited, we compared the time scales for molecular diffusion and reaction with the Thiele Modulus derived for zero-order kinetics in spherical catalyst pellets, eq.SI-C1.

$$\Phi = \sqrt{\frac{k_{obs} \cdot a^2}{D \cdot C_{cyclohexene}^0}} \quad \text{eq. SI-C1}$$

where; k_{obs} is the observed reaction rate constant at $t = 0$, a : pellet's volume to surface ratio, $R/3$ for sphere pellets, radius of a zeolite crystallite was measured from electron microscopy images, D : liquid phase counter-diffusion coefficients for cyclohexene and cyclohexene³ $C_{cyclohexene}^0$: concentration of cyclohexene at $t = 0$. $r_{obs} = k_{obs} \approx 1.9 \times 10^{-2}$ mol/L.s, $R \approx 2.5 \times 10^{-6}$ m, $D \approx 1.9 \times 10^{-16}$ m²/s, $C_{cyclohexene}^0 = 1.6$ mol/L.

Thiele modulus is calculated as 0.65 and accordingly effectiveness factor, η is obtained from the respective table elsewhere⁴ as 0.98. Effectiveness factor being close to 1 indicates that the system is not diffusion-limited. Hence, the active Ir centers at interior pores of the catalyst are being accessed without significant diffusion limitations so that chemical reaction kinetics are being observed, as desired.

Just for comparison to our previous studies⁵ of ethylene hydrogenation in a gas-solid reaction, starting with the same Ir(C₂H₄)₂/zeolite Y catalyst, the Thiele modulus for ethylene hydrogenation is estimated to be 0.13 ($r_{obs} \approx 7.1 \times 10^{-2}$ mol/L.s, $R \approx 2.5 \times 10^{-6}$ m, $D \approx 3.4 \times 10^{-15}$ m²/s,⁶ $C_{ethylene}^0 = 7.5$ mol/L) and the effectiveness factor is ≈ 1 obtained as described above.

REFERENCES

- ¹ Wilkins, R.G. *Kinetics and Mechanisms of Reactions of Transition Metal Complexes*, 2nd ed.; VCH: New York, 1991.
- ² Vaarkamp, M.; Linders, J.C.; Koningsberger, D.C. *Physica B* **1995**, 209, 159.
- ³ Ruthven, D. M.; Stapleton, P. *Chemical Engineering Science*, **1993**, 48, 89.
- ⁴ Fogler, S. H. *Elements of Chemical Reaction Engineering*; 4th Ed.; Prentice Hall PTR: Upper Saddle River, NJ, 2006; pp 830.
- ⁵ Uzun, A.; Gates, B. C. *Angew. Chem., Int. Ed.* **2008**, 47, 9245.
- ⁶ Cen, P. L. *AIChE J.*, **1990**, 36, 789.

CHAPTER VII

QUANTITATIVE 1,10-PHENANTHROLINE CATALYST-POISONING KINETIC STUDIES OF Rh(0) NANOPARTICLE AND Rh₄ CLUSTER BENZENE HYDROGENATION CATALYSTS: ESTIMATES OF THE POISON $K_{\text{association}}$ BINDING CONSTANTS, OF THE EQUIVALENTS OF POISON BOUND AND OF THE NUMBER OF CATALYTICALLY ACTIVE SITES FOR EACH CATALYST

This dissertation chapter contains a paper submitted for publication with a co-author (Finke, R.G.). This chapter presents more detailed analysis of the quantitative 1,10-phenanthroline catalyst poisoning of two model catalysts, Rh(0)_n nanoparticles and Rh₄ clusters, and provides detailed analyses of linear as well as non-linear kinetic quantitative poisoning plots. The resulting quantitative kinetic catalyst poisoning studies of Rh(0)_n nanoparticles and Rh₄ clusters led to estimates of the equivalents of poison bound, quantitative catalyst poisoning association constants, and the numbers of active sites for each catalyst.

The additional quantitative 1,10-phenanthroline poisoning experiments for Rh(0)_n nanoparticles were performed by first author Ercan Bayram. The analysis of data and calculations were done by Ercan Bayram and Richard G. Finke with valuable insights from Jordan Stracke.

The drafts of the complete manuscript were written by Ercan Bayram. The final manuscript was prepared via 12 versions via editing by Professor Richard G. Finke.

Overview

Quantitative catalyst poisoning studies are of fundamental interest and importance since: (a) knowledge of the number of true active sites is required for calculation of the *true* turnover frequency = (moles of product)/(moles of actual *active sites*)(time), and (b) quantitative catalyst poisoning is proving to be a key, required piece of data en route to distinguishing single metal (M_1), small metal cluster (e.g., M_4), or metal nanoparticle (M_n) catalysis. In evidence of the latter point, quantitative catalyst poisoning experiments using 1,10-phenanthroline as the poison proved to be crucial in the recent identification of Rh_4 sub-nanometer clusters as the true benzene hydrogenation catalyst in a system beginning with $[RhCp^*Cl_2]_2$ (Cp^* : ($^5-C_5(CH_3)_5$)) at 100 °C and 50 atm initial H_2 pressure (Bayram et al. *J. Am. Chem. Soc.* 2011, *133*, 18889). However and despite the success of those quantitative poisoning studies, five questions about such poisoning studies remained unanswered, questions posed and then addressed herein. In addition, the analysis herein of the 1,10-phenanthroline poisoning of both $Rh(0)_n$ nanoparticle and Rh_4 sub-nanometer benzene hydrogenation catalysts results in kinetic models for, respectively, strong-binding and weak-binding poisons. Also provided are quantitative estimates of the poison binding constants, of the number of equivalents required to completely poison each catalyst, and of the number of active sites on each catalyst. The weak-binding poison kinetic model is then shown to have immediate applicability towards analyzing extant literature data via its application to literature CS_2 quantitative poisoning data for ammonia-borane dehydrocoupling beginning with a $[Ru(cod)(cot)]$ (cod: cyclooctadiene and cot: cyclooctatriene) precatalyst. The significance of the results is then summarized in a Conclusions section.

Introduction

Catalyst poisoning is a fundamental and important topic to any and all catalysis.^{1,2,3,4,5,6,7,8,9} Indeed, one cannot even calculate a true turnover frequency, defined as $\text{TOF} = \text{moles of product}/(\text{moles of catalytically active sites} \times \text{time})$, without knowledge of the true number of catalytically active sites. Moreover, quantitative catalyst poisoning experiments are proving increasingly important in the identification of the true catalyst in a given reaction, a task that can involve distinguishing single-metal homogeneous from smaller metal cluster and larger, polymetallic nanoparticle catalysis.^{10,11} Poisoning studies are proving powerful in distinguishing such classes of catalysts since on going from a single metal, single-active-site homogeneous catalyst to a heterogeneous, nanoparticle catalyst, the required equivs of poison per total equivs of metal present needed to deactivate completely the catalyst typically decreases from ≥ 1 to $\ll 1$.^{10,11}

Recently, quantitative catalyst poisoning studies using 1,10-phenanthroline as the poison proved crucial in identifying sub-nanometer Rh_4 clusters of average composition $\text{Rh}_4\text{Cp}^*_{2.4}\text{Cl}_4\text{H}_c$ (hereafter abbreviated as Rh_4) as the true catalysts in benzene hydrogenation performed at 100 °C and 50 atm initial H_2 pressure beginning from $[\text{RhCp}^*\text{Cl}_2]_2$ as the precatalyst.¹² In that study, *in operando*¹³ X-ray absorption fine structure (XAFS) studies showed that $98 \pm 2\%$ of the initial Rh present in the $[\text{RhCp}^*\text{Cl}_2]_2$ precatalyst evolved to Rh_4 clusters; however, the 70-fold faster reactivity of model polyethyleneglycol-dodecylether hydrosol stabilized $\text{Rh}(0)_n$ nanoparticles studied in control reactions meant that $\text{Rh}(0)_n$ nanoparticles *would have been* the dominant and kinetically competent catalysts *if* even ca. $\geq 1.4\%$ of the initial $[\text{RhCp}^*\text{Cl}_2]_2$ precatalyst had been converted to $\text{Rh}(0)_n$ nanoparticles. Significantly, 1,10-phenanthroline quantitative catalyst poisoning experiments, reproduced in Figures 7.1 and 7.2 herein, were, in the end analysis, what

distinguished Rh₄ clusters as the true catalyst from larger, 2-3 nm Rh(0)_n nanoparticles as an alternative hypothesis for the true catalyst.¹²

The poisoning data in Figures 7.1 and 7.2 were analyzed previously¹² via the common literature practice^{1,11} of drawing straight lines to the linear portion of plot to find $x_{\text{intercept}}$: the $x_{\text{intercept}}$ for the Rh(0)_n nanoparticles¹⁴ is 0.10 ± 0.02 , Figure 7.1, whereas, for the Rh₄ clusters $x_{\text{intercept}}$ is 4.0 ± 0.4 , Figure 7.2—the Rh₄ sub-nanometer cluster catalyst requiring significantly more poison in comparison to the Rh(0)_n nanoparticle catalyst, as expected since only a fraction of the total Rh in the nanoparticle case is on the surface, and thus accessible. Hence and as already mentioned, the quantitative 1,10-phenanthroline poisoning experiments proved to be crucial in identifying Rh₄ sub-nanometer clusters as the true benzene hydrogenation catalyst when beginning with the [RhCp*Cl₂]₂ precatalyst.¹²

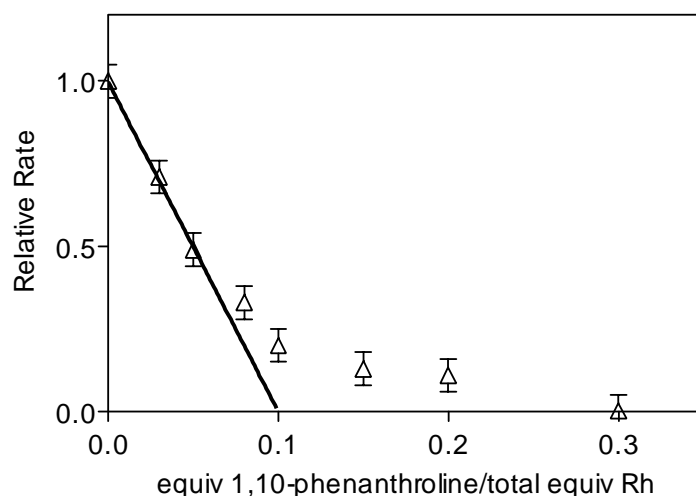


Figure 7.1. Plot of the relative rate vs equivs of 1,10-phenanthroline per equivs of total rhodium present for benzene hydrogenation beginning with model polyethyleneglycol-dodecylether hydrosol stabilized Rh(0)_n nanoparticles at 100 °C and 50 atm initial H₂ pressure. The value of the $x_{\text{intercept}}$ is 0.10 ± 0.02 for the straight line drawn.¹⁴

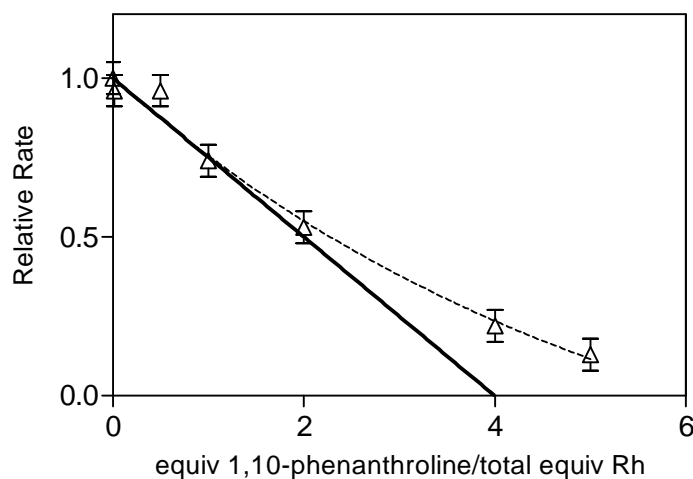


Figure 7.2. Plot of the relative rate vs equivs of 1,10-phenanthroline per equivs of total, fully evolved rhodium present in the form of $98 \pm 2\%$ Rh_4 clusters identified via *in operando*-XAFS¹² for benzene hydrogenation at 100 °C and 50 atm initial H_2 pressure. The value of the $x_{\text{intercept}}$ is 4.0 ± 0.4 for the tangent, straight line drawn.

Despite the seemingly definitive nature^{11,15} of the quantitative poisoning studies in Figures 7.1 and 7.2, five questions remain to be addressed following the prior work.¹² First, (i) what does the $x_{\text{intercept}}$ value of 0.10 in Figure 7.1 really mean in terms of the amount of poison required to deactivate the nanoparticles completely? Is a more rigorous, quantitative interpretation of such poisoning curves possible? Second, (ii) although the approximately linear dependence of $\text{Rh}(0)_n$ nanoparticle activity on the equivs of 1,10-phenanthroline implies a strong association between $\text{Rh}(0)_n$ nanoparticles and 1,10-phenanthroline, Figure 7.1, can one estimate a quantitative value for the binding constant of the 1,10-phenanthroline poison to the $\text{Rh}(0)_n$ nanoparticle catalyst, $K_{\text{association}}$ (hereafter abbreviated as $K_{\text{assoc.}}$)?^{16,17} Also, can the $K'_{\text{assoc.}}$ for 1,10-phenanthroline binding to the Rh_4 clusters also be obtained? Third, (iii) can one estimate a narrower range of values for the ratio of poison to the number of catalytic sites deactivated than, for example, the previously reported¹¹ $\text{CS}_2/\text{Rh}(0)_n$ ratios of ca. 1/1.5 to 1/20? This ratio is needed to calculate the number of

active sites, and thus the true turnover frequency, from the experimentally observed ratio of $\text{CS}_2:\text{Rh}(0)_n$ needed to fully poison the catalyst. We previously identified this ratio as the “Achilles Heel” of otherwise powerful catalyst poisoning studies aimed at determining the true number of catalytically active sites.¹¹ Fourth, (iv) since a closer look at the poisoning curve in Figure 7.2 shows a slightly sigmoidal shape, qualitatively implying a smaller K_{assoc} constant compared to Figure 7.1, is the use of this classic “straight-line extrapolation”^{1,11} method, and resultant $x_{\text{intercept}}$, *not justified* as it seems? Can a more appropriate, quantitative kinetic poisoning model be applied, and if so, what does constructing such a weak-binding poison kinetic model teach us? Fifth and finally, (v) what is the best method(s) of analyzing nanoparticle and sub-nanometer cluster catalysts poisoning data obtained in solution? Solid-gas phase, supported nanoparticle catalyst poisoning data are traditionally and commonly handled by Langmuir adsorption isotherms,^{16,17,18,19,20} while enzyme poisoning data are analyzed by a Michaelis-Menten kinetic treatments.^{21,22,23,24,25,26}

To start, a careful search of the literature relevant to the five questions above yielded the following literature insights as a foundation from which to build the present contribution. First, historically,¹ quantitative poisoning data (plotted typically as *catalyst activity vs concentration of the poison*, with tangential straight lines being drawn; see Figure 8 elsewhere¹) were then treated by Maxted using the linear equation $k_c = k_0(1 - \alpha c)$, where k_0 is the activity without any poison present, k_c is the activity when c concentration of poison is present, and α is the relative susceptibility of different catalysts to a poison under, ideally, otherwise identical conditions.¹ Later, others^{27,28} and we¹¹ analyzed quantitative catalyst poisoning data via plots of the *relative rate vs equivs of poison per total equivs of metal present*, with an eye here towards making apparent the number of equivalents of poison required to poison the total metal present. Again

tangential straight lines were drawn which were now analyzed by the simple, classic expression $y = -ax + b$ where y is the relative rate, $-a$ is the slope of the resultant line, x is the eqivs of poison per total eqivs of metal present, and b is 1, as in Figures 7.1 and 7.2, vide supra, a treatment that is equivalent to Maxted's equation¹ if $y = \text{relative rate} = k_c/k_0$ and $-\infty c = -ax$. The value of this treatment of the data is that the $x_{\text{intercept}}$ (i.e., value of x when $y=0$) provides an estimate of the eqivs of poison per total metal present required to fully poison the catalyst. However, the $x_{\text{intercept}}$ is only an estimate in the more general case where the poisoning plot is not strictly linear—that is, when one is drawing a straight-line tangent to the curved plot, as in Figures 7.1 and 7.2. A more rigorous, quantitative interpretation of $x_{\text{intercept}}$ in this more general case is lacking, but is addressed herein.

Returning to what else can be gleaned from the catalyst poisoning literature, catalyst poisoning data have been treated extensively in the chemical engineering literature,⁵ including the extraction of thermodynamic data (such as $K_{\text{assoc.}}$) via engineering models focused on industrial catalysts and their reactors. However, those typically reactor-based studies (a) necessarily include variables such as (but not limited to) reactor type, flow gas rate, and catalyst bed type, and often for solid-gas phase catalytic reaction conditions;^{29,30,31} (b) usually are, therefore, specific to a given system with resultant complex mathematical equations that obfuscate ready interpretation of the underlying, basic chemistry;^{4,5,32} and hence and as Bartholomew has noted³³ (c) provide “comprehensive mathematical models that will enable more effective design and optimization of the processes deactivating catalysts”,³³ but lack the ability to understand the poisoning phenomena at the molecular level^{34,35,36,37,38}—the latter being the goal of quantitative catalyst poisoning *mechanistic* studies such as the present work.

Unfortunately but not surprisingly, phenomenology based words and nomenclature have arisen in the chemical engineering literature from such non-mechanistic treatments, for example the term of “antiselective poisoning”⁵ (really just sigmoidal poisoning curves signifying relatively weak poisoning binding) just to pick an example, nomenclature that further obfuscates what is really occurring chemically. This is not a trivial point. The use of phenomenological, “physical” models, in place of disproof-based mechanistic models, in science is an insidious problem *that often results in the wrong concepts and words being used*,³⁹ in the final analysis, to (incorrectly) describe the resultant chemistry. More on this important topic is available elsewhere³⁹ for the interested reader.

Herein, we address the questions (i)-(v) raised above in-so-far as possible by (a) deriving and justifying the $x_{\text{intercept}}$ term rigorously en route to calculating the required amount of poison (i.e., variable m in what follows) needed to deactivate the catalyst completely, (b) estimating the average $K_{\text{assoc.}}$, and (c) estimating the number of catalytically active surface sites, with the first part of what follows focusing on the 1,10-phenanthroline quantitative poisoning data¹² for Rh(0)_n nanoparticle catalyzed benzene hydrogenation at 100 °C and 50 atm initial H₂ pressure. We also (d) propose a mechanism-based kinetic model from which to analyze rigorously the 1,10-phenanthroline quantitative poisoning data for Rh₄ cluster-based benzene hydrogenation at 100 °C and 50 atm initial H₂ pressure, an example of the probably more general case where a slightly sigmoidal poisoning plot is obtained, cases where drawing straight-line tangents makes little sense. The resultant kinetic model and quantitative analysis of the poisoning data then (e) allows us to extract the required amount of poison to deactivate Rh₄ cluster catalyst completely (i.e., m), and (f) estimates of the quantitative $K'_{\text{assoc.}}$. Finally, (g) literature CS₂ quantitative poisoning data for ammonia-borane dehydrocoupling beginning with a [Ru(cod)(cot)] precatalyst are analyzed

using the weak-binding poison kinetic model developed herein, results which demonstrate the immediate applicability of that poisoning kinetic model.

Experimental

Materials. Benzene (Aldrich, 99.8%, anhydrous, packaged under N₂), 2-propanol (Aldrich, 99.5%, anhydrous, packaged under N₂), and 1,10-phenanthroline (Aldrich, 99%) were transferred to and stored in a drybox, then used as received. Hydrogen gas (General Air, 99.5%) was used as received. Rh(0)_n nanoparticles (polyethyleneglycol-dodecylether hydrosol stabilized, ~9 wt%-Rh, ~2 nm Rh(0)_n nanoparticles) were purchased from Strem Chemicals, stored in the drybox, and used as received.

General Procedures for Quantitative 1,10-Phenanthroline Poisoning Experiments with Rh(0)_n Nanoparticles and Rh₄ Clusters. All experimental preparations and manipulations were performed under oxygen- and moisture-free conditions in a Vacuum Atmosphere N₂-drybox (<2 ppm of O₂ as continuously monitored by a Vacuum Atmosphere O₂-monitor). All quantitative 1,10-phenanthroline poisoning experiments for benzene hydrogenation reaction with either Rh(0)_n nanoparticles or Rh₄ clusters were performed in a Parr pressure reactor (model 4561) made of Monel 400 alloy. The reactor is equipped with a pressure gauge marked at intervals of 20 psig (~1.36 atm) and an automatic temperature controller (±3 °C). The inside of the reactor contains a stainless steel (i.e., non-Monel) impeller, thermocouple, cooling loop, and dip tube, all of which are in contact with the reaction solution. A glass-liner was used to avoid contacting the reaction solution with the rest of the reactor. The glass-liner was dried overnight in a 160 °C drying oven before being transferred into the drybox and prior to use. Pressurizing the reactor took about 1 min, and $t = 0$ was set after this time and once the reactor was fully pressurized. Pressure gauge readings vs time data were then collected and recorded manually.

1,10-Phenanthroline Quantitative Poisoning Experiments in Benzene Hydrogenation Reaction Beginning with Polyethyleneglycol-dodecylether Hydrosol Stabilized Rh(0)_n Nanoparticles. Recently reported¹² relative rate data for the quantitative poisoning of polyethyleneglycol-dodecylether hydrosol stabilized Rh(0)_n nanoparticles were used with three additional experiments being added. For those additional experiments, the same experimental procedure was repeated as detailed elsewhere¹² (in the Experimental section titled “1,10-Phenanthroline Quantitative Poisoning Experiments for Polyethyleneglycol-dodecylether Hydrosol Stabilized Rh(0)_n Nanoparticles”¹²), but now using the addition of 0.03, 0.08, and 0.15 equivs of 1,10-phenanthroline per total rhodium (1.1, 2.9, and 5.4 mg of 1,10-phenanthroline, respectively) to the initial solution in three separate, additional poisoning experiments. The resultant hydrogenation curves for each trial were fit to a polynomial and the initial rate was calculated as detailed previously¹² (in the Experimental Section titled “Kinetic Data Treatment: Initial Rate Method”) and as shown in the Supporting Information herewith, Figure SI-D3. Each poisoning trial was repeated three times and yielded identical initial rates within ±15% experimental error. The other 1,10-phenanthroline poisoning hydrogenation curves and initial rates are available as Figure SI-9 elsewhere.¹²

*1,10-Phenanthroline Quantitative Poisoning Experiments for Benzene Hydrogenation Beginning with, on average, Rh₄Cp*_{2.4}Cl₄H_c Clusters.* Recently reported¹² relative rate data for the quantitative poisoning of Rh₄Cp*_{2.4}Cl₄H_c clusters with 1,10-phenanthroline were used. See Figure 7, Figures SI-8(b-f), and the experimental procedures elsewhere.¹²

Data Handling. The non-linear least squares fit of the experimental data for the 1,10-phenanthroline quantitative kinetic poisoning of the Rh₄ clusters was performed using GraphPad

Prism version 5 for Mac OS X, GraphPad Software, San Diego California USA, www.graphpad.com.

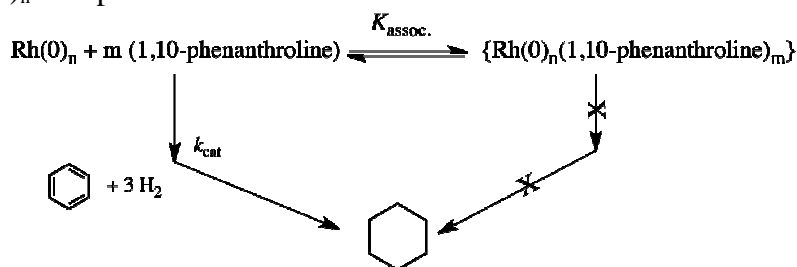
Results and Discussion

Analysis of 1,10-Phenanthroline Poisoning of Rh(0)_n Nanoparticles.

Correlation of $x_{intercept}$ with the amount of poison “m” required to deactivate the catalyst completely.

The quantitative poisoning plot of polyethyleneglycol-dodecylether hydrosol stabilized Rh(0)_n nanoparticles with 1,10-phenanthroline is given in Figure 7.1. The relative rate initially decreases linearly with increasing poison equivs, as is commonly seen in the literature.^{1,11} The typical literature practice^{1,11} of the linear regression analysis of this linear portion of the plot yields $x_{intercept}$ of 0.10 ± 0.02 , Figure 7.1.¹⁴ In order to justify the $x_{intercept}$ as well as analyze the basic underlying chemistry, a simple 1,10-phenanthroline poisoning scheme is proposed, Scheme 7.1. A full derivation of the kinetics corresponding to Scheme 7.1, eq. 7.1, is provided in the Supporting Information.

Scheme 7.1. A minimalistic, strong-binding poison kinetic model for 1,10-phenanthroline poisoning of Rh(0)_n nanoparticles.



$$\text{relative rate} = \left(-\frac{1}{m}\right) \left\{ \frac{[1,10\text{-phenanthroline}]_{\text{initial}}}{[\text{Rh}(0)_n]_{\text{initial}}} \right\} + 1 \quad \text{eq. 7.1}$$

Briefly, the initially linear decrease in catalytic activity with added 1,10-phenanthroline implies a strong association between the Rh(0)_n nanoparticles and the 1,10-phenanthroline, one where all the added 1,10-phenanthroline binds to the Rh(0)_n nanoparticles, at least in the initial, linear region. Hence, in the initial linear region, the initial 1,10-phenanthroline concentration will be equal to the poisoned catalyst concentration, that is, [1,10-phenanthroline]_{initial} ≈ m[{Rh(0)_n(1,10-phenanthroline)_m}. The resultant relative rate equation is then eq. 7.1, which is in the form of the standard linear function: $y=ax+b$, where y is the relative rate; a is the slope, $(-1/m)$; x is {[1,10-phenanthroline]_{initial}/[Rh(0)_n]_{initial}}, namely the equivs of poison per equivs of *total metal present*;⁴⁰ and b is 1.

The linear regression analysis of the initially linear portion of Figure 7.1 yields $y=-9.9x+1$ with a $x_{\text{intercept}}$ equal to 0.10. The slope of the line is $-(1/m) = -9.9$ making $m = 0.10$, m being the required equivs of 1,10-phenanthroline per total equivs of metal needed to deactivate the catalyst completely. Hence, m is equal to $x_{\text{intercept}}$.

Overall, the analysis of Scheme 7.1 reveals the $x_{\text{intercept}}$ ($= m$) is indeed the amount of 1,10-phenanthroline required to deactivate completely the Rh(0)_n nanoparticles catalyst, as expected given the tight binding of the poison, [1,10-phenanthroline]_{initial} ≈ m[{Rh(0)_n(1,10-phenanthroline)_m}] assumption used in the derivation of eq. 7.1. There is, then and also, an equivalence between eq. 7.1 and the $k_c=k_0(1-\infty c)$ equation used classically to treat strong-binding poisoning data:¹ the two are equivalent if the relative rate = k_c/k_0 so that, therefore, also $\infty c = (1/m)\{[1,10\text{-phenanthroline}]_{\text{initial}} / [\text{Rh}(0)_n]_{\text{initial}}\}$.

Estimate of the Approximate K_{assoc} .

One can also in principle calculate the K_{assoc} in Scheme 7.1 via eq. 7.2 where now, for simplification in writing the equilibrium expression, the amount of poisoned catalyst, $[\{\text{Rh}(0)_n(1,10\text{-phenanthroline})_m\}] = [P]$, $[\text{Rh}(0)_n]_{\text{initial}} = [A_0]$, and $[1,10\text{-phenanthroline}]_{\text{initial}} = [B_0]$. However, recalling the $[1,10\text{-phenanthroline}]_{\text{initial}} \approx m[\{\text{Rh}(0)_n(1,10\text{-phenanthroline})_m\}]$ (or, now, equivalently in the simplified nomenclature $[B_0] \approx m[P]$) assumption used to derive eq. 7.1, vide supra, the $[B_0] - m[P]$ term in the denominator of eq. 7.2 is approximately zero, and as a result K_{assoc} “blows up” / becomes undefined.

$$K_{assoc} = \frac{[P]}{\{[A_0] - [P]\} \{[B_0] - m[P]\}^m} \quad \text{eq. 7.2}$$

However, one can calculate via eq. 7.3 the poisoned catalyst concentration, $[P]$, from the experimentally determined relative rate values. Then, substituting the eq. 7.3 $[P]$ values into eq. 7.2 followed by simplification yields eq. 7.4 (see the Supporting Information for details). Then, using the experimentally determined $m = 0.1$ value, an estimate of $K_{assoc} \leq 1.4 \text{ M}^{-0.10}$ is obtained via eq. 7.4. Note that the unusual units ($\text{M}^{-0.10}$) of K_{assoc} in this strong-binding case mean that this specific K_{assoc} can be compared quantitatively only to other K_{assoc} that have identical m values (i.e., and thus identical units). Worth noting here is that, as one might expect, 1,10-phenanthroline is known to bind relatively tightly to other metal nanoparticles. For example, 1,10-phenanthroline binds tightly to Pd nanoparticles with polyvinyl pyrrolidone (PVP) as an added stabilizer employed in olefin hydrogenations.⁴¹

$$[P] = [A_0] \times (1 - \text{relative rate}) \quad \text{eq. 7.3}$$

$$K_{\text{assoc.}} = \frac{\{1 - \text{relative rate}\}}{\{\text{relative rate}\} \{ [B_0] - m \{ [A_0] \{1 - \text{relative rate}\} \} \}^m} \quad \text{eq. 7.4}$$

Estimate of the Number of the Catalytically Active Sites.

The Rh(0)_n nanoparticles are 2-3 nm according to TEM analysis (see Figure SI-6 elsewhere¹²), which in turn corresponds to Rh(0)_{~300} and Rh(0)_{~1100} nanoparticles, respectively,^{42,43} that is, on average Rh(0)_{~700} nanoparticles for the purposes of the following estimate of the number of catalytically active sites. Such average Rh(0)₇₀₀ nanoparticles have ca. 40% of their total rhodium present on the surface,^{42,43} where catalysis occurs. With the assumption that one 1,10-phenanthroline poisons one surface rhodium (i.e., if one assumes a Rh:1,10-phenanthroline ratio is 1:1), then the $x_{\text{intercept}}$ of 0.10 equiv of 1,10-phenanthroline poison per total rhodium becomes 0.25 equiv of 1,10-phenanthroline per total *surface* rhodium. (If, on the other hand, two or three catalytically active sites are poisoned by one 1,10-phenanthroline simultaneously, then, the fraction of catalytically active surface Rh atoms becomes 0.50 and 0.75, respectively.) Noteworthy here is that simultaneous deactivation of four surface rhodium atoms by one 1,10-phenanthroline is an upper limit to since at a Rh:1,10-phenanthroline ratio is 4:1, 100% of the surface Rh would have to be active (so called completely “naked nanoparticles”,⁴⁴ which are unknown⁴⁴). Hence, the useful implication is that one 1,10-phenanthroline molecule poisons between 1-3, and rigorously ≤ 4 , surface Rh atoms, at least under these specific conditions of our benzene hydrogenation experiments and within the Rh(0)_{~700} average nanoparticle size assumption.

Quantitative Analysis of 1,10-Phenanthroline Poisoning of Rh₄ Clusters. The poisoning plot of Rh₄ clusters by 1,10-phenanthroline, Figure 7.2, is slightly but detectably sigmoidal, implying a weaker association of 1,10-phenanthroline to the Rh₄ clusters and concomitant smaller K_{assoc} . Quantitatively, when $[\text{Rh}_4]_{\text{initial}} = 1.15 \times 10^{-3} \text{ M}$ and $[\text{1,10-phenanthroline}]_{\text{initial}} = 2.3 \times 10^{-3} \text{ M}$, a relative rate of 0.96 was observed¹²—that is, the benzene hydrogenation catalytic activity is virtually unaffected, yielding the same relative rate within $\pm 10\%$ experimental error to that seen *without* any 1,10-phenanthroline addition. This is arguably consistent with the small, approaching homogeneous catalysts by the Rh₄Cp*_{2.4}Cl₄H_c,¹² such homogeneous catalysts having been previously claimed to be less sensitive to poisons,^{45,46} at least when coordinated to sterically bulky ligands¹ such as the Cp* in Rh₄Cp*_{2.4}Cl₄H_c. The most important initial point here, then, is that the classic, linear treatment of fitting with a straight line (i.e., with $k_c = k_0(1 - \alpha c)$ or its relative rate vs equivs of poison per equivs of metal catalyst version, eq. 7.1) *is inappropriate and should not be used*^{1,11} due to the non-linear, sigmoidal nature of the poisoning plot, Figure 7.2.

Scheme 7.2 presents an alternative, minimalistic kinetic model from which to analyze the 1,10-phenanthroline poisoning of the Rh₄ clusters under the weak-binding assumption where also experimentally $[\text{1,10-phenanthroline}]_{\text{initial}} \gg m'[\{\text{Rh}_4(\text{1,10-phenanthroline})_{m'}\}]$ so that $[\text{1,10-phenanthroline}]_{\text{initial}} \approx [\text{1,10-phenanthroline}]_{\text{equilibrium}}$. Eq. 7.5 gives the resultant relative rate expression, with now its K'_{assoc} and m' constants, that were used to analyze quantitatively the poisoning data back in Scheme 7.2 for 1,10-phenanthroline poisoning of the Rh₄ clusters. The Supporting Information provides the full details of the derivation of eq. 7.5.

axis is the $[1,10\text{-phenanthroline}]_{\text{initial}}$ concentration required for the curve-fitting by eq. 7.5 (i.e., and not the equivs 1,10-phenanthroline per total equivs Rh present, Figure 7.1).

The good fit seen in Figure 7.3 supports the assumption of $[1,10\text{-phenanthroline}]_{\text{initial}} \approx [1,10\text{-phenanthroline}]_{\text{equilibrium}}$ that was used to derive eq. 7.5 and as detailed in the Supporting Information. In addition, ex-post-facto calculations support the $[1,10\text{-phenanthroline}]_{\text{initial}} \approx [1,10\text{-phenanthroline}]_{\text{equilibrium}}$ assumption by showing that ca. 90% of $[1,10\text{-phenanthroline}]_{\text{initial}}$ is $[1,10\text{-phenanthroline}]_{\text{equilibrium}}$ for each value of $[1,10\text{-phenanthroline}]_{\text{initial}}$ actually used (the Supporting Information presents the details of these calculations for the interested reader).

Estimates of the K_{assoc} Value and the Number of the Catalytically Active Sites.

As noted above, the association constant for the 1,10-phenanthroline binding to the Rh_4 clusters is $K'_{\text{assoc}} = 6.1 \pm 4.4 \times 10^3 \text{ M}^{-1.86}$. The m' is 1.86 ± 0.15 (i.e., ca. 2), so that a ca. 2 equivs of 1,10-phenanthroline per $\text{Rh}_4\text{Cp}^*_{2,4}\text{Cl}_4\text{H}_c$ are required to completely deactivate the Rh_4 catalyst—a result that makes physical sense, that is, that there are ca. 2 sites of coordinative unsaturation in the ligated, Rh_4 sub-nanometer cluster. Significantly, a m' of ca. 2 is more reasonable than a linear treatment of the data and then resultant $x_{\text{intercept}}$ value of 4.0 ± 0.4 and its implied ca. 4 equiv of 1,10-phenanthroline per total rhodium, ca. 16 equivs of 1,10-phenanthroline per Rh_4 cluster available previously from the data in Figure 7.2.¹² The refined $m' = \text{ca. } 2$ value implies that, on average, one 1,10-phenanthroline binds one of the ca. two total vacant coordination sites on the Rh_4 cluster, at least under the specific benzene hydrogenation catalysis conditions employed of 2-propanol at 100 °C and 50 atm initial H_2 pressure.^{47,48}

Quantitative Analysis of Recent Literature Poisoning Data: CS_2 Poisoning of Ammonia-Borane Dehydrocoupling at 25 °C Beginning with $[\text{Ru}(\text{cod})(\text{cot})]$. Zahmakıran and coworkers recently reported quantitative CS_2 poisoning data for ammonia-borane

dehydrocoupling beginning with a [Ru(cod)(cot)] precatalyst.⁴⁹ Although TEM and zero contrast-TEM investigation of the resultant reaction mixture revealed the presence of agglomerated ca. 60 nm Ru nanoparticles, quantitative poisoning experiments using the CS₂ method we developed for nanoparticles in 2002¹¹ showed that the addition (once the hydrogen evolution was 40% complete) of even 2 equivs of CS₂ per total Ru did not completely poison the catalyst (Table SI-D2 of the Supporting Information herein); instead, ca. 13% of the initial activity still remained. Their quantitative CS₂ poisoning data are reproduced in Figure 7.4 and caught our eye, since they are also slightly sigmoidal, suggesting that the use of a linear, strong-binding poison model is not appropriate but, instead, that the weak-binding kinetic model in Scheme 7.2 developed herein might be applicable and a better treatment of the data.

To test if Scheme 7.2 and eq. 7.5 herein could fit their data, a curve-fit was carried out in the data in Figure 7.4 using the weak-binding poison model in Scheme 7.2 and its associated eq. 7.5. A good fit to the data is seen, one that makes apparent the sigmoidal nature of the poisoning curve and, therefore, the *inappropriateness of the strong-binding, linear extrapolation fit approach in Scheme 7.1 for the analysis of this data.* (*Ex-post-facto* checks on the weak-binding assumption are also provided as part the Supporting Information.) The results from the poisoning curve-fitting yield a $m''=2.9 \pm 0.4$, one a value consistent with the reported⁴⁹ $x_{\text{intercept}}$ of ≥ 2.0 (that ≥ 2.0 value being obtained, however, via drawing a tangent line to an incomplete set of the poisoning data, one where data at 0.0 and 0.2 equiv CS₂ per total Ru appear to have been arbitrarily excluded; see Figure SI-9 elsewhere⁴⁹). Hence, the fit in Figure 7.4 at least illustrates the need for and value of Scheme 7.2 and its associated eq. 7.5 to begin to think more rigorously about how one might account for non-linear, sigmoidal poisoning curves that look to be weak-binding cases.

The authors see 0.6-2.2 nm particles by microscopy (once the hydrogen evolution was ca. 30% complete), but on the basis of the poisoning studies propose sub-nanometer, Ru_n cluster catalysis, the precise identity and nuclearity of which remain to be determined. The finding herein of $m''=2.9 \pm 0.4$ (i.e., and not a value closer to 0.1 for example) is in general support of their conclusion, although *in-operando* spectroscopy¹³ is needed to identify the dominant form(s) of Ru present under the reaction conditions (i.e., only if the sub-nanometer cluster is the dominant form of the Ru mass present can one say that the finding of $m''=2.9 \pm 0.4$ strongly supports a sub-nanometer, Ru_n cluster—vs for example a larger nanoparticle—catalyst). This literature example again illustrates both the importance of quantitative kinetic poisoning experiments in determining the true catalyst, as well as the value of the treatment and equations herein for treating such non-linear poisoning plot data in a more rigorous fashion.

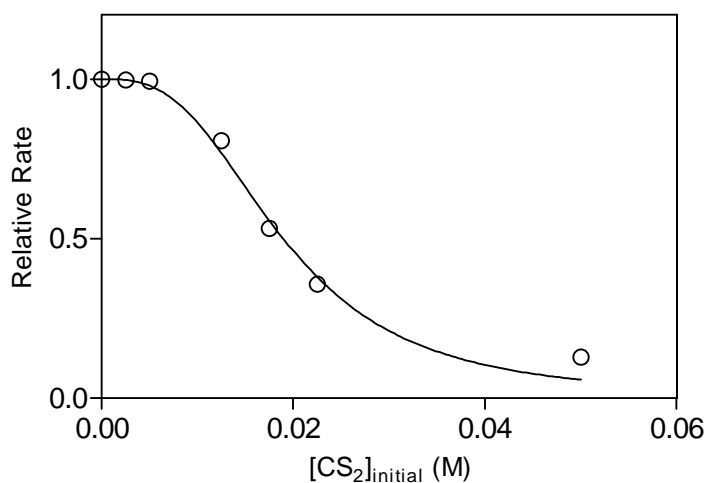


Figure 7.4. Curve-fit (—) of the reported⁴⁹ CS_2 poisoning data (O), Table SI-D2, by eq. 7.5 herein, $R^2=0.989$.

Conclusions

Analysis of 1,10-phenanthroline quantitative poisoning kinetic experiments, for Rh(0)_n nanoparticles as well as Rh₄ clusters undergoing benzene hydrogenation reaction at 100 °C and 50 atm initial H₂ pressure, led to several insights, including:

- (i) A strong-binding model for 1,10-phenanthroline attachment to the Rh(0)_n nanoparticles can account for the observed catalyst poisoning data, and in a closer, more rigorous look at the data. A minimalist, strong-binding mechanistic model, Scheme 7.1, clarifies the common practice^{1,11} of drawing a tangent to the often at least somewhat curved poisoning plot of the relative rate vs equivs of poison/equivs of total metal present. The $x_{\text{intercept}}$ of such classical treatments of the data does in fact give the total number of equivalents of poison needed to deactivate completely the catalyst, with $x_{\text{intercept}}=m$ of the strong-binding mechanistic model, Scheme 7.1. In addition, a correspondence with eq. 7.1 from Scheme 7.1 and the historical $k_c=k_0(1-\infty c)$ equation used to analyze poisoning data since the 1950s was, while perhaps obvious at least in hindsight, clarified and mathematically equated. The data were then used to see what limit resulted for K_{assoc} in the strong-binding case, and the m value and the average size of the nanoparticles were used to estimate the fraction of surface catalytically active sites.
- (ii) Second, a weak-binding model for 1,10-phenanthroline attachment to Rh₄ sub-nanometer clusters was shown to account for that observed catalyst poisoning data. The initially non-linear, slightly sigmoidal poisoning curve was shown to very nicely and quantitatively fit the data, yielding physically reasonable K'_{assoc} and m' values. The m' value was then used to provide a probably good estimate of the number of vacant coordination sites (two) on the Rh₄ cluster catalyst of average composition Rh₄Cp*_{2.4}Cl₄H_c.¹²

(iii) Third, an example of interesting, recent CS₂-based catalyst poisoning data from the literature⁴⁹ was analyzed and shown to be quantitatively accounted for by the weak-binding poison kinetic model developed herein. The results provide credence to both the broader applicability of the weak-binding model as well as the emphasized value¹² of quantitative catalyst poisoning experiments in correctly and rapidly identifying the true catalyst in a given system.

(iv) The results presented herein also are important in that they fortify our recent conclusion,¹² that Rh₄Cp*_{2,4}Cl₄H_c sub-nanometer clusters are the true catalyst in benzene hydrogenation beginning with Maitlis' classic system discovered some 35 years ago⁵⁰ of [RhCp*Cl₂]₂ and at 100 °C and 50 atm initial H₂ pressure. Specifically, the results herein disprove the alternative hypothesis we raised¹² of "...1,10-phenanthroline poison could be bound first by the Rh₄ clusters, with no poisoning reaching the (in this case hypothesized, true) Rh(0)_n catalyst until the 1,10-phenanthroline binding capacity of the Rh₄ clusters had been saturated."¹² The results herein rule out this possibility since the Rh(0)_n nanoclusters have the higher affinity for the 1,10-phenanthroline poison than do the heavily ligated, apparently sterically more congested, Rh₄Cp*_{2,4}Cl₄H_c sub-nanometer clusters.

(v) Finally, the results herein and those of others^{26,51} provide additional evidence for our assertion¹² that quantitative catalyst poisoning experiments can provide some of the strongest, often necessary, evidence for correctly identifying the true catalyst in multiple types of catalytic reactions, be they the benzene hydrogenations¹² and amine-borane dehydrocoupling catalysis data⁴⁹ treated herein or the transfer hydrogenation of ketones⁵¹ or CO oxidation catalysts²⁶ reported by others.

Acknowledgments

Authors would like to thank Finke-group members Jordan Stracke, Dr. Joseph Mondloch, and Will Laxson for valuable discussions during the preparation of the manuscript. Financial support was provided by the Department of Energy, Grant DE-FG02-03ER15453.

Supporting Information Available. Derivation of the equations for the strong-binding poison case; Analysis of the sigmoidal quantitative 1,10-phenanthroline poisoning plot for Rh₄ subnanometer clusters; Ex-post-facto confirmation of $[B'_0] \gg m'[P']$ with the $K'_{\text{assoc.}}$ and m' values obtained via non-linear least-squares fitting of the poisoning data; Comparison of $K'_{\text{assoc.}}$ values obtained by the controls of using the now available $[B'_0]-m'[P']$ values and fit the poisoning data; Additional 1,10-phenanthroline poisoning experiment results with Rh(0)_n nanoparticles; Analysis of the recently published quantitative CS₂ poisoning of ammonia-borane dehydrocoupling reaction beginning with [Ru(cod)(cot)] at 25 °C, including *ex-post-facto* justification of the weak-binding assumption. This material is free of charge via the Internet at <http://pubs.acs.org>.

REFERENCES

- ¹ Maxted, E.B. *Adv. Catal.* **1951**, 3, 129-177.
- ² Butt, J.B. *Stud. Surf. Sci. Catal.* **1997**, 111, 69-86.
- ³ Bartholomew, C.H.; Agrawal, P.K.; Katzer, J.R. *Adv. Catal.* **1982**, 31, 135-242.
- ⁴ Butt, J.B. *Adv. Chem. Ser.* **1972**, 109, 259-496.
- ⁵ Bartholomew, C.H.; Farrauto, R.J. In *Fundamentals of Industrial Catalytic Processes*, 2nd ed.; John Wiley&Sons, Inc.: Hoboken, New Jersey, 2006; p 262.
- ⁶ Hegedus, L.L.; McCabe, R.W. *Catal. Rev. Sci. Eng.* **1981**, 23, 377-476.
- ⁷ Hegedus, L.L.; McCabe, R.W. In *Catalyst Poisoning*; Marcel Dekker: New York & Basel, 1984; p 1.
- ⁸ Gonzalez-Tejuca, L.; Alka, K.; Namba, S.; Turkevich, J. *J. Phys. Chem.* **1977**, 81, 1399-1406.
- ⁹ Snelders, D.J.M.; Yan, N.; Gan, W.; Laurenczy, G.; Dyson, P.J. *ACS Catal.* **2012**, 2, 201-207.
- ¹⁰ Widegren, J.A.; Finke, R.G. *J. Mol. Cat. A: Chem.* **2003**, 198, 317-341.
- ¹¹ Hornstein, B.J.; Aiken III, J.D.; Finke, R.G. *Inorg. Chem.* **2002**, 41, 1625-1638.
- ¹² Bayram, E.; Linehan, J.C.; Fulton, J.L.; Roberts, J.A.S.; Szymczak, N.K.; Smurthwaite, T.D.; Özkaz, S.; Balasubramanian, M.; Finke, R.G. *J. Am. Chem. Soc.* **2011**, 133, 18889-18902.

¹³ Tinnemans, S. J.; Mesu, J. G.; Kervinen, K.; Visser, T.; Nijhuis, T. A.; Beale, A. M.; Keller, D. E.; van der Eerden, A. M. J.; Weckhuysen, B. M. *Catal. Today* **2006**, 113, 3-15.

¹⁴ Note here that, in addition to previously reported data,¹² three additional 1,10-phenanthroline poisoning experiments were performed herein with the Rh(0)_n nanoparticles (i.e., 0.03, 0.08, and 0.15 equivs of 1,10-phenanthroline per total rhodium, see the Experimental section for details). The inclusion of these three additional data points changed slightly the previously reported¹² $x_{\text{intercept}}$ from 0.12 ± 0.02 to the 0.10 ± 0.02 value reported herein and shown in Figure 7.1, a change not significant within the stated experimental errors, however.

¹⁵ Vargaftik, M.N.; Zagorodnikov, V.P.; Stolarov, I.P.; Moiseev, I.I.; Kochubey, D.I.; Likholobov, V.A.; Chuvilin, A.L.; Zamaraev, K.I. *J. Mol. Cat.* **1989**, 53, 315-348.

¹⁶ For example, Satterfield and coworkers have reported the adsorption constants of nitrogen-based poisons for NiMo/Al₂O₃ catalyst in a flow reactor under solid gas phase reactions analyzed via Langmuir isotherms.¹⁷

¹⁷ Satterfield, C.N.; LaVopa, V. *J. Catal.* **1988**, 110, 375-387.

¹⁸ Use of the Langmuir adsorption isotherm¹⁹ is a common method to analyze the adsorption of gaseous molecules or atoms on solid catalyst surfaces (e.g., the adsorption of gaseous poisons). Some basic assumptions behind that treatment are that:²⁰ (i) the gaseous-phase molecule is adsorbed on an immobile solid surface; (ii) all adsorption sites are energetically equivalent; (ii) lateral interactions between the adsorbate are absent; and that (iv) the adsorbate per surface site is always *one*.¹⁹ Then, coverage fraction, Q , is defined:¹⁹ $Q = \{k_a[\text{poison}]^1\} / \{k_d + k_a[\text{poison}]^1\}$, which is readily rewritten in the $Q = \{b[\text{poison}]^1\} / \{1 + b[\text{poison}]^1\}$, where k_a and k_d are adsorption and desorption rate constants, respectively, and their ratio, $k_a/k_d = b$, is the adsorption coefficient.

¹⁹ Langmuir, I. *J. Am. Chem. Soc.* **1916**, 38, 2221-2295.

²⁰ Lercher, J.A. In *Catalysis: An Integrated Approach Second, Revised and Enlarged Edition*; van Santen, R.A., van Leeuwen, P.W.N.M., Moulijn, J.A., Averill, B.A., Eds.; Elsevier: Amsterdam, The Netherlands, 1999; p 543.

²¹ The Michaelis-Menten (M-M) kinetic treatment, developed for enzymatic sugar inversion²² in 1913 and widely used for enzymatic catalysis kinetics,²³ enzyme inhibition kinetics,²⁴ and homogeneous catalysis kinetics,²⁵ has been applied by Chandler and coworkers to TiO₂ supported gold nanoparticle heterogeneous catalysts, specifically to NaBr poisoning to estimate the percentage of catalytically active sites.²⁶

²² Michaelis, M.; Menten, M.L. *Biochem. Zeit.* **1913**, 49, 333-369.

²³ Lobban, M.D.; Irons, L.I.; van Heyningen, S. *Biochim. Biophys. Acta* **1991**, 1078, 155-160.

²⁴ Woodbury Jr., C.P. In *Biochemistry for the Pharmaceutical Sciences*; Jones&Bartlett Learning, LLC: Sudbury, Massachusetts, 2012; p 171.

²⁵ Rothenberg, G. In *Catalysis Concepts and Green Applications*; Wiley-VCH: Weinheim, 2008; p 39.

²⁶ Chandler, B.D.; Kendell, S.; Doan, H.; Korkosz, R.; Grabow, L.C.; Pursell, C.J. *ACS Catal.* **2012**, 2, 684-694.

²⁷ Chen, S.-Y.; Smith, J.M.; McCoy, B.J. *J. Catal.* **1986**, 102, 365-376.

²⁸ Palinko, I. *Stud. Surf. Sci. Catal.* **1994**, 88, 603-608.

²⁹ Lewnard, J.J.; Hsiung, T.H.; Brown, T.M.; Roberts, G.W. *Ind. Eng. Chem. Res.* **1993**, 32, 1610-1621.

³⁰ Xu, D.; Carbonell, R.G.; Kiserow, D.J.; Roberts, G.W.; *Ind. Eng. Chem. Res.* **2005**, 44, 6164-6170.

³¹ Nguyen, D.; Ho, T.C. *Chem. Eng. Commun.* **2006**, 193, 460-477.

³² Forzatti, P.; Lietti, L. *Catal. Today* **1999**, 52, 165-181.

³³ Bartholomew, C.H. *Appl. Catal. A: General* **2001**, 212, 17-60.

³⁴ Note also that there is an extensive literature for single-crystal model catalysts, under ultra-high vacuum (UHV) conditions, where precise quantitative poisoning data are reported, for example, where the equivs of metal sites deactivated by one equiv of poison are reported³⁷ or poison adsorption energies on metal surfaces are reported.³⁸ However, bridging the pressure, temperature, and material gaps between these ultra-clean, high-vacuum model systems and practical heterogeneous catalysts remains to be accomplished. For additional discussion of and lead references to these gaps, see ref 35 and 36.

³⁵ Mondloch, J.E.; Bayram, E.; Finke, R.G. *J. Mol. Catal. A: Chem.* **2012**, 355, 1-38.

³⁶ Thomas, J.M. *J. Chem. Phys.* **2008**, 128, 182502(1)-182502(19).

³⁷ Goodman, D.W. *J. Vac. Sci. Technol.* **1982**, 20, 522-526.

³⁸ Ku, R.; Bonzel, H.P. *J. Chem. Phys.* **1973**, 58, 4617-4624.

³⁹ Finney, E. E.; Finke, R. G. *Chem. Mater.* **2009**, 21, 4692-4705.

⁴⁰ In line with the literature, in the relative rate vs equivs of poison per *total* metal plots such as Figure 7.1 herein, we used the *total rhodium concentration* rather than the (rigorously unknown)

Rh(0)_n nanoparticle concentration. That total rhodium concentration will, then, be an upper limit to the true concentration of Rh(0)_n nanoparticles.

⁴¹ Pillai, U.R.; Sahle-Demessie, E. *J. Mol. Catal. A: Chem.* **2004**, 222, 153-158.

⁴² Schmid, G. *Endeavour* **1990**, 14, 172-178.

⁴³ Lin, Y.; Finke, R.G. *J. Am. Chem. Soc.* **1994**, 116, 8335-8353.

⁴⁴ Bayram, E.; Zahmakıran, M.; Özkar, S.; Finke, R.G. *Langmuir* **2010**, 26, 12455-12464.

⁴⁵ Birch, A.J.; Walker, A.M. *Tetrahedron Lett.* **1967**, 8, 1935-1936.

⁴⁶ Harmon, R.E.; Gupta, S.K.; Brown, D.J. *Chem. Rev.* **1973**, 73, 21-52.

⁴⁷ Note that following the original recipe for catalysis in this system,¹² 15 equivs of Et₃N are added per initial Rh employed. One role of the added Et₃N is to capture HCl formation produced from heterolytic H₂ activation.⁴⁸ Assuming our previously proposed¹² stoichiometry for the formation of Rh₄ clusters of $2[\text{RhCp}^*\text{Cl}_2]_2 + 4\text{Et}_3\text{N} + (5.6+c)/2 \text{H}_2 \rightarrow \text{Rh}_4\text{Cp}^*_{2.4}\text{Cl}_4\text{H}_c + 4\text{Et}_3\text{NH}^+\text{Cl}^- + 1.6(\text{Cp}^*\text{-H})$, then only 1 equiv Et₃N per equiv of Rh will form Et₃NH⁺Cl⁻, leaving 14 equivs of Et₃N “free” and thus itself a “potential” ligand / poison.¹⁰ However, and as a control to test for the rate effect of the added 15 equivs of Et₃N, a Standard Conditions benzene hydrogenation with [RhCp*Cl₂]₂ was performed as detailed elsewhere¹² *without any added Et₃N* followed by a subsequent benzene hydrogenation with the fully evolved catalyst (i.e., with Rh₄ clusters). That control yielded the same kinetics within ±15% experimental error as reported previously; see Figure 1 and Figure 7, respectively, elsewhere,¹² implying a minimal rate effect of the added 15 equivs of Et₃N. In addition, the 1,10-phenanthroline poisoning data analyzed herein are *relative rates*, so that any small effect of the 15 equivs of Et₃N should cancel out (i.e., any small effects of the 15 equivs of Et₃N are also in the initial rate of benzene hydrogenation beginning with Rh₄ clusters without any added 1,10-phenanthroline, Figure SI-D3a). In short, the evidence would seem to rule out the hypothesis that the 15 equivs of Et₃N, that are part of the original recipe for this system,¹² are somehow distorting the analysis or interpretation of the 1,10-phenanthroline poisoning experiments reported herein.

- ⁴⁸ Maitlis, P.M. *Acc. Chem. Res.* **1978**, 11, 301-307.
- ⁴⁹ Zahmakıran, M.; Ayvalı, T.; Philippot, K. *Langmuir* **2012**, 28, 4908-4914.
- ⁵⁰ Russell, M.J.; White, C.; Maitlis, P.M. *J. Chem. Soc. Chem. Commun.* **1977**, 427-428.
- ⁵¹ Sonnenberg, J.F.; Coombs, N.; Dube, P.A.; Morris, R.H. *J. Am. Chem. Soc.* **2012**, 134, 5893-5899.

APPENDIX-D

SUPPORTING INFORMATION FOR:

QUANTITATIVE 1,10-PHENANTHROLINE CATALYST-POISONING KINETIC STUDIES

OF Rh(0)_n NANOPARTICLE AND Rh₄ CLUSTER BENZENE HYDROGENATION

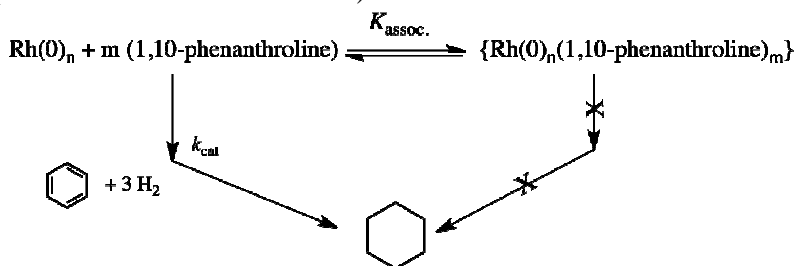
CATALYSTS: ESTIMATES OF THE POISON $K_{\text{association}}$ BINDING CONSTANTS, OF THE

EQUIVALENTS OF POISON BOUND AND OF THE NUMBER OF CATALYTICALLY

ACTIVE SITES FOR EACH CATALYST

Derivation of the Equations for the Strong-Binding Poison Case. To start, Scheme 7.1 from the main text is reproduced below as Scheme SI-D1.

Scheme SI-D1. The minimalistic, strong-binding poison model for poisoning of the $\text{Rh}(0)_n$ nanoparticles (reproduced from the main text).



To simplify the nomenclature and resultant equations, we set $[\text{Rh}(0)_n]_{\text{initial}} = [A_0]$, $[1,10\text{-phenanthroline}]_{\text{initial}} = [B_0]$, and the equilibrium concentration of the poisoned catalyst, $[\text{Rh}(0)_n(1,10\text{-phenanthroline})_m] = [P]$. It then follows that the equilibrium concentrations of $[\text{Rh}(0)_n]$ and $[1,10\text{-phenanthroline}]$ become $[A_0 - P]$ and $[B_0 - (mP)]$, respectively.

Since the at least initially linear decrease in the relative rate with added $[1,10\text{-phenanthroline}]$ indicates strong binding of the poison to the catalyst (i.e., and at least within that linear region), we make the assumption for the strong binding limit that all the added poison binds to the catalyst (i.e., and again at least in that linear region), that is, that:

$$[B_0] \approx m[P] \quad \text{eq. SI-D1}$$

Given that the rate law is typically first order with respect to the nanoparticle concentration,¹ $[A_0]$, eq. SI-D2 can be written;

$$\left\{ -\frac{d(\text{benzene})}{dt} \right\} = k_{\text{cat}} [A_0] [\text{benzene}]^b [H_2]^c \quad \text{eq. SI-D2}$$

The initial rate can then be identified as:

$$\left\{-\frac{d(\text{benzene})}{dt}\right\}_i = \{k_{cat}[\text{benzene}]_i^b [H_2]_i^c\} [A_0] \quad \text{eq. SI-D3}$$

Defining the observed rate constant for the initial rate as $k_{obs,i}$, where $k_{obs,i} = \{k_{cat}[\text{benzene}]_i^b [H_2]_i^c\}$, yields;

$$\left\{-\frac{d[\text{benzene}]}{dt}\right\}_i = k_{obs,i} [A_0] \quad \text{eq. SI-D4}$$

Since the poisoned catalyst, [P], does not have any catalytic activity, one can write the relative rate equation for Scheme SI-D1 as:

$$\text{Relative rate} = \frac{k_{obs,i} \{[A_0] - [P]\}}{k_{obs,i} [A_0]} \quad \text{eq. SI-D5}$$

Rearranging eq. SI-D5 yields eq. SI-D6;

$$\text{Relative rate} = 1 - \frac{[P]}{[A_0]} \quad \text{eq. SI-D6}$$

Solving eq. SI-D1 for [P] and substituting in eq. SI-D5 followed by simplification yields;

$$\text{Relative rate} = \left\{-\frac{1}{m}\right\} \frac{[B_0]}{[A_0]} + 1 \quad \text{eq. SI-D7}$$

Eq. SI-D7 is a simple linear equation of the form: $y = ax + b$ where $y =$ relative rate, slope $a =$

$\left\{-\frac{1}{m}\right\}$, $x = \left\{\frac{[B_0]}{[A_0]}\right\}$, and $b = 1$. Hence, one can analyze via linear regression the initially linear

portion of the relative rate vs equivalents of 1,10-phenanthroline per total rhodium (i.e., vs

$\left\{\frac{[B_0]}{[A_0]}\right\}$), plot.

The linear regression analysis of the linear portion of Figure 7.1 of the main text fits eq. SI-D7

with $y = -9.9x + 1$. By definition, the slope is $\left\{-\frac{1}{m}\right\} = -9.9$ making $m = 0.10$.

Further, in order to calculate the $K_{\text{assoc.}}$ via Scheme SI-D1, $K_{\text{assoc.}}$ can be written as;

$$K_{\text{assoc.}} = \frac{[P]}{\{[A_0] - [P]\}\{[B_0] - m[P]\}^m} \quad \text{eq. SI-D8}$$

Rearranging eq. SI-D6 for [P] yields;

$$[P] = [A_0] \times \{1 - \text{relative rate}\} \quad \text{eq. SI-D9}$$

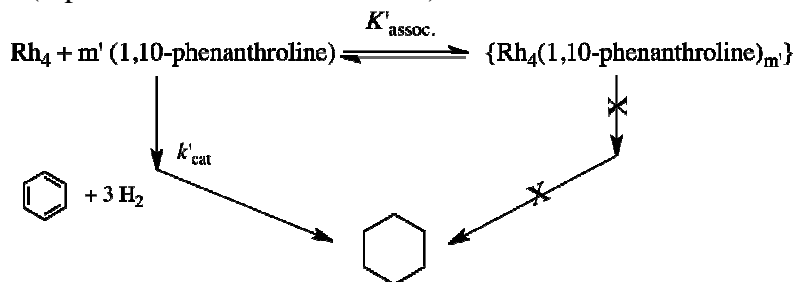
Substituting [P] in eq. SI-D8 with eq. SI-D9 yields;

$$K_{\text{assoc.}} = \frac{\{1 - \text{relative rate}\}}{\{\text{relative rate}\}\{[B_0] - m\{[A_0]\{1 - \text{relative rate}\}\}\}^m} \quad \text{eq. SI-D10}$$

Analysis of the Slightly Sigmoidal Quantitative 1,10-Phenanthroline Poisoning Plot for Rh₄

Sub-nanometer Clusters. To start, Scheme 7.2 from the main text is reproduced below as Scheme SI-D2.

Scheme SI-D2. The minimalistic, weak-binding poison model for poisoning of the Rh₄ sub-nanometer clusters (reproduced from the main text).



Again, we make analogous equation-simplifying definitions of $[\text{Rh}_4]_{\text{initial}} = [A'_0]$, $[1,10\text{-phenanthroline}]_{\text{initial}} = [B'_0]$ and the equilibrium concentration of poisoned catalyst, $[\text{Rh}_4(1,10\text{-phenanthroline})_{m'}] = [P']$. From this it follows that the equilibrium concentrations of $[\text{Rh}_4]$ and $[1,10\text{-phenanthroline}]$ are $[A'_0 - P']$ and $[B'_0 - (mP')]$, respectively.

K'_{assoc} equation is then and by definition:

$$K'_{\text{assoc}} = \frac{[P']}{\{[A'_0] - [P']\}\{[B'_0] - m'[P']\}^{m'}} \quad \text{eq. SI-D11}$$

Since the somewhat sigmoidal 1,10-phenanthroline poisoning of the Rh₄ clusters indicates weak association of the poison, we make the approximation that most of the added poison is not bound to the catalyst, especially when an excess of poison is present. Hence:

$$[B'_0] \gg m'[P'] \quad \text{eq. SI-D12}$$

This in turn simplifies the K'_{assoc} expression to:

$$K'_{\text{assoc}} = \frac{[P']}{\{[A'_0] - [P']\}[B'_0]^{m'}} \quad \text{eq. SI-D13}$$

Rearranging the above equation to give $[P']$ yields:

$$[P'] = \frac{K'_{\text{assoc}} [A'_0][B'_0]^{m'}}{1 + K'_{\text{assoc}} [B'_0]^{m'}} \quad \text{eq. SI-D14}$$

Previously, we reported² that the reaction is first order with respect to the Rh₄ clusters; hence a reasonable rate law will have some general form such as:

$$\left\{ -\frac{d(\text{benzene})}{dt} \right\} = k'_{\text{cat}} [A'_0] [\text{benzene}]^b [H_2]^c \quad \text{eq. SI-D15}$$

The initial rate will therefore be given by:

$$\left\{ -\frac{d(\text{benzene})}{dt} \right\}_i = \{k'_{\text{cat}} [\text{benzene}]_i^b [H_2]_i^c\} [A'_0] \quad \text{eq. SI-D16}$$

Defining the observed initial rate constant, $k'_{\text{obs},i}$, as $k'_{\text{obs},i} = \{k'_{\text{cat}} [\text{benzene}]_i^b [H_2]_i^c\}$ yields:

$$\left\{ -\frac{d[\text{benzene}]}{dt} \right\}_i = k'_{\text{obs},i} [A'_0] \quad \text{eq. SI-D17}$$

Since the poisoned catalyst, $[P']$, does not have any catalytic activity, one can write the relative rate equation as follows and according to Scheme SI-D2:

$$\text{Relative rate} = \frac{k'_{obs,i} \{[A'_0] - [P']\}}{k'_{obs,i} [A'_0]} \quad \text{eq. SI-D18}$$

Substituting [P'] from eq. SI-D14 into the above relative rate equation, eq. SI-D18, yields the desired:

$$\text{Relative rate} = \frac{1}{1 + K'_{assoc.} [B'_0]^{m'}} \quad \text{eq. SI-D19}$$

Ex-post-facto Confirmation of $[B'_0] \gg m'[P']$ with the $K'_{assoc.}$ and m' values Obtained via Non-Linear Least-Squares Fitting of the Poisoning Data. The non-linear least-squares fitting of the 1,10-phenanthroline poisoning of Rh₄ clusters via eq. SI-D19 and using GraphPad Prism software (ver 5.0) yields the $K'_{assoc.}$ and m' values of $6.1 \pm 4.4 \times 10^3 \text{ M}^{-1.86}$ and 1.86, respectively, and as detailed in the main text. Next, ex-post-facto calculations were performed with these fit $K'_{assoc.}$ and m' values to confirm (or refute) the initial assumption of $[B'_0] \gg m'[P']$. To do so, m' was rounded to 2 in order to simplify the calculations and avoid the complication of having to expanding to the power of 1.86 (see the justification below for this approximation). For each added 1,10-phenanthroline concentration, the $m'[P']$ value was calculated via eq. SI-D11 and compared to the $[B'_0]$. One example calculation is provided below for $[B'_0] = 2.3 \times 10^{-3} \text{ M}$. All other $[B'_0]$ concentrations were also performed in the same manner and are tabulated in Table SI-D1.

Sample Calculation when $[B'_0] = 2.3 \times 10^{-3} \text{ M}$: $[A'_0] = 1.15 \times 10^{-3} \text{ M}$ (0.202 mmol Rh in 44 mL solution: 36 mL of 2-propanol, 4 mL of benzene, 4 mL of cyclohexane). For $[B'_0] = 2.3 \times 10^{-3} \text{ M}$, the $K'_{assoc.}$ equation becomes (with m' rounded from 1.86 to 2.0);

$$6.1 \times 10^3 = [P'] / \{ (1.15 \times 10^{-3} - [P']) \times (2.3 \times 10^{-3} - 2[P'])^2 \} \quad \text{eq. SI-D20}$$

When the above equation is solved, $[P'] = 3.7 \times 10^{-5}$ M, so that $m'[P']$ then becomes $m'[P'] = 7.4 \times 10^{-5}$ M. Since $[B'_0] = 2.3 \times 10^{-3}$ M for this case, $m'[P']$ is ~3% of $[B'_0]$, confirming that $[B'_0] \gg m'[P']$. Repeating the same calculation for the other $[B'_0]$ concentrations yields the results shown in Table SI-D1.

Table SI-D1. The percentage of $m'[P']$ with respect to the initial $[B'_0]$ for all 1,10-phenanthroline concentrations used in the poisoning experiments performed.² The results show that at most, $m'[P']$ consists of $\leq 13\%$ of $[B'_0]$ confirming ex-post-facto the initial $[B'_0] \gg m'[P']$ assumption.

$[B'_0]$ (M)	$m'[P']$ (M)	$\left\{ \frac{m'[P']}{[B'_0]} \right\} \times 100$
4.6×10^{-5}	2.8×10^{-8}	0.06%
2.3×10^{-3}	7.4×10^{-5}	3%
4.6×10^{-3}	3.0×10^{-4}	7%
9.2×10^{-3}	1.2×10^{-3}	13%
18.4×10^{-3}	1.6×10^{-3}	9%
2.3×10^{-2}	3.0×10^{-4}	1%

Comparison of K'_{assoc} Values Obtained by the Controls of Using the Now Available $[B'_0]$ - $m'[P']$ Values and Fit the Poisoning Data (i) By Constraining $m' = 2$, and (ii) By Leaving m' Unconstrained. Ex-post-facto calculations using the fit-obtained K'_{assoc} and m' values of $6.1 \times 10^3 \text{ M}^{-1.86}$ and 1.86, respectively, revealed that $m'[P']$ is $\leq \sim 13\%$ of $[B'_0]$, justifying the $[B'_0] \gg m'[P']$ approximation used in the derivation of eq. SI-D19. However, and as controls, the poisoning plot was re-constructed using the now available, more accurate $[B'_0]$ - $m'[P']$ values for

each set of poisoning data as the x -axis (i.e., instead of the initial assumption of $[B'_0] \gg m'[P']$ and, in that case, using $[B'_0]$ as the x -axis). Constraining m' to 2 and fitting that data to eq. SI-D19 yields $R^2=0.994$ and $K'_{\text{assoc.}} = 8.1 \pm 4.5 \times 10^3 \text{ M}^{-2}$, the same value within experimental error of the prior $6.1 \pm 4.4 \times 10^3 \text{ M}^{-1.86}$ value (save the small difference in the units). This also justifies the rounding up of m' to 2, Figure SI-D1.

Next, if m' is *not constrained* to 2, fitting according to eq. SI-D19 with the new $[B'_0]-m'[P']$ values as the x -axis yields Figure SI-D2 and $K'_{\text{assoc.}} = 7.4 \pm 4.5 \times 10^3 \text{ M}^{-1.86}$, $m' = 1.86$, and $R^2=0.994$. Again, no significant difference is seen from the original fit results within the stated experimental errors.

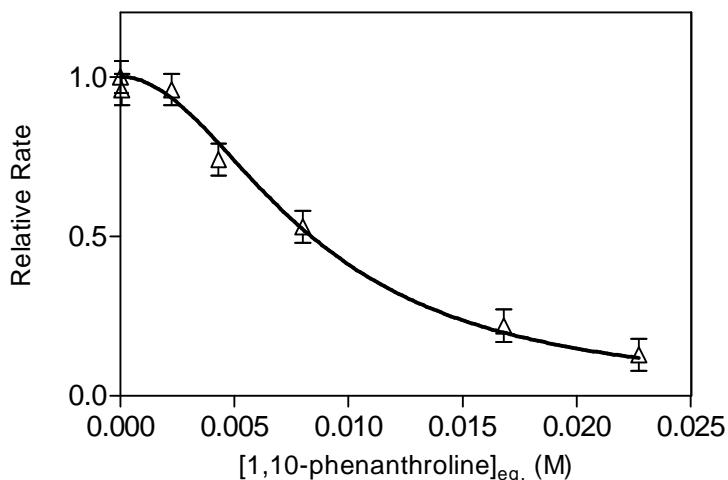


Figure SI-D1. Poisoning data (\triangle) and fit (—) according to eq. SI-D19 with the new $[B'_0]-m'[P']$ values as the x -axis and constraining $m' = 2$. The fitting yields $K'_{\text{assoc.}} = 8.1 \pm 4.5 \times 10^3 \text{ M}^{-2}$ with $R^2=0.994$.

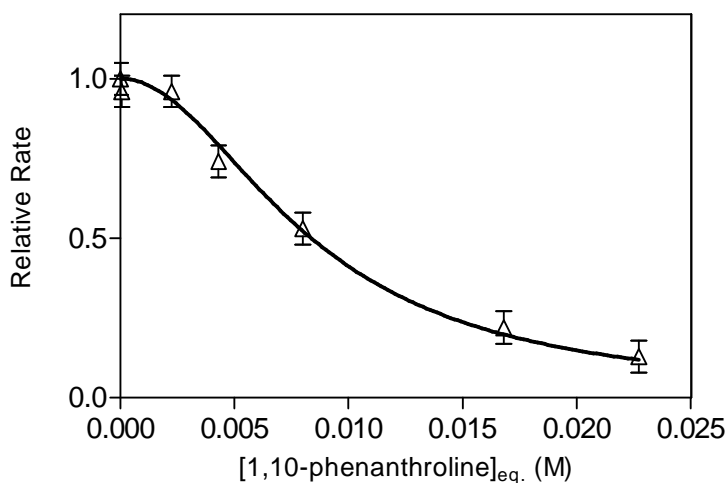
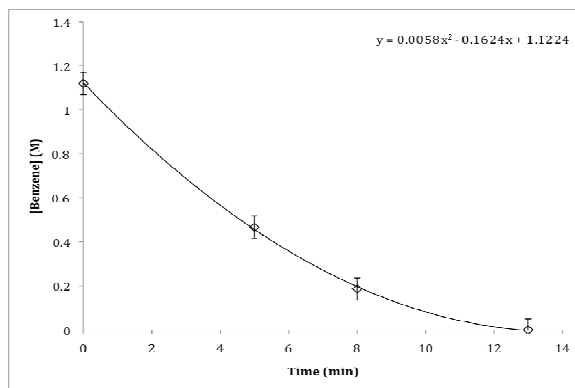


Figure SI-D2. Poisoning data (\triangle) and fit (—) according to eq. SI-D19 with the new $[B'_0]-m'[P']$ values as the x -axis, but now with an unconstrained m' . The fitting yields $K'_{\text{assoc.}} = 7.4 \pm 4.5 \times 10^3 \text{ M}^{-1.86}$, $m' = 1.86$ with $R^2 = 0.994$.

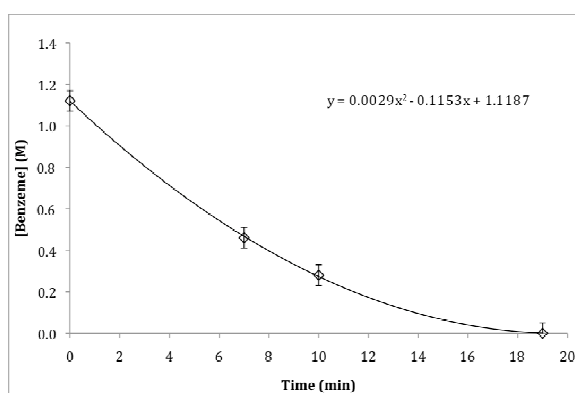
Overall, these two controls yield the same $K'_{\text{assoc.}}$ values within experimental error compared to the original fit of the poisoning data using the initial 1,10-phenanthroline concentration in place of equilibrium 1,10-phenanthroline concentration and with the assumption of $[B'_0] \gg m'[P']$.

Additional 1,10-Phenanthroline Poisoning Experiment Results with Rh(0)_n Nanoparticles.

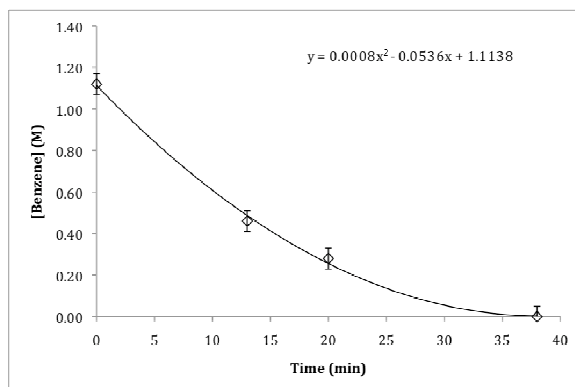
Three additional quantitative kinetic 1,10-phenanthroline poisoning experiments for the Rh(0)_n nanoparticles were performed as detailed in the Experimental section of the main text. Those experiments yielded the following benzene hydrogenation plots for (a) 0, (b) 0.03, (c) 0.08, and (d) 0.15 equivs 1,10-phenanthroline (i.e., 0, 1.1, 2.9, and 5.4 mg, respectively) per total Rh, Figure SI-D3.



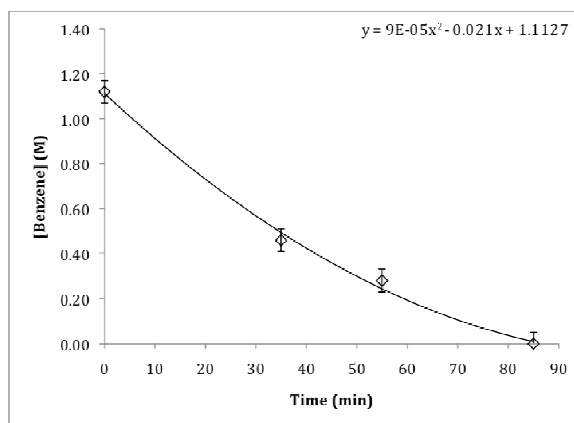
(a)



(b)



(c)



(d)

Figure SI-D3. Plots of the poisoning data (\diamond) with 1,10-phenanthroline and the 2nd degree polynomial fit (—) according to the specific equation provided within each graph. For each quantitative poisoning experiment, a separate “Benzene Hydrogenation Reaction Starting with Polyethyleneglycol-dodecylether Hydrosol Stabilized Rh(0)_n Nanoparticles” was performed by adding the required quantitative, predetermined amount of 1,10-phenanthroline to the initial solution as detailed elsewhere.² Specifically, (a) 0, (b) 0.03, (c) 0.08, and (d) 0.15 equivs of 1,10-phenanthroline (i.e., 0, 1.1, 2.9, and 5.4 mg, respectively) per total Rh were added in the three separate poisoning experiments. Each poisoning trial was repeated three times yielding identical initial rates within $\pm 15\%$ experimental error. The method of initial rates was used to analyze the kinetic data: the derivative of the polynomial equation fitted to each experiment was evaluated at $t = 0$, yielding the initial rate for that experiment from the coefficient of the second, t^1 term of the polynomial.

Overall, the initial rates for the three additional 1,10-phenanthroline poisoning experiments were calculated² to be 0.1153, 0.0536, and 0.0210 M/min, respectively, for 0.03, 0.08, and 0.15 equivs of 1,10-phenanthroline per total Rh. Since the initial rate of without any added 1,10-phenanthroline was previously reported² to be 0.1624 M/min, the relative rates for 0.03, 0.08, and 0.15 equivs of 1,10-phenanthroline per total Rh becomes 0.71, 0.33, and 0.13, respectively.

Analysis of the Recently Published Quantitative CS₂ Poisoning of Ammonia-Borane Dehydrocoupling Reaction Beginning with [Ru(cod)(cot)] (where cod: cyclooctadiene and cot: cyclooctatriene) at 25 °C. Table SI-D2 summarizes the quantitative CS₂ poisoning data from the literature study³ that were fit with eq. SI-D19 (or, equivalently, eq. 7.5 from the main

text) under the weak-binding poison assumption of $[CS_2]_{\text{initial}} \approx [CS_2]_{\text{equilibrium}}$. The resultant fit is reported in Figure 7.4 of the main text and yields $R^2=0.989$ and $m''=2.9 \pm 0.4$, although the $K''_{\text{assoc.}}$ value could not be determined from the limited set of literature data available (an ill-defined $K''_{\text{assoc.}} \sim 8.9 \pm 9.3 \times 10^5 \text{ M}^{-2.9}$ with error bars as large as the value itself resulted from the curve fitting).

Table SI-D2. The CS_2 quantitative poisoning data for dehydrocoupling of ammonia-borane when starting with $[Ru(\text{cod})(\text{cot})]$ at 25°C . For all data, the $[Ru]_{\text{initial}}=2.5 \times 10^{-2} \text{ M}$.

<i>Equivs of CS_2 per total Ru (CS_2/Ru)</i>	<i>Initial Rate (mL H_2/min)</i>	<i>$[CS_2]_{\text{initial}}$ (M)</i>	<i>Relative Rate</i>
0.0	0.0342	0.0	1.000
0.1	0.0341	2.5×10^{-3}	0.997
0.2	0.0340	5.0×10^{-3}	0.994
0.5	0.0276	1.25×10^{-2}	0.807
0.7	0.0182	1.75×10^{-2}	0.532
0.9	0.0122	2.25×10^{-2}	0.357
2.0	0.0044	5.0×10^{-2}	0.129

What one would like to do at this point is to perform *ex-post-facto* calculations to confirm, or refute, the assumption $[CS_2]_{\text{initial}} \approx [CS_2]_{\text{equilibrium}}$. However, for such ex-post-facto calculations one needs (a) a precise $K''_{\text{assoc.}}$ value; (b) the precise nature of the catalyst, specifically its nuclearity, n , in Ru_n , as well as (c) the number of active sites in each Ru_n that each equiv of CS_2 poisons. None of these are available for the present system. However, reflection reveals that such

calculations can provide further evidence for the true catalyst in that if the weak-binding poison model fits the data, then whatever the catalyst is, it should be consistent with the $[CS_2]_{\text{initial}} \approx [CS_2]_{\text{equilibrium}}$ assumption of the model in *ex-post-facto* calculations. Hence, we illustrate one of these below, just as an example that may assist others who might use the weak-binding model in the future.

Zahmakıran and coworkers added CS_2 when 40% of the their H_2 evolution reaction was complete, ca. 50 min after the reaction was initiated.³ Ex situ TEM investigation after 40 min of reaction revealed the presence of 0.6-2.2 nm particles with an average particle diameter of 1.4 ± 0.72 nm corresponding to on average $Ru_{\sim 147}$ nanoparticles^{4,5} (and deliberately citing more significant figures in the “ ~ 147 ” than is justified, just for the purposes of this calculation). Assuming (i) that there is no significant change in the diameter of the Ru_n species from 40 min to 50 min, and assuming (ii) that the ex situ TEM investigation reflects all the Ru species in solution during the reaction, then one can calculate the concentration of $Ru_{\sim 147}$ as 1.7×10^{-4} M (via the known $[Ru]_{\text{total,initial}} = 2.5 \times 10^{-2}$ M). Then, *ex-post-facto* calculations show $m' [Ru_{\sim 147} \cdot CS_2]$ is <10% of $[CS_2]_{\text{initial}}$ for all $[CS_2]_{\text{initial}}$ concentrations tabulated in Table SI-D2 (when m'' is rounded to 3) confirming the $[CS_2]_{\text{initial}} \approx [CS_2]_{\text{equilibrium}}$ assumption for the case of *if* the $Ru_{\sim 147}$ were the true catalyst.

The total number of surface atoms^{4,5} for $Ru_{\sim 147}$ is 92 which requires ca. 3 equivs of CS_2 per total Ru for the complete poisoning of the catalyst (i.e., $m'' = 3$ was obtained via fitting the reported data to eq. SI-D19). Previously, $CS_2:Rh(0)_n$ ratios of 1:1.5 to 1:20 were reported.⁶ If the upper limit of 1:20 is adopted for the sake of argument, then ca. 60 surface Ru atoms are poisoned out of available 92 surface Ru atoms—a physically not unreasonable value.

With a bit of reflection, it is probably apparent that more and more of the $[\text{CS}_2]_{\text{initial}}$ will be bound as one goes from a Ru_n to, say, a Ru_4 to a Ru_1 catalyst. In this regard, such calculations can at least in principle help support or refute hypotheses for the true catalyst. In the present literature example case, assumption will become less viable as one goes down to smaller $\text{Ru}_{\sim 4}$, say, clusters and more *in operando* investigation to follow the evolution of $[\text{Ru}(\text{cod})(\text{cot})]$ precatalyst under the reaction conditions will be required to gain a better idea of the true catalyst. Then, quantitative CS_2 or other poisoning experiments, and analysis by presumably the weak-binding model, will also need to be done, including *ex-post-facto* calculations analogous to those above to confirm, or refute, the assumption $[\text{CS}_2]_{\text{initial}} \approx [\text{CS}_2]_{\text{equilibrium}}$ for the proposed catalyst(s).

REFERENCES

¹ The statement, that the rate law is typically first order with respect to the nanoparticle concentration, tends to generally be true so long as the Rh(0)_n nanoparticle catalyst does not evolve to other forms such as, but not limited to, agglomerated bulk metal. In the present case, agglomeration is ruled out by TEM analysis of the catalyst from the product solution which showed unagglomerated, 2-3 nm Rh(0)_n nanoparticles (see Figure SI-6 elsewhere²), identical to the starting Rh(0)_n nanoparticles. Also supporting a first-order dependence on the 2-3 nm Rh(0)_n nanoparticle catalyst is the absence of any observable induction period for the benzene hydrogenation followed by an exponential, first-order reaction decay.

² Bayram, E.; Linehan, J.C.; Fulton, J.L.; Roberts, J.A.S.; Szymczak, N.K.; Smurthwaite, T.D.; Özkar, S.; Balasubramanian, M.; Finke, R.G. *J. Am. Chem. Soc.* **2011**, 133, 18889-18902.

³ Zahmakıran, M.; Ayvalı, T.; Philippot, K. *Langmuir* **2012**, 28, 4908-4914.

⁴ Schmid, G. *Endeavour* **1990**, 14, 172-178.

⁵ Lin, Y.; Finke, R.G. *J. Am. Chem. Soc.* **1994**, 116, 8335-8353.

⁶ Hornstein, B.J.; Aiken, III, J.D.; Finke, R.G. *Inorg. Chem.* **2002**, 41, 1625-1638.

CHAPTER VIII

SUMMARY

Brief but critical reviews of the pertinent literature revealed that identification of the true catalyst for a given catalyst system (i) is an important, fundamental issue in all catalytic systems since key catalytic properties such as—but not limited to—activity, selectivity, lifetime, recovery, regeneration, and poisoning all depend on the identity of the true catalyst, and (ii) M_4 (M: transition metal) cluster catalysis is an interesting, increasingly important, and evolving area for catalysis. This latter point follows since M_4 clusters are poised between mononuclear metal complexes and larger, $M(0)_n$ metal nanoparticles and offer their own, distinctive catalytic properties in-between single-metal homogeneous and polymetallic-nanoparticle heterogeneous catalysis. In addition, the reviews of the literature presented herein revealed that determining the identity of the true catalyst (iii) is often challenging if not perplexing, and hence (iv) requires multiple, complimentary methods, since no single experiment can convincingly identify the true catalyst of the system. Nonetheless, the work presented in this thesis and the two published and two submitted papers were able to identify the true catalyst in three systems: (a) $Ir(0)_n$ nanoparticles and aggregates, (b) Rh_4 sub-nanometer clusters, and (c) mononuclear Ir_1 /zeolite Y catalysts for benzene and cyclohexene hydrogenations, respectively.

The final work presented in this thesis and submitted for publication was able to understand linear and non-linear 1,10-phenanthroline quantitative kinetic poisoning data for $Rh(0)_n$

nanoparticles and Rh₄ clusters catalysts, respectively. The methodology employed yielded the estimates of the equivalents of poison bound, the quantitative catalyst poisoning association constants, and the numbers of active sites for each catalyst. The latter is required for calculation of the important quantity of the turn-over frequency (TOF) of a catalyst.

There are several other potential avenues for future research stemming directly from the results described herein. For example, investigation of the true catalyst for dehydrocoupling of dimethylaminoborane at 25 °C when beginning with [(1,5-COD)RhCl]₂ precatalyst is important and should be pursued. There is still¹ a controversy as to whether the true catalyst is Rh(0)_n nanoparticles² or Rh₄ clusters³ as detailed in Chapter III. Additional kinetic experiments will be needed (such as the order of the reaction with respect to the total metal present when starting with the fully evolved catalyst) as well as quantitative kinetic poisoning experiments; even these two experiments will help to definitively identify the true catalyst of the aforementioned system as has been done for the studies detailed in Chapter V.

In a general sense, the work herein shows that employing multiple, complimentary methods including *in operando* spectroscopic studies, kinetics, and quantitative kinetic poisoning experiments are key to identify the true active catalyst of any catalyst system, be it weakly ligated/labile ligand nanoparticles and aggregates, sub-nanometer metal clusters or an atomically dispersed mononuclear metal catalyst supported on a solid-oxide surface. However, one should also adopt and utilize the Platt's method⁴ while investigating the true catalyst for any and all catalyst systems: namely hypothesis driven research, in which all the hypotheses for the identity of the true catalyst tested with attempts made to disprove them. In the case that more than one hypothesis are probable and consistent with all the evidence, one should proceed with Ockham's

razor:⁵ the simplest answer is conditionally taken as the best answer, at least until new method or approaches allow additional testing.

Finally, the results described and resultant four papers show that the methodology developed and employed is able to identify the true catalyst and differentiate single-active-site homogeneous, and multiple-active-sites heterogeneous catalysts. As such, the evidence is that the work performed, and resultant publications from this thesis, promise to be a lasting contribution to the scientific literature of the important topic of chemical catalysis.

REFERENCES

¹ Staubitz, A.; Robertson, A.P.M.; Sloan, M.E.; Manners, I. *Chem. Rev.* **2010**, *110*, 4023.

² (a) Jaska, C.A.; Temple, K.; Lough, A.J.; Manners, I. *J. Am. Chem. Soc.* **2003**, *125*, 9424. (b) Jaska, C.A.; Manners, I. *J. Am. Chem. Soc.* **2004**, *126*, 9776.

³ (a) Chen, Y.; Fulton, J.L.; Autrey, T.; Linehan, J.C. *J. Am. Chem. Soc.* **2005**, *127*, 3254. (b) Szymczak, N.K.; Chen, Y.; Balasubramanian, M.; Autrey, T.; Fulton, J.L.; Linehan, J.C. *J. Am. Chem. Soc.* **2007**, *129*, 11936.

⁴ Platt, J.R.; *Science* **1964**, *146*, 3642.

⁵ William of Ockham, 1285-1349, as cited in E. A. Moody (1967) *The Encyclopedia of Philosophy*, Vol. 7, MacMillan, New York.

APPENDIX-E

GENERAL STATEMENT ON “JOURNALS-FORMAT” THESES

(Written by Professor Richard G. Finke)

The Graduate School at Colorado State University allows, and the Finke Group in particular encourages, so-called journals-format theses. Journals-format theses, such as the present one, consist of a student written and lightly edited literature background section, chapters corresponding (in the limiting, ideal case) to final-form papers either accepted or at least submitted for publication, a summary or conclusions chapter, and short bridge or transition sections between the chapters as needed to make the thesis cohesive and understandable to the reader. The “bridge” sections and summary are crucial so that the thesis fulfills the requirement that the thesis be an entity (an official requirement of most Graduate Schools). All chapters (manuscripts) in a journals-format thesis must of course be written initially by the student, with subsequent (ideally light) editing by the Professor, the student’s committee, and even the student’s colleagues where appropriate and productive.

The advantages for doing a journals-format thesis are several-fold and compelling. Specifically, some of the major advantages are: the level of science (i.e., of refereed, accepted publications) is at the highest level; the student and Professor must interact closely and vigorously (i.e., to bring both the science and the writing to their highest level), hence the student is getting the best education possible and is being at least exposed to (if not held to) the highest

standards; the needed clean-up or control experiments that invariably come up have all been identified and completed before the student leaves; there are no further time demands once the student has left the University (since all publications are at least submitted; it is terribly inefficient to try to complete either writing or often specialized experiments once the student has left); and the American tax payers, who ultimately pay the bill for the research, are getting their money's worth since all the research is published and thus widely disseminated in the highest form, as refereed science. Professorial experience teaches that a student who has achieved a journals-format thesis has indeed received a better education and has learned critical thinking and clear writing skills that will serve them well for a lifetime.

Experience also teaches, however, that much more than light editing is often needed in at least some student theses; it follows, then, that considerable professorial writing and editing might be needed for at least the initial chapters of most journals-format theses. Indeed, a journals-format thesis is not recommended (and may not even be possible) for less strong students. Hence, the issue arises of exactly how much of the science and the writing, in the final (or submittable) chapters, is due to the student vs. the Professor and whether or not this level of contribution constitutes that acceptable of a new Ph.D. and independent investigator.

To deal with this issue, several recommendations are made.

Recommendations

The recommendations are:

- (i) That the present pages be enclosed in the thesis until such a time as it is no longer needed (i.e., when the policies and procedures for journals-format theses become routine);
- (ii) That for each chapter it is detailed, and to the satisfaction of the committee and the advisor, who made what contributions, both of intellectual substance and writing. Substantial

contributions of other students or Professors should of course be acknowledged. In the case of disagreements, the various drafts (i.e., as their electronic files) can be examined by the committee (in light of a knowledge of who wrote which draft) to easily determine who contributed what. In possible borderline or controversial cases it may even be advisable to keep all (electronic) drafts of the papers as a record;

(iii) That it be specifically stated whether or not all the experimental work is the Ph.D. candidate's (as is usually the case, although the increasing (desirable) collaboration among scientists worldwide makes this a non-trivial point).

(iv) Furthermore, it is recommended that allowances be made for the expectation that a greater degree of involvement of the professorial advisor is likely in a journals-format thesis than in a traditional thesis. That this is reasonable follows from the fact that some Professors write 100% of all their papers; this, unfortunately, robs the student of the valuable experience of participating in the science and the end product as practiced at the highest levels. It also creates an unmanageable writing burden for Professors involved in all but the narrowest of research areas or for Professors involved in more than one competitive research area;

(v) Notwithstanding (iv), there needs to be ideally no more than ca. 40% Professorial writing contribution in a given *early* chapter in the thesis, and there should be a clear evolution in the thesis of a decreasing professorial involvement to, say, a 10-20% direct contribution in the last chapter or two.

(vi) As a further aid towards separating out the candidate's and the professorial (and other) contributions, it is recommended that the Introductory (usually literature background) chapter(s) and at least the final chapter be lightly edited only, so that authentic examples of the student's contributions are documented in an unambiguous form.